IOWA STATE UNIVERSITY
Digital Repository

Retrospective Theses and Dissertations

Iowa State University Capstones, Theses and Dissertations

2007

Wireless multiuser communication systems: diversity receiver performance analysis, GSMuD design, and fading channel simulator

Dongbo Zhang
Iowa State University

Follow this and additional works at: https://lib.dr.iastate.edu/rtd

 Part of the Electrical and Electronics Commons

Recommended Citation
Zhang, Dongbo, "Wireless multiuser communication systems: diversity receiver performance analysis, GSMuD design, and fading channel simulator" (2007). *Retrospective Theses and Dissertations*. 15587.
https://lib.dr.iastate.edu/rtd/15587

This Dissertation is brought to you for free and open access by the Iowa State University Capstones, Theses and Dissertations at Iowa State University Digital Repository. It has been accepted for inclusion in Retrospective Theses and Dissertations by an authorized administrator of Iowa State University Digital Repository. For more information, please contact digirep@iastate.edu.

www.manaraa.com

Wireless multiuser communication systems: diversity receiver performance analysis, GSMuD design, and fading channel simulator

by

Dongbo Zhang

A dissertation submitted to the graduate faculty

in partial fulfillment of the requirements for the degree of

DOCTOR OF PHILOSOPHY

Major: Electrical Engineering

Program of Study Committee:
Yao Ma, Major Professor
Julie Dickerson
Daji Qiao
Zhengdao Wang
Huaiqing Wu

Iowa State University

Ames, Iowa

2007

Copyright © Dongbo Zhang, 2007. All rights reserved.

www.manaraa.com

UMI Number: 3289389

UMI

UMI Microform 3289389

Copyright 2008 by ProQuest Information and Learning Company.
All rights reserved. This microform edition is protected against
unauthorized copying under Title 17, United States Code.

ProQuest Information and Learning Company
300 North Zeeb Road
P.O. Box 1346
Ann Arbor, MI 48106-1346

www.manaraa.com

Dedicated

To My Parents

www.manaraa.com

TABLE OF CONTENTS

www.manaraa.com

www.manaraa.com

www.manaraa.com

www.manaraa.com

LIST OF TABLES

www.manaraa.com

LIST OF FIGURES

www.manaraa.com

www.manaraa.com

www.manaraa.com

www.manaraa.com

www.manaraa.com

www.manaraa.com

LIST OF ACRONYMS

AAS	advanced antenna systems
AF	amount of fading
AAP	average access probability
AAR	average access rate
AAT	average access time
AFD	average fade duration
AMC	adaptive modulation and coding
a-SNR	absolute-SNR
AWT	average wait time
BER	bit error rate
CARA	channel-aware resource allocation
CDF	cumulative distribution function
CDMA	code-division multiple-access
CIRA	channel-independent resource allocation
CSI	channel state information
CSIT	CSI at transmitter
DV	decision varible
EGC	equal gain combining
FDMA	frequency-division multiple-access
GCQ	Gauss-Chebyshev quadrature
GSC	generalized selection combining
GSMuD	generalized selection multiuser diversity
MMSE-CE	minimum mean squared-error channel estimator

www.manaraa.com

i.i.d	independent and identically distributed
i.n.d	independent but not necessarily identically distributed
ICE	imperfect channel estimation
IDFT	inverse discrete Fourier transform
LCR	level crossing rate
MGF	moment generating function
MIMO	multiple-input multiple-output
MRC	maximal ratio combining
MUD	multiuser detection
n-SNR	normalized-SNR
OFDM	orthogonal frequency-division multiplexing
PDF	probability density function
PER	packet error rate
PFS	proportional fair scheduling
PSAM	pilot symbol assisted modulation
QAM	quadrature amplitude modulation
QoS	quality of service
RV	random variable
SDMA	spacial-division multiple-access
SER	symbol error rate
SMuD	selection multiuser diversity
SNR	signal-to-noise ratio
TDMA	time-division multiple-access
PAM	pulse amplitude modulation
WF	waterfilling

www.manaraa.com

ACKNOWLEDGEMENTS

It is my honor and pleasure to thank so many people who helped me with through those years at Iowa State University. First and foremost, it is impossible to overstate my deepest gratitude and respect to my advisor, Dr. Yao Ma, for his inspiration, his helpful instructions, and his tremendous efforts and dedication to guide me through my study and research over the years. He always led me to the right track when I felt confused and his insightful viewpoints broadened my horizon on many areas of interesting problems. Throughout my dissertation writing, he provided me lots of advices, lots of ideas, and certainly endless kind encouragements. I would have been lost without his great guidance.

I also would like to thank my program of study committee members- Dr. Julie Dickerson, Dr. Daji Qiao, Dr. Zhengdao Wang, and Dr. Huaiqing Wu for their wonderful and inspirational teaching of the invaluable classes I attended, and their great and enthusiastic help on my research. I would also like to thank Dr. Aleksandar Dogandzic for his guidance throughout the initial stages of my graduate career.

During my study, I have collaborated with many fellow students for whom I have great regard, and I would like to extend my warmest thanks to the members of communication and signal processing group , Wei Mo, Jinghua Jin, Peng Yu, Xiaofan Yang, Benhong Zhang, Wei Zhou, Lei Zhao and Weitan Hsu. Also, I am grateful to my friends, especially Cheng Cheng for making life more interesting and enjoyable in Ames.

Lastly, and most importantly, I would like to thank my Mom and Dad. They bore me, raised me, always support me, teach me, and love me. To them I dedicate this dissertation. I cannot complete the dissertation without their constant love and support.

www.manaraa.com

ABSTRACT

Multipath fading phenomenon is central to the design and analysis of wireless communication systems including multiuser systems. If untreated, the fading will corrupt the transmitted signal and often cause performance degradations such as increased communication error and decreased data rate, as compared to wireline channels with little or no multipath fading. On the other hand, this multipath fading phenomenon, if fully utilized, can actually lead to system designs that provide additional gains in system performance as compared to systems that experience non-fading channels.

The central question this thesis tries to answer is how to design and analyze a wireless multiuser system that takes advantage of the benefits the diversity multipath fading channel provides. Two particular techniques are discussed and analyzed in the first part of the thesis: quadrature amplitude modulation (QAM) and diversity receivers, including maximal ratio combining (MRC) and generalized selection combining (GSC). We consider the practical case of imperfect channel estimation (ICE) and develop a new decision variable (DV) of MRC receiver output for M-QAM. By deriving its moment generating function (MGF), we obtain the exact bit error rate (BER) performance under arbitrary correlated Rayleigh and Rician channels, with ICE. GSC provides a tradeoff between receiver complexity and performance. We study the effect of ICE on the GSC output effective SNR under generalized fading channels and obtain the exact BER results for M-QAM systems. The significance of this part lies in that these results provide system designers means to evaluate how different practical channel estimators and their parameters can affect the system's performance and help them distribute system resources that can most effectively improve performance.

In the second part of the thesis, we look at a new diversity technique unique to multiuser

www.manaraa.com

systems under multipath fading channels: the multiuser diversity. We devise a generalized selection multiuser diversity (GSMuD) scheme for the practical CDMA downlink systems, where users are selected for transmission based on their respective channel qualities. We include the effect of ICE in the design and analysis of GSMuD. Based on the marginal distribution of the ranked user signal-noise ratios (SNRs), we develop a practical adaptive modulation and coding (AMC) scheme and equal power allocation scheme and statistical optimal 1-D and 2-D power allocation schemes, to fully exploit the available multiuser diversity. We use the convex optimization procedures to obtain the 1-D and 2-D power allocation algorithms, which distribute the total system power in the "waterfilling" fashion alone the user (1-D) or both user and time (2-D) for the power-limited and energy-limited system respectively. We also propose a normalized SNR based GSMuD scheme where user access fairness issues are explicitly addressed. We address various fairness-related performance metrics such as the user's average access probability (AAP), average access time (AAT), and average wait time (AWT) in the absolute- and normalized- SNR based GSMuD. These metrics are useful for system designers to determine parameters such as optimal packet size and delay constraints.

We observe that Nakakagami-m fading channel model is widely applied to model the real world multipath fading channels of different severity. In the last part of the thesis, we propose a Nakagami-m channel simulator that can generate accurate channel coefficients that follow the Nakagami-m model, with independent quadrature parts, accurate phase distribution and arbitrary auto-correlation property. We demonstrate that the proposed simulator can be extremely useful in simulations involving Nakagami-m fading channel models, evident from the numerous simulation results obtained in earlier parts of the thesis where the fading channel coefficients are generated using this proposed simulator.

www.manaraa.com

CHAPTER 1. INTRODUCTION

1.1 Overview of Multiuser Wireless Communication Systems

Wireless communication industry has seen explosive growth in the past decade, as numerous new applications and network services such as wireless local area network (WLAN), third generation (3G) and beyond wireless cellular system, wireless metropolitan area network (WMAN), and Worldwide Interoperability for Microwave Access (WiMAX)are now getting increasingly popular. Some of the common goal of those new technologies and systems are to support simultaneous access of multiple users and to provide users with better throughput, lower power consumption and larger coverage area. Research efforts on multiuser wireless communication systems will create exciting new opportunities that have the potential to fundamentally change the way people communicate.

The unique nature of wireless channels presents many challenges as well as opportunities to the system designers. First of all, wireless channel exhibits fading of different scale, from the long-term path loss and shadowing to the more volatile multipath fading, which will greatly corrupt the received signal and degrade system performance if left untreated. On the other hand, multipath fading presents the potential to improve the system performance if diversity combining receivers are utilized. Secondly, any wireless communication system must operate with the limited and usually expensive spectral resources. A major challenge is to design the wireless communication system such that this limited resource can be utilized to the fullest extent. For uncoded communication, a straightforward solution is to use the modulation schemes that have high spectral efficiency such as M-ary QAM, and thus provide high-speed communication with limited bandwidth. The price to pay for this increased spectral efficiency is less reliable reception given the same transmitting power level, but this can be mitigated by

www.manaraa.com

diversity combiners.

Furthermore, due to the multiuser nature of many practical wireless communication systems, harmful interference from unintended users also poses a problem. This often results in lower reception reliability, lower capacity or both. Numerous multiple access schemes such as time-division multiple access (TDMA), frequency-division multiple access (FDMA), and code-division multiple access (CDMA) have been proposed to separate different users, by putting their traffic on orthogonal channels thus minimizing mutual interference. A problem with orthogonal multiuser system is the inefficient use of total system resources, especially in wireless multipath fading environment. If the system assigns the orthogonal channels to users without considering the fading channel state of those particular uses, total system throughput could suffer. On the other hand, channel scheduling algorithms that actively use the information on fading channel conditions by assigning channels to users who have the biggest the channel gains, can provide a gain in terms of total system capacity. This additional gain due to wireless fading channel and multiuser nature is called multiuser diversity gain [64, 75].

Finally, it's evident from the preceding discussion that fading phenomenon in wireless channels is utterly important to system design and performance analysis. An additional challenge for system designers is how to accurately model and simulate the multipath fading channel. Only after the successful designing of an accurate fading channel simulator, can system performance under actual physical fading conditions be simulated and new algorithms be verified.

In what follows, we introduce some of the major techniques to address the important issues identified above.

1.2 Diversity Combining

Multipath fading channels provide multiple replicas of the transmitted signal arriving with different phase and magnitude. Diversity combining technique takes advantage of this fading phenomenon, by combining these distinct replicas. If the wireless channel provides a rich scattering environment that results in the multiple copies of the transmitted signal being almost independent of each other, diversity reception technique can provide a significant *diversity gain*

www.manaraa.com

over the flat fading channels where there is no multipath fading. This is possible because of the fact that it is a rare event that all available replicas will experience deep fading at any given time where there's significant signal attenuation. As long as the signal levels of some of the replicas are reasonably high, the system could still correctly determine the transmitted signal, and provide diversity gain.

Depending on how to combine available diversity branches, diversity combiner can be classified into MRC or equal gain combiner (EGC). In MRC, the output is the weighted and co-phased sum of signals from all available branches, where the weight assigned is the complex conjugate of each branch's respective channel gain normalized by its noise power. MRC provides maximal output SNR and consequently maximal performance gain under white noise assumption. EGC only requires the estimation of channel phase and combines the co-phased branches but provides smaller diversity gain.

Judged by how many of the available diversity branches are being used in the combiner, we could differentiate the diversity combiners into "maximal" combiners where all detectable diversity branches are used, or "generalized selection" combiners (GSCs), also called hybrid selection/maximum ratio combining (HS/MRC) [35, 36, 41], where only a fraction of the total diversity branches are used. We can further dissect those general selection combiners into different subgroups based on what criteria are used in the selection process. If the selection is based on a predefined fixed number of diversity branches to be combined, it's the conventional GSC. The number of branches selected can be determined by the system designer based on desired level of performance, quality of service (QoS) and system complexity requirements, and thus bridges the gap between MRC and SC. GSC will usually provide a BER performance that is comparable to that of MRC and at the same time with reduced implementation complexity. If the selection of diversity branches is based on a predetermined threshold of SNR, it is actually called threshold-GSC or minimal selection-GSC [7].

Besides multipath diversity, there are other forms of diversity as long as multiple replicas of the same signal are available at the receiver. The same principal and method of analysis of diversity combining techniques developed for the multipath diversity (MRC, EGC and GSC)

www.manaraa.com

can be easily extended to those scenarios. For example, spatial diversity is possible in multiple-input multiple-output (MIMO) system, and frequency diversity can be available in frequency hopping, orthogonal frequency-division multiplexing (OFDM), and multi-carrier CDMA (MC-CDMA) systems.

1.3 Imperfect Channel Estimation

Many communication systems require channel state information (CSI) either at the receiver, at the transmitter or both. Systems with coherent detection, receive beamforming, diversity combining are the examples that CSI is needed at receiver. Transmit beamforming would be an example that requires CSI at the transmitter (CSIT). The process to obtain CSI is called channel estimation. Generally speaking, channel estimation is usually realized either by the using of training symbols called pilot symbols assisted modulation (PSAM), by the so-called blind estimation approaches that don't rely on pilot symbols, instead on some known higher order statistics of the data symbols being transmitted, or by the decision feedback (DF) estimator where soft- or hard-decoded data symbols are fed back to update channel estimation iteratively.

In practice, it is hard to obtain the CSI accurately in wireless channel because of delay and complexity constraints and the inherent nature of wireless channel such as multipath fading, doppler shift, among others. More often, the practical channel estimator output is stochastic and imperfect, thus the adverse effect of ICE as compared to the perfect CSI case must be considered. Intuitively, the inherent channel estimation error will degrade the system performance. An important problem to answer next is how to model the effects of the ICE on system performance and how to design better channel estimators and fine-tune their parameters to achieve the optimal tradeoff of performance, complexity and overhead.

1.4 Multiuser Communication

Many wireless communication systems are multiuser systems, where system resources are usually divided among users. In centralized systems, multiple users communicate with a cen-

www.manaraa.com

tral node or base station. The communication channels to and from this base station are called uplink and downlink channels, respectively. The technique of allocating channels to specific users is called *resource allocation* technique, which divides the total available signaling dimensions (time, frequency, code, and sector) into channels and then assigns these channels to different users. In *ad hoc* systems, there are no central stations to coordinate or relay user traffic. Instead, all the resource allocation and actual communications happen entirely via the coordination of participating users, usually through contention-based procedure.

Some of the most commonly used multiple access techniques divide the signaling space along the time, frequency, and code dimensions.TDMA and FDMA are mostly orthogonal channelization methods whereas CDMA can be orthogonal or non-orthogonal, depending on the code design. All the orthogonal schemes are equivalent in the sense that they orthogonally divide up the signaling dimensions and will have the same channel capacity in AWGN. Under fading channel conditions, those schemes sometimes will provide different capacities, depending on the criteria they use to assign the available orthogonal channel resources to users.

There are categorically two kinds of channel resource allocation schemes. The first is what we call channel independent resource allocation (CIRA), where users are assigned the channel resources in a predetermined fashion independent of the current fading channel condition they experience. One widely used CIRA scheme is round robin, where resources are assigned to users in the order of their index. The other type of resource allocation scheme is channel aware resource allocation (CARA) where user's channel condition is considered in the allocation process. CARA has the potential to provide larger capacity in multiuser wireless communication systems by using the multiuser diversity.

Multiuser Diversity (MuD) is inherent in any multiuser systems with fading channels and can be exploited by tracking the individual user channel quality between the transmitter and the receiver and transmits to the receiver with the largest channel gain. MuD gain is a diversity gain in addition to any existing point-to-point "normal" diversity gain discussed in Section 1.2. It arises from the fact that in a network with many independent users, there is likely to be a user with a very high channel quality. We noticed that the "normal" diversity combiner improves

www.manaraa.com

the lower tail of the PDF of the received SNR, reducing the probability that the effective SNR of the combined output signal from the diversity combiners is low. MuD exploits the higher tail of the PDF of the received SNR, by always picking those user channels at the fading stage that are in the high SNR region. As a matter of fact, the potential performance gain due to MuD in rich fading environment prompts some work [75] to "create" artificial rich fading multiuser channels when the physical channel exhibits moderate fading, to fully exploit the MuD.

An example of MuD is given in [64] for uplink channel in a single cell with multiple users communicating to the base station via time-varying fading channels. It is assumed that the channel is tracked at the base station and CSI is fed back to the subscribers. The maximal total information-theoretic capacity for a TDMA system is achieved by an optimal strategy to let the user with best channel to transmit at any given interval and this capacity is greater than that of a single user system under the same setup. Multiuser diversity gain is possible because of the inherent fading phenomenon in wireless channels just as diversity receivers are possible in wireless communication. They both utilize the fact that the fading channel can provide received signals with wider dynamic range and that the system can choose to use. We'll show that this underlying similarity also prompts to similar approaches in tackling with these two seemingly different problems.

In any practical multiuser systems, not all users are equal in terms of amount of traffic created and QoS requirements. These users could be one of several typical QoS classes [73]: non-real-time variable bit rate, available bit rate, unspecified bit rate, constant bit rate and real-time variable bit rate. And even in the same class, the demanded bit rate will differ from one user to another. Consequently, one of the most important tasks in a multiuser system is how and when to assign the available multiuser channel resources to those users and this task is called *multiuser scheduling*. Multiuser scheduling algorithms aim to meeting the following goals: (1) satisfying the individual user's required QoS (i.e. BER), (2) providing maximal combined throughput for all users, and (3) other system considerations (i.e. power constraints, fairness requirements, and system lifetime requirements).

www.manaraa.com

Multiuser scheduling is a cross-layer design problem because it balances requirements of different layers in terms of QoS(throughput, BER, latency), capacity, and power constraints. In addition, the algorithm that always schedules the strongest user may cause some channel access fairness issue because some users with the stronger average channel strengths (e.g., the user who is closer to the base station) may monopolize channel access resources. Other multiuser scheduling algorithms [65,66,75,79] take into account the fairness issue and although the multiuser sum rate may not be as large, each user will have more fair share of access to the channel resources.

1.5 Fading Channel Simulator

As discussed above, the fading phenomenon in wireless channel is inherent to any wireless communication system. Accurate and realistic models of the fading channel will provide us with the ability to design new systems and analyze their performance. Another important yet under-researched topic is the computer simulation of the real-world fading channels. We need accurate, manageable, repeatable and computationally efficient fading channel simulators for research and development of various wireless communication systems under popular fading channel models. First, it will help the researcher to verify the correctness and accuracy of the theoretical results obtained against the simulation results. In many scenarios, the researcher usually assumes certain popular fading channel models and based their results on such models. An accurate fading channel simulator that literally adheres to such models is a prerequisite for the simulation results to be comparable to analytical results. More importantly, the availability of such simulators will greatly aid the engineers in accelerating the rate of discovery and evaluation of many emerging technologies and schemes. System designers will be able to simulate system performance under practical fading models that resembles the physical world closely during the conceptual design stage. Once the concept is proved, during the system design stage, optimal system parameters could be obtained efficiently by using the simulator without the need to build and test actual systems in real fading channels, which tend to be expensive and time consuming.

www.manaraa.com

Stochastic models are used to describe the fading channel response characteristics. The models are considered to be time-variant because the scatter or reflector that causes the multipath transmission in fixed wireless application almost certainly will move during any given period of time and thus change the received multipath components, and cause its time-variant behavior. In mobile application, the movement of wireless transmitter and/or receiver will only make the channel more time-variant. Because the movements of the scatters and/or wireless transmitters and receivers are correlated in time, and thus the multipath received signals, wireless fading channels are usually temporally correlated. The resulting power spectrum density for wireless channels can take various forms. One widely adopted model is Jakes' fading spectrum [121, 122] for isotropic scattering environment where there are large number of scatters causing reflected multipath components arriving at all angles uniformly at the receiver.

Fading channels can be divided into frequency non-selective fading and frequency selective fading channels. Models and simulators for the two cases are treated differently. For frequency non-selective channels, the signal symbol duration is larger than the maximal delay spread of the multipath components and thus the fading channel effects can be modeled as a single tap. The baseband equivalent channel can then be modeled as a complex number with its amplitude and phase follow certain families of distribution. The specific distribution parameters are dependent on the fading environment and the chosen models.

One particular example is the Rayleigh fading channel model where the in-phase and the quadrature parts of the channel coefficients follow zero-mean Gaussian distribution. The resulting envelop follows the Rayleigh distribution and the phase follows a uniform distribution. Rayleigh fading model describes the physical fading condition where there are abundant reflectors but no direct line-of-sight (LOS) component. One approach to generate Rayleigh fading channel is the sum of sinusoids, which uses the central limit theorem to approximate the Gaussian distribution of the Rayleigh fading channel quadrature and in-phase components. In [126], a Rayleigh channel simulator using an inverse discrete Fourier transform (IDFT) was proposed. In [108], Young and Beaulieu designed an improved method for Rayleigh channel simulation for the Clarke's fading spectrum (i.e., the Jakes' model) using the IDFT and frequency domain

www.manaraa.com

filtering where white signal is multiplied by the desired power spectrum density in frequency domain and time samples are obtained by IDFT. In [109] a method based on auto-regressive model was proposed to generate Rician fading channels with both pre-specified temporal correlation and mult-channel spatial correlation.

A more general fading model that gained significant interest in recent years is Nakagami-m fading model, which can account for fading conditions more severe or less severe than the Rayleigh case, including the non-fading channel. A significant amount of research on wireless system design and performance analysis has adopted the Nakagami-m fading channel model [98–102, 104, 105]. In addition, several experimental and theoretical works have shown that the Nakagami-m distribution is the best-fit for the amplitude by data obtained from many urban multipath wireless channels [113, 114, 123]. We notice that it's a non-trivial task to generate in computer simulations the fading channel coefficients that follow the Nakagami-m channel model. The difficulties lie in the fact that (1) it's difficult to generate random variable (RV) that follows the Nakagami-m distribution which is non-Gaussian (thus not directly applicable to utilize the central limit theorem), (2) it's hard to generate the channel with a correct phase distribution, and (3) difficulties in providing correct auto-correlation properties.

Different approaches in the literature were taken to build a Nakagami-m channel simulator, with limited success. In [117, 131], techniques to generate spatially correlated Nakagami sequences are designed using the correlation matrix decomposition method and other techniques. The method proposed in [95] is useful for generating Nakagami-m distributed RV with integer and half-integer values of m. A method to generate Nakagami-m fading channels for $0.5 \leq m \leq 1$ is proposed in [110]. The amplitude of the channel coefficient produced by the simulator proposed in [111] follows the Nakagami-m distribution with arbitrary m, but its phase distribution and temporal correlation are inaccurate.

1.6 Problem Formulations and Main Results

In the preceding sections, we discussed some of the challenges in wireless communication design and analysis and the possible solutions. The topics discussed are essential and unique

www.manaraa.com

to the wireless communication systems where the multipath fading phenomenon is prominent. The goal of this thesis is to investigate the three major issues we have identified above and to provide new analytical approaches and possible solutions to tackle the problems for real-world situations.

The combination of spectrum-efficient M-QAM modulation, diversity-combining techniques such as MRC, and robust channel estimators will generate a practical receiver structure for wireless communication systems. It's an important yet often under-researched topic that how the different types of channel estimators and their parameters will affect the performance of the MRC diversity combiner under Rayleigh and Rician fading channels. The diversity branches available to MRC combiner can be either statistically independent of each other or correlated. In rich scattering environment, those branches tend to have smaller correlation while in scenarios where there is LOS or near LOS present, the available diversity branches show more correlation among each other. Thus this prompts a valid problem that merits further investigation. We formulate the first problem we wish to solve as:

- **Problem 1.** *Investigate the BER performance of the MRC diversity receiver with M-QAM under correlated Rayleigh and Rician fading channels with ICE, and characterize the performance loss due to ICE and the choice of their parameters.*

Our approach to this problem is to derive new DVs for the M-QAM MRC with ICE under Gaussian (Rayleigh and Rician, because of the quadratures of the baseband equivalent channel follow the Gaussian distribution) fading channels. By expressing the BER of the receiver in terms of the DVs and using MGF-based performance analysis approach for Gaussian quadratic forms, we derive exact and easy-to-compute analytical expressions for the BER of square and rectangular M-QAM with ICE for independent and identical distributed (i.i.d.), independent but not identical distributed (i.n.d.), as well as arbitrarily correlated Rayleigh and Rician fading channels. The major contributions in this work include: (1) Deriving BER of the M-QAM MRC receiver using the distribution of a new DVs, (2) Developing closed-form BER expressions, taking into account the effect of ICE and other system design parameters for i.i.d and i.n.d branches, as well as arbitrary correlated Rayleigh and Rician fading channels, and (3)

www.manaraa.com

Predicting whether an error floor will occur under given fading channel condition and channel estimator parameters.

These results have their theoretical significance in that a closed-form expression for the exact BER performance results for correlated diversity branches is presented that does not involve major approximation or calculation of numerically unstable special functions. More importantly, these results will have a significant impact on the design and analysis of practical receivers. The results in this study are particularly well-suited to quantify and predict the exact performance of the MRC combiner utilized at the receiver and will provide the system designers a valuable tool to investigate how the different system parameters will affect the BER. For example, one particular application of the study will aid the engineers in determining whether there will be an error floor with a certain type of channel estimator used and its parameters under any given channel conditions. This information is extremely helpful in that if the system designers would predict the existence of an error floor beforehand, a lot of time and resources can be saved by directing available system resources accordingly to avoid possible waste of signal power on the region where error floor occurs or to avoid the existence of the error floor all together by tuning the channel estimator parameters. Another possible application of the BER result is to guide the system engineers in optimally distributing limited system resources to provide the most reliable and efficient communication. One example is that with PSAM, there will be a tradeoff between the number of pilot symbols and the number of data-bearing symbols in a given block. The more are the pilot symbols used, the less are the channel estimation errors and BER, but at the cost of reduced throughput. The results obtained in this study will help choose an optimal frequency of pilot symbol insertion to maximize the system throughput while maintaining a certain BER.

Performance of GSC under perfect CSI conditions has been studied in several papers in the literature [34–36]. Intuitively, it makes more sense not to combine some of the weaker branches under ICE conditions. The reason is that the lower the SNR on a particular branch, the less accurate the channel estimation is, and consequently the less additional benefit can the combiner provide. This is an issue of diminishing return of investment in combiner complexity,

www.manaraa.com

since the complexity to combine the strong and weak branches are the same. It would be interesting to investigate the exact performance and complexity tradeoff for GSC receivers under practical ICE considerations.

- **Problem 2.** *Investigate the BER performance of the GSC diversity receiver with M-QAM under generalized fading channels with ICE; characterize the performance loss due to different channel estimators and the choice of their parameters; and investigate the tradeoff between performance and complexity in the proposed scheme.*

The main technique we used in solving this problem is based on the the idea to use the effective SNR of the combined branches to obtain the BER performance results. By taking this effective SNR based approach, we obtained the BER on Rayleigh, Rician as well as non-Gaussian type, such as Nakagami-m, fading channels.

The major contributions in this work include: (1) Derivation of signal-constellation-dependent effective SNRs with GSC and ICE, (2) Formulation of accurate BER expressions for square and rectangular M-QAM with GSC and ICE based on MGF of the derived SNR under generalized fading conditions with independent diversity branches, and (3) Provision of an accurate analytical result for GSC performance using different modulations, different channel estimators and different levels of GSC complexity (number of branches combined). The importance of this work lies in the fact that under the ICE condition, combining all the diversity branches may not be the most cost-benefit efficient solutions considering the tradeoffs. The results are instrumental to system designers who want to know exactly how much performance gain there will be by combining one extra diversity branch. As a matter of fact, as shown in Chapter 3, with a certain type of channel estimator configuration, combining all available diversity branches (MRC) won't have any significant performance gain (in terms of SNR gain for the same BER) than only combining some of the branches (GSC), in spite of the added complexity of the MRC combiners.

The broadcast nature of the wireless channels determines that the issue of multiuser communication has its unique importance to wireless communication. More specifically, the issue of multiuser scheduler design is one of the most important topics in this area that has the

www.manaraa.com

potential to drastically increase the total system throughput. In this thesis, we concentrate on the problem of designing multiuser schedulers that can exploit the inherent multiuser diversity gain.

We discussed in Section 1.4 that there are several multiuser scheduling schemes available in literature [64–66, 75, 78, 79]. All of them schedule a single user to monopoly all the available power for transmission, in a TDMA fashion. The criterion to choose such a user is based on its rank in terms of a chosen metric (instantaneous SNR, normalized SNR, or any other metrics based on instantaneous or statistical channel conditions). An alternative signal space division method is CDMA which can provide a practical benefit over TDMA scheme in that it's feasible to assign multiple users for simultaneous transmissions. For example, in CDMA networks, scheduling parallel independent transmissions are feasible due to the availability of multiple orthogonal (or quasi-orthogonal) spreading codes in a single time slot.

The design criterion of many existing multiuser scheduling algorithms is the multiuser diversity gain measured in terms of Shannon information theoretic capacity gain or the SNR gap. In practical wireless networks, the throughput for a given target packet error rate (PER) or BER may be a more feasible performance metric. For example, with AMC the transmission rate is discrete and upper-bounded with SNR; while for Shannon capacity, it's unbounded. Furthermore, it is desirable to have an efficient scheduling algorithm operating per time slot. In this research, we consider the scenario of simultaneous multiuser transmissions under a CDMA scheme, and propose a generalized selection multiuser diversity (GSMuD) scheme. In this scheme, in each time slot (e.g. a packet duration) among all the L users awaiting transmissions up to N_c (with $N_c \leq L$) users with the largest SNRs are selected.

We also propose a sub-optimal yet efficient equal power allocation algorithm, which imposes a minimum-throughput-rate constraint on each selected user so that the low-efficiency transmission is cut off and the power is re-allocated to users with stronger channels. The power allocation algorithm needs to be implemented only once for the period that the multiuser channel statistics remain unchanged. We assign equal amount of power to all users selected for transmission in this scheme, which apparently is not the optimal way of disputing

www.manaraa.com

power to provide maximal total throughput. It would be of interest to know the optimal way of allocating total system power to selected users based on their channel conditions.

Though the SNR-ranking based multiuser scheduling is an efficient and promising technique, its performance (e.g., error rate and throughput) with adaptive modulation has not been evaluated in the literature. A technical difficulty lies in the analysis of order statistics for the ranked users. Furthermore, with minimum-throughput-rate power allocation being included, the accurate analysis becomes even more difficult.

It would also be of interest to know how our proposed scheme works under practical considerations, namely ICE. The channel information provided to the GSMuD scheduler won't be perfect, and ICE and anticipated feedback delay are unavoidable. Furthermore, in order to fully evaluate the usefulness of the proposed scheme, several metrics related to multiuser scheduling algorithm need to be evaluated. Among the most important of them are metrics related to the fairness, such as the average channel access rate (AAR), the average access time (AAT), and the average waiting time (AWT). It is also important to know how we would improve the proposed GSMuD scheme to maintain better fairness by changing the way we select users.

We thus propose the third major problem we wish to tackle in this thesis:

- **Problem 3.** *Design a generalized selection multiuser diversity (GSMuD) scheme and related power allocation scheme (optimal and sub-optimal). Evaluate the impact of ICE on the scheduler's performance. Propose a modified GSMuD scheme to provide better access fairness for all users and analyze how different system parameters in the scheduler affects the user channel access metrics.*

The main novelties in our design of GSMuD lie in that we can accommodate more than one user per time slot to maximize the total system throughput under AMC and generalized fading channel models (Rayleigh, Rician, Nakagami-m, etc.), in systems where each user is assigned one orthogonal channel. The approaches we used in our design and analysis of the AMC thresholds, BER performance analysis and throughput calculation is based on obtaining the marginal distribution of the effective SNR of the users selected for transmission.

www.manaraa.com

The major contributions in this thesis on solving Problem 3 include (1) Design of the absolute-SNR (**a**-SNR)-based GSMuD scheduling algorithm and related sub-optimal equal power allocation scheme, (2) Derivation of individual-rate and sum-rate for users under utilization of AMC, (3) Construction and analysis of optimal power allocation scheme under GSMuD scheduler, (4) Analysis of GSMuD performance under ICE considerations, and (5) Derivation and analysis of channel access statistics under GSMuD scheme and propose a normalized-SNR (**n**-SNR)-based ranking that improves user access fairness.

The significance of this work lies in that we propose a new multiuser scheduler that aims to increase total system throughput under AMC scheme. The new scheduler can also accommodate multiple user's traffic in the same time slot, unlike previously proposed SMuD scheme that only allows a single user to monopolize the total system resources in a given time slot. We also provide detailed discussion and modifications required on the proposed scheme to work under practical considerations such as ICE and feedback delay. In the aspect of the accompanying power allocation scheme, we proposed and analyzed both the statistical optimal power allocation scheme and simple-to-implement equal power allocation scheme. To ensure that our algorithm will provide a fair channel access opportunity for the users, we derived several metrics that measures the extend of fairness for the proposed **a**-SNR and **n**-SNR-based ranking GSMuD and discussed the relationship with the scheduler parameters.

Now we turn our attention to the Nakagami-m channel simulator. We identified in Section 1.5 that Nakagami-m channel model is widely used [98–102, 104, 105]. An efficient algorithm to generate such channel coefficients is essential to accurately simulate such channel model for wireless communication and signal processing algorithm development.

We observed that the existing methods introduced in Section 1.5 are not adequate. Both methods in [95, 110] are only suitable for a certain range of m values where, in reality, m parameter in Nakagami-m fading channels could be anywhere in the range of $0.5 \leq m \leq \infty$. The method proposed in [111] could account for all m in its range. We observed that there are still several points that have not been addressed in the existing Nakagami-m channel generation algorithms: (1) The property of independent real and imaginary parts of the gen-

www.manaraa.com

erated Nakagami-m fading channel realizations are not guaranteed in those schemes, which may cause problems for the simulations verifying certain analytical results assuming they are independent. (As in Rayleigh and Rician cases, where the channel tap coefficients are considered circular symmetric RVs), (2) The temporal autocorrelation property in the generated Nakagami-m channel realization is not addressed explicitly and no methods are in place to ensure the generated sequence has the desired property, and (3) ambiguity regarding the correct phase distribution of the generated Nakagami-m channel coefficients.

Phase distribution in Nakagami-m fading channel is recently derived in [112]. In [95, 110], phase distribution is not explicitly addressed. In [111], the authors try to address the phase distribution issue but the approach taken therein will not produce channel coefficients with the correct phase distribution as prescribed in [112]. We observe that the phase characteristic is an important aspect of the channel simulator.

Based on the above observations, we propose the last problem we will solve in this thesis:

- **Problem 4.** *Design a Nakagami-m fading channel simulator that produces Nakagami-m distributed channel coefficients, with mutually independent quadrature parts, with arbitrary prescribed power spectrum, and with the correct phase distribution.*

To design such a simulator that satisfies the prescribed requirements, our intuition is to consider first of how to obtain the channel coefficients that follows the Nakagami-m distribution. In our design, we envisioned that by using inverse-CDF approaches, we can turn RVs that follows any arbitrary distribution into RVs that follow the Nakagami-m distribution. We generate the Rayleigh fading channel coefficients as the first step, in that the in-phase and quadrature part of them are Gaussian distributed and relatively easy to generate. We then mapped the in-phase and quadrature parts of the baseband-equivalent channel coefficients independently into the Nakagami-m distributed channel coefficients. We preserved the independence of the in-phase and quadrature part of the channel coefficients, which guarantees that the resulting phase distribution would follow the theoretical results given in [112]. To make sure the generated sequence fits any prescribed power spectrum density, we devised gradient search algorithms that find the mapping of the autocorrelation functions between the Rayleigh

www.manaraa.com

channel coefficients and the generated Nakagami-m channel coefficients. By generating the Rayleigh sequence with the calculated autocorrelation function, the simulator will output the Nakagami-m sequence with the desired autocorrelation function.

In summary, the major contributions of our work include the following. First we proposed a novel Nakagami-m fading channel simulator that generates sequences that satisfy (1) proper phase distribution, (2) arbitrary power spectrum properties, (3) any m parameter and signal power, and (4) independent in-phase and quadrature parts. Secondly, we independently verified by simulation, the correctness of the phase distribution proposed in [112], thus solved the phase ambiguity problem discussed in [111].

Throughout this chapter, we use the superscript $*$ to denote the complex conjugate. $E[x]$ and $\text{var}\{x\}$ are the expected value and the variance of x, respectively, and $\text{sign}(x) = \begin{cases} 1 & x \geq 0 \\ -1 & x < 0 \end{cases}$ is the sign of x. $N(\boldsymbol{\mu}, \boldsymbol{\Sigma})$ (and $\text{CN}(\boldsymbol{\mu}, \boldsymbol{\Sigma})$) denotes the Gaussian (and complex Gaussian) distribution with mean $\boldsymbol{\mu}$ and variance $\boldsymbol{\Sigma}$, respectively.

www.manaraa.com

CHAPTER 2. ACCURATE PERFORMANCE ANALYSIS OF QAM MRC RECEIVERS WITH IMPERFECT CHANNEL ESTIMATION

2.1 Introduction

High rate, high spectrum efficiency communication is the basis for future generation of wireless communication systems. Bandwidth has always been a very limited and expensive resource especially when the system is providing high date rate services to a large amount of users. QAM is a widely used modulation scheme that can provide high date rate and high spectrum efficiency with moderate implementation complexity compared to some lower-efficiency modulation schemes. The performance analysis of QAM communication system has always been a classic communication problem and has provided valuable information on communication system design and implementation.

M-QAM system structure and performance are extensively studied in several books [6, 9, 125]. The symbol error probability (SER) of M-QAM system is relatively easy to calculate and exact results can be found in common communication textbooks. The BER performance has also been investigated by several authors. The exact BER for 16-QAM and 64-QAM in an additive white Gaussian noise (AWGN) channel is derived in [4]. However, the BER results for M-QAM when M is large are usually given in approximation terms. Cho and Yoon [14] proposed an exact and general closed form BER expression of non-diversity M-QAM with arbitrary constellation size under AWGN channel and Gray code bit mapping assumption. It's valid to point out that the approach therein is based on a recursive relation between the BER and the signal amplitude levels and the complimentary error function, which is only immediately valid for the AWGN case but can be extended to the fading channels with CSI.

Diversity reception technique is one of the most widely used methods to mitigate the effect

www.manaraa.com

of multipath fading at the receiver by combining the multiple replicas of the transmitted signal. MRC provides maximal output SNR if different branches have the same noise statistics and thus maximal performance gain. MRC receiver requires CSI at the receiver and some of existing performance analysis [3, 14] are based on the assumption that perfect estimation of this information is available. In [3], the authors derived the bit error rate (BER) for QAM with MRC in a Rayleigh fading channel. The formula derived therein is obtained by averaging the BER of QAM in AWGN channel over a chi-square distribution with $2L$ degrees of freedom. The process of deriving the formula involves the integration of an infinite series expansion of the *erf* function which is not strictly a closed form expression and will introduce unwanted numerical instability for certain cases. Further more, the results obtained assumed perfect CSI case and are not readily expendable to more practical case, where the channel estimates cannot be perfect in fading channels, and thus the adverse effect of ICE on the BER performance must be taken into account.

Performance results for special cases of ICE are present such as BER results for MRC diversity square M-QAM with PSAM in i.i.d Rayleigh [18] and Rician [19] fading channels and an integral form BER expression for 16-QAM with MRC and ICE in a Rayleigh fading channel with i.i.d diversity branches [17]. We note that the analysis in the existing literatures are based on the assumption of independence among all diversity branches. In many practical scenarios, the receiver diversity branches have non-equal signal gains, and they may even be arbitrarily correlated.

An approximate expression for the BER of 16-QAM and 64-QAM with ICE and specifically with PSAM channel estimator over Rayleigh fading channels is proposed in [13]. In [10], an approximate BER for M-QAM with PSAM was obtained for a Rayleigh fading channel. In [11], the BER for the minimum mean-squared-error (MMSE)-based channel estimator for a non-diversity Rician fading channel was derived. In [12], the exact BERs for pulse amplitude modulation (PAM) and QAM signals in Rayleigh and Rician fading channel with ICE were obtained, respectively, by deriving the received data's probability density function (PDF) and expressing the BER in integrals of the obtained PDF. Though their results are applicable

www.manaraa.com

to channel estimators whose output channel estimates are complex Guassian distributed, the closed-form integrals are only obtained for 16 QAM with 1 or 2 diversity branches in the Rayleigh case and non-diversity case in Rician channels. In [15, 16] a SER formula involving a two-fold integral was developed for arbitrary two-dimensional signalling formats in a non-diversity Rician fading channel. In [17], the authors provided a BER expression (in the form of a two-fold integral of a parabolic cylinder function) for 16-QAM with MRC and ICE in a Rayleigh fading channel with i.i.d. diversity branches. The BER expressions derived in [13,17] are obtained by evaluating the effective SNRs in terms of estimation-error-rotated signal in-phase and quadrature components and the decision boundaries.

Recently, closed-form BER expressions for MRC diversity square M-QAM with PSAM in i.i.d. Rayleigh and Rician fading channels with arbitrary number of diversity branches were derived in [18] and [19], respectively. However their results are only valid for independent and identically distributed (i.i.d.) fading channels. In many practical scenarios, the receiver diversity branches have non-equal signal gains, and they may even be arbitrarily correlated. The approaches used in [18, 19] to find the BER expressions were to compare the receiver output with decision boundaries using a characteristic function method. The authors in [2] extended this approach to find BER expression of an arbitrary square/ rectangular QAM with MRC and channel estimation error, applicable to square/rectangular M-QAM constellation with MRC and ICE in i.n.d. Rayleigh fading channels. However, the exact closed-form result for i.n.d Rayleigh fading with MRC and ICE is not presented in the paper but rather only a general approach or how to obtain the closed-form results by comparing the receiver output with decision boundaries using an MGF-based method. It's valid to point out that the proposed approach in [2] is only applicable to Rayleigh fading and not readily applicable to Rician case.

In this chapter, we will present an accurate and closed-form performance result for diversity M-QAM with PSAM and MRC combiner valid for correlated fading channels (including arbitrary spatial and temporal fading correlation and noise correlation) that has not been obtained yet in the literature, despite its theoretical importance and practical relevance.

www.manaraa.com

2.2 System and Signal Model

2.2.1 Signal Model

We use (I, J)-QAM to denote the general rectangular QAM modulation with I and J signal levels in the horizontal and vertical directions, respectively, where $I, J \in \{2^n\}$, $n = \{1, 2, \ldots\}$. The total number of signal levels M is given by $M = I \times J$. We denote the data signals received in the ith symbol interval over all L diversity branches by

$$\mathbf{y}(i) = \mathbf{c}(i)d(i) + \mathbf{n}(i) \tag{2.1}$$

where $d(i) = \sqrt{E_a}(\alpha_h + j\alpha_v)$ is an M-QAM symbol, with $j = \sqrt{-1}$, $\alpha_h \in \{-I+1, \ldots, -1, 1, \ldots, I-1\}$, and $\alpha_v \in \{-J+1, \ldots, -1, 1, \ldots, J-1\}$. E_a is used to normalize the data symbol energy to unity, i.e., $E_d = E[|d(i)|^2] = 1$. For square M-QAM $E_a = \frac{3}{2(M-1)}$; and for rectangular (I, J)-QAM $E_a = \frac{3}{I^2+J^2-2}$ [14]. $\mathbf{c}(i) = [c_1(i), \ldots, c_L(i)]^\top$ is the channel-coefficient vector for the L branches. In Rician fading channels, $\mathbf{c}(i)$ can be written as $c(i) = \boldsymbol{\mu}_c(i) + \mathbf{c}_f(i)$, where $\boldsymbol{\mu}_c(i) = E[\mathbf{c}(i)] = [\mu_{c_1}(i), \ldots, \mu_{c_L}(i)]^\top$ and $\mathbf{c}_f(i) = [c_{f_1}(i), \ldots, c_{f_L}(i)]^\top$ are the line-of-sight (LOS) and diffuse components of $\mathbf{c}(i)$, respectively. At the lth branch, $\mu_{c_l}(i) = |\mu_{c_l}(i)|e^{j2\pi(f_{d_l}+f_{o_l})iT_s+\theta_l}$, where f_{d_l} is the Doppler shift of the LOS component, f_{o_l} is the frequency offset, θ_l is a random residual phase, and T_s is the symbol duration. The Rician factor is defined as $K_l = |\mu_{c_l}(i)|^2/\sigma_{c_l}^2$, where $\sigma_{c_l}^2 = E[|c_{f_l}(i)|^2]$ is the variance of the diffuse fading component of the lth branch.

The normalized temporal channel correlation coefficient at the lth branch is defined as $\tilde{R}_{c_l}(n) = E[c_{f_l}(i)c_{f_l}^*(i-n)]/\sigma_{c_l}^2$. For Clarke's fading spectrum [121,122], $\tilde{R}_{c_l}(n) = J_0(2\pi n B_{f_l} T_s)$ $e^{j2\pi f_{o_l} n T_s}$; and for the Gaussian fading spectrum, $\tilde{R}_{c_l}(n) = \exp(-(\pi n B_{f_l} T_s)^2)e^{j2\pi f_{o_l} n T_s}$, where $J_0(x)$ is the zeroth order Bessel function and B_{f_l} is the Doppler fading bandwidth of the diffuse component, at the lth branch.

The additive background noise vector, $\mathbf{n}(i) = [n_1(i), \ldots, n_L(i)]^\top$, is a zero-mean circularly symmetric complex Gaussian process, with average power $E[|n_l(i)|^2] = N_0$, $l = 1, \ldots, L$. In (2.1), $\mathbf{n}(i)$ may be temporally and spatially correlated. The average bit SNR of the lth branch is given by $\bar{\gamma}_{b,l} = E[|c_l(i)|^2]/N_0 = (|\mu_{c_l}(i)|^2 + \sigma_{c_l}^2)/N_0$.

www.manaraa.com

2.2.2 PSAM-Based Channel Estimators

PSAM-based channel estimation is widely adopted in actual wireless systems, due to its applicability to various channels and/or modulation schemes, and its robustness and low complexity. Instead of using a long sequence of training symbols at the beginning of a block of transmission, a pilot symbol is inserted into the data stream every P symbol intervals in the PSAM we consider. To estimate the channel coefficient vector $\mathbf{c}(i)$ for the desired symbol $d(i)$, F pilot symbols are employed which may be written as an $F \times 1$ vector $\mathbf{d}_{\rm PS} = [d(i - PF_1 + i_{\rm off}), \ldots, d(i - P + i_{\rm off}), d(i + i_{\rm off}), \ldots, d(i + P(F_2 - 1) + i_{\rm off})]^\top$, where F_1 and F_2 (with $F_1 + F_2 = F$) are the numbers of pilot symbols on the left and right sides of $d(i)$, respectively, and $i_{\rm off}$ ($i_{\rm off} = 1, 2, \ldots, P-1$) is the offset of the desired symbol $d(i)$ to the closest pilot symbol on its right side. The received signals at the pilot symbols' positions for estimating channel $\mathbf{c}(i)$ may be written as an $FL \times 1$ vector $\mathbf{y}_{\rm PS}$, expressed in a compact form as

$$\mathbf{y}_{\rm PS} = (\mathrm{diag}(\mathbf{d}_{\rm PS}) \otimes \mathbf{I}_L)\mathbf{c}_{\rm PS} + \mathbf{n}_{\rm PS}, \tag{2.2}$$

where $\otimes$ denotes the Kronecker product [22], $\mathbf{c}_{\rm PS} = [\mathbf{c}^\top(i - PF_1 + i_{\rm off}), \ldots, \mathbf{c}^\top(i + i_{\rm off}), \ldots, \mathbf{c}^\top(i + P(F_2 - 1) + i_{\rm off})]^\top$ and $\mathbf{n}_{\rm PS} = [\mathbf{n}^\top(i - PF_1 + i_{\rm off}), \ldots, \mathbf{n}^\top(i + i_{\rm off}), \ldots, \mathbf{n}^\top(i + P(F_2 - 1) + i_{\rm off})]^\top$ are the channel gain and noise components of all the L branches at the pilot symbols' positions, respectively.

Without loss of generality, we assume $\mathbf{d}_{\rm PS} = \sqrt{P_{\rm PS}}\mathbf{1}_{L\times 1}$, where $P_{\rm PS}$ is the transmitted power of the pilot symbols, and may be different from P_d, the transmitted power of the data symbols. Thus, equation (2.2) simplifies to $\mathbf{y}_{\rm PS} = \sqrt{P_{\rm PS}}\mathbf{c}_{\rm PS} + \mathbf{n}_{\rm PS}$.

The channel estimate for $\mathbf{c}(i)$, denoted as $\hat{\mathbf{c}}(i)$, is given by $\hat{\mathbf{c}}(i) = \mathbf{W}\mathbf{y}_{\rm PS}$, where $\mathbf{W} = [\mathbf{w}_1^\top, \ldots, \mathbf{w}_L^\top]^\top$ is an $L \times FL$ channel estimator filter matrix. $\hat{c}_l(i) = \mathbf{w}_l\mathbf{y}_{\rm PS}$ is true, where $\mathbf{w}_l$ is the filter (lth row of $\mathbf{W}$) to estimate the channel gain $c_l(i)$.

Although the analysis of this chapter is applicable to any linear channel estimator $\mathbf{W}$, we outline two types of channel estimators below which have attracted particular research interest.

Sinc-CE: For the sinc-interpolator-based CE with rectangular window, we have $\mathbf{W}_{\rm sinc} = [h_{\rm sinc}(-PF_1 + i_{\rm off}), \ldots, h_{\rm sinc}(i_{\rm off}), \ldots, h_{\rm sinc}(P(F_2 - 1) + i_{\rm off})] \otimes \mathbf{I}_L$, where $h_{\rm sinc}(x) = \sin(\pi x)/(\pi x)$.

www.manaraa.com

A Hamming window may also be employed. Our numerical results in Section 2.5.2 show that the relative performance of rectangular and Hamming windows depends on the operating channel and system parameters.

MMSE-CE: We derive the linear MMSE channel estimator (MMSE-CE) for the PSAM in generalized Rician fading channels below. A detailed exposition here is necessary to elaborate the relation between the channel estimator and the BER performance of M-QAM. By using the Wiener filter [23], the MMSE-CE is given by $\mathbf{W}_{\text{mmse}} = \mathbf{R}_{c,y_{\text{PS}}}\mathbf{R}_{y_{\text{PS}}}^{-1}$, where $\mathbf{R}_{c,y_{\text{PS}}} = E[\mathbf{c}(i)\mathbf{y}_{\text{PS}}^H]$ is the cross-correlation matrix between $\mathbf{c}(i)$ and $\mathbf{y}_{\text{PS}}$ (taking into account the LOS component), and $\mathbf{R}_{y_{\text{PS}}} = E[\mathbf{y}_{\text{PS}}\mathbf{y}_{\text{PS}}^H]$ the auto-correlation matrix of $\mathbf{y}_{\text{PS}}$. After some manipulations, we can show that

$$\mathbf{R}_{c,y_{\text{PS}}} = \sqrt{P_{\text{PS}}}[\mathbf{R}_c(PF_1 - i_{\text{off}}), \ldots, \mathbf{R}_c(-i_{\text{off}}) \ldots, \mathbf{R}_c(-P(F_2 - 1) - i_{\text{off}})] \tag{2.3}$$

and $\mathbf{R}_{y_{\text{PS}}}$ is given by (2.4):

$$\mathbf{R}_{y_{\text{PS}}} = \begin{bmatrix} P_{\text{PS}}\mathbf{R}_c(0) + \mathbf{\Sigma}_n(0) & P_{\text{PS}}\mathbf{R}_c^H(P) + \mathbf{\Sigma}_n^H(P) & \ldots & \\ P_{\text{PS}}\mathbf{R}_c(P) + \mathbf{\Sigma}_n(P) & P_{\text{PS}}\mathbf{R}_c(0) + \mathbf{\Sigma}_n(0) & \ldots & \\ \vdots & & \ddots & \\ P_{\text{PS}}\mathbf{R}_c(P(F-1)) + \mathbf{\Sigma}_n(P(F-1)) & & \ldots & P_{\text{PS}}\mathbf{R}_c(0) + \mathbf{\Sigma}_n(0) \end{bmatrix} \tag{2.4}$$

where $\mathbf{R}_c(m) = E[\mathbf{c}(i)\mathbf{c}^H(i-m)] = \mathbf{\Sigma}_c(m) + \boldsymbol{\mu}_c(i)\boldsymbol{\mu}_c^H(i-m)$ is the spatial-temporal correlation matrix of $\{\mathbf{c}(i)\}_{i=0,1,\ldots}$ (including the LOS components). $\mathbf{\Sigma}_c(m) = E[\mathbf{c}_f(i)\mathbf{c}_f^H(i-m)]$ is the channel spatial-temporal covariance matrix. Assuming the noise $\mathbf{n}(i)$ is a zero-mean process, $\mathbf{\Sigma}_n(m) = E[\mathbf{n}(i)\mathbf{n}^H(i-m)]$ is defined as the noise spatial-temporal covariance matrix. For i.i.d. white noise, we obtain that $\mathbf{\Sigma}_n(0) = N_0\mathbf{I}_L$, and $\mathbf{\Sigma}_n(m) = \mathbf{0}_{L\times L}$, when $m \neq 0$. In summary, our channel model includes arbitrary joint spatial-temporal fading correlation, noise correlation, and Rician fading. Thus, it is much more general than the i.i.d. Rayleigh and Rician fading models studied in [17–19].

www.manaraa.com

2.2.3 Channel Estimation Error Model

The estimate for channel vector $\mathbf{c}(i)$ is denoted by $\hat{\mathbf{c}}(i) = [\hat{c}_1(i), \ldots, \hat{c}_L(i)]^\top$. For i.i.d. signal branches, without loss of generality, we assume $E[|\hat{c}_l(i)|^2] = \sigma_{\hat{c}}^2$, for all l. Let the normalized correlation coefficient between $\hat{c}_l(i)$ and $c_l(i)$ be defined as $\rho = E[\hat{c}_l^*(i)c_l(i)]/[\sigma_c\sigma_{\hat{c}}]$. For i.n.d signal branches, define the normalized correlation coefficient ρ_l for each branch as $\rho_l = E[\hat{c}_l^*(i)c_l(i)]/[\sigma_{c_l}\sigma_{\hat{c}_l}]$. In general, ρ or ρ_l is a function of the average SNR (ASNR), the fading channel parameter (e.g. fading power spectra, the Doppler fading bandwidth) and the PSAM parameters (e.g. P, F, and i_{off}). A popular channel estimation error model for PSAM and MMSE-CE is given by [10, 11]

$$c_l(i) = \hat{c}_l(i) + z_l(i), \tag{2.5}$$

where $\{z_l(i)\}_{l=1}^L$ are the i.i.d. channel estimation errors for i.i.d branches independent of $\{\hat{c}_l(i)\}_{l=1}^L$, and follow a complex Gaussian distribution with zero mean and variance $\sigma_z^2 = (1-|\rho|^2)\sigma_c^2$. We obtain this result by using the orthogonality principle between $\hat{c}_l(i)$ and z_l, and we also get the relationship that $\sigma_{\hat{c}}^2 = |\rho|^2\sigma_c^2$. For the ideal MMSE-CE, ρ is real-valued. The model (2.5) is also applicable for some non-MMSE channel estimators (e.g. sinc-interpolators), yielding an accurate approximation of the BER. The explicit relation between ρ, channel model parameters and different channel estimator parameters will be shown in Section 2.4.2.2.

2.2.4 Symbol Detection

By using the estimated channel vector $\hat{\mathbf{c}}(i)$ to detect $d(i)$, the complex decision variable for MRC is given by $\tilde{D} = \hat{\mathbf{c}}^{\text{H}}(i)\mathbf{y}(i)/[\hat{\mathbf{c}}^{\text{H}}(i)\hat{\mathbf{c}}(i)] = \sum_{l=1}^L \hat{c}_l^*(i)y_l(i)/\sum_{l=1}^L |\hat{c}_l(i)|^2$. The transmitted symbol $d(i)$ can be recovered by comparing $\tilde{D}$ with the horizontal and vertical QAM decision boundaries [13, 14, 17].

2.3 BER Formulation for M-QAM

We derive the BER for horizontal and vertical PAM first, and then extend the result to both square and rectangular M-QAM.

www.manaraa.com

2.3.1 I-PAM

Consider horizontal I-PAM with $d(i) = \alpha_h\sqrt{E_a}$, where $E_a = \frac{3}{I^2-1}$. For $I = 4$, the two bits b_1b_2 are Gray-coded and mapped to four possible transmitted symbols. Let $\tilde{D}_R = \mathrm{Re}(\tilde{D})$ be the real part of $\tilde{D}$. The error probabilities for b_1 and b_2 are, respectively, given by

$$P_{4,H}(1) = \frac{1}{2}[P\{\tilde{D}_R < 0|\alpha_h = 3\} + P\{\tilde{D}_R < 0|\alpha_h = 1\}],$$

$$\begin{aligned} P_{4,H}(2) = \frac{1}{2}[&P\{\tilde{D}_R < 2a|\alpha_h = 3\} - P\{\tilde{D}_R < -2a|\alpha_h = 3\} \\ &+P\{\tilde{D}_R < -2a|\alpha_h = 1\} + P\{\tilde{D}_R > 2a|\alpha_h = 1\}], \end{aligned}$$

where a is given by $a = \sqrt{E_a}$, and $P\{A|B\}$ denotes the conditional probability of event A given event B.

For vertical 4-PAM with $d(i) = j\alpha_v\sqrt{E_a}$, let $\tilde{D}_I = \mathrm{Im}(\tilde{D})$ be the imaginary part of $\tilde{D}$. The BERs for b_1, b_2 can be obtained as $P_{4,V}(1) = \frac{1}{2}[P\{\tilde{D}_I < 0|\alpha_v = 3\} + P\{\tilde{D}_I < 0|\alpha_v = 1\}]$, and $P_{4,V}(2) = \frac{1}{2}[P\{\tilde{D}_I < 2a|\alpha_v = 3\} - P\{\tilde{D}_I < -2a|\alpha_v = 3\} + P\{\tilde{D}_I < -2a|\alpha_v = 1\} + P\{\tilde{D}_I > 2a|\alpha_v = 1\}]$. For horizontal and vertical PAM, respectively, let us define the conditional BERs as

$$\tilde{P}_H(\beta_n|\alpha_n) = P\{\tilde{D}_R < a\beta_n|d(i) = a\alpha_n\} \tag{2.6}$$

$$\tilde{P}_V(\beta_n|\alpha_n) = P\{\tilde{D}_I < a\beta_n|d(i) = ja\alpha_n\}. \tag{2.7}$$

where β_n is an integer specifying the decision boundary. Thus, we obtain $P_{4,H}(1) = \frac{1}{2}[\tilde{P}_H(0|3) + \tilde{P}_H(0|1)]$ and $P_{4,H}(2) = \frac{1}{2}[\tilde{P}_H(2|3) - \tilde{P}_H(-2|3) + \tilde{P}_H(-2|1) + 1 - \tilde{P}_H(2|1)]$. Here we use the $P_{4,H}(1)$ to denote the probability that the MSB (b_1 in Fig. 2.1) is decoded wrong and the term $\tilde{P}_H(\beta|\alpha)$ denotes the probability that the received signal falls below the decision boundary β when the transmitted constellation point is α. For example, the probability $P_{4,H}(1)$ can be obtained by averaging the probability of the MSB being wrongly decoded when $\alpha = -3a, -a, a$, and $3a$ is transmitted. Due to the symmetrical nature of the constellation points and decision boundaries, we only need to calculate for the average provability when two points a and $3a$ are

www.manaraa.com

Table 2.1 Coefficients for BER calculation for 4-PAM

n	1	2	3	4	5	6
β_n	2	-2	-2	2	0	0
α_n	3	3	1	1	3	1
w_n	1	-1	1	-1	1	1

transmitted, which is $\tilde{P}_H(\beta|\alpha)$ for $\alpha = a$, and $\alpha = 3a$ respectively. $\beta = 0$ for both cases and we drop a in α and β without causing any confusions.

Here, for deriving $P_{4,H}(2)$ we used the equality that $P\{\tilde{D}_R > 2a|\alpha_h = 1\} = 1 - P\{\tilde{D}_R < 2a|\alpha_h = 1\} = 1 - \tilde{P}_H(2|1)$. We can express the average BERs for horizontal and vertical 4-PAM, respectively, as

$$\begin{aligned} \bar{P}_{4,H} &= \frac{1}{2}[P_{4,H}(1) + P_{4,H}(2)] \\ &= \frac{1}{4}[C_4 + \sum_{n=1}^{N_4} w_n \tilde{P}_H(\beta_n|\alpha_n)] \qquad (2.8) \\ \bar{P}_{4,V} &= \frac{1}{4}[C_4 + \sum_{n=1}^{N_4} w_n \tilde{P}_V(\beta_n|\alpha_n)] \qquad (2.9) \end{aligned}$$

where $C_4 = 1$, $N_4 = 6$, and the coefficients w_n, β_n, and α_n are given in Table 2.1.

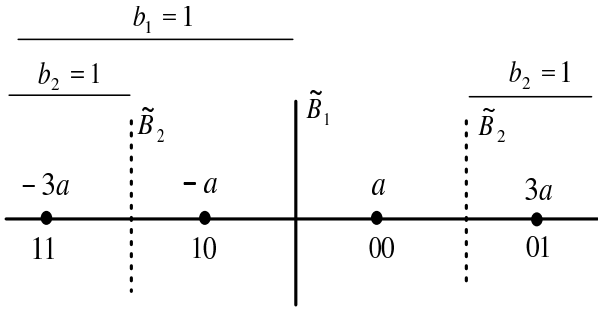

Figure 2.1 Decision boundaries and bit-symbol mapping (b_1, b_2) for 4-PAM. $\tilde{B}_1$ and $\tilde{B}_2$ denote the bit decision boundaries for b_1 and b_2, respectively.

For horizontal 8-PAM, the bit-symbol mapping is shown by Fig. 2.2. Using the definition

www.manaraa.com

in (2.6), we can express the BERs for the bits b_1, b_2, and b_3, respectively, as

$$P_{8,H}(1) = \frac{1}{4}[\tilde{P}_H(0|1) + \tilde{P}_H(0|3) + \tilde{P}_H(0|5) + \tilde{P}_H(0|7)], \tag{2.10}$$

$$\begin{aligned} P_{8,H}(2) = \frac{1}{4}[&2 + \tilde{P}_H(4|5) - \tilde{P}_H(-4|5) + \tilde{P}_H(4|7) - \tilde{P}_H(-4|7) \\ &+\tilde{P}_H(-4|3) + \tilde{P}_H(-4|1) - \tilde{P}_H(4|3) - \tilde{P}_H(4|1)], \end{aligned} \tag{2.11}$$

$$\begin{aligned} P_{8,H}(3) = \frac{1}{4}\Big[&2 + \tilde{P}_H(6|7) - \tilde{P}_H(2|7) + \tilde{P}_H(-2|7) - \tilde{P}_H(-6|7) - \tilde{P}_H(6|5) + \tilde{P}_H(2|5) \\ &-\tilde{P}_H(-2|5) + \tilde{P}_H(-6|5) - \tilde{P}_H(6|3) + \tilde{P}_H(2|3) - \tilde{P}_H(-2|3) + \tilde{P}_H(-6|3) \\ &-\tilde{P}_H(2|1) + \tilde{P}_H(6|1) + \tilde{P}_H(-2|1) - \tilde{P}_H(-6|1)\Big]. \end{aligned}$$

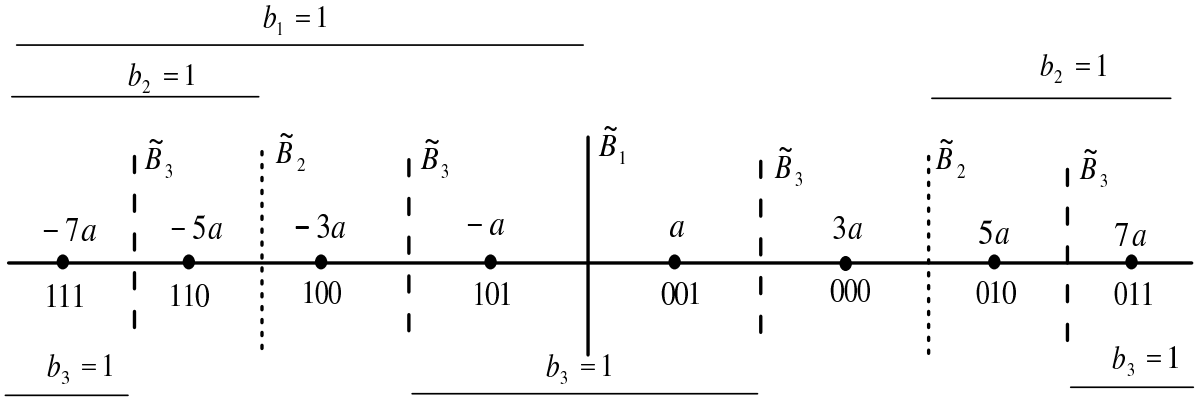

Figure 2.2 Decision boundaries and bit-symbol mapping (b_1, b_2, b_3) for 8-PAM. $\tilde{B}_1$, $\tilde{B}_2$, and $\tilde{B}_3$ denote the bit decision boundaries for b_1, b_2, and b_3, respectively.

The average BER for horizontal 8-PAM can be obtained as

$$\bar{P}_{8,H} = \frac{1}{3}[P_{8,H}(1) + P_{8,H}(2) + P_{8,H}(3)] = \frac{1}{12}[C_8 + \sum_{n=1}^{N_8} w_n \tilde{P}_H(\beta_n|\alpha_n)] \tag{2.12}$$

where $C_8 = 4$ and $N_8 = 28$, and the w_n, β_n, and α_n are given in Table 2.2, respectively. Similarly, using the symmetry, it follows that the average BER for vertical 8-PAM is $\bar{P}_{8,V} = \frac{1}{12}[C_8 + \sum_{n=1}^{N_8} w_n \tilde{P}_V(\beta_n|\alpha_n)]$.

Similar results for 16-PAM are obtained and given in the Appendix 2.A.

We underscore that when both $\mathbf{c}(i)$ and $\hat{\mathbf{c}}(i)$ are circularly symmetric complex Gaussian processes, as they usually are, we have that $\bar{P}_{I,H} = \bar{P}_{I,V}$, for $I = 2^n, n \in \{1, 2, 3, \ldots\}$. However,

www.manaraa.com

Table 2.2 Coefficients for BER calculation for 8-PAM

n	β_n	α_n	ω_n	n	β_n	α_n	ω_n
1	0	1	1	15	-2	7	-1
2	0	3	1	16	-6	7	-1
3	0	5	1	17	6	5	-1
4	0	7	1	18	2	5	1
5	4	5	1	19	-2	5	-1
6	-4	5	-1	20	-6	5	1
7	4	7	1	21	6	3	-1
8	-4	7	-1	22	2	3	1
9	-4	3	1	23	-2	3	-1
10	-4	1	1	24	-6	3	1
11	4	3	-1	25	2	1	-1
12	4	1	-1	26	6	1	1
13	6	7	1	27	-2	1	1
14	2	7	-1	28	-6	1	-1

when either $\mathbf{c}(i)$ or $\hat{\mathbf{c}}(i)$ are not circularly symmetric (e.g. for an improper process [24]), the detection error probabilities for the real and imaginary parts of $d(i)$ may not be equal, i.e., $\bar{P}_{I,H} \neq \bar{P}_{I,V}$. Therefore, our framework is valid for both proper and improper fading processes.

2.3.2 M-QAM

For rectangular (I,J)-QAM (with $M = I \times J$), let us define the conditional BERs conditioned on the transmitted symbol $d(i) = (\alpha_h + j\alpha_v)\sqrt{E_a}$, for the horizontal and vertical components of QAM as

$$\tilde{P}_H(\beta_n|\alpha_h, \alpha_v) = P\{\tilde{D}_R < \beta_n \cdot \sqrt{E_a}|d(i) = (\alpha_h + j\alpha_v)\sqrt{E_a}\}, \tag{2.13}$$

$$\tilde{P}_V(\beta_n|\alpha_h, \alpha_v) = P\{\tilde{D}_I < \beta_n \cdot \sqrt{E_a}|d(i) = (\alpha_h + j\alpha_v)\sqrt{E_a}\}. \tag{2.14}$$

Note that for Gray-coded (I,J)-QAM, the decision boundaries for horizontal signals (real part of $d(i)$) are independent of the vertical signal levels (imaginary part of $d(i)$), and vice versa, see e.g. [13, 14]. Thus, we can directly extend the BER result for PAM obtained in

www.manaraa.com

Subsection 2.3.1 to the case of M-QAM, and obtain

$$\bar{P}_{I,H} = \frac{2}{I \log_2 I}[C_I + \frac{1}{J}\sum_{m=1}^{J}\sum_{n=1}^{N_I} w_n \tilde{P}_H(\beta_n|\alpha_n, J-2m+1)], \tag{2.15}$$

$$\bar{P}_{J,V} = \frac{2}{J \log_2 J}[C_J + \frac{1}{I}\sum_{m=1}^{I}\sum_{n=1}^{N_J} w_n \tilde{P}_V(\beta_n|I-2m+1, \alpha_n)], \tag{2.16}$$

where $C_4 = 1$, $C_8 = 4$ and $C_{16} = 12$, $N_4 = 6, N_8 = 28$ and $N_{16} = 120$, respectively. When I (or J) $= 4, 8$ and 16 respectively, the values of $\{w_n,\ \beta_n,\ \alpha_n\}$ have to be selected from Table 2.1, 2.2 and 2.3 respectively. The average BER is given by

$$\bar{P}_M = \frac{1}{\log_2(I \cdot J)}[(\log_2 I)\bar{P}_{I,H} + (\log_2 J)\bar{P}_{J,V}]. \tag{2.17}$$

We emphasize that for non-Gray-coded bit-mappings, our results are applicable with slight modifications. In detail, equation (2.15) has to be rewritten as

$$\bar{P}_{I,H} = \frac{2}{I \log_2 I}\frac{1}{J}\sum_{m=1}^{J}\left[C_I(m) + \sum_{n=1}^{N_I} w_n(m)\tilde{P}_H(\beta_n(m)|\alpha_n(m), J-2m+1)\right] \tag{2.18}$$

where $C_I(m), w_n(m), \beta_n(m)$, and $\alpha_n(m)$ are now dependent on the signal level m ($m = 1, \ldots J$) in the vertical direction, and we just need to tabulate them for each m, following the same procedure as for generating Table 2.1, 2.2 and 2.3. Similar steps can be taken to re-evaluate $\bar{P}_{J,V}$. Thus, our new result is applicable to arbitrary symbol-bit mappings.

When both $\mathbf{c}(i)$ and $\hat{\mathbf{c}}(i)$ are circularly symmetric Gaussian processes, we obtain that $\tilde{P}_H(\beta_n|\alpha_n, \alpha_m) = \tilde{P}_V(\beta_n|\alpha_m, \alpha_n)$. For Gray-coded square M-QAM, (2.17) simplifies to

$$\bar{P}_M = \frac{4}{\sqrt{M}\log_2 M}\left[C_{\sqrt{M}} + \frac{1}{\sqrt{M}}\sum_{m=1}^{\sqrt{M}}\sum_{n=1}^{N_{\sqrt{M}}} w_n \tilde{P}_H(\beta_n|\alpha_n, \sqrt{M}-2m+1)\right]. \tag{2.19}$$

When $M = 16, 64$ and 256, the values of $\{w_n,\ \beta_n,\ \alpha_n\}$ again have to be selected from Table 2.1, 2.2 and 2.3, respectively. Next, we re-formulate the conditional BERs $\tilde{P}_H(\beta_n|\alpha_h, \alpha_v)$ and $\tilde{P}_V(\beta_n|\alpha_h, \alpha_v)$ for QAM in terms of the distribution of some new DVs. $\tilde{P}_H(\beta_n|\alpha_h)$ and $\tilde{P}_V(\beta_n|\alpha_v)$ for PAM can be obtained as special cases.

We note that in [14] the BER of M-QAM is obtained by extending the result of I-PAM to QAM. The result in [14] is valid for the case of perfect CSI and a non-fading channel, and is based on a recursive relation (valid for Gray-coded bit mapping) between the BER and the

www.manaraa.com

signal amplitude levels. For the case of ICE the SNR penalty due to ICE is a function of the signal amplitude, and thus such a recursive relation [14] is no longer applicable, and the BER analysis method in [14] cannot be straightforwardly extended to the ICE case. In comparison, we used a different framework by evaluating the distribution of some new decision variables, and our result includes the effects of both generalized fading and ICE.

2.4 Evaluating the BERs

We now evaluate the exact BER results by exploiting the property of the DV we derive. We use the MGF-based approach, and find the easy-to-compute BER expressions in the form of an infinite integral of the obtained MGF for both i.i.d, i.n.d and arbitrary correlated Rayleigh and Rician fading channels for MRC diversity combiner. The results are easily computed numerically and could be further derived into a closed-form using methods similar to what is given in [29].

2.4.1 Reformulation of the BERs

By definition, $\tilde{P}_H(\beta_n|\alpha_h,\alpha_v) = P\{\tilde{D}_R < \beta_n \cdot \sqrt{E_a}|d(i) = (\alpha_h + j\alpha_v)\sqrt{E_a}\}$. Using the equalities $\tilde{D}_R = \mathrm{Re}(\sum_{l=1}^{L} \hat{c}_l^*(i)y_l(i))/\sum_{l=1}^{L}|\hat{c}_l(i)|^2$ and $y_l(i) = c_l(i)\sqrt{E_a}(\alpha_h + j\alpha_v) + n_l(i)$, we obtain $\tilde{P}_H(\beta_n|\alpha_h,\alpha_v) = P\{D_H(\beta_n|d(i)) < 0\}$, where $D_H(\beta_n|d(i))$ is a new DV defined as

$$D_H(\beta_n|d(i)) = \mathrm{Re}\left(\sum_{l=1}^{L}\hat{c}_l^*(i)y_l(i)\right) - \sqrt{E_a}\beta_n\sum_{l=1}^{L}|\hat{c}_l(i)|^2. \tag{2.20}$$

Similarly, we define the conditional BER for the vertical signal components as $\tilde{P}_V(\beta_n|\alpha_h,\alpha_v) = P\{D_V(\beta_n|d(i)) < 0\}$, where

$$D_V(\beta_n|d(i)) = \mathrm{Im}\left(\sum_{l=1}^{L}\hat{c}_l^*(i)y_l(i)\right) - \sqrt{E_a}\beta_n\sum_{l=1}^{L}|\hat{c}_l(i)|^2.$$

Below, we drop the symbol index i of $d(i)$ when no confusion arises. To evaluate the cumulative distribution functions (CDFs) $P\{D_H(\beta_n|d) < 0\}$ and $P\{D_V(\beta_n|d) < 0\}$, we derive the MGFs of the new DVs $D_H(\beta_n|d)$ and $D_V(\beta_n|d)$, and then use the inverse Laplace transform to obtain these CDFs.

www.manaraa.com

2.4.2 Evaluating the Distributions of the New DVs

We first obtain the CDFs of the new DVs for generalized correlated Rician fading channels, and then discuss special-case results for Rayleigh fading and independent diversity branches.

2.4.2.1 Rician Fading Channels

We study the general case of arbitrary spatial and temporal correlations between diversity branches and between different symbol intervals.

To obtain the MGFs of $D_H(\beta_n|d)$ and $D_V(\beta_n|d)$, we express them in Gaussian quadratic forms as

$$\begin{aligned} D_H(\beta_n|d) &= \mathbf{v}^{\mathrm{H}}(\mathbf{d})\mathbf{Q_H}(\beta_\mathbf{n})\mathbf{v}(\mathbf{d}) \\ D_V(\beta_n|d) &= \mathbf{v}^{\mathrm{H}}(\mathbf{d})\mathbf{Q_V}(\beta_\mathbf{n})\mathbf{v}(\mathbf{d}) \end{aligned}$$

where

$$\begin{aligned} \mathbf{v}(\mathbf{d}) &= \begin{bmatrix} \hat{\mathbf{c}}(i) \\ \mathbf{c}(i)d + \mathbf{n}(i) \end{bmatrix}, \\ \mathbf{Q}_H(\beta_n) &= \begin{bmatrix} -\beta_n \cdot a\mathbf{I}_L & 0.5\mathbf{I}_L \\ 0.5\mathbf{I}_L & \mathbf{0}_{L\times L} \end{bmatrix}, \\ \mathbf{Q}_V(\beta_n) &= \begin{bmatrix} -\beta_n \cdot a\mathbf{I}_L & -0.5j\mathbf{I}_L \\ 0.5j\mathbf{I}_L & \mathbf{0}_{L\times L} \end{bmatrix}. \end{aligned}$$

Using a property of Gaussian quadratic forms [25, 26], we obtain the MGF of $D_H(\beta_n|d)$ in Rician channels as

$$\Phi_{D_H(\beta_n|d)}(s) = \frac{\exp(\bar{\mathbf{v}}^{\mathrm{H}}(d)[\mathbf{Q}_H^{-1}(\beta_n)s^{-1} - \mathbf{\Sigma}_v(d)]^{-1}\bar{\mathbf{v}}(d))}{\det(\mathbf{I}_{2L} - s\mathbf{\Sigma}_v(d)\mathbf{Q}_H(\beta_n))}, \tag{2.21}$$

where $\bar{\mathbf{v}}(d)$ and $\mathbf{\Sigma}_v(d)$ are the mean vector and the covariance matrix of $\mathbf{v}(\mathbf{d})$, respectively. The procedure to find $\bar{\mathbf{v}}(d)$ and $\mathbf{\Sigma}_v(d)$ for generalized Rician fading and any linear channel estimators is outlined below. Let $\hat{\mathbf{c}}(i) = \hat{\boldsymbol{\mu}}_c(i) + \hat{\mathbf{c}}_f(i)$, where $\hat{\boldsymbol{\mu}}_c(i)$ and $\hat{\mathbf{c}}_f(i)$ are the LOS and diffusive component vectors of $\hat{\mathbf{c}}(i)$, respectively.

www.manaraa.com

The mean and the auto-covariance matrix of $\mathbf{v}(\mathbf{d})$ are, respectively, given by

$$\bar{\mathbf{v}}(d) = [\hat{\boldsymbol{\mu}}_c^{\top}(i), \boldsymbol{\mu}_c^{\top}(i)d]^{\top} \tag{2.22}$$

$$\boldsymbol{\Sigma}_v(d) = \begin{bmatrix} \boldsymbol{\Sigma}_{\hat{c},\hat{c}} & \boldsymbol{\Sigma}_{\hat{c},c}d^* \\ \boldsymbol{\Sigma}_{\hat{c},c}^{\mathrm{H}}d & \boldsymbol{\Sigma}_{c,c}|d|^2 + \boldsymbol{\Sigma}_n(0) \end{bmatrix} \tag{2.23}$$

where $\boldsymbol{\Sigma}_{\hat{c},c} = E[\hat{\mathbf{c}}_f(i)\mathbf{c}_f^{\mathrm{H}}(i)]$ is the cross-covariance matrix between $\hat{\mathbf{c}}(i)$ and $\mathbf{c}(i)$, $\boldsymbol{\Sigma}_{\hat{c},\hat{c}} = E[\hat{\mathbf{c}}_f(i)\hat{\mathbf{c}}_f^{\mathrm{H}}(i)]$, and $\boldsymbol{\Sigma}_{c,c} = E[\mathbf{c}_f(i)\mathbf{c}_f^{\mathrm{H}}(i)]$. Note that $\boldsymbol{\Sigma}_{\hat{c},\hat{c}}$, $\boldsymbol{\Sigma}_{\hat{c},c}$, and $\boldsymbol{\Sigma}_{c,c}$ completely model the effect of ICE on the diffuse channel components, and the signal correlation between different branches.

Next, we show how to evaluate $\boldsymbol{\Sigma}_v(d)$ and $\bar{\mathbf{v}}(d)$ for a given channel estimator $\mathbf{W}$. Let $\mathbf{c}_{\mathrm{PS}} = \boldsymbol{\mu}_{\mathrm{PS}} + \mathbf{c}_{f_{\mathrm{PS}}}$, where $\boldsymbol{\mu}_{\mathrm{PS}}$ and $\mathbf{c}_{f_{\mathrm{PS}}}$ are the vectors of the LOS and diffuse components of $\mathbf{c}_{\mathrm{PS}}$, respectively. Then, $\mathbf{y}_{\mathrm{PS}} = \sqrt{P_{\mathrm{PS}}}\boldsymbol{\mu}_{\mathrm{PS}} + \tilde{\mathbf{y}}_{\mathrm{PS}}$, where $\tilde{\mathbf{y}}_{\mathrm{PS}} = \sqrt{P_{\mathrm{PS}}}\mathbf{c}_{f_{\mathrm{PS}}} + \mathbf{n}_{\mathrm{PS}}$ is a zero-mean vector. We can show that

$$\hat{\boldsymbol{\mu}}_c(i) = \sqrt{P_{\mathrm{PS}}}\mathbf{W}\boldsymbol{\mu}_{\mathrm{PS}} \tag{2.24}$$

$$\begin{aligned} \boldsymbol{\Sigma}_{\hat{c},c} &= E[\mathbf{W}\tilde{\mathbf{y}}_{\mathrm{PS}}\mathbf{c}_f^H(i)] \\ &= \mathbf{W}E[(\sqrt{P_{\mathrm{PS}}}\mathbf{c}_{f_{\mathrm{PS}}} + \mathbf{n}_{\mathrm{PS}})\mathbf{c}_f^H(i)] = \mathbf{W}\boldsymbol{\Sigma}_{c,y_{\mathrm{PS}}}^H \end{aligned} \tag{2.25}$$

$$\begin{aligned} \boldsymbol{\Sigma}_{\hat{c},\hat{c}} &= E[\mathbf{W}(\sqrt{P_{\mathrm{PS}}}\mathbf{c}_{f_{\mathrm{PS}}} + \mathbf{n}_{\mathrm{PS}})(\sqrt{P_{\mathrm{PS}}}\mathbf{c}_{f_{\mathrm{PS}}} + \mathbf{n}_{\mathrm{PS}})^H\mathbf{W}^H] \\ &= \mathbf{W}\boldsymbol{\Sigma}_{y_{\mathrm{PS}}}\mathbf{W}^H \end{aligned} \tag{2.26}$$

where $\boldsymbol{\Sigma}_{c,y_{\mathrm{PS}}} = E[\mathbf{c}_f(i)\tilde{\mathbf{y}}_{\mathrm{PS}}^H]$ is the cross-covariance matrix between $\mathbf{c}(i)$ and $\mathbf{y}_{\mathrm{PS}}$, and $\boldsymbol{\Sigma}_{y_{\mathrm{PS}}} = E[\tilde{\mathbf{y}}_{\mathrm{PS}}\tilde{\mathbf{y}}_{\mathrm{PS}}^H]$ is the auto-covariance matrix of $\mathbf{y}_{\mathrm{PS}}$. They can be obtained by replacing $\mathbf{R}_c(m)$ in (2.3) and (2.4) with $\boldsymbol{\Sigma}_c(m)$, respectively, as shown by the equations (2.27), (2.28).

$$\boldsymbol{\Sigma}_{c,y_{\mathrm{PS}}} = \sqrt{P_{\mathrm{PS}}}[\boldsymbol{\Sigma}_c(PF_1 - i_{\mathrm{off}}), \ldots, \boldsymbol{\Sigma}_c(-i_{\mathrm{off}}), \ldots, \boldsymbol{\Sigma}_c(-P(F_2 - 1) - i_{\mathrm{off}})] \tag{2.27}$$

www.manaraa.com

$$\mathbf{\Sigma}_{y_{\rm PS}} = \begin{bmatrix} P_{\rm PS}\mathbf{\Sigma}_c(0)+\mathbf{\Sigma}_n(0) & P_{\rm PS}\mathbf{\Sigma}_c^H(P)+\mathbf{\Sigma}_n^H(P) & \dots & \\ P_{\rm PS}\mathbf{\Sigma}_c(P)+\mathbf{\Sigma}_n(P) & P_{\rm PS}\mathbf{\Sigma}_c(0)+\mathbf{\Sigma}_n(0) & \dots & \\ \vdots & & \ddots & \\ P_{\rm PS}\mathbf{\Sigma}_c(P(F-1))+\mathbf{\Sigma}_n(P(F-1)) & & \dots & P_{\rm PS}\mathbf{\Sigma}_c(0)+\mathbf{\Sigma}_n(0) \end{bmatrix} \tag{2.28}$$

A special case is discussed below. For the case of white noise, independent diversity branches, and identical fading correlation functions at all the branches (i.e., $\tilde{R}_{c_1}(n) = \ldots = \tilde{R}_{c_L}(n) = \tilde{R}_c(n)$), we have

$$\mathbf{\Sigma}_{c,y_{\rm PS}} = \sqrt{P_{\rm PS}}[\tilde{R}_c(PF_1 - i_{\rm off}), \ldots, \tilde{R}_c(-i_{\rm off}), \ldots, \tilde{R}_c(-P(F_2-1)-i_{\rm off})] \otimes \text{diag}(\sigma_{c_1}^2, \ldots, \sigma_{c_L}^2),$$

and

$$\mathbf{\Sigma}_{y_{\rm PS}} = N_0\mathbf{I}_{FL} + P_{\rm PS}\begin{bmatrix} 1 & \tilde{R}_c^*(P) & \dots & \tilde{R}_c^*(P(F-1)) \\ \tilde{R}_c(P) & 1 & \ldots, & \\ \vdots, & & \ddots & \\ \tilde{R}_c(P(F-1)) & & \dots & 1 \end{bmatrix} \otimes \text{diag}(\sigma_{c_1}^2, \ldots, \sigma_{c_L}^2).$$

Applying (2.22) – (2.26) to (2.21), we can evaluate the MGF of the new DV. The CDF $P\{D_H(\beta_n|d) < 0\}$ can be evaluated by the inverse Laplace transform of the MGF, as shown by

$$P\{D_H(\beta_n|d) < 0\} = \frac{1}{2\pi}\text{Re}\left(\int_{c-j\infty}^{c+j\infty} \frac{\Phi_{D_H(\beta_n|d)}(-s)}{js} ds\right) \tag{2.29}$$

where c is a small real constant in the convergence region [27]. The MGF of $\Phi_{D_V(\beta_n|d)}(s)$ can be obtained by replacing $\mathbf{Q}_H(\beta_n)$ with $\mathbf{Q}_V(\beta_n)$ in (2.21), and the CDF $P\{D_V(\beta_n|d) < 0\}$ can be obtained by replacing $\Phi_{D_H(\beta_n|d)}(-s)$ with $\Phi_{D_V(\beta_n|d)}(-s)$ in (2.29).

Equation (2.29) can be evaluated by a Gauss-Chebyshev quadrature (GCQ) formula [28],

$$P\{D_H(\beta_n|d) < 0\} = \frac{1}{2N}\sum_{n=1}^{N} \hat{\Phi}\left(\frac{(2n-1)}{2N}\pi\right) + \hat{R}_N,$$

www.manaraa.com

where $\hat{\Phi}(\theta) = \Phi_{D_H(\beta_n|d)}(-c - jc\tan(\theta/2))(1 - j\tan(\theta/2))$, and $\hat{R}_N$ is a residual term which vanishes for $N \to \infty$. The GCQ formula with (2.17)–(2.19) gives accurate BER results for M-QAM in arbitrary Rician fading channels taking ICE into account.

2.4.2.2 Rayleigh Fading Channels

The results for arbitrarily correlated branches in Rayleigh channels can be obtained using (2.21) and (2.29) by setting $\bar{\mathbf{v}}(d)$ to a zero vector. Below, we consider the case of independent diversity branches.

I.N.D. Diversity

To gain more insight into the relation between channel estimation accuracy and BER performance of M-QAM with PSAM, we derive the BER formula for i.n.d. diversity Rayleigh channels. To our knowledge, an exact BER result for MRC M-QAM in i.n.d. Rayleigh fading channels is not available. Define the normalized correlation coefficient ρ_l between $c_{f_l}(i)$ and $\hat{c}_{f_l}(i)$ as

$$\rho_l = E[\hat{c}^*_{f_l}(i)c_{f_l}(i)]/[\sigma_{c_l}\sigma_{\hat{c}_l}], \tag{2.30}$$

where $E[\hat{c}^*_{f_l}(i)c_{f_l}(i)] = [\mathbf{\Sigma}_{\hat{c},c}]_{l,l}$, $\sigma_{\hat{c}_l} = \sqrt{[\mathbf{\Sigma}_{\hat{c},\hat{c}}]_{l,l}}$, and $\mathbf{\Sigma}_{l,l}$ is the (l,l)-th entry of matrix $\mathbf{\Sigma}$. Thus, we obtain that $\rho_l = \frac{1}{\sigma_{c_l}}[\mathbf{\Sigma}_{c,y_{\rm PS}}\mathbf{W}^H]_{l,l}/\sqrt{[\mathbf{W}\mathbf{\Sigma}_{y_{\rm PS}}\mathbf{W}^H]_{l,l}}$, which is a function of the estimation filter $\mathbf{W}$ (which may be non-MMSE-CE) and various fading channel parameters.

For i.n.d. Rayleigh fading branches, the MGF for the DV $D_H(\beta_n|d)$ is given by

$$\Phi_{D_H(\beta_n|d)}(s) = \prod_{l=1}^{L} \det(\mathbf{I}_2 - s\mathbf{\Sigma}_{v_l}(d)\mathbf{Q}_{H,2}(\beta_n))^{-1},$$

where $\mathbf{Q}_{H,2}(\beta_n) = \begin{bmatrix} -a\beta_n & 0.5 \\ 0.5 & 0 \end{bmatrix}$ and $\mathbf{\Sigma}_{v_l}(d) = \begin{bmatrix} \sigma^2_{\hat{c}_l} & \rho^*_l\sigma_{\hat{c}_l}\sigma_{c_l}d^* \\ \rho_l\sigma_{\hat{c}_l}\sigma_{c_l}d & \sigma^2_{c_l}|d|^2 + N_0 \end{bmatrix}$. Let the two eigenvalues of $\mathbf{\Sigma}_{v_l}(d)\mathbf{Q}_{H,2}(\beta_n)$ be denoted by $\lambda^{\pm}_l(\beta_n, d)$. Since the signals in all the L branches are independent, all the poles of $\Phi_{D_H(\beta_n|d)}(s)$ are given by $\{1/\lambda^-_l(\beta_n,d), 1/\lambda^+_l(\beta_n,d)\}_{l=1}^{L}$.

From the results obtained in (2.43) of Appendix 2.B, we sort the $2L$ eigenvalues in the ascending order so that $\{\lambda_l(\beta_n,d)\}_{l=1}^{L}$ are negative, and $\{\lambda_l(\beta_n,d)\}_{l=L+1}^{2L}$ are positive. Assuming

www.manaraa.com

all the negative eigenvalues of $\mathbf{\Sigma}_v(d)\mathbf{Q}_H(\beta_n)$ are distinct, we obtain

$$P\{D_H(\beta_n|d) < 0\} = \sum_{l=1}^{L} \prod_{m=1, m\neq l}^{2L} \frac{\lambda_l(\beta_n, d)}{\lambda_l(\beta_n, d) - \lambda_m(\beta_n, d)} \tag{2.31}$$

The BER of M-QAM can be obtained by substituting (2.31) into (2.17)–(2.19), respectively.

Obviously, from (2.31) we observe that an error floor appears if $\lambda_l(\beta_n, d) < 0$ for $l = 1, \ldots, L$ (i.e., $\mathbf{\Sigma}_{v_l}(d)\mathbf{Q}_{H,2}(\beta_n)$ has negative eigenvalues), when the noise power $N_0 \to 0$, or the average SNR goes to infinity. We observe that when $N_0 = 0$ and $\rho_l = 1$ for all l, it follows from (2.43) in Appendix 2.B that $\lambda_l^-(d, \beta_n) = 0$ for all l, which shows that an error floor does not occur in this case.

I.I.D. Diversity

In the literature, a substantial part of the research effort on the BER evaluation of M-QAM has been devoted to i.i.d. Rayleigh fading channels, c.f. [12, 17, 18]. Here, we derive results for this case based on our new approach for the purpose of comparison. For i.i.d. branches, we obtain that $\rho_l = \rho$, $\sigma_{\hat{c}_l}^2 = \sigma_{\hat{c}}^2$, and $\sigma_{c_l}^2 = \sigma_c^2$ for $l = 1, \ldots, L$. In this case, $\mathbf{\Sigma}_v(d)\mathbf{Q}_H(\beta_n)$ has only two distinct eigenvalues with each of them being repeated L times, and we denote them as $\lambda^{\pm}(\beta_n, d)$. Using a result in [30], the CDF $P\{D_H(\beta_n|d) < 0\}$ can be obtained as

$$P\{D_H(\beta_n|d) < 0\} \quad = \quad [A(\beta_n|d)]^L \sum_{l=0}^{L-1} \binom{L+l-1}{l} \times [1 - A(\beta_n|d)]^l \tag{2.32}$$

where $A(\beta_n|d) = \frac{\lambda^-(\beta_n,d)}{\lambda^-(\beta_n,d) - \lambda^+(\beta_n,d)}$. Exact formulation of the BER is given in Appendix 2.C.

Let us rewrite $A(\beta_n|d)$ as $A(\beta_n|d) = A(\beta_n|\alpha_h, \alpha_v)$, where $d = a(\alpha_h + j\alpha_v)$. Then, we obtain a closed-form average BER expression for M-QAM with L-fold MRC as (2.45).

For comparison, the result given in [17, eq. (37)] is in the form of a two-dimensional (2-D) integral of the $2L$-order parabolic cylinder function, and thus is numerically intensive to evaluate. In [18, eqs. (9), (12)], an alternative closed-form BER expression for M-QAM with PSAM was presented. Our result given by (2.45) and (2.44) of Appendix 2.C explicitly shows the relation between ρ_l and the BER, and thus provides more insight into the behavior of

www.manaraa.com

PSAM, as will be discussed next in Subsection 2.4.2.2.

MMSE-CE

The MMSE channel estimator for PSAM has attracted a lot of research interest in the literature, and it provides a performance benchmark for other linear channel estimators. For MMSE-CE with i.n.d. branches, we can show that

$$\rho_l = \sqrt{[\mathbf{W}_{\text{mmse}}\mathbf{\Sigma}_{y_{\text{PS}}}\mathbf{W}_{\text{mmse}}^H]_{l,l}}/\sigma_{c_l} = \sqrt{[\mathbf{\Sigma}_{c,y_{\text{PS}}}\mathbf{\Sigma}_{y_{\text{PS}}}^{-1}\mathbf{\Sigma}_{c,y_{\text{PS}}}^H]_{l,l}}/\sigma_{c_l}, \tag{2.33}$$

$$\mathbf{\Sigma}_{v_l}(d) = \begin{bmatrix} |\rho_l|^2\sigma_{c_l}^2 & |\rho_l|^2\sigma_{c_l}^2 d^* \\ |\rho_l|^2\sigma_{c_l}^2 d & \sigma_{c_l}^2|d|^2 + N_0 \end{bmatrix} \tag{2.34}$$

Obviously, ρ_l is real-valued for MMSE-CE. Using (2.43) we get the eigenvalue pairs as

$$\lambda_l^{\pm}(d,\beta_n) = \frac{1}{2}\sigma_{c_l}^2 a\rho_l^2(\alpha_h - \beta_n) \pm \frac{1}{2}\rho_l\{\sigma_{c_l}^4 a^2 \times [\alpha_h^2 + \rho_l^2\beta_n^2 + (1-\rho_l^2)\alpha_v^2 - 2\rho_l^2\beta_n\alpha_h] + \sigma_{c_l}^2 N_0\}^{1/2} \tag{2.35}$$

By substituting (2.35) into (2.31), we obtain a closed-form BER expression for QAM with MMSE-CE in i.n.d. Rayleigh fading.

For MMSE-CE and i.i.d. Rayleigh fading channels, it follows that the BER of M-QAM is given by (2.45), where $A(\beta_n|d)$ therein is replaced by

$$A(\beta_n|d) = \frac{1}{2} - \frac{1}{2}[a\sigma_c\rho(\alpha_h - \beta_n)] \times [\sigma_c^2 a^2(\alpha_h^2 + \rho^2\beta_n^2 + (1-\rho^2)\alpha_v^2 - 2\rho^2\beta_n\alpha_h) + N_0]^{-1/2} \tag{2.36}$$

The study of the detection error floor of QAM with PSAM is of practical interest. Let us consider the BER of MRC QAM with MMSE-CE for the asymptotic case of high SNR. We note that when $\alpha_h - \beta_n > 0$ and $\alpha_h - \beta_n < 0$, the conditional BERs are given by $P\{D_H(\beta_n|d) < 0\}$ and $1 - P\{D_H(\beta_n|d) < 0\}$, respectively. Thus, for brevity of presentation, we assume $\alpha_h - \beta_n > 0$ and study $P\{D_H(\beta_n|d) < 0\}$ below.

For MMSE-CE the effect of ICE at the lth branch is manifested by the fact that $\rho_l < 1$. When $N_0 = 0$ and $\rho_l < 1$, using (2.35) we observe that $\lambda_l^-(d,\beta_n) < 0$ is true. Note that

www.manaraa.com

the negative eigenvalues of $\mathbf{\Sigma}_{v_l}\mathbf{Q}_{H,2}(\beta_n)$ for $N_0 = 0$ mean that a detection error floor occurs. When $N_0 = 0$ and $\rho_l = 1$ for all l, using (2.35) again we observe that $\lambda_l^-(d, \beta_n) = 0$ and $\lambda_l^+(d, \beta_n) = \sigma_{c_l}^2 a(\alpha_h - \beta_n)$, which shows that an error floor does not occur in this case. Thus, $\{\rho_l\}_{l=1}^L$ is closely related to the performance of diversity QAM with PSAM. The error floor for M-QAM with MMSE-CE can be analytical evaluated by using (2.33)–(2.36) with (2.31) or (2.32). We note that the normalized residual MSE (which is proportional to $1 - |\rho_l|^2$ defined in Section 2.2.3) of MMSE-CE in a non-diversity Rayleigh channel has recently been studied in [31, Appendix]. It was shown that for a bandlimited fading process (e.g., the Jakes' model) with $B_f T_s P < 1/2$ and infinite PSAM interpolation order ($F \to \infty$), the normalized residual MSE decreases proprotionally as the SNR increases, which suggests that under these conditions an error floor does not occur.

Finally, we underscore that we have verified that for all the square and rectangular M-QAM constellations obtained in this chapter, our new BER results, when simplified to the case of perfect CSI, are numerically identical to the known results given in [14, 125].

2.5 Numerical Examples and Discussions

In this section, we provide some numerical results for the performance of the M-QAM MRC receiver in general Rician fading channels taking into account the effects of ICE and various system and channel parameters. We assume the same data symbol power P_d and pilot symbol power P_{PS} unless otherwise stated. To clearly illustrate the effects of Doppler fading bandwidth and the Rician K factor, we also assume $B_{f,l} = B_f$, $f_{d,l} = f_d$, and $K_l = K$ (for all l) for all the cases studied.

2.5.1 Verification of the BER Analysis

For correlated fading, the popular constant spatial correlation model [125] (with correlation coefficient ρ_c) is assumed. For example, for balanced branches and $L = 3$, $\mathbf{\Sigma}_c(0) =$

www.manaraa.com

$\sigma_c^2 \begin{bmatrix} 1 & \rho_c & \rho_c \\ \rho_c & 1 & \rho_c \\ \rho_c & \rho_c & 1 \end{bmatrix}$. To show the effect of the phase vector $\boldsymbol{\theta} = [\theta_1, \cdots, \theta_L]^T$ of the LOS components, we assume $f_d T_s = 0$ and $B_f T_s = 0.02$. In our simulation, we assume $\mathbf{R}_c(n) = \mathbf{R}_c(0) J_0(2\pi n B_f T_s)$, i.e., the spatial and temporal correlations can be separated.

First, we present the simulated and calculated BER results (averaged over all possible i_{off}'s) for 16-QAM receivers with $L = \{1, 2, 3\}$ in i.i.d. and correlated Rician fading channels in Fig. 2.3, and the results for the effect of ρ_c in Fig. 2.4, respectively. The simulation results (markers) verify the validity and accuracy of our new BER analysis approach. Fig. 2.3 shows that the correlated fading (with $\boldsymbol{\theta}$ being an all-zero vector) severely degrades the performance of MRC QAM in Rician fading channels. As L increases, the degradation of BER for MMSE-CE caused by correlated branches becomes larger. Fig. 2.4 shows that as ρ_c increases, the performance of MRC QAM with CSI, MMSE-CE, and sinc-CE becomes worse for $\boldsymbol{\theta} = [0, 0, 0]$, but becomes better than the independent fading case for $\boldsymbol{\theta} = [0, \pi/2, \pi]$ (i.e., a non-cophased LOS vector). This observation may be explained by the fact that the phase vector $\boldsymbol{\theta}$ significantly affects the MRC output Rician-K factor and the SNR gain in correlated Rician fading channels, first discussed in [32].

Next, we present the BER results for the 32-QAM MRC receiver in i.n.d. Rayleigh and Rician fading channels in Fig. 2.5, and those for 16-QAM in i.i.d. Rayleigh and Rician fading channels in Fig. 2.6. For independent Rician channels the distribution of the LOS phase vector $\boldsymbol{\theta}$ does not affect the BER performance, and thus we set $\boldsymbol{\theta}$ to a zero vector for all the remaining numerical examples. In Fig. 2.5, for $B_f T_s = 0.02$, QAM with MMSE-CE gives a performance close to that of the perfect CSI case, and the SNR loss is within 2 dB for all SNRs shown in the figure; while in Fig. 2.6, for a larger $B_f T_s$ ($B_f T_s = 0.03$) and a larger P the relevant SNR gap becomes larger. Fig. 2.5 shows that the BER of sinc-CE with Hamming window (sinc-Hamm-CE) is uniformly lower than that of sinc-CE with rectangular window (sinc-rect-CE). On the contrary, for the parameters studied in Fig. 2.6, QAM with sinc-rect-CE performs significantly better than QAM with sinc-Hamm-CE. In addition, the SNR gaps between sinc-

www.manaraa.com

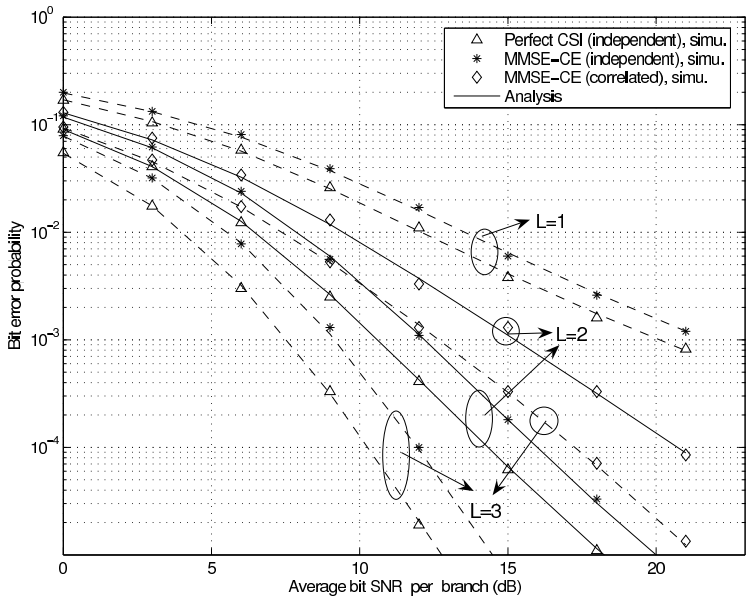

Figure 2.3 BER (averaged over all i_{off}'s) vs. average bit SNR per branch for 16-QAM MRC receivers with CSI and the MMSE-CE, respectively, in independent and correlated Rician ($K = 5$ dB) fading channels. $\boldsymbol{\theta} = \mathbf{0}_{1\times L}$, $L = \{1, 2, 3\}$, $P = 10$, $F_1 = F_2 = 5$, $B_f T_s = 0.02$, $f_d T_s = 0$, and $f_o = 0$.

CE and MMSE-CE depend on the average SNR, P, F, $B_f T_s$, and other parameters. This observation demonstrates that the relative performance between sinc-rect-CE and sinc-Hamm-CE, and the performance gap between sinc-CE and MMSE-CE, crucially depend on the channel and system parameters.

2.5.2 Effects of Design Parameters

In the following, we show the effects of some design parameters, including the pilot symbol insertion interval P, number of pilot symbols F, and the ratio P_{PS}/P_d on the performance of the MRC M-QAM.

We show the effect of P on the BER of 16-QAM with MMSE-CE and sinc-CE in Fig. 2.7, assuming $L = 2$ and $i_{\text{off}} = \lfloor P/2 \rfloor$. Our results show that the BER degrades slowly when $P \leq 14$. When $P > 14$, both the performances of MMSE-CE and sinc-Hamm-CE start to degrade rapidly. Sinc-Hamm-CE may give a performance very close to (though uniformly

www.manaraa.com

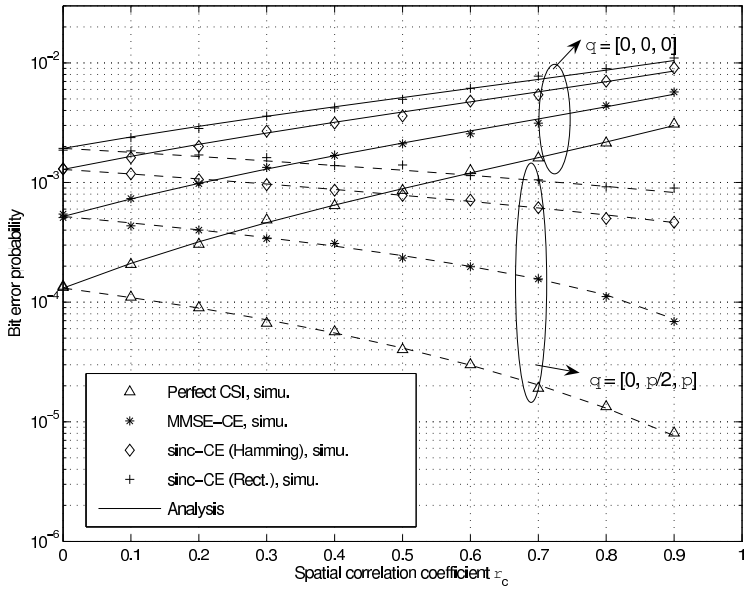

Figure 2.4 BER (averaged over all i_{off}'s) vs. spatial correlation coefficient ρ_c for 16-QAM MRC receivers with CSI, MMSE- and sinc-interpolator-based (with rectangular and Hamming windows) channel estimators, respectively, in Rician ($K = 5$ dB) fading channels. $\boldsymbol{\theta} = [0, 0, 0]$ and $[0, \pi/2, \pi]$, $\bar{\gamma}_b = 10$ dB, $L = 3$, $P = 10$, $F_1 = F_2 = 5$, $B_f T_s = 0.02$, $f_d T_s = 0$, and $f_o = 0$.

worse than) that of MMSE-CE, especially for $P = 12$.

Next, we study the effect of P_{PS}/P_d, the power ratio between pilot and data symbols in Fig. 2.8. The total average transmission power is given by $P_t = \frac{1}{P}(\alpha+(P-1))P_d$, where $\alpha = P_{\text{PS}}/P_d$. For a fair comparison between the cases of $P_{\text{PS}}/P_d \neq 1$ and $P_{\text{PS}}/P_d = 1$, we let P_t to be identical for both cases. When α increases, the power allocated to the data symbol P_d decreases which degrades the BER, while at the same time the channel estimation accuracy becomes better which improves the BER. Without power normalization, $\hat{\mathbf{c}}(i)$ could be directly obtained as $\hat{\mathbf{c}}(i) = \mathbf{W}\mathbf{y}_{\text{PS}}$. We study the case with channel gain power normalization where $\hat{\mathbf{c}}(i)$ is obtained from $\hat{\mathbf{c}}(i) = \mathbf{W}\mathbf{y}_{\text{PS}}/\sqrt{\alpha}$. To evaluate the corresponding BER, we need to modify (2.24)–(2.26) as follows: $\hat{\boldsymbol{\mu}}_c(i) = \mathbf{W}\sqrt{P_{\text{PS}}}\boldsymbol{\mu}_{\text{PS}}/\sqrt{\alpha}$, $\boldsymbol{\Sigma}_{\hat{c},c} = \mathbf{W}\boldsymbol{\Sigma}_{c,y_{\text{PS}}}/\sqrt{\alpha}$, and $\boldsymbol{\Sigma}_{\hat{c},\hat{c}} = \mathbf{W}\boldsymbol{\Sigma}_{y_{\text{PS}}}\mathbf{W}^H/\alpha$.

Fig. 2.8 shows that $P_{\text{PS}}/P_d \in [2, 3]$ gives optimal BER performance for MMSE-CE and sinc-CE, and compared to the case of $P_{\text{PS}}/P_d = 1$ the BERs can be reduced by a factor of about $1.5 - 2.5$. We note that for non-constant modulus formats, such as M-QAM, the power

www.manaraa.com

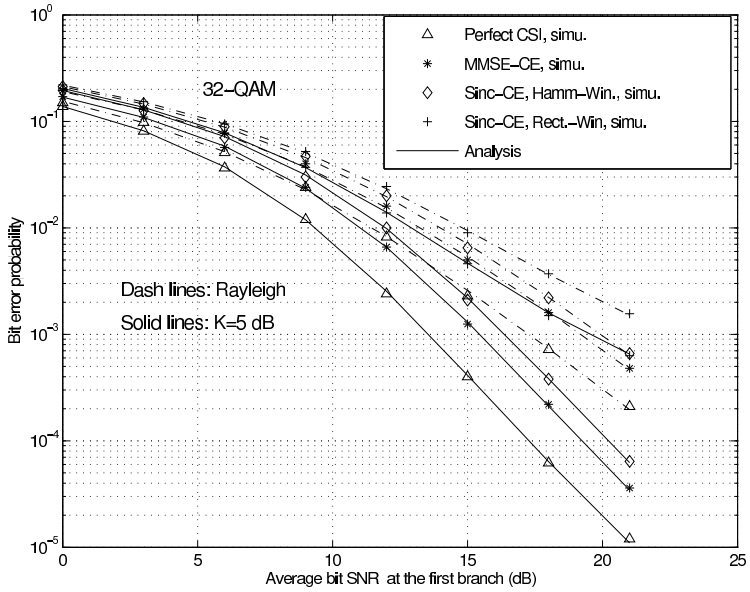

Figure 2.5 BER (averaged over all i_{off}'s) vs. average bit SNR of the first branch for 32-QAM MRC receivers with CSI, MMSE- and sinc-interpolator-based channel estimators, respectively, in i.n.d. Rayleigh and Rician ($K = 5$ dB) fading channels. $L = 2$, $P = 10$, $F_1 = F_2 = 4$, $B_f T_s = 0.02$, $f_d T_s = 0.01$, and $f_o = 0$. The SNR of the first branch is 2 dB larger than that of the second branch.

normalization of the channel estimate is necessary (except for the MMSE-CE where the power normalization has been taken into account in $\mathbf{W}_{\text{mmse}}$). Otherwise, the case of $P_{\text{PS}}/P_d \neq 1$ (e.g., for sinc-CE) may severely degrade the performance.

We study the effects of F_2 and F on the BER of the M-QAM MRC receivers with MMSE-CE and sinc-CE. We present the BER vs. F_2 for 32-QAM in i.i.d. Rician and Rayleigh fading channels in Fig. 2.9 for $F = 24$. The cases of $F_2 = 0$ and $F_2 = 12$ correspond to a prediction-based (thus one-sided) and a centered observation window, respectively. Our result shows that the centered observation window ($F_1 = F_2 = 12$) gives a better performance than the case of $F_2 \neq 12$ for MMSE-CE and sinc-rect-CE, as expected. Furthermore, MMSE-CE is less sensitive to a non-centered window than sinc-CE.

The BER vs. F for 16- and 64-QAM with MMSE-CE and sinc-CE is presented in Fig. 2.10. We observe that as F increases, the BER performances of QAM with MMSE-CE and

www.manaraa.com

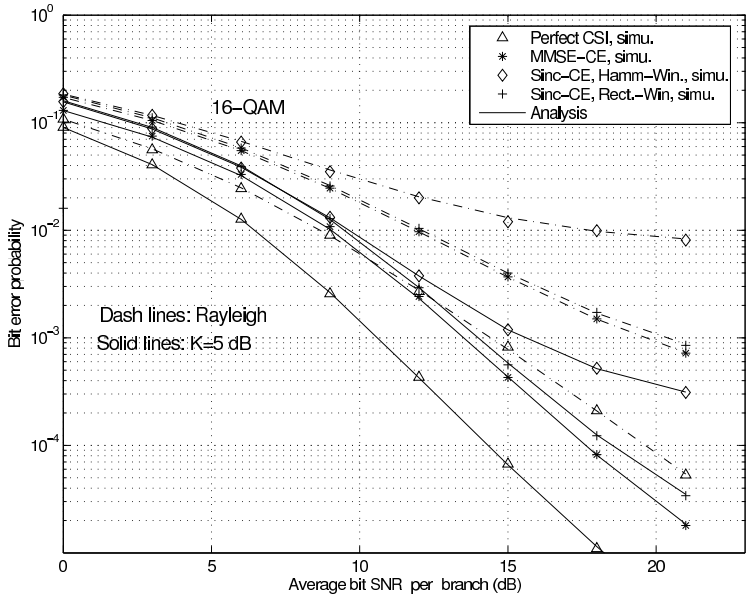

Figure 2.6 BER (averaged over all i_{off}'s) vs. average bit SNR per branch for 16-QAM MRC receivers with CSI, MMSE- and sinc-interpolator-based channel estimators, respectively, in i.i.d. Rayleigh and Rician ($K = 5$ dB) fading channels. $L = 2$, $P = 15$, $F_1 = F_2 = 5$, $B_f T_s = 0.03$, $f_d T_s = 0.015$, and $f_o = 0$.

sinc-CE improve monotonically. For a small to medium F, sinc-Hamm-CE may be worse than sinc-rect-CE, while for a larger F (e.g. $F \geq 15$), sinc-Hamm-CE performs uniformly better than the latter, and its performance converges to that of the MMSE-CE. This observation confirms that the relative performance of sinc-rect-CE and sinc-Hamm-CE depends on the system parameters.

2.6 Summary

In this chapter, we derived the exact BER formulas of diversity square and rectangular M-QAM with ICE for Rician and Rayleigh fading channels. The novelty in our approach is that we derived new DVs of the MRC combiner and then expressed the BER of MRC combiner in terms of the distribution of them, thus avoiding many of the difficulties faced by other approaches. More importantly, by doing this, our new result is valid for arbitrary linear channel estimators, and unbalanced and correlated diversity branches. In addition, we discussed the

www.manaraa.com

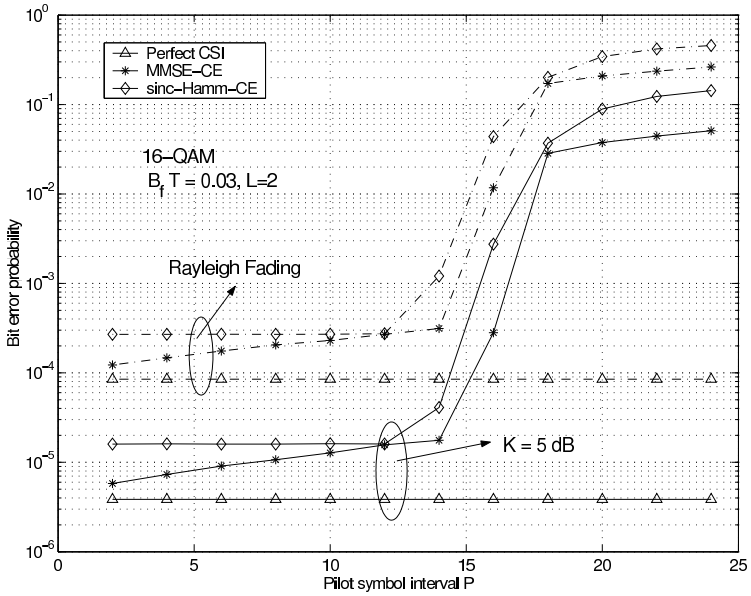

Figure 2.7 BER versus the pilot symbol insertion interval P for MRC 16-QAM with MMSE-CE and sinc-CE, respectively, in i.i.d. Rayleigh and Rician ($K = 5$ dB) fading channels. $\bar{\gamma}_b = 20$ dB, $L = 2$, $i_{\text{off}} = \lfloor P/2 \rfloor$, $F_1 = F_2 = 6$, $B_f T_s = 0.03$, $f_d T_s = 0.015$, $f_o = 0$.

relation between channel estimation accuracy and BER floor, and evaluated the performance of MRC M-QAM with the practical PSAM MMSE-CE and sinc-CE with different real-world parameter settings using numerical examples. One highlight of our results that's immediately applicable to practice is we clearly showed the relative performance of Hamming window and rectangular window for sinc-CE, and the performance gap between sinc-CE and MMSE-CE, depend on the system and channel parameters. These results provide valuable insights for the design of PSAM-based channel estimation schemes for diversity QAM in arbitrarily correlated or uncorrelated Rician or Rayleigh channels.

2.7 Appendix 2.A Formulation of BER of 16-PAM

Similar to what we developed in Section 2.3.1, the BERs for bits b_1, b_2, b_3 and b_4 in 16-PAM are expressed respectively as:

www.manaraa.com

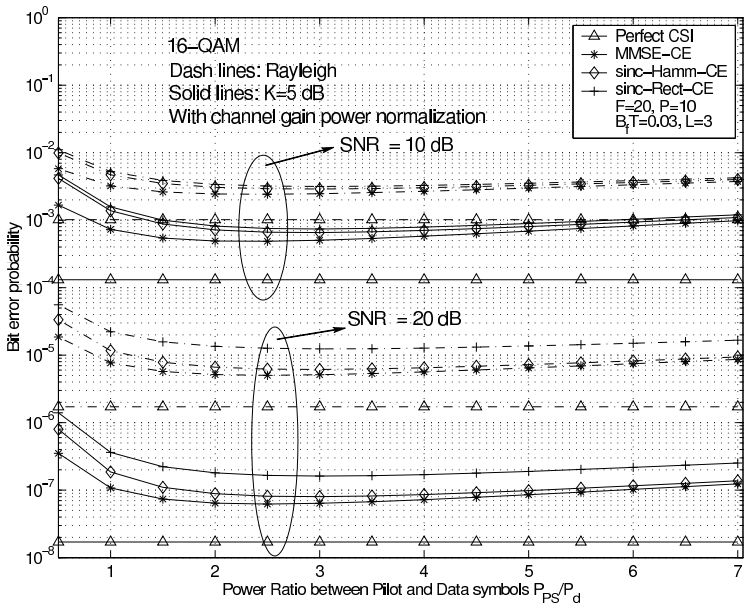

Figure 2.8 BER vs. the power allocation ratio $P_{\rm PS}/P_d$ for MRC 16-QAM with MMSE-CE and sinc-CE (with power normalization), respectively, in i.i.d. Rayleigh and Rician ($K = 5$ dB) fading channels. $\bar{\gamma}_b = \{10, 20\}$ dB, $L = 3$, $P = 10$, $i_{\rm off} = 5$, $F_1 = F_2 = 10$, $B_f T_s = 0.03$, $f_d T_s = 0.015$, $f_o = 0$.

$$P_{16,H}(1) = \frac{1}{8}[\tilde{P_H}(0|1)+\tilde{P_H}(0|3)+\tilde{P_H}(0|5)+\tilde{P_H}(0|7)+\tilde{P_H}(0|9)+\tilde{P_H}(0|11)+\tilde{P_H}(0|13)+\tilde{P_H}(0|15)] \tag{2.37}$$

$$\begin{aligned} P_{16,H}(2) \;=\; & \tfrac{1}{8}[4 + \tilde{P_H}(8|9) - \tilde{P_H}(-8|9) + \tilde{P_H}(8|11) - \tilde{P_H}(-8|11) + \tilde{P_H}(8|13) - \tilde{P_H}(-8|13) \\ & +\tilde{P_H}(8|15) - \tilde{P_H}(-8|15) + \tilde{P_H}(-8|7) + \tilde{P_H}(-8|5) + \tilde{P_H}(-8|3) + \tilde{P_H}(-8|1) \\ & -\tilde{P_H}(8|7) - \tilde{P_H}(8|5) - \tilde{P_H}(8|3) - \tilde{P_H}(8|1)] \end{aligned} \tag{2.38}$$

www.manaraa.com

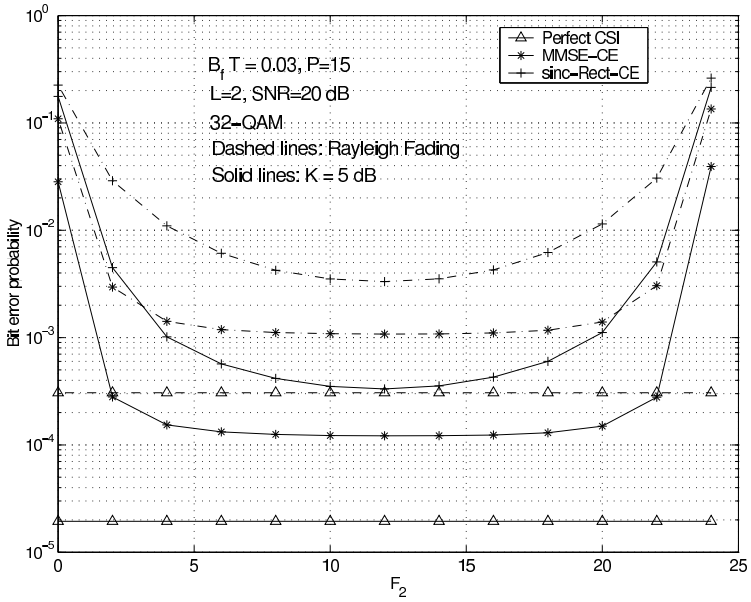

Figure 2.9 BER versus F_2 for MRC 32-QAM with MMSE-CE and sinc-rect-CE, respectively, in i.i.d. Rayleigh and Rician ($K = 5$ dB) fading channels. $\bar{\gamma}_b = 20$ dB, $L = 2$, $P = 15$, $i_{\text{off}} = 7$, $F = 24$, $B_f T_s = 0.03$, $f_o = 0$.

$$
\begin{aligned}
P_{16,H}(3) \;=\; & \tfrac{1}{8}[4 + \tilde{P_H}(12|13) - \tilde{P_H}(4|13) + \tilde{P_H}(-4|13) - \tilde{P_H}(-12|13) + \tilde{P_H}(12|15) - \tilde{P_H}(4|15) \\
& + \tilde{P_H}(-4|15) - \tilde{P_H}(-12|15) + \tilde{P_H}(4|11) - \tilde{P_H}(-4|11) + \tilde{P_H}(-12|11) - \tilde{P_H}(12|11) \\
& + \tilde{P_H}(4|9) - \tilde{P_H}(-4|9) + \tilde{P_H}(-12|9) - \tilde{P_H}(12|9) + \tilde{P_H}(4|7) - \tilde{P_H}(-4|7) \\
& + \tilde{P_H}(-12|7) - \tilde{P_H}(12|7) + \tilde{P_H}(4|5) - \tilde{P_H}(-4|5) + \tilde{P_H}(-12|5) - \tilde{P_H}(12|5) \\
& + \tilde{P_H}(-4|3) - \tilde{P_H}(-12|3) - \tilde{P_H}(4|3) + \tilde{P_H}(12|3) + \tilde{P_H}(-4|1) - \tilde{P_H}(-12|1) \\
& - \tilde{P_H}(4|1) + \tilde{P_H}(12|1)
\end{aligned}
\tag{2.39}
$$

www.manaraa.com

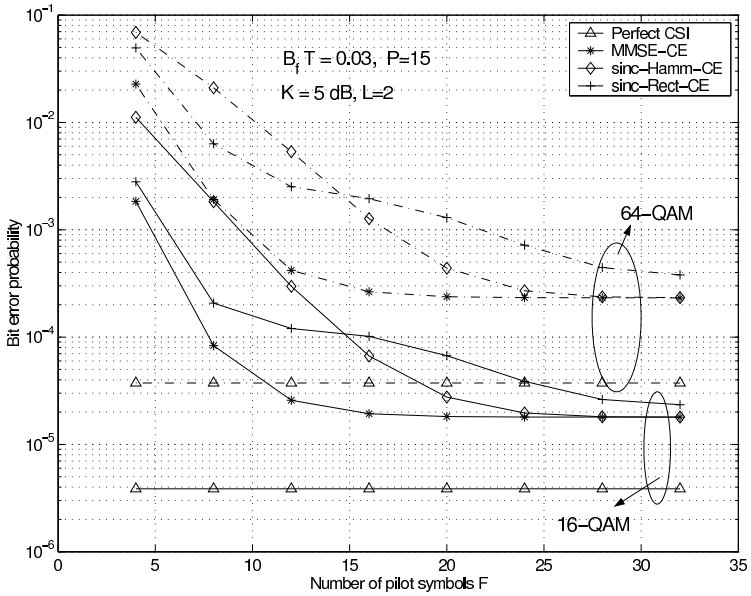

Figure 2.10 BER versus F for MRC 16- and 64-QAM receivers with MMSE-CE and sinc-CE, respectively, in an i.i.d. Rician fading channel. $K = 5$ dB, $\bar{\gamma}_b = 20$ dB, $L = 2$, $i_{\text{off}} = 7$, $F_1 = F_2 = F/2$, $B_f T_s = 0.03$, $f_o = 0$.

$$
\begin{aligned}
P_{16,H}(4) \;=\; & \tfrac{1}{8}[4 + \tilde{P_H}(14|15) - \tilde{P_H}(10|15) + \tilde{P_H}(6|15) - \tilde{P_H}(2|15) + \tilde{P_H}(-2|15) - \tilde{P_H}(-6|15) \\
& + \tilde{P_H}(-10|15) - \tilde{P_H}(-14|15) - \tilde{P_H}(14|13) + \tilde{P_H}(10|13) - \tilde{P_H}(6|13) + \tilde{P_H}(2|13) \\
& - \tilde{P_H}(-2|13) + \tilde{P_H}(-6|13) - \tilde{P_H}(-10|13) + \tilde{P_H}(-14|13) - \tilde{P_H}(14|11) + \tilde{P_H}(10|11) \\
& - \tilde{P_H}(6|11) + \tilde{P_H}(2|11) - \tilde{P_H}(-2|11) + \tilde{P_H}(-6|11) - \tilde{P_H}(-10|11) + \tilde{P_H}(-14|11) \\
& - \tilde{P_H}(10|9) + \tilde{P_H}(14|9) + \tilde{P_H}(6|9) - \tilde{P_H}(2|9) + \tilde{P_H}(-2|9) - \tilde{P_H}(-6|9) + \tilde{P_H}(-10|9) \\
& - \tilde{P_H}(-14|9) - \tilde{P_H}(10|7) + \tilde{P_H}(14|7) + \tilde{P_H}(6|7) - \tilde{P_H}(2|7) + \tilde{P_H}(-2|7) - \tilde{P_H}(-6|7) \\
& + \tilde{P_H}(-10|7) - \tilde{P_H}(-14|7) - \tilde{P_H}(6|5) + \tilde{P_H}(10|5) - \tilde{P_H}(14|5) + \tilde{P_H}(2|5) - \tilde{P_H}(-2|5) \\
& + \tilde{P_H}(-6|5) - \tilde{P_H}(-10|5) + \tilde{P_H}(-14|5) - \tilde{P_H}(6|3) + \tilde{P_H}(10|3) - \tilde{P_H}(14|3) + \tilde{P_H}(2|3) \\
& - \tilde{P_H}(-2|3) + \tilde{P_H}(-6|3) - \tilde{P_H}(-10|3) + \tilde{P_H}(-14|3) - \tilde{P_H}(2|1) + \tilde{P_H}(6|1) - \tilde{P_H}(10|1) \\
& + \tilde{P_H}(14|1) + \tilde{P_H}(-2|1) - \tilde{P_H}(-6|1) + \tilde{P_H}(-10|1) - \tilde{P_H}(-14|1)]
\end{aligned}
\tag{2.40}
$$

The average BER for horizontal 16-PAM can be obtained as

www.manaraa.com

$$\begin{aligned}\hat{P}_{16,H} &= \tfrac{1}{4}[P_{16,H}(1)+P_{16,H}(2)+P_{16,H}(3)+P_{16,H}(4)] \\ &= \tfrac{1}{32}\left[C_{16}+\sum_{n=1}^{N_{16}}\omega_n\tilde{P}_H(\beta_n|\alpha_n)\right]\end{aligned} \tag{2.41}$$

where $C_{16}=12$ and $N_{16}=120$, and the w_n, β_n, and α_n are given in Table 2.3, respectively. The average BER for vertical 16-PAM can be obtained similarly.

2.8 Appendix 2.B Derivation of Eigenvalues of $\mathbf{\Sigma}_{v_l}(d)\mathbf{Q}_{H,2}(\beta_n)$

We now derive the exact form of the eigenvalue pair $\lambda_l^{\pm}(\beta_n,d)$ at the lth branch. For simplicity, we suppress the subscript l below. Let $\mathbf{\Sigma}_v(d)=\begin{bmatrix}\sigma_{\hat{c}}^2 & \rho^*\sigma_{\hat{c}}\sigma_c d^* \\ \rho\sigma_{\hat{c}}\sigma_c d & \sigma_c^2|d|^2+N_0\end{bmatrix}$ and $\mathbf{Q}_{H,2}(\beta_n)=\begin{bmatrix}-a\beta_n & 0.5 \\ 0.5 & 0\end{bmatrix}$, where $d=(\alpha_h+j\alpha_v)a$ and $\rho=\rho_R+j\rho_I$. Here, ρ_R and ρ_I are the real and imaginary parts of ρ, respectively. It follows that $\mathbf{\Sigma}_v(d)\mathbf{Q}_{H,2}(\beta_n)=$
$\begin{bmatrix}-\beta_n a\sigma_{\hat{c}}^2+0.5\rho^*\sigma_{\hat{c}}\sigma_c d^* & 0.5\sigma_{\hat{c}}^2 \\ -\beta_n a\rho\sigma_{\hat{c}}\sigma_c d+0.5\sigma_c^2|d|^2+0.5N_0 & 0.5\rho\sigma_{\hat{c}}\sigma_c d\end{bmatrix}$.

For a matrix of the form $\begin{bmatrix}c_1 & c_2 \\ c_3 & c_4\end{bmatrix}$ we obtain its two eigenvalues as [33],

$$\lambda_{\pm}=\frac{1}{2}\left[(c_1+c_4)\pm\sqrt{4c_2c_3+(c_1-c_4)^2}\right] \tag{2.42}$$

Based on this observation, we obtain $(c_1-c_4)^2=\beta_n^2a^2\sigma_{\hat{c}}^4-\sigma_{\hat{c}}^2\sigma_c^2[\mathrm{Im}(\rho d)]^2+j2\beta_n a\sigma_{\hat{c}}^3\sigma_c\mathrm{Im}(\rho d)$, $4c_2c_3=-2\beta_n a\rho\sigma_{\hat{c}}^3\sigma_c d+\sigma_{\hat{c}}^2\sigma_c^2|d|^2+\sigma_{\hat{c}}^2N_0$, and $c_1+c_4=\mathrm{Re}(d\rho)\sigma_{\hat{c}}\sigma_c-\beta_n a\sigma_{\hat{c}}^2$. Applying these equalities to (2.42), we obtain the two eigenvalues of $\mathbf{\Sigma}_v\mathbf{Q}_{H,2}(\beta_n)$ as:

$$\begin{aligned}\lambda_l^{\pm}(\beta_n,d) &= \frac{1}{2}[(\rho_{l,R}\alpha_h-\rho_{l,I}\alpha_v)a\sigma_{\hat{c}_l}\sigma_{c_l}-\beta_n a\sigma_{\hat{c}_l}^2]\pm\frac{1}{2}\sigma_{\hat{c}_l}\{a^2[\sigma_{c_l}^2(1-\rho_{l,R}^2)\alpha_v^2+\sigma_{c_l}^2(1-\rho_{l,I}^2)\alpha_h^2 \\ &\quad -2\sigma_{c,l}^2\rho_{l,R}\rho_{l,I}\alpha_h\alpha_v-2\beta_n\sigma_{\hat{c}_l}\sigma_{c_l}\times(\rho_{l,R}\alpha_h-\rho_{l,I}\alpha_v)+\beta_n^2\sigma_{\hat{c}_l}^2]+N_0\}^{1/2}\end{aligned} \tag{2.43}$$

where $\rho_{l,R}=\mathrm{Re}(\rho_l)$ and $\rho_{l,I}=\mathrm{Im}(\rho_l)$.

www.manaraa.com

Table 2.3 Coefficients for BER calculation for 16-PAM

n	β_n	α_n	ω_n	n	β_n	α_n	ω_n	n	β_n	α_n	ω_n	n	β_n	α_n	ω_n
1	0	1	1	31	-4	15	1	61	-2	15	1	91	6	7	1
2	0	3	1	32	-12	15	-1	62	-6	15	-1	92	2	7	-1
3	0	5	1	33	4	11	1	63	-10	15	1	93	-2	7	1
4	0	7	1	34	-4	11	-1	64	-14	15	-1	94	-6	7	-1
5	0	9	1	35	-12	11	1	65	14	13	-1	95	-10	7	1
6	0	11	1	36	12	11	-1	66	10	13	1	96	-14	7	-1
7	0	13	1	37	4	9	1	67	6	13	-1	97	6	5	-1
8	0	15	1	38	-4	9	-1	68	2	13	1	98	10	5	1
9	8	9	1	39	-12	9	1	69	-2	13	-1	99	14	5	-1
10	-8	9	-1	40	12	9	-1	70	-6	13	1	100	2	5	1
11	8	11	1	41	4	7	1	71	-10	13	-1	101	-2	5	-1
12	-8	11	-1	42	-4	7	-1	72	-14	13	1	102	-6	5	1
13	8	13	1	43	-12	7	1	73	14	11	-1	103	-10	5	-1
14	-8	13	-1	44	12	7	-1	74	10	11	1	104	-14	5	1
15	8	15	1	45	4	5	1	75	6	11	-1	105	6	3	-1
16	-8	15	-1	46	-4	5	-1	76	2	11	1	106	10	3	1
17	-8	7	1	47	-12	5	1	77	-2	11	-1	107	14	3	-1
18	-8	5	1	48	12	5	-1	78	-6	11	1	108	2	3	1
19	-8	3	1	49	-4	3	1	79	-10	11	-1	109	-2	3	-1
20	-8	1	1	50	-12	3	-1	80	-14	11	1	110	-6	3	1
21	8	7	-1	51	4	3	-1	81	10	9	-1	111	-10	3	-1
22	8	5	-1	52	12	3	1	82	14	9	1	112	-14	3	1
23	8	3	-1	53	-4	1	1	83	6	9	1	113	2	1	-1
24	8	1	-1	54	-12	1	-1	84	2	9	-1	114	6	1	1
25	12	13	1	55	4	1	-1	85	-2	9	1	115	10	1	-1
26	4	13	-1	56	12	1	1	86	-6	9	-1	116	14	1	1
27	-4	13	1	57	14	15	1	87	-10	9	1	117	-2	1	1
28	-12	13	-1	58	10	15	-1	88	-14	9	-1	118	-6	1	-1
29	12	15	1	59	6	15	1	89	10	7	-1	119	-10	1	1
30	4	15	-1	60	2	15	-1	90	14	7	1	120	-14	1	-1

www.manaraa.com

2.9 Appendix 2.C Closed Form BER Result for I.I.D Rayleigh

The eigenvalue obtained in (2.43) in Appendix 2.B is for i.n.d case, thus the terms therein have subscript l to dentate the branches. In i.i.d case, we can drop the l subscript because each branch are identically distributed. We arrive at (2.44).

$$\begin{aligned} A(\beta_n|d) &= \frac{1}{2} - \frac{1}{2}[(\rho_R\alpha_h - \rho_I\alpha_v)a\sigma_c - \beta_n a\sigma_{\hat{c}}]\left(a^2[\sigma_c^2(1-\rho_R^2)\alpha_v^2 + \sigma_c^2(1-\rho_I^2)\alpha_h^2 \right. \\ &\left. -2\sigma_c^2\rho_R\rho_I\alpha_h\alpha_v - 2\beta_n\sigma_{\hat{c}}\sigma_c(\rho_R\alpha_h - \rho_I\alpha_v) + \beta_n^2\sigma_{\hat{c}}^2] + N_0\right)^{-1/2} \end{aligned} \tag{2.44}$$

By plugging this result back into (2.32), we obtain the closed-form BER for i.i.d Rayleigh case.

$$\begin{aligned} \bar{P}_M &= \frac{4}{\log_2 M}\{C_{\sqrt{M}} + \frac{1}{\sqrt{M}}\sum_{m=1}^{\sqrt{M}}\sum_{n=1}^{N_{\sqrt{M}}} w_n[A(\beta_n|\alpha_n, \sqrt{M}-2m+1)]^L \\ &\times \sum_{l=0}^{L-1}\binom{L+l-1}{l}[1 - A(\beta_n|\alpha_n, \sqrt{M}-2m+1)]^l\}. \end{aligned} \tag{2.45}$$

www.manaraa.com

CHAPTER 3. PERFORMANCE OF GSC COMBINER UNDER GENERALIZED FADING CHANNELS WITH IMPERFECT CHANNEL ESTIMATION

3.1 Introduction

Generalized selection combining [34–36] is a type of diversity receivers in which a subset of available diversity branches is selected and combined based on the branch SNRs. It bridges the gap between MRC and selection combining (SC), and is a very useful diversity combining technique for dense multipath channels, and has recently attracted a lot of research interest in many applications.

GSC involves an selection mechanism that the receiver will only combine the selected branches based on their SNR measurements. In the perfect CSI case, the combiner will select the branches that have the N highest SNRs. In practice, the adverse effect of ICE on the performance must be accurately evaluated and taken into account in the system design [10, 11, 13, 17, 37–40]. The additional difficulty for the analysis lies in how to quantify the ICE's effect on the selection of the available diversity branches for combining, in addition to its effect on the combining operation itself as in the MRC case.

One approach to evaluate the BER performance of GSC diversity receivers is to derive the PDF of the GSC combiner output SNR. The SNR dependent BER can then be obtained by plugging the SNR into the BER expressions for different modulation schemes. The actual BER for the certain modulation under a particular model of fading channels can be obtained by integrating the obtained BER expression over the PDF of the SNR. The main difficulty lies in how to obtain the correct SNR output statistics. Particularly important for ICE case is how to arrive at the effective SNR distribution which takes into account the effect of ICE under

www.manaraa.com

different fading channel conditions. A popular approach to evaluate the PDF of the diversity output SNR with ICE was provided in [37], which, however, involves a major approximation, as analytically illustrated and numerically verified in [39, 40]. Using the PDF result in [37], the performance of GSC diversity QAM with Gaussian weighting errors in an i.i.d. Rayleigh fading channel was analyzed in [38], which consequently involves a major approximation and may be regarded as a loose performance upper bound (see [40]). To our knowledge, an accurate BER result for M-QAM with GSC and ICE applicable to different fading channel types is not available in the literature. Even for the Rayleigh fading channel an exact closed-form BER expression for M-QAM diversity receivers with ICE is not known.

In this chapter, we take the approach to relate the BER performance of M-QAM with ICE to the signal-constellation-dependent effective GSC combiner output SNRs, and derive its MGF for independent channels. Based on this result we derive accurate BER expressions for square and rectangular M-QAM with GSC and ICE. Our new BER expressions are simple and elegant, and simplify to closed-form for the Rayleigh fading case. Furthermore, they provide new insight into the performance loss caused by ICE compared to the case of perfect CSI. Finally, we evaluate the performance of MMSE- and sinc-interpolator-based channel estimators with PSAM, and report some new observations.

3.2 System and Channel Model

3.2.1 Signal Model and Channel Estimation Error Model

We basically follow the same model for the M-QAM modulation schemes discussed in 2.2.1. We also follow the same framework introduced in 2.2.3 to model the effect of ICE.

3.2.2 GSC Combining

In GSC, there are a total of L available diversity branches, out of which we combine N branches with the highest SNRs. We call this GSC scheme GSC(L, N). Assuming all the branches have the same noise level, we rank the estimated channel coefficients $\{\hat{c}_l(i)\}_{l=1}^{N}$ by their instantaneous powers in a non-increasing order, such that $|\hat{c}_{(1)}(i)|^2 \geq |\hat{c}_{(2)}(i)|^2 \geq \cdots \geq$

www.manaraa.com

$|\hat{c}_{(N)}(i)|^2$. Here and throughout this chapter we use subscript (n) to denote the branch with the nth largest SNR. The signals and channel estimates of the first N strongest branches are selected and used to detect the data $d(i)$ per MRC rule. Accordingly, the complex decision variable for GSC is given by $\tilde{D} = \sum_{l=1}^{N} \hat{c}^*_{(l)}(i) y_{(l)}(i) / \sum_{l=1}^{N} |\hat{c}_{(l)}(i)|^2$. The transmitted symbol $d(i)$ can be recovered by comparing $\tilde{D}$ with the horizontal and vertical QAM decision boundaries [13, 14, 17].

The BER performance of the GSC combiner can be expressed in terms of the conditional BER $\tilde{P}_H(B_i|A_h, A_v)$ conditioned on the decision boundaries and transmitted constellation points. We can then obtain the signal-constellation-dependent BER by averaging the conditional BER obtained in (2.13).

Next, we derive the conditional BER $\tilde{P}_H(B_i|A_h, A_v)$ for PAM by evaluating the signal-constellation-dependent effective SNRs for ICE. We assume Gray bit-mapping throughout this chapter. Once we obtain the signal-constellation-dependent effective SNRs for ICE, the conditional BER can then be obtained by integrating out the SNR with regard to their respective distributions under different fading models. The average BER for the GSC receiver can then obtained by plugging the results into (2.17) for the rectangular M-QAM case. In the following sections, we first look at some of the existing results on the MGF for the SNR output of GSC under CSI case. Aided by this result, we then develop the MGF of the effective SNR under the ICE case.

3.3 MGF of GSC Output SNR Under CSI

In this section, we looked into the problem of obtaining the MGF of the GSC output SNR over generalized fading channels. For a GSC(L, N) combiner, the ordered SNR vector from the N selected branches is represented as: $\hat{\gamma} = [\gamma_{(1)}, \gamma_{(2)}, \ldots, \gamma_{(N)}]^T$ and its joint PDF is given in [46] and [36] as:

$$f_{\gamma_{(1)},\ldots,\gamma_{(N)}}(y_1, \ldots, y_N) = \sum_{\substack{n_1,\ldots,n_N \\ n_1 \neq n_2 \neq \ldots \neq n_N}} f_{n_1}(y_1) \ldots f_{n_N}(y_N) \prod_{l'=N+1}^{L} F_{n_{l'}}(y_N) \tag{3.1}$$

www.manaraa.com

Here, the $y_1, \ldots, y_N$ are the SNRs of the diversity branches with y_1 being the largest SNR. The indexes $n_1, \ldots, n_N$ are the N branches that are selected out of the total L diversity branches. Here the $f_{n_k}(y)$ is the PDF of the output SNR of the n_kth diversity branch, where $k = 1, \ldots, L$. $F_{n_{l'}}(y)$ is the corresponding CDF.

Specific PDF expressions for generalized fading channels such as Rayleigh, Rician, and Nakagami-m fading channels that are used to evaluate the joint PDF in (3.1) can be found in Table I in [36] and also in [35], relist here in the first column of Table 3.1. We express the GSC output SNR as $\gamma_s = \sum_{k=1}^{N} \gamma_{(k)}$, and its MGF is defined as $\Phi_{\gamma_s}(s) = E[e^{-\gamma_s s}]$. Using joint PDF results in (3.1), the MGF for the GSC output under CSI case is given in [36] as:

$$\Phi_{\gamma_s}(s) = \sum_{\substack{n_1,\ldots,n_N \\ n_1 \neq n_2 \neq \ldots \neq n_N}} \sum_{n_N} \int_0^\infty e^{-sx} f_{n_N}(x) \left[\prod_{l=1}^{N-1} \Phi_{n_l}(s,x) \right] \left[\prod_{l'=N+1}^{L} F_{n_{l'}}(x) \right] dx \tag{3.2}$$

where $\Phi_{n_l}(s,x)$ is the complementary incomplete MGF expression given by:

$$\Phi_{n_l}(s,x) = \int_x^\infty f_{n_l} e^{-sy} dy \tag{3.3}$$

The closed-form expression of the complementary incomplete MGF for different fading cases are presented in the second column of Table 3.1. The summation $\sum_{\substack{n_1,\ldots,n_N \\ n_1 \neq n_2 \neq \ldots \neq n_N}} \sum_{n_N}$ means the $\binom{L}{N-1}$ possible combinations of selecting the $(N-1)$ branches with the largest SNRs out of the total L branches, and the summation $\sum_{n_N}$ denotes the branch index n_N is selected from the pool of remaining $L - N + 1$ available branches.

3.4 Constellation-Dependent Effective SNRs

In this section, we derive the MGF for the QAM GSC effective output SNR (dependent on d and B_i) with ICE, which allows us to obtain the conditional BER $\tilde{P}_H(\beta_i|\alpha_h, \alpha_v)$.

Given that $d = (\alpha_h + j\alpha_v)a$, $y_{(l)} = c_{(l)}d + n_{(l)}$, and $c_{(l)} = \hat{c}_{(l)} + z_{(l)}$, for $l = 1, \ldots, N$, we obtain that

$$\tilde{D}_R = \sum_{l=1}^{N} \mathrm{Re}\left(\hat{c}^*_{(l)} y_{(l)}\right) / \sum_{l=1}^{N} |\hat{c}_{(l)}|^2 = \mathrm{Re}(d) + \tilde{n}_R = a\alpha_h + \tilde{n}_R. \tag{3.4}$$

www.manaraa.com

Fading Type	PDF expressions	Incomplete MGF expressions
Rayleigh	$\frac{1}{\bar{\gamma}_{n_k}} \exp(\frac{-y}{\bar{\gamma}_{n_k}})$	$1/(1+s\bar{\gamma}_{n_k}) \exp(-x[s+1/\bar{\gamma}_{n_k}])$
Rician	$\frac{1+K_{n_k}}{\bar{\gamma}_{n_k}} \exp(-K_{n_k} - \frac{(1+K_{n_k})y}{\bar{\gamma}_{n_k}})$ $\cdot I_0(2\sqrt{K_{n_k}(K_{n_k}+1)y/\bar{\gamma}_{n_k}})$	$\frac{1+K_{n_k}}{1+K_{n_k}+s\bar{\gamma}_{n_k}} \exp\left(-\frac{sK_{n_k}\bar{\gamma}_{n_k}}{1+K_{n_k}+s\bar{\gamma}_{n_k}}\right)$ $\cdot Q_1\left(\sqrt{\frac{2K_{n_k}(K_{n_k}+1)}{K_{n_k}+1+s\bar{\gamma}_{n_k}}}, \sqrt{2(s\bar{\gamma}_{n_k}+K_{n_k}+1)x/\bar{\gamma}_{n_k}}\right)$
Nakagami-m	$(\frac{m_{n_k}}{\bar{\gamma}_{n_k}})^{m_{n_k}} \frac{y^{m_{n_k}-1}}{\Gamma(m_{n_k})} \exp(-\frac{m_{n_k}}{\bar{\gamma}_{n_k}}y)$	$\frac{1}{\Gamma(m_{n_k})}[\frac{m_{n_k}}{m_{n_k}+s\bar{\gamma}_{n_k}}]^{m_{n_k}} \Gamma(m_{n_k}, x[s+m_{n_k}/\bar{\gamma}_{n_k}])$

Table 3.1 The PDF and incomplete MGF expressions for the SNR in the n_kth branch (for $k = 1, \ldots, L$) over Rayleigh, Rician, and Nakagami-m fading channels. In the table, $\bar{\gamma}_{n_k}$ is the average SNR per branch. For the Rician fading channels, K_{n_k} is the Rice-K factor, $I_0(x)$ is the zeroth-order modified Bessel function of the first kind, and $Q_1(a,b)$ is the first-order Marcum-Q function defined as $Q_1(a,b) = \int_b^\infty xe^{-(x^2+a^2)/2} I_0(ax)dx$. For the Nakagami fading channel, m_{n_k} is the fading parameter, $\Gamma(a,x)$ is the incomplete Gamma function defined as $\Gamma(a,x) = \int_x^\infty e^{-t}t^{a-1}d\,t$, and $\Gamma(m)$ is the gamma function.

where $\tilde{n}_R = \text{Re}\left[\sum_{l=1}^N \hat{c}_{(l)}^*(z_{(l)}d + n_{(l)}) / \sum_{l=1}^N |\hat{c}_{(l)}|^2\right]$.

Applying (3.4) in (2.13) leads to

$$\begin{aligned} \tilde{P}_H(\beta_i|\alpha_h, \alpha_v) &= P\{\tilde{n}_R < -|\beta_i - \alpha_h|a\} \\ &= P\left\{\text{Re}\left(\sum_{l=1}^N \hat{c}_{(l)}^*[z_{(l)}d + n_{(l)}]\right) < -|\beta_i - \alpha_h|a \sum_{l=1}^N |\hat{c}_{(l)}|^2\right\} \end{aligned} \tag{3.5}$$

The equation above leads to the effective GSC output SNR with ICE (conditioned on d and β_i) as

$$\gamma_{\text{ICE}|d,\beta_i}^{\text{GSC}} = (|\beta_i - \alpha_h|a)^2 / \text{var}\{\tilde{n}_R\},$$

which, after some simplifications, yields

$$\gamma_{\text{ICE}|d,\beta_i}^{\text{GSC}} = S_{0,\text{GSC}}/(2N_{0,\text{GSC}}), \tag{3.6}$$

where $S_{0,\text{GSC}} = |\beta_i - \alpha_h|^2 a^2 (\sum_{l=1}^N |\hat{c}_{(l)}|^2)^2$ and $N_{0,\text{GSC}} = \text{var}\left\{\text{Re}(\sum_{l=1}^N \hat{c}_{(l)}^*[z_{(l)}d + n_{(l)}])\right\}$. We have $\tilde{P}_H(\beta_i|\alpha_h, \alpha_v) = \int_0^\infty Q(\sqrt{\gamma}) f_{\gamma_{\text{ICE}|d,\beta_i}^{\text{GSC}}}(\gamma)d\gamma$, where $f_{\gamma_{\text{ICE}|d,\beta_i}^{\text{GSC}}}(\gamma)$ is the PDF of $\gamma_{\text{ICE}|d,\beta_i}^{\text{GSC}}$.

www.manaraa.com

Using the property that $\hat{c}_l$, z_l, and n_l are mutually independent, and that $(z_l + n_l)$ is a zero-mean circularly symmetric Gaussian noise with variance $(1-|\rho|^2)\sigma_c^2 + N_0$, we obtain that conditioned on $\hat{c}_l$, $N_{0,\mathrm{GSC}} = \frac{1}{2}\sum_{l=1}^{N} |\hat{c}_{(l)}|^2((1-|\rho|^2)|d|^2 + N_0)$. Thus, it follows from (3.6) that

$$\gamma_{\mathrm{ICE}|d,\beta_i}^{\mathrm{GSC}} = \frac{(\beta_i - \alpha_h)^2 E_a \sum_{l=1}^{N} |\hat{c}_{(l)}|^2}{(1-|\rho|^2)\sigma_c^2|d|^2 + N_0}, \tag{3.7}$$

With the assumption that $E[|\hat{c}_{(l)}|^2] = |\rho|^2 E[|c_{(l)}|^2]$, and $\hat{c}_{(l)}$ and $c_{(l)}$ have the same distributions (e.g., with identical Rician-K or Nakagami-m factors), we can obtain

$$\gamma_{\mathrm{ICE}|d,\beta_i}^{\mathrm{GSC}} = \frac{|\rho|^2(\beta_i - \alpha_h)^2 E_a \sum_{l=1}^{N} \gamma_{(l)}}{(1-|\rho|^2)|d|^2\bar{\gamma} + 1} \tag{3.8}$$

where $\bar{\gamma} = \sigma_c^2/N_0$ is the input average SNR per branch, and $\gamma_{(l)}$ is the lth largest input SNR. Equation (3.8) gives the QAM GSC effective output SNR with ICE, and it is constellation and boundary-dependent. Strictly speaking, $\hat{c}_{(l)}$ and $c_{(l)}$ will have the same distributions only under Rayleigh fading conditions, but it is a very accurate approximation for Rician and Nakagami fading channels nonetheless.

Using a procedure similar to that for deriving (3.8), we can show that the effective SNR at the lth branch now is

$$\gamma_{\mathrm{ICE},l|d,\beta_i} = \frac{|\rho|^2(\beta_i - \alpha_h)^2 E_a \gamma_l}{(1-|\rho|^2)|d|^2\bar{\gamma} + 1} \tag{3.9}$$

where $\gamma_l = |c_l|^2/N_0$ is the instantaneous input SNR at the lth branch. For the perfect CSI case, the constellation-dependent SNR at the lth branch is given by

$$\gamma_{\mathrm{CSI},l|d,\beta_i} = (\beta_i - \alpha_h)^2 E_a \gamma_l \tag{3.10}$$

Using the results (3.2) for the GSC output SNR in the CSI case [35,36], we can obtain the MGF of (3.8) for fading channels (valid for, e.g., Rayleigh, Rician, and Nakagami fading) as

$$\Phi_{\gamma_{\mathrm{ICE}|d,\beta_i}^{\mathrm{GSC}}}(s) = N\binom{L}{N}\int_0^\infty e^{-sx} f_{\gamma_{\mathrm{ICE}|d,\beta_i}}(x)\left[\Phi_{\gamma_{\mathrm{ICE}|d,\beta_i}}(s,x)\right]^{N-1}\left[F_{\gamma_{\mathrm{ICE}|d,\beta_i}}(x)\right]^{L-N} dx. \tag{3.11}$$

where $f_{\gamma_{\mathrm{ICE}|d,\beta_i}}(x)$, $\Phi_{\gamma_{\mathrm{ICE}|d,\beta_i}}(s,x)$, and $F_{\gamma_{\mathrm{ICE}|d,\beta_i}}(x)$ are the PDF, truncated MGF, and CDF expressions for the effective SNR $\gamma_{\mathrm{ICE}|d,\beta_i}$ at each i.i.d. branch, and can be obtained by replacing $\bar{\gamma}$ with $\bar{\gamma}_{\mathrm{ICE}|d,\beta_i}$ in the relevant expressions in Table 3.1.

www.manaraa.com

Equation (3.11) leads to the conditional BER as

$$\tilde{P}_H(\beta_i|\alpha_h,\alpha_v) = \frac{1}{\pi}\int_0^{\pi/2} \Phi_{\gamma^{\rm GSC}_{{\rm ICE}|d,\beta_i}}\left(\frac{1}{\sin^2\theta}\right) d\theta \tag{3.12}$$

For Rayleigh fading, by using [34, eq. (28)] and [41, eq.(13)], we obtain a closed-form expression for (3.11) as

$$\Phi_{\gamma^{\rm GSC}_{{\rm ICE}|d,\beta_i}}(s) = \frac{1}{(1+s\bar{\gamma}_{{\rm ICE}|d,\beta_i})^{N+1}} \prod_{n=1}^{L-N} \frac{(-1)^n \binom{L}{N}\binom{L-N}{n}}{1+\frac{n}{N}+s\bar{\gamma}_{{\rm ICE}|d,\beta_i}}.$$

Furthermore, using [41, eq. (40)]), we can simplify (3.12) to a closed-form expression as

$$\tilde{P}_H(\beta_i|\alpha_h,\alpha_v) = \frac{1}{\pi}\binom{L}{N}\sum_{l=0}^{L-N}\frac{(-1)^l\binom{L-N}{l}}{1+l/N} \times I_{N-1}\left(\pi/2;\bar{\gamma}_{{\rm ICE}|d,\beta_i},\frac{\bar{\gamma}_{{\rm ICE}|d,\beta_i}}{1+l/N}\right) \tag{3.13}$$

where $I_n(\theta;c_1,c_2)$ is defined as $I_n(\theta;c_1,c_2) = \frac{1}{\pi}\int_0^\theta (\frac{\sin^2\phi}{\sin^2\phi+c_1})^n(\frac{\sin^2\phi}{\sin^2\phi+c_2})d\phi$, which has a closed-form expression given by [41, eq. (79)].

Some comments are in order. First, a comparison of (3.9) and (3.10) shows that the ASNR loss per branch caused by ICE at the GSC output is given by

$$\kappa(\gamma) = \frac{(1-|\rho|^2)|d|^2\bar{\gamma}+1}{|\rho|^2}. \tag{3.14}$$

For a larger $|d|^2$, the loss is larger. When $\rho = 1$, there is no loss. Second, when the ASNR $\bar{\gamma}$ increases, ρ may also increase, and the factor $(1-|\rho|^2)\bar{\gamma}$ will determine whether or not there is an error floor. If $(1-|\rho|^2)\bar{\gamma}$ is not upper-bounded, a detection error floor occurs.

3.5 Numerical Results

In Fig. 3.1, we present the BER for 16-QAM with GSC ($L = 4$) and PSAM, in Rayleigh and Rician fading channels ($K = 5$ dB) with i.i.d. branches, and with a symmetric observation window ($F_1 = F_2 = 10$, $P = 15$, and $i_{\rm off} = 8$). The MMSE-CE gives a performance close to that of the perfect CSI case, and the SNR loss is within 2.5 dB in both Rayleigh and Rician channels for all SNRs shown in the figure. The BER of sinc-CE with Hamming window (sinc-Hamm) is uniformly worse than that of MMSE-CE, with an additional SNR loss close to 1 dB. The sinc-CE with rectangular window (sinc-Rect) gives the worst performance, and entails an error floor at medium-to-high SNRs.

www.manaraa.com

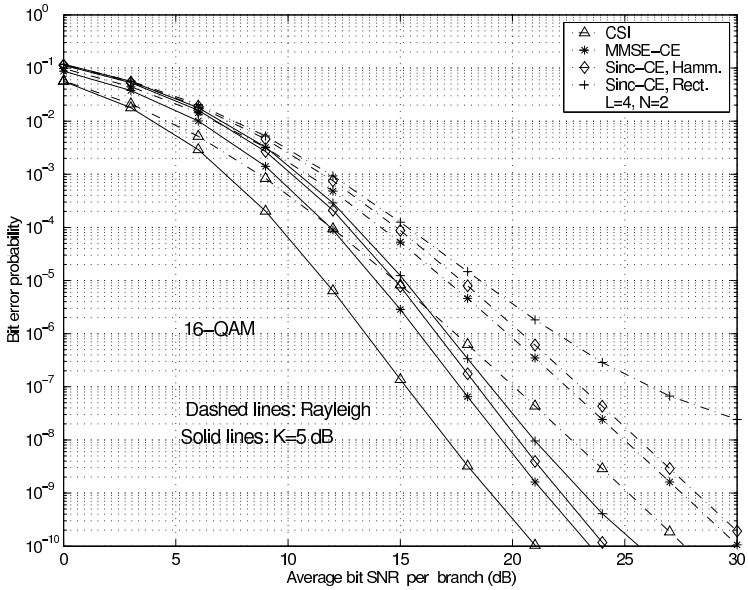

Figure 3.1 BER versus the average bit SNR per branch for the 16-QAM GSC receiver with CSI, MMSE- and Sinc-interpolator-based (with rectangular and Hamming windows) channel estimators, respectively. Rayleigh and Rician ($K = 5$ dB) fading. $L = 4$, $N = 2$, $P = 15$, $i_{\text{off}} = 8$, $F_1 = F_2 = 10$, $B_f T_s = 0.02$.

Next, in Fig. 3.2, we present the BER for the 64-QAM GSC receiver ($L = 4$) with CSI and MMSE-CE, respectively, in a Rayleigh fading channel. The performance loss for MMSE-CE compared to CSI is almost constant for different N. The SNR loss of 64-QAM with MMSE-CE is very close to that of 16-QAM with MMSE-CE.

Finally, we show the effect of the pilot symbol insertion interval P on the BERs of 16-QAM with GSC in an i.i.d. Rayleigh channel in Fig. 3.3, where we assume $F_1 = F_2 = 10$, and $i_{\text{off}} = \lfloor P/2 \rfloor$, e.g. the data symbol is in the middle of two pilot symbols. The result shows that when P increases from 2 to 14, the BER of MMSE-CE degrades slowly. When $P = 14$, the BERs of the MMSE-CE starts to grade very fast as P increases. The same trends are observed for different N.

In summary, our results above suggest that (1) the performance gap between sinc-Hamm-CE and MMSE-CE highly depends on the PSAM parameters (e.g., P, F, i_{off}), but is less sensitive to the SNR (before the error floor occurs). Sinc-CE with Hamming window may have

www.manaraa.com

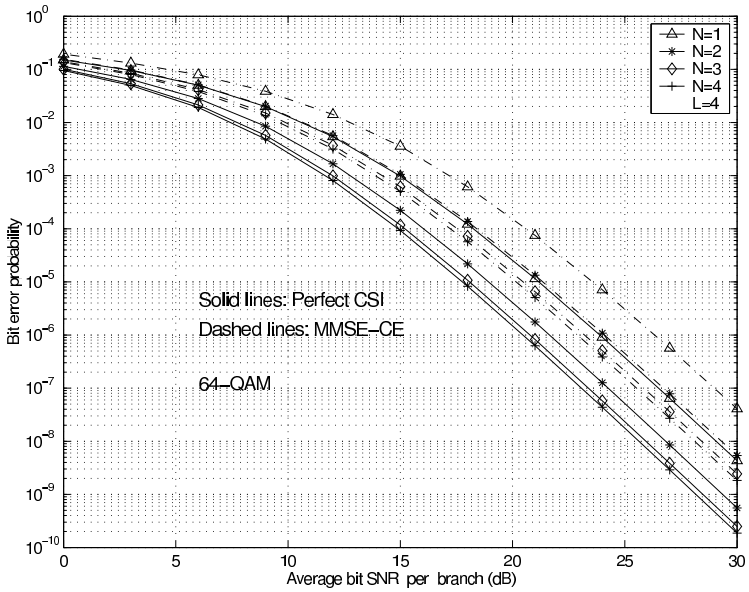

Figure 3.2 BER versus the average bit SNR per branch for the 64-QAM GSC receiver with CSI and MMSE-CE, respectively. Rayleigh fading channel. $L = 4$, $P = 15$, $i_{\text{off}} = 8$, $F_1 = F_2 = 10$, and $B_f T_s = 0.02$.

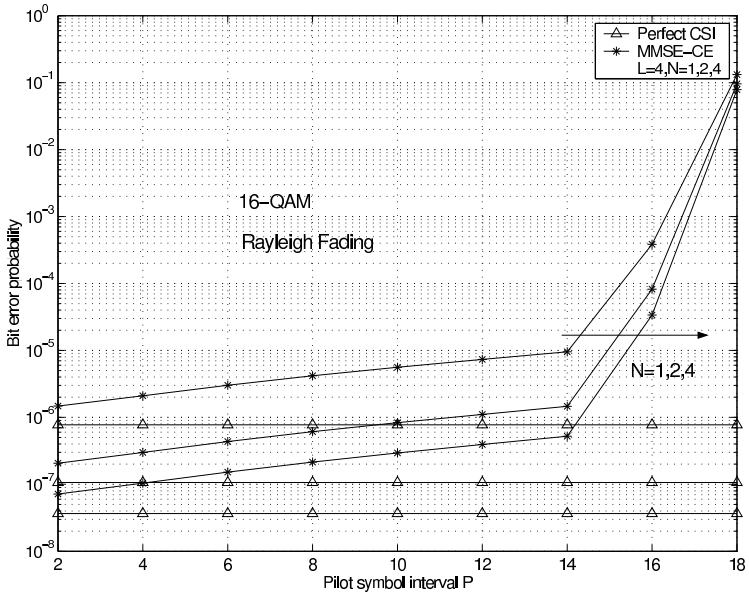

Figure 3.3 BER versus P for 16-QAM with MMSE-CE. Rayleigh fading channel. $i_{\text{off}} = \lfloor P/2 \rfloor$, $F_1 = F_2 = 10$, $\bar{\gamma}_b = 20$ dB, and $B_f T_s = 0.03$.

www.manaraa.com

a performance very close to that of MMSE-CE for some setting of PSAM parameters (P, F), but with a substantial gap for some other case. (2) The trends for BER vs. P can be very different for different i_{off}, P, F_1, F_2, but they may be quite similar for different diversity order L and signal size M.

3.6 Summary

In this chapter, we identify a novel approach for accurate BER evaluation of M-QAM GSC diversity receivers with PSAM and MMSE-CE in generalized fading channels (including Rayleigh, Rician and Nakagami-m and Nakagami-q fading). We concentrate our efforts on deriving the constellation-dependent effective SNR formulas for M-QAM with ICE, and then integrate the BER expression over the SNR distribution for different fading channel models respectively. Our new BER formulas are general and easy to evaluate, and provided new insight into the performance loss caused by ICE. As an example, we simplify the BER results for Rayleigh fading case to a closed-form expression, which was not available in the literature. One of the important implications of this result is that we can now use the analytical means to evaluate the relation of the anticipated BER performance and the type of practical channel estimators used (such as MMSE- and sinc-interpolator-based channel estimators) and their parameters, in Rician and Nakagami-m or Nakagami-q fading channels. The evaluation process of our derived analytical results are in the form of either closed-form (Rayleigh) or easy-to-compute integrations.

www.manaraa.com

CHAPTER 4. GENERALIZED SELECTION MULTIUSER DIVERSITY

4.1 Introduction

Many large-scale wireless communication systems such as cellular networks, WLAN and WiMax systems, are multiuser systems that divide total system resources among all users. One of the central problems in these systems is how to schedule users to share the resources effectively, thus providing better coverage and higher capacity in terms of number of users supported and data throughput. Compared to single user communication, multiuser systems in fading channels can provide an additional diversity gain: multiuser diversity gain, a term coined by Knopp and Humblet in [64]. We can exploit this extra diversity by designing CARA type multiuser scheduling algorithms. Consider the uplink channel in a single cell in a cellular multiuser network. The channel was considered to be a time-varying fading channel and it was tracked at both the receiver and the transmitter (via feedback) and TDMA scheme was utilized. Intuitively, the multiuser diversity comes from the fact that in a system with many users and whose channels change independently, there is more likely that a specific user's channel is near its peak SNR at any one time slot. If scheduler always select the "best" user to communicate to base station at any time slot, total system capacity is maximized because the channel resources are given to the user who can best exploit it at all time. It is noted that similar result for downlink was presented in [53–59, 78].

TDMA is assumed in most of the above-mentioned schemes, where one and only one "best" user could transmit at a given time slot, using all the available power. As proved in [64], such a scheme will provide maximum total information-theoretic capacity. This result will translate to maximal total data throughput only under certain conditions. However, for a CDMA system with a fixed spreading gain and the assumption that each user could be assigned one

www.manaraa.com

codeword at any given time slot, scheduling one user at a time is no longer optimal. It's readily feasible to schedule multiple users for transmission in many wireless networks, such as the wideband CDMA (WCDMA) [68] and ultra-wideband (UWB) networks [62, 63]. In those systems, multiple parallel channels are available due to the availability of multiple orthogonal (or quasi-orthogonal) spreading code and thus a parallel multiuser scheduling design is possible and sometimes required. In [68], scheduling algorithms which maximize the sum throughput of all the L users were proposed. In these schemes, the scheduling for each time slot requires to solve a multi-dimensional nonlinear optimization problem for optimal power allocation, multi-code assignment, and adaptive modulation. In [67], the authors proposed to schedule a number of users for simultaneous transmission based on their instantaneous normalized SNRs. The performance gain with respect to the conventional CDMA systems is evaluated based on the Shannon information capacity criterion.

In this chapter, we propose a novel generalized selection multiuser diversity (GSMuD) scheme where multiple users are scheduled to share the system resources according to their respective channel conditions. Here "generalized" is in reference to legacy selective multiuser diversity (SMuD) where only one user is selected for transmission in any time slot. In GSMuD, the N_c out of total L users with the largest received SNR will be scheduled for communication. Our goal in designing GSMuD is to recognize the need to provide better total system throughput under practical AMC scheme and generalized fading channels, and under the practical assumption that each user will be assigned one channel at a time. We also maintain the prescribed QoS (in terms of BER and PER) levels of the scheduled users. Our approach in the design and analysis is based on obtaining the marginal distributions of SNRs of ordered users, and thus determine the optimal AMC modulation-switching SNR threshold to guarantee the desired QoS. We also design an equal power allocation scheme that automatically shut down certain users in poor fading conditions and redirect the available system power to other users.

We observe that many legacy selective multiuser scheduling systems are based on the assumption that perfect CSI is available at the receiver and that such information is fed back to the scheduler at the BS perfectly. In practice, it's not always possible to obtain perfect

www.manaraa.com

CSI at the receiver. There are some results in the literature discussing effect of ICE on the performance of the SMuD scheduler. Performance results for the effects of limited-rate feedback of received SNR from the MS to BS, with SMuD schedulers using absolute-SNR (**a**-SNR) and normalized-SNR-based (**n**-SNR) thresholding are obtained in [65, 66]. The analysis showed that the essential part of the scheduling gain could be preserved with the substantially reduced feedback load. In [81], the effect of outdated channel feedback on the performance of multiuser diversity with adaptive modulation and absolute- and normalized-SNR-based ranking was evaluated.

We observe that the ICE at the multiple receivers significantly affects the design and analysis of multiuser scheduling. However, none of the existing results in literature explicitly proposed new scheduler design approaches in light of their analysis on the effects of ICE on the legacy selective multiuser schedulers. We argue that the adverse effect of ICE must be included in the GSMuD design to guarantee the QoS, such as the target PER and the spectral efficiency (SE). Thus, in later part of this chapter, the effect of ICE caused by the MMSE channel estimator are studied and the GSMuD algorithms are developed in light of the knowledge that ICE is present in the system. In our design and analysis, the SNR-ranking now is based on the effective SNRs of the users after the effect of ICE is included. To guarantee the target PER in the presence of channel estimation errors, the AMC design and throughput-rate calculation are optimized on the effective SNRs rather than the input SNRs. In our analysis, we consider the practical scenario where different users could experience different fading severity, or even different families of fading channels.

The major contributions of this work include: (1) We derive the statistics of the ordered effective-SNR set due to ICE for L users, including the PDF and MGF of the Nth largest SNR ($N = 1, 2, \ldots, L$), and then evaluate the error and outage probabilities of each ranked user; (2) We derive the individual-rate and sum-rate for the SNR-ranked users including the effect of adaptive modulation and power allocation. The multiuser scheduling gain, defined as the ratio of the GSMuD sum-rate with respect to that of conventional CDMA systems, is also calculated; (3) Based on the derived BER, and outage probabilities of each ranked user

www.manaraa.com

and the individual-rate and sum-rate in CSI and ICE case, we design an AMC algorithm and determined its optimal switching SNR threshold, and (4) Based on the above results, we design a multiuser scheduling and power allocation scheme. The CSI case can be obtained as a special case of our design and analysis.

4.2 System Model

4.2.1 GSMuD System Model

In the downlink of a typical centralized wireless network (e.g. synchronous CDMA downlink channels), there are a total of L users awaiting for channel assignment. For simplicity, we assume the queue buffer is not empty at any time for every user, and the data link layer design problem, as that considered in [76, 77], is not studied in this chapter.

In our model, we assume the multiuser signals are orthogonal, and the mutual interference and external interference [67, 68, 79] are not explicitly modeled. The scheduler ranks the instantaneous SNRs of all the L users in a descending order, denoted by $\gamma_{(1)}, \gamma_{(2)}, \ldots, \gamma_{(L)}$ (with $\gamma_{(1)} \geq \gamma_{(2)} \geq \cdots \geq \gamma_{(L)}$), where $\gamma_{(k)}$ is the kth largest SNR. The scheduler chooses the N_c users with the largest SNRs for simultaneous transmission in the next available time slot (a packet duration). We assume a block-wise static fading channel, for which the channel remains constant for a packet duration, and then varies from one block to another.

The fading channels for different users may follow different fading types and the channel for different users may have different short-term mean signal strengths and channel parameters. We assume the total power at the BS is a constant, and the available transmission power is allocated equally among the selected users. User traffic is separated by different orthogonal spreading code. We assume that each user can use one such spreading code at any given time slot. Due to the limited number of available orthogonal spreading codes there are a maximum of N_c users which can be scheduled for simultaneous transmission at any time slots. As we will show later in this chapter, to achieve a target PER and a minimum throughput requirement for each selected user, the number of simultaneous users could be less than N_c.

For each selected user, adaptive modulation with different levels of M-QAM or BPSK is

www.manaraa.com

employed. For the AMC design, our method to find the SNR thresholds for all the operating modes is adopted from that proposed in [45], but with the effect of SNR-ranking being included. This design guarantees that the average target PER is achieved for all the operating modes (except the non-transmission mode). In AMC the power for each user remains constant and only the signal constellation size is adapted according to the channel conditions.

4.2.2 Channel Estimation Error Model

We employ the PSAM type of channel estimator in the modeling of ICE. In each packet, F pilot symbols (each with power $P_{\rm PS}$) are inserted. The remaining N_p symbols are data symbols (payload). Denote the channel gain of the kth user in pth packet as $c_k(p)$, which remains constant over a packet duration and varies from one packet to another. $c_k(p)$ may follow different types of fading distributions, such as Rayleigh, Nakagami-m, -q, and Weibull models [125]. Furthermore, the channel gains for different users may have different mean signal strengths and fading parameters.

Let $\hat{c}_k(p)$ be the received feedback of $c_k(p)$. If we assume a perfect feedback process, the imperfect channel estimates is entirely contributed by the channel estimator. Define $\rho = E[\hat{c}_k^*(p)c_k(p)]/[\sigma_c\sigma_{\hat{c}}]$. For the MMSE-CE, ρ_k may be obtained as in [31] and [8]:

$$\rho_k = \sqrt{\mathbf{1}_{F\times 1}^T(\mathbf{1}_{F\times F} + \mathbf{I}_F/(P_{\rm PS}\bar{\gamma}_k))^{-1}\mathbf{1}_{F\times 1}} \tag{4.1}$$

where $\mathbf{1}_{M\times N}$ and $\mathbf{I}_F$ are the $M \times N$ all-one matrix and the $F \times F$ identity matrix, and superscripts T and -1 denote the transpose and matrix inverse, respectively. We have

$$c_k(i) = \hat{c}_k(i) + z_k(i) \tag{4.2}$$

where $z_k(i)$ is an effective channel estimation error with zero mean and variance $(1-|\rho_k|^2)\sigma_{c_k}^2$. Equation (4.2) is exact for MMSE-CE over Rayleigh channels, and is a very tight approximation for Nakagami-m, -q, and Weibull channels [5].

Following what we have developed for GSC output effective SNR, for (I_1, I_2)-QAM modulation formats, $\tilde{\gamma}_k(d)$ (the effective SNR including the effect of ICE for a signal point with

www.manaraa.com

modulus d) was given in (3.9), rewritten here:

$$\tilde{\gamma}_k(d) = \beta_k(d)\gamma_k \tag{4.3}$$

where $\beta_k(d) = \frac{|\rho|^2}{(1-|\rho|^2)|d|^2\bar{\gamma}_k+1}$, and $|d|^2 = (i_1^2 + i_2^2)E_a$, for $i_1 = \{\pm 1, \ldots, \pm(I_1 - 1)\}$ and $i_2 = \{\pm 1, \ldots, \pm(I_2 - 1)\}$, and again E_a is used to normalized the total symbol energy to unity. For rectangular (I_1, I_2)-QAM $E_a = \frac{3}{I_1^2+I_2^2-2}$ [14], which reduces to $E_a = \frac{3}{2(M-1)}$ for square M-QAM (where $M = I_1 I_2$). To utilize (4.3) for AMC design, we need to obtain a relation between the effective SNR $\tilde{\gamma}_k$ and the input SNR γ_k independent of d. Using the numerical search approach proposed in [31], we found the optimal fixed coefficient to replace the constellation-dependent d in (4.3). The obtained "fixed" relationship will most accurately approximate the BER obtained by simulation. The tight approximation for d obtained are

$$\tilde{\gamma}_k \simeq \beta_k \gamma_k \tag{4.4}$$

where $\beta_k = \begin{cases} \frac{|\rho|^2}{(1-|\rho|^2)\bar{\gamma}_k+1} & M = 2, 4 \\ \frac{|\rho|^2}{(1-|\rho|^2)1.3\bar{\gamma}_k+1} & M > 4 \end{cases}$

Given a target PER value $\mathrm{PER}_{\mathrm{th}}$, we need to find target SER $P_{s,\mathrm{th}}$ and bit error rate $P_{b,\mathrm{th}}$ for the design of adaptive modulation. For uncoded transmission and medium-to-high ASNRs, $\mathrm{PER}_{\mathrm{th}}$ is related to $P_{s,\mathrm{th}}$ and $P_{b,\mathrm{th}}$ by

$$\mathrm{PER}_{\mathrm{th}} = 1 - (1 - P_{s,\mathrm{th}})^{N_s} \simeq 1 - (1 - P_{b,\mathrm{th}})^{N_b} \tag{4.5}$$

Consequently,

$$P_{s,\mathrm{th}} = 1 - (1 - \mathrm{PER}_{\mathrm{th}})^{1/N_s} \tag{4.6}$$

and $P_{b,\mathrm{th}} \simeq P_{s,\mathrm{th}} / \log_2 M_j$. For coded transmission, an empirical fitting between the ASNR and the PER may be employed, such as that given in [45, eq. (5)].

4.3 Performance Metrics

4.3.1 Statistics of the Ranked Users

The scheduler will rank the SNRs of all L users in a descending order and select no more than N_c users for transmission. For convenience, throughout this chapter we refer to the user

www.manaraa.com

with the Nth largest instantaneous SNR as *the* (N)*th user*.

In the presence of channel estimation errors, the scheduler will rank the effective SNRs of all L users, $\tilde{\gamma}_1, \ldots, \tilde{\gamma}_L$, in a descending order and select no more than N_c users for transmission. This is reasonable because the receiver could only rank the users based on the channel estimation $\hat{c}_k(p)$ instead of the actual channel coefficient $c_k(p)$ which is unknown to the scheduler. Throughout this chapter, we will assume that the channel estimation is not perfect. The result for the perfect CSI case can be obtained as a special case when $\rho = 1$ in (4.3).

For scheduling purpose, it is critical to evaluate the SER, BER and throughput of the (N)th user $(N = 1, \ldots, L)$, denoted by $P_{s,(N)}$, $P_{b,(N)}$, and $C_{(N)}$, respectively. Here, the evaluation of the SNR of the (N)th user is similar to but different from a problem of GSC studied in the literature [36,88,90,125] and in Chapter 3. In GSC, the first N largest SNRs are combined per MRC rule. For multiuser scheduling, however, we are interested in the marginal statistics of the Nth largest SNR only, for $N = 1, \ldots, L$. To approach this problem, we employ the MGF approach and tailor a result for order statistics given in [36] and in section 3.3 to the GSMuD model. Define the MGF for the Nth largest effective SNR as

$$\Phi_{\tilde{\gamma}_{(N)}}(s) = E[\exp(-\tilde{\gamma}_{(N)}s)] \tag{4.7}$$

We also define

$$\tilde{\gamma}_t(a_1, \ldots, a_{N-1}, a_N) = a_1\tilde{\gamma}_{(1)} + a_2\tilde{\gamma}_{(2)} + \ldots + a_N\tilde{\gamma}_{(N)}, \tag{4.8}$$

where $a_k \in (0, 1)$ for $k = 0, 1, \ldots, N$. When $a_k = 1$ for all k, $\tilde{\gamma}_t$ is the output SNR for GSC. We also observe that $\tilde{\gamma}_{(N)}(s) = \tilde{\gamma}_t(0, \ldots, 0, 1)$, which is useful for GSMuD. Below, we derive the MGF of $\tilde{\gamma}_t(a_1, \ldots, a_{N-1}, a_N)$, which yields the MGF of $\tilde{\gamma}_{(N)}(s)$ as a special case.

For convenience, we will rewrite the complementary incomplete MGF in (3.3) as

$$\Phi_{\tilde{\gamma}_l}(s, x) = \int_x^\infty f_{\tilde{\gamma}_l}(y)e^{-sy}dy \tag{4.9}$$

where $f_{\tilde{\gamma}_l}(x)$ is the PDF expression for the instantaneous SNR $\tilde{\gamma}_l$ for the lth user (before the SNR ranking). Note that $\Phi_{\tilde{\gamma}_l}(s, 0) = \Phi_{\gamma_l}(s)$, and $\Phi_{\tilde{\gamma}_l}(0, x) = 1 - F_{\tilde{\gamma}_l}(x)$, where $F_{\tilde{\gamma}_l}(x) = \int_0^x f_{\tilde{\gamma}_l}(y)d\,y$ is the CDF of the SNR $\tilde{\gamma}_l$. For simplicity, we also call $\Phi_{\tilde{\gamma}_l}(s, x)$ the truncated MGF (TMGF) in this chapter.

www.manaraa.com

Using a result on the order statistics of GSC given in [36, 46], we may express the joint PDF of $[\tilde{\gamma}_{(1)}, \tilde{\gamma}_{(2)}, \ldots, \tilde{\gamma}_{(N)}]$ as (for the i.n.d. users)

$$f_{\tilde{\gamma}_{(1)},\ldots,\tilde{\gamma}_{(N)}}(y_1, y_2, \ldots, y_N) = \sum_{\substack{n_1,\ldots,n_N \\ n_1 \neq n_2 \neq \ldots \neq n_N}} f_{\tilde{\gamma}_{n_1}}(y_1) f_{\tilde{\gamma}_{n_2}}(y_2) \cdots f_{\tilde{\gamma}_{n_N}}(y_N) \prod_{l'=N+1}^{L} F_{\tilde{\gamma}_{n_{l'}}}(y_N), \tag{4.10}$$

where $y_1, \ldots, y_N$, $f_{\tilde{\gamma}_{n_l}}(y)$, and $F_{\tilde{\gamma}_{n_{l'}}}(y)$ are defined similar to that of Section 3.3, only here it represents the statistics from different users instead of diversity branches.

Using a procedure similar to that for deriving the output SNR for GSC [36], we obtain the MGF of $\tilde{\gamma}_t(a_1, \ldots, a_N) = \sum_{k=1}^{N} a_k \tilde{\gamma}_{(k)}$ valid for i.n.d. users as

$$\Phi_{\tilde{\gamma}_t}(s) = \sum_{n_1,\ldots,n_N \in \mathcal{I}} \int_0^\infty e^{-s a_N x} f_{\tilde{\gamma}_{n_N}}(x) \left[\prod_{l=1}^{N-1} \Phi_{\tilde{\gamma}_{n_l}}(a_l s, x) \right] \left[\prod_{l'=N+1}^{L} F_{\tilde{\gamma}_{n_{l'}}}(x) \right] dx. \tag{4.11}$$

where $f_{\tilde{\gamma}_{n_l}}(y)$ is the PDF for the output SNR in the n_lth user, $l = 1, \ldots, L$. $F_{\tilde{\gamma}_{n_{l'}}}(y)$ is the CDF of the SNR of the $n_{l'}$th user. For example, for Nakagami-m fading channels,

$$f_{\tilde{\gamma}_l}(x) = \frac{1}{\Gamma(m_l)} (m_l / \bar{\tilde{\gamma}}_l)^{m_l} x^{m_l - 1} \exp(-m_l x / \bar{\tilde{\gamma}}_l),$$

where $\bar{\tilde{\gamma}}_l$ and m_l are the symbol ASNR and m-parameter of the lth user, respectively. In $\sum_{n_1,\ldots,n_N \in \mathcal{I}}$, $\mathcal{I}$ is the set for all combinations of $\{n_1, \ldots, n_L\}$ in which the subset $\{n_1, \ldots, n_N\}$ are the indices of N users with largest SNRs. Note that $\sum_{n_1,\ldots,n_N \in \mathcal{I}}$ is equivalent to $\sum_{\substack{n_1,\ldots,n_N \\ n_1 < n_2 < \ldots < n_N - 1}} \sum_{n_N}$, which was defined in [36]. Therefore, the summation in (4.11) contains $\binom{L}{N}$ terms in total.

By setting $a_1 = \cdots = a_{N-1} = 0$ and $a_N = 1$ in (4.11), we obtain the MGF of $\tilde{\gamma}_{(N)}$ as

$$\Phi_{\tilde{\gamma}_{(N)}}(s) = \sum_{n_1,\ldots,n_N \in \mathcal{I}} \int_0^\infty e^{-sx} f_{\tilde{\gamma}_{n_N}}(x) \times \left[\prod_{l=1}^{N-1} (1 - F_{\tilde{\gamma}_{n_l}}(x)) \right] \left[\prod_{l'=N+1}^{L} F_{\tilde{\gamma}_{n_{l'}}}(x) \right] dx, \tag{4.12}$$

where we used the equality that $\Phi_{\tilde{\gamma}_{n_l}}(0, x) = 1 - F_{\tilde{\gamma}_{n_l}}(x)$. The PDF, CDF and TMGF of $\tilde{\gamma}_l$ are easy to derive and related with those of CSI γ_l as

$$\begin{aligned} f_{\tilde{\gamma}_l}(x) &= \frac{1}{\beta_k} f_{\gamma_l}(x/\beta_k) \\ \Phi_{\tilde{\gamma}_l}(s, x) &= \Phi_{\gamma_l}(s\beta_k, x/\beta_k) \\ F_{\tilde{\gamma}_l}(x) &= F_{\gamma_l}(x/\beta_k) = 1 - \Phi_{\gamma_l}(0, x/\beta_k) \end{aligned}$$

www.manaraa.com

Here, f_{γ_l}, Φ_{γ_l}, and F_{γ_l} are the PDF, TMGF and CDF of the actual channel SNRs. Their expression over several types of fading channels have been derived and tabulated in Table 3.1. The marginal PDF of $\tilde{\gamma}_{(N)}$, $f_{\tilde{\gamma}_{(N)}}(x)$, may be obtained as follows. We compare (4.12) with the definition of the MGF $\Phi_{\tilde{\gamma}_{(N)}}(s) = \int_0^\infty e^{-sx} f_{\tilde{\gamma}_{(N)}}(x)dx$, and obtain the marginal PDF of $\tilde{\gamma}_{(N)}$ as

$$f_{\tilde{\gamma}_{(N)}}(x) = \sum_{n_1,\ldots,n_N \in \mathcal{I}} f_{\tilde{\gamma}_{n_N}}(x) \times \left[\prod_{l=1}^{N-1}(1 - F_{\tilde{\gamma}_{n_l}}(x))\right]\left[\prod_{l'=N+1}^{L} F_{\tilde{\gamma}_{n_{l'}}}(x)\right]. \tag{4.13}$$

For L i.i.d. users, (4.12) simplifies to

$$\Phi_{\tilde{\gamma}_{(N)}}(s) = \binom{L}{N} N \times \int_0^\infty e^{-sx} f_{\tilde{\gamma}}(x)[1 - F_{\tilde{\gamma}}(x)]^{N-1} F_{\tilde{\gamma}}(x)^{L-N} dx. \tag{4.14}$$

Consequently, the PDF of $\tilde{\gamma}_{(N)}$ for i.i.d. users is

$$f_{\tilde{\gamma}_{(N)}}(x) = \binom{L}{N} N f_{\tilde{\gamma}}(x)[1 - F_{\tilde{\gamma}}(x)]^{N-1} F_{\tilde{\gamma}}(x)^{L-N}. \tag{4.15}$$

Equations (4.13) and (4.15) will be used to calculate the statistics of the (N)th user with adaptive modulation.

4.3.2 Outage probabilities

The outage probability for the (N)th user with pre-specified SNR threshold $\tilde{\gamma}_{\text{th}}$ is defined as $P_{\text{OT},\tilde{\gamma}_{(N)}}(\tilde{\gamma}_{\text{th}}) = \int_0^{\tilde{\gamma}_{\text{th}}} f_{\tilde{\gamma}_{(N)}}(\tilde{\gamma})d\tilde{\gamma}$. Using a CDF evaluation technique [125] and the MGF of $\tilde{\gamma}_{(N)}$ derived in this chapter, an efficient formula to evaluate $P_{\text{OT},\tilde{\gamma}_{(N)}}(\tilde{\gamma}_{\text{th}})$ can be obtained, as

$$P_{\text{OT},\tilde{\gamma}_{(N)}}(\tilde{\gamma}_{\text{th}}) \simeq \frac{e^{A/2}}{2Q} \sum_{\beta=\pm(\pi/2-\pi/M)} \sum_{q=0}^{Q} \binom{Q}{q} \sum_{n=0}^{N+q} \frac{(-1)^n}{c_n} \times \text{Re}\left(\Phi_{\tilde{\gamma}_{(N)}}\left(-\frac{A + jn2\pi}{2\sqrt{\tilde{\gamma}_{\text{th}}}}\right)/(A + jn2\pi)\right) + E_{A,N,Q}, \tag{4.16}$$

where $E_{A,N,Q}$ is a remainder term that vanishes when Q becomes large, A is a constant to ensure the fast convergence of (4.16), and $c_n = 1$ for $n = 0$; $c_n = 0.5$ for $n = 1, \ldots, N + Q$.

For i.i.d. users, using the integration of parts we obtain a closed-form expression for $P_{\text{OT},\tilde{\gamma}_{(N)}}(\tilde{\gamma}_{\text{th}})$ as

$$P_{\text{OT},\tilde{\gamma}_{(N)}}(\tilde{\gamma}_{\text{th}}) = \binom{L}{N} N \sum_{n=0}^{N-1} (-1)^n \binom{N-1}{n} \times [F_{\tilde{\gamma}}(\tilde{\gamma}_{\text{th}})]^{L-N+n+1}/(L - N + n + 1). \tag{4.17}$$

www.manaraa.com

4.3.3 BER Performance Under Given Thresholding

We now derive the BER performance of the individual user with an arbitrary given set of thresholds. For the (N)th user with adaptive modulation and J operating modes, let the thresholds of the effective SNRs be denoted by $[\tilde{\gamma}_{\text{th},0}(N), \tilde{\gamma}_{\text{th},1}(N), \ldots, \tilde{\gamma}_{\text{th},J}(N), \tilde{\gamma}_{\text{th},J+1}(N)]$, where $\tilde{\gamma}_{\text{th},0}(N) = 0$ and $\tilde{\gamma}_{\text{th},J+1}(N) = \infty$. The constellation sizes for the J modes are given by $[M_1, M_2, \ldots, M_J]$. When $\tilde{\gamma}_{(N)} \in [\tilde{\gamma}_{\text{th},j}(N), \tilde{\gamma}_{\text{th},j+1}(N))$, the jth mode is selected with constellation size M_j, for $j = 1, \ldots, J$. When $\tilde{\gamma}_{(N)} \in [0, \tilde{\gamma}_{\text{th},1}(N))$, no data is transmitted for the (N)th user.

To determine the SNR threshold set $[\tilde{\gamma}_{\text{th},1}(N), \ldots, \tilde{\gamma}_{\text{th},J}(N))$, we need to evaluate the probability given by

$$\begin{aligned} P_j(N) &= \Pr\{\tilde{\gamma}_{(N)} \in [\tilde{\gamma}_{\text{th},j}(N), \tilde{\gamma}_{\text{th},j+1}(N))\} \\ &= \int_{\tilde{\gamma}_{\text{th},j}(N)}^{\tilde{\gamma}_{\text{th},j+1}(N)} f_{\tilde{\gamma}_{(N)}}(\tilde{\gamma}) d\tilde{\gamma}. \end{aligned} \tag{4.18}$$

For the general case,

$$P_j(N) = P_{\text{OT},\tilde{\gamma}_{(N)}}(\tilde{\gamma}_{\text{th},j+1}(N)) - P_{\text{OT},\tilde{\gamma}_{(N)}}(\tilde{\gamma}_{\text{th},j}(N)) \tag{4.19}$$

where $P_{\text{OT},\tilde{\gamma}_{(N)}}(\tilde{\gamma}_{\text{th}})$ is the outage probability given in (4.17).

For the i.i.d. case we obtain

$$\begin{aligned} P_j(N) &= \int_{\tilde{\gamma}_{\text{th},j}(N)}^{\tilde{\gamma}_{\text{th},j+1}(N)} \binom{L}{N} N f_{\tilde{\gamma}}(x)[1 - F_{\tilde{\gamma}}(x)]^{N-1} \times F_{\tilde{\gamma}}(x)^{L-N} dx \\ &= \binom{L}{N} N \sum_{n=0}^{N-1} (-1)^n \binom{N-1}{n} \times \int_{\tilde{\gamma}_{\text{th},j}(N)}^{\tilde{\gamma}_{\text{th},j+1}(N)} f_{\tilde{\gamma}}(x)[F_{\tilde{\gamma}}(x)]^{L-N+n} dx. \end{aligned} \tag{4.20}$$

Define $I_k = \int_{r_1}^{r_2} f(x)[F(x)]^k dx$. Using the integration by parts we can show that:

$$I_k = [F(x)]^{k+1} \,|_{r_1}^{r_2} - k \int_{r_1}^{r_2} f(x)[F(x)]^k dx = [F(r_2)]^{k+1} - [F(r_1)]^{k+1} - kI_k, \tag{4.21}$$

and thus $I_k = \frac{1}{1+k}\left[[F(r_2)]^{k+1} - [F(r_1)]^{k+1}\right]$. Substituting this result into (4.20), we get a closed-form expression as

$$\begin{aligned} P_j(N) = \binom{L}{N} N \sum_{n=0}^{N-1} \frac{(-1)^n}{(L-N+n+1)} \binom{N-1}{n} \\ \times \left[[F(\tilde{\gamma}_{\text{th},j+1}(N))]^{L-N+n+1} - [F(\tilde{\gamma}_{\text{th},j}(N))]^{L-N+n+1}\right]. \end{aligned} \tag{4.22}$$

www.manaraa.com

For example, $P_{b,j}(\tilde{\gamma}) = Q(\sqrt{2\tilde{\gamma}})$ for BPSK and for M-QAM,

$$P_{b,j}(\tilde{\gamma}) \simeq \frac{4}{\log_2 M}\left[\left(1-\frac{1}{\sqrt{M}}\right)Q(\sqrt{g_{\text{qam},j}\tilde{\gamma}}) - \left(1-\frac{1}{\sqrt{M}}\right)^2 Q^2(\sqrt{g_{\text{qam},j}\tilde{\gamma}})\right],$$

where $g_{\text{qam},j} = \frac{3}{2(M_j-1)}$ is BER of M_j-QAM in the non-fading channel, and $f_{\tilde{\gamma}_{(N)}}(\tilde{\gamma})$ is the PDF of $\tilde{\gamma}_{(N)}$ given by (4.13) and (4.15) for i.n.d. and i.i.d. cases, respectively.

We now derive the BER for the jth AMC mode ($j \geq 0$). Note that $j = 0$ is the case of no transmission, $j = 1$ is BPSK mode, and for $j \geq 2$ square M_j-QAM modulation is used. This result is essential to the design of AMC because one of its design criteria is to set $\bar{P}_{b,j}(N) = P_{b,\text{th}}$ for all j except $j = 0$ (i.e., the case of no transmission.).

The average BER of the (N)th user in the jth mode (with signal size M_j) is given by

$$\bar{P}_{b,j}(N) = \frac{1}{P_j(N)}\int_{\tilde{\gamma}_{\text{th},j}(N)}^{\tilde{\gamma}_{\text{th},j+1}(N)} P_{b,j}(\tilde{\gamma}) f_{\tilde{\gamma}_{(N)}}(\tilde{\gamma}) d\tilde{\gamma}, \tag{4.23}$$

where $P_{b,j}(\tilde{\gamma})$ is the conditional BER in the non-fading channel.

If the jth mode uses BPSK modulation, using (4.23), we have:

$$\bar{P}_{b,j}(N) = \frac{1}{P_j(N)}\int_{\tilde{\gamma}_{\text{th},j}(N)}^{\tilde{\gamma}_{\text{th},j+1}(N)} Q(\sqrt{2\tilde{\gamma}}) f_{\tilde{\gamma}_{(N)}}(\tilde{\gamma}) d\tilde{\gamma}. \tag{4.24}$$

Using the MGF-based approach, we obtain the closed-form BER as

$$\bar{P}_{b,j}(N) \simeq \frac{1}{\pi P_j(N)}\left\{\int_0^{\pi/2}\left[\Phi_{\tilde{\gamma}_{(N)}}\left(1/\sin^2\theta, \tilde{\gamma}_{\text{th},j}(N)\right) - \Phi_{\tilde{\gamma}_{(N)}}\left(1/\sin^2\theta, \tilde{\gamma}_{\text{th},j+1}(N)\right)\right] d\theta\right\}, \tag{4.25}$$

where $\Phi_{\tilde{\gamma}_{(N)}}(s, \tilde{\gamma}_{\text{th}})$ is the TMGF of $\tilde{\gamma}_{(N)}$ defined in (4.9).

Similarly, for square M-QAM, assuming Gray coding, we obtain the BER for mode j as

$$\begin{aligned}\bar{P}_{b,j}(N) \simeq\ & \frac{1}{P_j(N)\log_2 M}\left\{\frac{4}{\pi}\left(1-\frac{1}{\sqrt{M}}\right)\int_0^{\pi/2}\left[\Phi_{\tilde{\gamma}_{(N)}}\left(\frac{g_{\text{qam}}}{\sin^2\theta}, \tilde{\gamma}_{\text{th},j}(N)\right)\right.\right. \\ & \left. - \Phi_{\tilde{\gamma}_{(N)}}\left(\frac{g_{\text{qam}}}{\sin^2\theta}, \tilde{\gamma}_{\text{th},j+1}(N)\right)\right] d\theta - \frac{4}{\pi}\left(1-\frac{1}{\sqrt{M}}\right)^2 \times \\ & \left.\int_0^{\pi/4}\left[\Phi_{\tilde{\gamma}_{(N)}}\left(\frac{g_{\text{qam}}}{\sin^2\theta}, \tilde{\gamma}_{\text{th},j}(N)\right) - \Phi_{\tilde{\gamma}_{(N)}}\left(\frac{g_{\text{qam}}}{\sin^2\theta}, \tilde{\gamma}_{\text{th},j+1}(N)\right)\right] d\theta\right\}. \end{aligned} \tag{4.26}$$

Thus, we can evaluate $\bar{P}_{b,j}(N)$ readily for different types of fading channels. Next adopting a technique proposed in [45], we propose our scheduling algorithms that searches the SNR thresholds for the (N)th user.

www.manaraa.com

4.4 GSMuD Algorithms

In this section, we propose a novel AMC design algorithm that searches for the optimal sets of thresholds for switching AMC modulations for the (N)th user. We based our algorithm on the performance results obtained in last section and the obtained threshold sets will maintain the designed performance level (in terms of BER) for each ranked user.

4.4.1 AMC Design Algorithm

For each ranked user, we perform the same operation to obtain the AMC threshold set. We only need to run this algorithm once during the initialization phase, or when the channel statistics changes significantly. For example, once the threshold set is obtained for the (N)th user, it will be used in each time slot for the user that ranked in the Nth place during that time slot. When the rank of the user is changed in the next time slot, no additional calculation is necessary to determine a new threshold set. Rather the scheduler simply assigns the AMC modulation according the the threshold set for the new rank that this user now holds.

We take similar approach in finding the threshold sets as first proposed in [76, 77]. We describe our algorithm as:

1. Initially, set $j = J$ and $\tilde{\gamma}_{\text{th},J+1}(N) = \infty$.

2. For each j, search for the unique $\tilde{\gamma}_{\text{th},j}(N) \in [0, \tilde{\gamma}_{\text{th},j+1}(N)]$ which satisfies

$$\bar{P}_{b,j}(N) = P_{b,\text{th}}(N). \tag{4.27}$$

   Here $\bar{P}_{b,j}(N)$ can be calculated using (4.25) and (4.26) for BPSK and QAM formats, respectively.

3. If $j > 1$, set $j = j - 1$, and go to step 2; otherwise, stop.

We underscore that since the conditional BER in (4.25) or (4.26) is a monotonically decreasing function as $\tilde{\gamma}_{\text{th},j}(N)$ increases, a simple numerical search can be implemented to solve (4.27) with low complexity. For example, we can utilize the binary search strategy to expedite the procedure.

www.manaraa.com

The total average BER of the (N)th user is given by

$$\bar{P}_b(N) = \frac{\sum_{j=1}^{J} \bar{P}_{b,j}(N) P_j(N) R_j}{\sum_{j=1}^{J} P_j(N) R_j}.$$

where $R_j = \log_2(M_j)$. Note that generally $\bar{P}_{b,j} \leq P_{b,\text{th}}$ is true. The throughput of the (N)th user is computed by

$$C_{(N)} = \sum_{j=1}^{J} R_j P_j(N). \tag{4.28}$$

4.4.2 Power Allocation Algorithm with Minimum-rate Constraint

In our scheme, no more than N_c strongest users out of L are scheduled for transmission. For low ASNRs, some users among the N_c strongest users may have a low throughput rate (say $C_{(N)} \leq 0.1$ bits/s/Hz). For this case, it is more beneficial to prohibit such users from transmission, and re-allocate their power to the users with stronger channel SNRs, and thus may achieve a higher sum throughput. Here, we propose a useful suboptimal power allocation scheme. This algorithm has a low complexity because it does not rely on instantaneous SNRs of all the users, but uses the statistical SNR knowledge of the first N_c ranked users and distribute the total power equally. Thus, when $C_{(N)} \leq C_{\text{th}}$, where C_{th} is a pre-specified rate threshold, the (N)th user is prohibited from transmission even when $N \leq N_c$, and its originally allocated transmission power is re-allocate to the former $N-1$ users. This testing is repeated until $C_{(N_{c,\text{eff}})} \geq C_{\text{th}}$ ($N_{c,\text{eff}}$ users are finally scheduled) or $N = 0$ (no transmission can be scheduled). Note that $N_{c,\text{eff}}$ could be zero.

Thus, it only has to be updated when the channel statistics for some users changes, for example, due to the long-term Lognormal shadowing or dynamic changes of the number of users. It requires the same amount of channel statistical knowledge as that required for the AMC design.

Assume the total normalized power for all the N_c users is $P_T = 1$. The normalized power assigned to the (N)th user is given by $P_N = 1/N_c$ for $N = 1, \ldots, N_c$. Let $N_{c,eff}$ be the effective number of users which are scheduled for channel access after power allocation. Assume all the L users are ranked in a descending order according to their SNRs.

www.manaraa.com

1. Initialization: let $N = N_c$ and $N_{c,\text{eff}} = N_c$.

2. Let $P_N = 1/N_{c,\text{eff}}$. Assume the total transmit power is $P_T = 1$ and the equal power allocation. The effective receive SNR of the (N)th user ($N \leq N_{c,\text{eff}}$) after power allocation is modified to $\tilde{\gamma}_{(N),\text{eff}} = \tilde{\gamma}_{(N)}/N_{c,\text{eff}}$. The PDF, TMGF and CDF of $\tilde{\gamma}_{(N),\text{eff}}$ are, respectively, given by

$$f_{\tilde{\gamma}_{(N),\text{eff}}}(x) = N_{c,\text{eff}} f_{\tilde{\gamma}_{(N)}}(xN_{c,\text{eff}}) \tag{4.29}$$

$$\Phi_{\tilde{\gamma}_{(N),\text{eff}}}(s,x) = \Phi_{\tilde{\gamma}_{(N)}}(s/N_{c,\text{eff}}, xN_{c,\text{eff}}) \tag{4.30}$$

$$F_{\tilde{\gamma}_{(N),\text{eff}}}(x) = 1 - \Phi_{\tilde{\gamma}_{(N),\text{eff}}}(0,x) \tag{4.31}$$

   Thus, we simply need to re-calculate $P_j(N)$, $\bar{P}_{b,j}(N)$ and $C_{(N)}$ based on $\tilde{\gamma}_{(N),\text{eff}}$ instead of $\tilde{\gamma}_{(N)}$. Calculate the effective ASNR (including effect of P_N) for the (N)th user, given by $\bar{\tilde{\gamma}}_N = P_N \bar{\tilde{\gamma}}_s = \bar{\tilde{\gamma}}_s/N_{c,\text{eff}}$.

3. Following the AMC Algorithm, find the SNR thresholds of the (N)th user. If $C_{(N)} \geq C_{\text{th}}$, go to step 4; If $C_{(N)} \leq C_{\text{th}}$, that is, the data rate for the (N)th user is smaller than a pre-specified threshold, then release its power allocation to the other $N-1$ users with larger SNRs, and let $N_{c,\text{eff}} = N_{c,\text{eff}} - 1$, then go to step 4.

4. Let $N = N-1$. If $N \geq 1$, go to step 2; otherwise, return $N_{c,\text{eff}}$ and $C_{(N)}$, $N = 0, \ldots, N_{c,\text{eff}}$, and the power allocation algorithm is done.

Note that in the extreme case, $N_{c,\text{eff}}$ could be zero if the throughput is low for all the N_c users.

For comparison purpose, we can show that the sum throughput of all the $N_{c,\text{eff}}$ users is computed by

$$C_{\text{tot},N_{c,\text{eff}}} = \sum_{N=1}^{N_{c,\text{eff}}} C_{(N)} = \sum_{N=1}^{N_{c,\text{eff}}} \sum_{j=1}^{J} R_j P_j(N).$$

The sum throughput of a conventional CDMA system which unwittingly schedules all the L users for simultaneous transmission regardless of channel conditions is given by

$$C_{\text{conv},L} = \sum_{N=1}^{L} \sum_{j=1}^{J} R_j \tilde{P}_j(N).$$

www.manaraa.com

where $\tilde{P}_j(N) = \Pr\{\tilde{\gamma}_N \in [\tilde{\tilde{\gamma}}_{\text{th},j}(N), \tilde{\tilde{\gamma}}_{\text{th},j+1}(N))\}$ and $\{\tilde{\tilde{\gamma}}_{\text{th},j}(N)\}_{j=0}^{J}$ is the SNR threshold set for the AMC design of the un-ordered SNR $\tilde{\gamma}_N$. $\tilde{P}_j(N)$ may be calculated based on (4.19) by replacing $\tilde{\gamma}_{(N)}$ with $\tilde{\gamma}_N$ for each user, and also under a constant total power constraint that $P_T = \sum_{N=1}^{L} P_N = 1$. We note that the statistical power allocation (which is based on the ordered SNR-set and cuts off low-rate transmissions) that we proposed for the GSMuD scheme is hard to be included in the conventional system.

Finally, we define the GSMuD gain obtained as

$$G_{N_{c,eff}} = C_{tot,N_{c,eff}}/C_{conv,L} \tag{4.32}$$

4.5 Numerical Examples

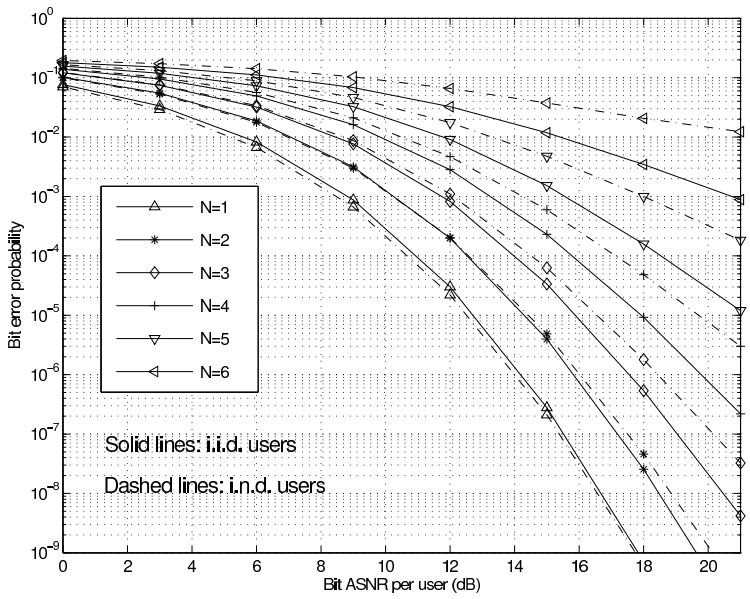

Figure 4.1 BER of 16-QAM vs. bit ASNR per user for all the $L = 6$ users over i.i.d and i.n.d. Nakagami-m fading channels. For i.i.d. users, $m = 2.1$; for the i.n.d. users, $m = [3, 2.6, 2.2, 1.8, 1.4, 1]$, and their ASNRs differ by 1 dB from the strongest user to the weakest one.

We provide some numerical examples to illustrate the performance of generalized selection multiuser scheduling with CSI and ICE, respectively, over Rayleigh and Nakagami-m fading channels, including the results of error rates and multiuser throughput.

www.manaraa.com

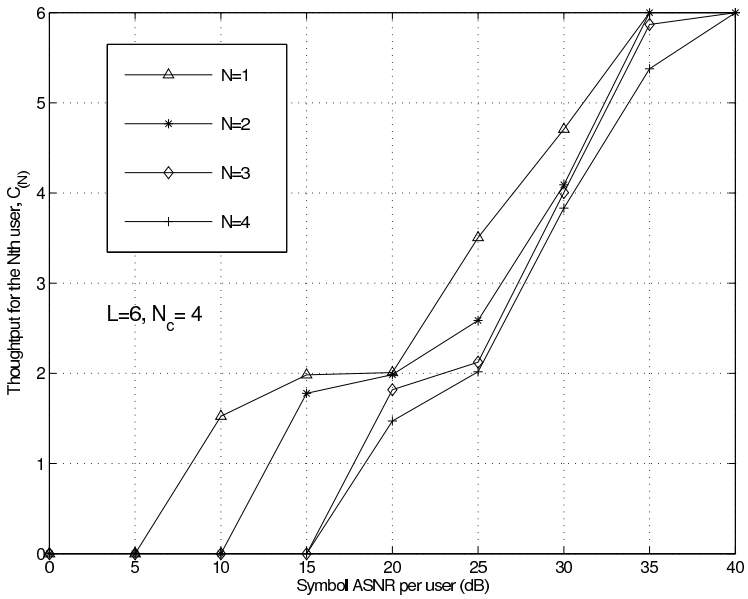

Figure 4.2 Throughput of every user vs. symbol ASNR over an i.i.d. Nakagami-m fading channel with $L = 6$, $C_{th} = 1$, $PER_{th} = 10^{-2}$, and $m = 2.1$.

First we investigate the BER performance of GSMuD under perfect CSI conditions. In Fig. 4.1 we present the BER of 16-QAM vs. bit ASNR for i.i.d. (shown in solid lines) and i.n.d. (in dashed lines) Nakagami-faded users with SNR ranking. For i.i.d. users in Nakagami channels, $m = 2.1$; and for i.n.d. users, the ASNRs differ by 1 dB from the strongest user to the weakest one, and following the same order, $m = [3, 2.6, 2.2, 1.8, 1.4, 1]$. For a fair comparison between the cases of i.i.d. and i.n.d. users, we assume the sum ASNRs $\sum_{k=1}^{L} \bar{\gamma}_k$ are identical for both cases.

Fig. 4.1 shows that as N increases the performance of the (N)th user degrades substantially, and the BER gap between the strongest (first) user and the weakest user is large. The (N)th user in the i.n.d. case has a substantially worse BER performance than in the i.i.d case, especially for a larger N.

Next, we study the throughput performance of GSMuD with adaptive modulation, which uses BPSK and M-QAM formats with symbol sizes [2,4,16,64] for $J = 4$ operating modes, and the packet length is $N_p = 128$ for all the N_c users. We emphasize that we assume a normalized total power $P_T = 1$, and thus $\sum_{N=1}^{N_{c,\text{eff}}} p_N = P_T = 1$ and $P_N = 1/N_{c,\text{eff}}$.

www.manaraa.com

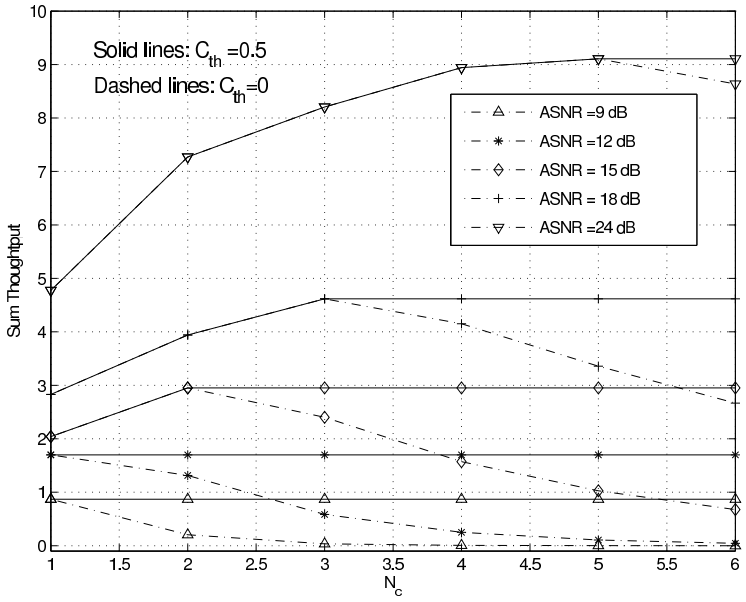

Figure 4.3 Sum throughput vs. N_c for different channel ASNRs over an i.i.d. Rayleigh fading channel with ICE. $L = 6$, $C_{\text{th}} = \{0, 0.5\}$, and $\text{PER}_{\text{th}} = 10^{-3}$.

In Fig. 4.2, we present each user's throughput $C_{(N)}$ among the first (strongest) $N_c = 4$ users in CSI case. For this and all the examples below, the ASNR is defined as the symbol ASNR per user before the statistical power allocation. The total symbol ASNR is defined as $\sum_{N=1}^{N_{c,\text{eff}}} p_N \bar{\gamma}_{N,\text{eff}} = \bar{\gamma}$, We observe that for the case of $N_c = N_{c,\text{eff}}$ and without SNR-ranking, we have

$$\sum_{N=1}^{N_{c,\text{eff}}} p_N \bar{\gamma}_{N,\text{eff}} = \sum_{N=1}^{N_c} p_N \bar{\gamma}_N = \bar{\gamma}, \tag{4.33}$$

i.e., the total symbol ASNR after power allocation is equivalent to the ASNR per user before power allocation. The result in Fig. 4.2 illustrates that stronger users have larger throughput rates. For large ASNRs, the throughput saturates to $\log_2 64 = 6$, as expected.

In Fig. 4.3 we present the sum throughput vs. N_c for different channel ASNRs, for $C_{\text{th}} = 0$ (without the minimum-rate constraint) and 0.5 (with the minimum-rate constraint), respectively for ICE case. Here and throughout the rest of this chapter, we assume a MMSE-CE, with parameters $F = 6$ and $P_{\text{PS}} = 1$ (i.e., the pilot symbols use the same transmission power as the data symbols). We assume that the channel information feedback mechanism is

www.manaraa.com

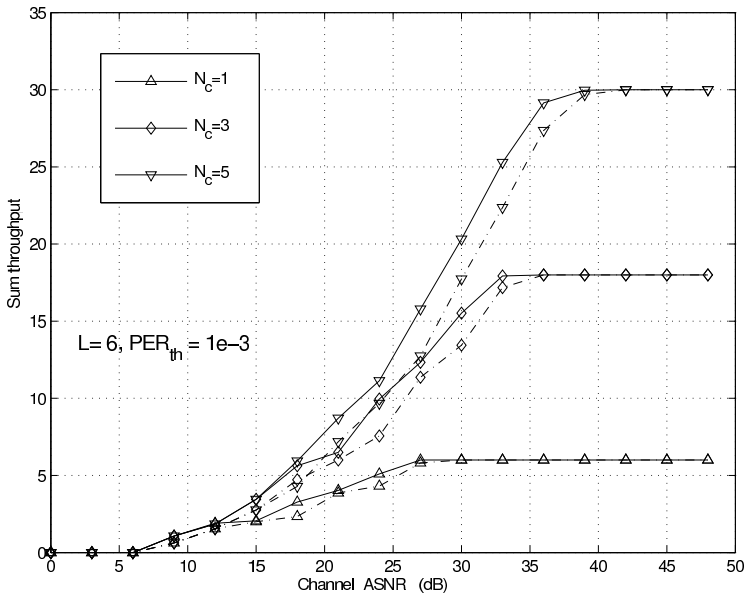

Figure 4.4 Sum throughput rate vs. channel ASNR over an i.i.d. Nakagami-m fading channel with perfect CSI (in solid lines) and ICE (in dashed lines). $L = 6$, $C_{\text{th}} = 0.5$, $\text{PER}_{\text{th}} = 10^{-3}$, and $m = 2.1$.

perfect in this case, with no delay or quantization error. Note that when $C_{\text{th}} = 0.5$ $N_{c,\text{eff}} < N_c$ may be true, while $C_{\text{th}} = 0$, $N_{c,\text{eff}} = N_c$ always holds. The result shows that the case of $C_{\text{th}} = 0.5$ has a larger sum throughput than $C_{\text{th}} = 0$ for all the ASNRs shown in Fig. 4.3. This is because for low-to-medium ASNRs splitting a given transmission power among more users may cause a lower rate for every user and result in a lower sum throughput. As the ASNR increases, however, scheduling more users becomes beneficial to the sum rate under the AMC assumption that highest modulation schemes attainable are upper bounded.

We show the sum throughput of all the N_c users vs. the channel ASNR per symbol over an i.i.d. Nakagami-m fading channel (with $L = 6$, $C_{\text{th}} = 1$, and $m = 2.1$) in Fig. 4.4, for both CSI and ICE case. Only for low ASNRs (e.g., $\bar{\gamma} \leq 10$ dB) scheduling more users ($N_c > 1$, CDMA-type) has little improvement over scheduling one user ($N_c = 1$, TDMA-type). As the ASNR increases, however, the improvement in the sum throughput becomes significant for a larger N_c than $N_c = 1$.

The effect of the target PER (PER_{th}) on the sum rate over an i.i.d. Rayleigh fading

www.manaraa.com

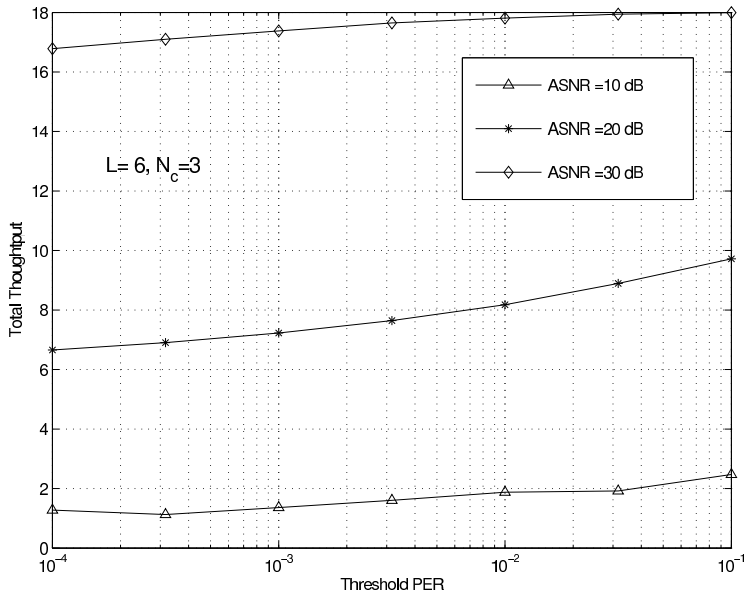

Figure 4.5 Sum throughput of all the N_c users vs. target PER over an i.i.d. Rayleigh fading channel, with $L = 6$, $Nc = 3$, $C_{th} = 0.1$.

channel (with $L = 6$, $Nc = 3$ and $C_{th} = 0.1$) is studied in Fig. 4.5. As PER_{th} increases, the multiuser throughput increases for all the ASNRs shown in the figure. A more strict (lower) target PER causes a lower sum rate. But compared to the sum rate for the less-stringent PER requirement, the reduction is quite smooth and tolerable.

Finally, the GSMuD gain is presented in Fig. 4.6. The result shows that for medium ASNRs the scheduling gain is significant. For high ASNR, the GSMuD gain vanishes due to the discrete-rate AMC.

4.6 Summary

In this chapter, we proposed a novel multiuser scheduling algorithm with practical AMC and under different fading models. In the GSMuD scheme, the scheduler ranks a total of L users awaiting for transmission by their received SNRs and selects no more than N_c number of users with the largest SNRs for channel access. We considered the scenario where the scheduler has perfect CSI as well as the case where only imperfect channel estimation is available at the receiver. We analyzed the error rates, the individual- and sum-rates of the proposed

www.manaraa.com

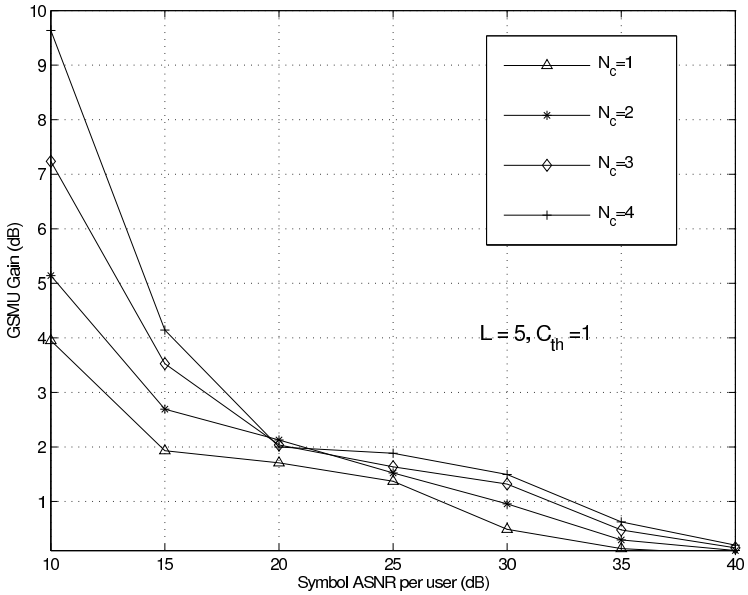

Figure 4.6 Multiuser scheduling gain (dB) vs. symbol ASNR over an i.i.d. Rayleigh fading channel, with $L = 5$, $N_c = 1 \sim 4$, and $C_{th} = 1$.

GSMuD schemes taking into account the effects of adaptive modulation, power allocation with minimum-rate-constraint, the accuracy of the channel estimation and generalized fading channels.

Numerical results show that as the ASNR increases, assigning more than one users for simultaneous transmission (for a fixed total transmission power) significantly improves the sum throughput compared to the TDMA-type of scheduling (i.e., SMuD). However, given the total BS transmission power and the ASNR, there are an optimum number of users $N_{c,\mathrm{opt}}$ to be scheduled, which is a function of channel statistics and packet error rate threshold. We also observed that in ICE case, under the block static fading assumption, the adverse effect of channel estimation errors on the spectral efficiency tends to decrease as the ASNR increases, and the performance of GSMuD with MMSE-CE approaches that with perfect CSI for high ASNRs. We defined the scheduling gain as a performance metric and found that the gain with respect to conventional CDMA systems is significant for low-to-medium ASNRs.

We observed that there are several interesting problems that we haven't covered in this chapter regarding the proposed GSMuD scheme. Equal power allocation strategy is used to

www.manaraa.com

distribute total transmitting power to selected users. Apparently it's not the optimal way of allocating power. In the next chapter, we will introduce optimal power allocation schemes that distribute total system power among scheduled users to provide maximal total capacity for GSMuD. Fairness is an important issue in multiuser scheduler. The GSMuD proposed in this chapter is based on absolute SNR ranking. It would be an interesting enhancement to GSMuD if normalized SNR are used instead that will provide considerations of user's average channel condition (e.g. distance from the BS) in the scheduler design. It would also be of interest to measure quantitatively the statistics of fairness (e.g., the channel access time) under proposed GSMuD schemes. Those problems will be proposed and discussed in following chapters as enhancements to the GSMuD scheme.

www.manaraa.com

CHAPTER 5. OPTIMAL POWER ALLOCATION FOR GSMuD

5.1 Introduction

Multiuser scheduling for cross-layer design has been a hot topic in recent years [73–77]. In selection multiuser diversity [64, 78], the scheduler assigns the channel access to the user with the largest SNR among the L users awaiting transmission. We extend the SMuD to GSMuD in Chapter 4, where the N_c out of L users are selected, and propose a suboptimal equal power allocation (EPA) scheme. In this chapter, we provide a low-complexity optimal solution to the following WCDMA parallel access rate-maximizing problem: Given a total of L users and no more than N_c ($N_c \leq L$) users can be scheduled using non-interfering parallel channels (e.g., using orthogonal spreading codes), for a fixed spreading gain N_s and a sum power P_T, how to allocate power to users to achieve the maximum sum rate? We propose a low-complexity optimal solution using optimal waterfilling (WF) power allocation for the N_c selected users, which ensures that the allocated power to every user optimally matches the channel conditions. Two optimal power allocation algorithms for the GSMuD are derived, namely (i) one-dimensional (1-D) optimal WF power allocation along the channels given a fixed peak power at each time slot; and (ii) two-dimensional (2-D) optimal waterfilling along both the time and the channels given a fixed average total power (energy). The channel distribution information (CDI) of all the users is required for the second case, but not needed for the first case. For the 2-D WF, we further require that the multiuser channels are wide-sense stationary and ergodic. We note that in this chapter, the sum-rate optimization is based on orthogonal parallel channels brought forth by spreading codes, and is different from the downlink broadcasting channel (BC) sum-rate optimization problem [71, 72]. For the latter, the multiuser superposition coding (non-orthogonal channels) and successive interference cancelation at the receivers have to

www.manaraa.com

be exploited.

Numerical results show that the 2-D WF yields the largest sum rate, while equal power allocation (EPA) along the channels proposed in Chapter 4 is near-optimal for many cases of practical interest. However, At low average SNRs (ASNRs) and as N_c increases, EPA may allocate too much transmit power into weak channels and the performance gap to the WF algorithms becomes larger. Our results provide a benchmark and useful tools for the analysis and design of WCDMA and UWB parallel-scheduling multiuser diversity schemes.

5.2 Signal Model

In a CDMA downlink there are a total of L users awaiting channel assignment using N_c parallel orthogonal channels ($N_c \leq L$). The spreading gain N_s of the considered CDMA system may be larger than N_c to provide a capability to suppress external interference. As in Chapter 4, the fading channels for different users may follow different fading types, such as Rayleigh, Rician, Nakagami-m, Nakagami-q, and Weibull channels [125], and may furthermore experience non-identical mean signal strengths and channel parameters. The channel SNR of user k is given by $\gamma_k = |h_k|^2/\mathcal{N}_k$, where h_k and $\mathcal{N}_k$ are the complex channel gain and the noise power of user k, respectively. The average channel SNR for user k is defined as by $\bar{\gamma}_k = E[\gamma_k]$.

We consider the GSMuD scheme to select users for transmission introduced in Chapter 4. In this scheme the scheduler ranks the instantaneous channel SNRs of all the L users in a descending order, denoted by $\gamma_{(1)}, \gamma_{(2)}, \ldots, \gamma_{(L)}$ (with $\gamma_{(1)} \geq \gamma_{(2)} \geq \cdots \geq \gamma_{(L)}$), where $\gamma_{(k)}$ is the kth largest SNR. The scheduler chooses the N_c users with the largest SNRs for simultaneous transmission in the next available time slot (e.g., a packet duration). The receiver SNR of the kth strongest user is given by $P_{(k)}\gamma_{(k)} = \gamma_{(k)}P_T/N_c$ ($k = 1, \ldots, N_c$).

In this chapter, we will propose a general approach to provide optimal power allocation to users based on their channel statistics in the framework of the proposed GSMuD scheme. Our goal is to design the power allocation criteria to maximize the possible theoretically achievable rates and thus we don't consider any specific AMC scheme like the one proposed in Chapter 4. Instead we take a more generalized approach of treating the information-theoretical capacity

www.manaraa.com

for each user as the actual rate provided by the AMC. Throughout this chapter, we also assume that we have CSI at the receiver and that the SNR feedback process is perfect. Next we present the model for the power allocation optimization problem for GSMuD.

We assume that in the GSMuD scheme, the total transmission power at the base station is $P_T(t)$, which is split among the N_c scheduled users, and $P_k(t)$ is the power allocated to the user with the kth largest channel SNR ($k = 1, \ldots, N_c$). Thus, $\sum_{k=1}^{N_c} P_k(t) = P_T(t)$.

Instead of the EPA scheme for power allocation proposed in Chapter 4, we propose schemes of optimally distributing the total system power to users based on their channel conditions. We consider the sum rate maximization for two different cases: (1) The sum power at any time t is bounded by fixed $P_T(t)$, i.e., $\sum_{k=1}^{N_c} P_k(t) \leq P_T(t)$ and $P_T(t) = P_T$ for all t's. (2) Only the average sum power is bounded by P_T, i.e., $E_t[\sum_{k=1}^{N_c} P_k(t)] = E_t[P_T(t)] \leq P_T$, where $E_x[\cdot]$ denotes the average with respect to (w.r.t.) x. Here $P_T(t)$ is the total power allocated to all users in time slot t, and may fluctuate in each time slot according to channel conditions. Simply speaking, these two scenarios correspond to the scenario where the system is peak power limited (case 1), or the system is average power (energy) constrained (case 2). Apparently, an energy constrained system would provide more headroom to GSMuD power allocator than the power limited system. We will show in Section 5.4 that indeed case 2 will provide larger total system sum rate than case 1.

Now we formally present our optimization problem. Under the fixed sum power constraint (case 1), the optimization problem to maximize the sum rate of the N_c selected users can be posed as:

$$\max_{P_1(t),\ldots,P_{N_c}(t)} \frac{B_w}{N_s} \sum_{k=1}^{N_c} C_{(k)}(P_k(t)) \qquad \text{s.t.} \qquad \sum_{k=1}^{N_c} P_k(t) \leq P_T \tag{5.1}$$

where B_w is the transmission bandwidth, and N_s is the spreading gain. $C_{(k)}(P_k(t))$ is the normalized rate (in nats/s/Hz) for the (k)th user at time t and is given by

$$C_{(k)}(P_k(t)) = \log(1 + P_k(t)\gamma_{(k)}(t)) \tag{5.2}$$

Here, $\log(x)$ is the natural logarithm. The goal of (5.1) is to maximize the instantaneous sum rate for every t. A 1-D waterfilling algorithm (along the channels) will be designed for this

www.manaraa.com

case.

Under the average sum power constraint (case 2), we propose to maximize the time-average sum rate of the N_c selected users. The optimization problem is expressed as:

$$\max_{P_1(t),\ldots,P_{N_c}(t)} \frac{B_w}{N_s} E_t \left[\sum_{k=1}^{N_c} C_{(k)}(P_k(t)) \right] \qquad \text{s.t.} \qquad E_t \left[\sum_{k=1}^{N_c} P_k(t) \right] \leq P_T \tag{5.3}$$

Since the average sum power constraint is less stringent than case 1, we may implement the WF algorithm along both the time and the channels, resulting in a 2-D WF algorithm. The 2-D WF results in a larger sum rate than the 1-D WF, but requires some channel distribution knowledge (such as the PDF of the channel SNRs) for its implementation. It also requires the multiuser channels to be stationary and ergodic.

5.3 Optimal Power Allocation Algorithms for a-GSMuD

In the equal power allocation scheme for GSMuD, $P_k(t) = P_T/N_c$ for $k = 1, \ldots, N_c$ and all t. The capacity for the (k)th user is (the index t in the absolute ranked SNR $\gamma_{(k)}(t)$ is suppressed for brevity)

$$C_{(k),\,\text{EPA}} = \int_0^\infty \log(1 + \frac{P_T}{N_c} y) f_{\gamma_{(k)}}(y) dy. \tag{5.4}$$

where $f_{\gamma_{(k)}}(y)$ is the PDF of the kth largest SNR. Using the result in (4.13), we write the PDF for the CSI case as

$$f_{\gamma_{(k)}}(x) = \sum_{n_1,\ldots,n_k \in \mathcal{I}} f_{\gamma_{n_k}}(x) \left[\prod_{l=1}^{k-1} (1 - F_{\gamma_{n_l}}(x)) \right] \cdot \left[\prod_{l'=k+1}^{L} F_{\gamma_{n_{l'}}}(x) \right], \tag{5.5}$$

where $f_{\gamma_n}(x)$ and $F_{\gamma_n}(x)$ are the PDF and CDF of the nth user (unranked), respectively.

The sum capacity is then $C_{\text{tot, EPA}} = \sum_{k=1}^{N_c} C_{(k),\,\text{EPA}}$. This algorithm is, however, suboptimal since the waterfilling power allocation can provide a larger capacity. To provide optimal solutions to (5.1) and (5.3), in the following subsections we derive two optimal WF algorithms for the GSMuD under the fixed- and the average-sum-power constraints, respectively. We also analyze their performances assuming multiple i.n.d.-faded users.

www.manaraa.com

5.3.1 1-D Waterfilling over the User Channels

We assume that the total power is a fixed constant $P_T(t) = P_T$ for any time slot t. Define the Lagrangian

$$\mathcal{L}(\lambda(t), P_1(t), \ldots, P_{N_c}(t)) = \frac{B_w}{N_s} \sum_{k=1}^{N_c} \log\left(1 + \frac{P_k(t)|h_{(k)}(t)|^2}{\mathcal{N}_k}\right) - \tilde{\lambda}(t)\left(\sum_{k=1}^{N_c} P_k(t) - P_T\right) \quad (5.6)$$

which may be rewritten as

$$\mathcal{L}(\lambda(t), P_1(t), \ldots, P_{N_c}(t)) = \sum_{k=1}^{N_c} \log(1 + \frac{P_k(t)|h_{(k)}(t)|^2}{\mathcal{N}_k}) - \lambda(t)\left(\sum_{k=1}^{N_c} P_k(t) - P_T\right) \quad (5.7)$$

where $\lambda(t) = \frac{N_s}{B_w}\tilde{\lambda}(t)$. We observe that the factor $\frac{N_s}{B_w}$ does not affect the WF power allocation result.

Taking the derivative of (5.7) w.r.t. $P_k(t)$ and setting the result to zero, we have the Kuhn-Tucker condition for the optimal power allocation as:

$$\frac{\partial \mathcal{L}}{\partial P_k(t)} = \begin{cases} = 0 & \text{if } P_k(t) > 0 \\ \leq 0 & \text{if } P_k(t) = 0. \end{cases} \quad (5.8)$$

Define $(x)^+ = \max(0, x)$, and the optimal power allocation satisfies (5.8) is obtained as:

$$P_k^*(t) = \left(\frac{1}{\lambda(t)} - \frac{1}{\gamma_{(k)}(t)}\right)^+ \quad \text{s.t.} \quad \sum_{k=1}^{N_c} P_k^*(t) = P_T, \quad (5.9)$$

where $P_k^*(t)$ denotes the waterfilling optimal solution of $P_k(t)$. At each time t, we have to find a waterfilling threshold $\lambda(t)$ which is time-varying, and then solve for $P_k^*(t)$.

After some manipulations, we obtain an equation equivalent to (5.9)

$$\lambda(t) = N_c(t) \Big/ \left[P_T + \sum_{k=1}^{N_c(t)} \frac{1}{\gamma_{(k)}(t)}\right] \qquad \text{s.t.} \qquad \lambda(t) \leq \gamma_{(k)}(t), \quad (5.10)$$

Let the number of scheduled users after 1-D WF at time t be denoted by $N_{c,\text{eff}}(t)$, which is the largest integer satisfying $\gamma_{(N_{c,\text{eff}}(t))}(t) \geq \lambda(t)$. All the selected channels' SNRs have to meet the WF threshold $\lambda(t)$, i.e., $\gamma_{(k)}(t) \geq \lambda(t)$. $N_{c,\text{eff}}(t)$ is a random variable and $1 \leq N_{c,\text{eff}}(t) \leq N_c$ holds. Equation (5.10) should be solved iteratively until $\lambda(t) \leq \gamma_{(k)}(t)$ is true for all k ($k = 1, \ldots, N_{c,\text{eff}}(t)$). We start from allocating power to all N_c users, and solve for $\lambda(t)$; if one of

www.manaraa.com

the uers power turns out to be zero according to (5.10), we will reduce the $N_{c,eff}$ by one and redistribute the power.

Once $N_{c,\text{eff}}(t)$ is obtained, we can rewrite the (5.10) as

$$\lambda(t) = N_{c,\text{eff}}(t) \Big/ \left[P_T + \sum_{k=1}^{N_{c,\text{eff}}(t)} \frac{1}{\gamma_{(k)}(t)} \right], \tag{5.11}$$

The algorithm for 1-D WF is summarized below (**Algorithm I**):

1. For each t, let $N_{c,\text{eff}}(t) = N_c$.
2. Find $\lambda(t)$ using (5.11).
3. Check if $\lambda(t) \leq \gamma_{(N_{c,\text{eff}}(t))}(t)$ is true. If true, go to step 4. Otherwise, remove $\gamma_{(N_{c,\text{eff}}(t))}(t)$ from the set $\{\gamma_{(1)}(t), \ldots, \gamma_{(N_{c,\text{eff}}(t))}(t)\}$, set $N_{c,\text{eff}}(t) = N_{c,\text{eff}}(t) - 1$, and go to step 2.
4. The $\lambda(t)$ and $N_{c,\text{eff}}(t)$ are now obtained. The allocated power for the (k)th user, $P_k^*(t)$, is given by (5.9), for $k = 1, \ldots, N_{c,\text{eff}}(t)$. ■

The instantaneous capacity for the (k)th user with 1-D WF is given by

$$C_{(k),\text{WF-1D}}\,(t) = \log(1 + P_k^*(t)\gamma_{(k)}(t)).$$

and the instantaneous sum capacity is

$$C_{\text{tot,WF-1D}}\,(t) = \frac{B_w}{N_s} \sum_{k=1}^{N_{c,\text{eff}}(t)} C_{(k),\text{WF-1D}}\,(t). \tag{5.12}$$

We observed that the instantaneous sum capacity is a function of time slot t and may fluctuate with it. The time-average sum rate is a better metric for comparison purposes because it's the effective sum rate. Assuming the channels for all users are ergodic, we have the time-average sum rate of the proposed 1-D WF scheme as:

$$\begin{aligned} C_{\text{tot,WF-1D}} &= E_t[C_{\text{tot,WF-1D}}\,(t)] \\ &= E_{\{\gamma_{(k)}(t)\}_{k=1}^{N_c}} \left[\frac{B_w}{N_s} \sum_{k=1}^{N_c} \log[1 + P_k^*(t)\gamma_{(k)}(t)] \right]. \end{aligned} \tag{5.13}$$

www.manaraa.com

Thus,

$$C_{\text{tot,WF-1D}} = \underbrace{\int_0^\infty \cdots \int_0^\infty}_{N_c \text{ fold}} \frac{B_w}{N_s} \sum_{k=1}^{N_c} \log[1 + p_k^*(\mathbf{y}) y_k] f_{\gamma_{(1)}}(y_1) dy_1 \cdots f_{\gamma_{(N_c)}}(y_{N_c}) dy_{N_c} \quad (5.14)$$

where $p_k^*(\mathbf{y}) = (1/\lambda(\mathbf{y}) - 1/y_k)^+$, $\mathbf{y} = [y_1, \ldots, y_{N_c}]^T$, and we denote $\gamma_{(k)}$ as y_k for notational simplicity. Here, the waterfilling threshold $\lambda(\mathbf{y})$ is the solution to (5.11). Since $\lambda(\mathbf{y})$ is a function of vector $\mathbf{y}$ and so an N_c-fold nested integral has to be evaluated. For the case of $N_c = 1$, the 1-D WF reduces to the EPA, and the waterfilling becomes unnecessary.

5.3.2 2-D Waterfilling over the User Channels and Time

We propose a statistical 2-D WF algorithm over both the channels and the time. We name it "statistical" because the statistical channel knowledge is required in the waterfilling design and we assume that the channel is stationary and ergodic.

Define the Lagrangian

$$\mathcal{L}(\lambda(t), P_1(t), \ldots, P_{N_c}(t)) = \sum_{k=1}^{N_c} \log(1 + P_k(t)|h_{(k)}(t)|^2/\mathcal{N}_k) - \lambda(t) \left(\sum_{k=1}^{N_c} P_k(t) - P_T(t) \right) \quad (5.15)$$

where, as in (5.7), $\lambda(t) = \frac{N_s}{B_w} \tilde{\lambda}(t)$, and $P_T(t)$ is the sum power for time t satisfying $E_t[P_T(t)] = P_T$.

Taking the derivative of (5.15) w.r.t. $P_k(t)$ and setting the resulting equalities to zero, we obtain

$$P_k^*(t) = (1/\lambda(t) - 1/\gamma_{(k)}(t))^+ \qquad \text{s.t.} \qquad \sum_{k=1}^{N_c} P_k^*(t) = P_T(t). \quad (5.16)$$

which leads to $\sum_{k=1}^{N_c} (1/\lambda(t) - 1/\gamma_{(k)}(t))^+ = P_T(t)$. Taking the time average of this equality we have

$$E_t \left[\sum_{k=1}^{N_c} (1/\lambda(t) - 1/y_k(t))^+ \right] = E_t[P_T(t)] = P_T \quad (5.17)$$

With the assumption of ergodic channels, the time average of the left side of (5.17) is replaced by the ensemble average of the channel SNRs and we obtain

$$\sum_{k=1}^{N_c} E_{\gamma_k}[(1/\lambda - 1/\gamma_k)^+] = \sum_{k=1}^{N_c} \int_\lambda^\infty (1/\lambda - 1/y) f_{\gamma_{(k)}}(y) dy = P_T \quad (5.18)$$

www.manaraa.com

We observe that the solution λ to (5.18) is a constant rather than a time-varying variable. Since $\gamma_k > 0$ holds and (5.18) is a monotonically non-increasing function of λ, an efficient numerical search algorithm can be designed for solving (5.18). When all the users are Rayleigh-faded, a closed form expression for (5.18) can be derived and efficient methods to evaluate it can be found in Appendix 5.A.

The statistical optimal 2-D power allocation algorithm is given below (**Algorithm II**).

1. Find λ using (5.18).

2. For each time slot t, the power allocated to the (k)th user is given by

$$P^*_{k,\text{WF-2D}}(t) = (1/\lambda - 1/\gamma_{(k)}(t))^+. \tag{5.19}$$

■

The 2-D WF algorithm above involves two steps, a design stage (to find λ) and an implementation stage (to find $P^*_{k,\text{WF-2D}}(t)$). The first step of the 2-D WF is more complex than that in the 1-D WF algorithm, but is done only once (given the channel statistics for all users are unchanged) while the 1-D WF requires solving $\lambda(t)$ for every t. The second step of 2-D WF has the same complexity to that of 1-D WF.

After λ is obtained, the time-average rate of the (k)th user is given by $C_{(k),\text{WF-2D}} = E_t[C_{k,\text{WF-2D}}(P^*_k(t))]$. With the assumption of ergodic channels, the time average is replaced by the ensemble average of the channel SNRs, and we obtain

$$\begin{aligned} C_{(k),\text{WF-2D}} &= E_t[\frac{B_w}{N_s}\log(1 + P^*_{k,\text{WF-2D}}(t)\gamma_{(k)}(t))] \\ &= \int_0^\infty \frac{B_w}{N_s}\log(1 + P^*_{k,\text{WF-2D}}(t)y) f_{\gamma_{(k)}}(y)dy \\ &= \int_\lambda^\infty \frac{B_w}{N_s}\log(y/\lambda) f_{\gamma_{(k)}}(y)dy. \end{aligned} \tag{5.20}$$

Assume Rayleigh fading channels. Let $x = y/\lambda$. A closed-form expression for (5.20) is derived

www.manaraa.com

as

$$C_{(k),\text{WF-2D}} = \frac{B_w}{N_s}\int_1^{\infty} \log(x)\, f_{\gamma_{(k)}}(x\lambda)\lambda dx \tag{5.21}$$

$$= \frac{B_w}{N_s}\sum_{n_1,\ldots,n_k\in\mathcal{I}}\sum_{\tau\in J_{L-k}} \frac{\lambda\cdot\text{sign}(\tau)}{\bar{\gamma}_{n_k}}\int_1^{\infty}(\log x)\exp(-x\lambda B)dx \tag{5.22}$$

$$= \frac{B_w}{N_s}\sum_{n_1,\ldots,n_k\in\mathcal{I}}\sum_{\tau\in J_{L-k}} \frac{\text{sign}(\tau)}{\bar{\gamma}_{n_k}} E_1(\lambda B)/B \tag{5.23}$$

where B is given by (5.28) and we exploited the equality that $\int_1^{\infty}\log(y)\exp(-yA)dy = E_1(A)/A$, where $E_1(A)$ is defined in Appendix 5.A.

The sum rate of the N_c selected users is given by

$$C_{\text{tot,WF-2D}} = \sum_{k=1}^{N_c} C_{(k),\text{WF-2D}}\,, \tag{5.24}$$

which is the maximum sum rate achievable under the average sum power constraint.

We may also use the time average of (5.19) for power allocation, leading to

$$P^*_{k,\text{WF-2D}} = E_t[P^*_{k,\text{WF-2D}}(t)] = E_t[(1/\lambda - 1/\gamma_{(k)}(t))^+] = \int_{\lambda}^{\infty}(1/\lambda - 1/y) f_{\gamma_{(k)}}(y)dy. \tag{5.25}$$

This results in a sub-optimal fixed-power statistical power allocation scheme. Some comments for Algorithm II are in order: (1) The λ is optimized by 2-D WF w.r.t to both user channels (index k) and time (t). The λ may be interpreted as the WF threshold, and it becomes a constant for different t's and k's based on the statistical knowledge of the channel SNRs and the assumption that the channels for all users are ergodic. Waterfilling among the channels is taken into account by the SNR order statistics $\gamma_{(k)}$. (2) In the implementation phase (step 2), the total allocated power for each time t $P_T(t) = \sum_{k=1}^{N_c} P^*_{k,\text{WF-2D}}(t)$ may not be a constant. With the assumption of the ergodic channels, the average sum power over a long time approaches the constant $E[P_T(t)] = P_T$. (3) For the case of single channel access and without multiuser diversity, the 2-D WF algorithm reduces to the 1-D time-domain WF power allocation studied in [71, Sec. 5.4.6].

5.4 Numerical Results

We provide some numerical results for the GSMuD (L, Nc), combined with the derived 1-D and 2-D WF power allocation algorithms and the EPA, assuming multiuser orthogonal

www.manaraa.com

CDMA downlink channels with different fading types and i.n.d. statistics. For all the i.n.d. channels considered in this section, we assume the average channel SNRs differ successively by 1.5 dB from the strongest user to the weakest one, i.e., $\bar{\gamma}_{k+1} = \bar{\gamma}_k 10^{-1.5/10}$, for $k = 1, \ldots, L-1$. Furthermore, following the same branch order $m = [3, 2.6, 2.2, 1.8, 1.4, 1]$ in the 6-user i.n.d. Nakagami-m channels. We assume the average (or the instantaneous) sum power is given by $P_T = 1$ for different N_c's and L's. All the rate results are plotted after converting nats/s/Hz to bits/s/Hz (i.e., the log to the $\log_2$ scale). For simplicity, we normalize the sum rate by B_w/N_s.

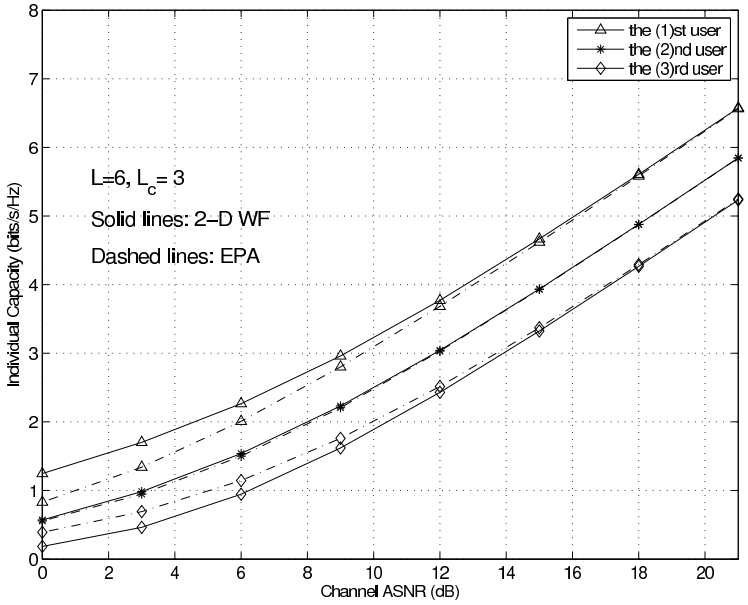

Figure 5.1 Individual rate of GSMuD (with 2-D WF and EPA) vs. ASNR with 6 users over the i.n.d. Nakagami fading channels.

In Fig. 5.1, we present the individual capacity of GSMuD (with 2-D WF and EPA) vs. ASNR with 6 users over i.n.d. Nakagami fading channels. The ASNR in the x-axis is defined as the average channel SNR over all the users, i.e., $\bar{\gamma} = \frac{1}{L}\sum_{l=1}^{L} \bar{\gamma}_l$. The result shows that compared to 2-D WF, the EPA gives a lower capacity for the strongest user but a higher capacity for the 3rd strongest user. As the ASNR increases, the EPA yields the same capacity as the 2-D WF.

Fig. 5.2 presents simulation and analytical results for the sum capacity of GSMuD (with 1-D WF) vs. ASNR for six independent and identically distributed (i.i.d.) Rayleigh-faded users.

www.manaraa.com

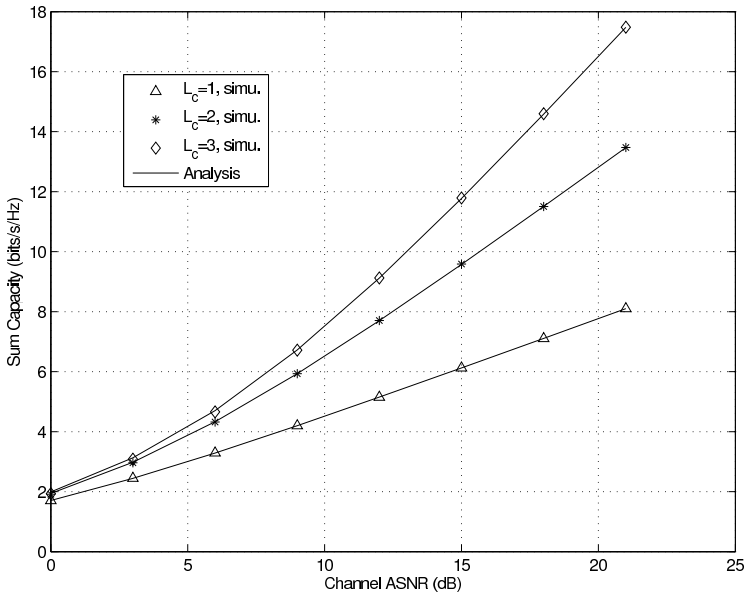

Figure 5.2 Simulation and analytical results for the sum capacity of GSMuD (with 1-D WF) vs. ASNR for 6 i.i.d. Rayleigh-faded users.

The analytical curves (given by (5.14)) excellently agree with the simulated ones (obtained by Algorithm I). Given a fixed sum power P_T and that each user has the same transmission bandwidth, splitting power between more users ($N_c = 3$) increases the sum rate compared to scheduling one user only ($N_c = 1$).

We compare the performance of the three power allocation algorithms (2-D WF, 1-D WF, and EPA) in Fig. 5.3 assuming i.n.d. Rayleigh fading ($L = 6$). The result shows that the 2-D WF has the highest rate for all the cases, and the EPA has the lowest one. The EPA with $N_c = 3$ yields even a lower sum rate than that with $N_c = 1$ for ASNRs less than 0 dB. For $N_c = 1$, the EPA has the same rate as the 1-D WF, as expected. However, for $N_c = 3$ the 1-D WF possesses a larger rate than the EPA. The performance advantage of the 2-D WF is most pronounced at low ASNRs, and the gaps between the 2-D WF, the 1-D WF and the EPA reduce as the ASNR increases. For Fig. 5.4 we assume the same system parameters as for Fig. 5.3, but now with a higher channel ASNRs, and $N_c = 1, 2, 3$. Fig. 5.4 shows that as the channel ASNR becomes high, all the three algorithms give almost identical sum rates.

In Fig. 5.5 we compare the sum rates of the 2-D WF and the EPA vs. N_c assuming 8 i.n.d.

www.manaraa.com

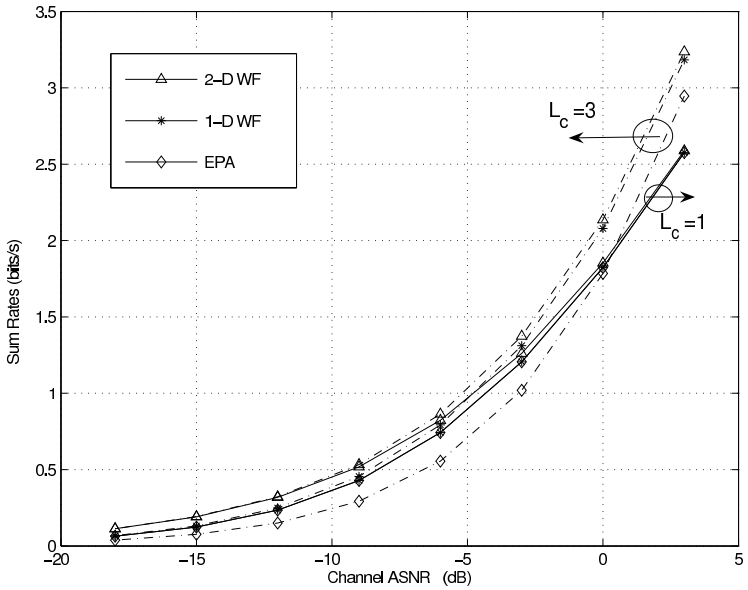

Figure 5.3 Sum capacity of GSMuD (with 2-D WF, 1-D WF, and EPA) vs. channel ASNR with 6 i.n.d. Rayleigh-faded users.

Rayleigh-faded users. We observe that increasing N_c over some threshold values (different for different ASNRs) degrades the performance of the EPA. For high ASNRs, EPA gives almost the same performance as the 2-D WF except for the case of a large N_c .

5.5 Conclusions

The equal power allocation scheme discussed in Chapter 4 provides a low-complexity solution for parallel channel access multiuser scheduling and power assignment. In this chapter, we proposed optimal power allocation schemes to achieve the maximum sum rate for GSMuD, namely 1-D or 2-D WF power allocation. The 1-D WF power allocation distribute powers among the user channels given a fixed total power at each time slot. The 2-D optimal statistical WF power allocation assigns power along both packet (time slot) and the user channels given the average total power, under the assumption of ergodic user channels and most suitable for scenarios where user channel statistics do not change over time. If user channel distribution changes over time significantly, 1-D WF algorithm will provide better performance because it allocates power over per time slot. Simulation results have verified the accuracy of our analy-

www.manaraa.com

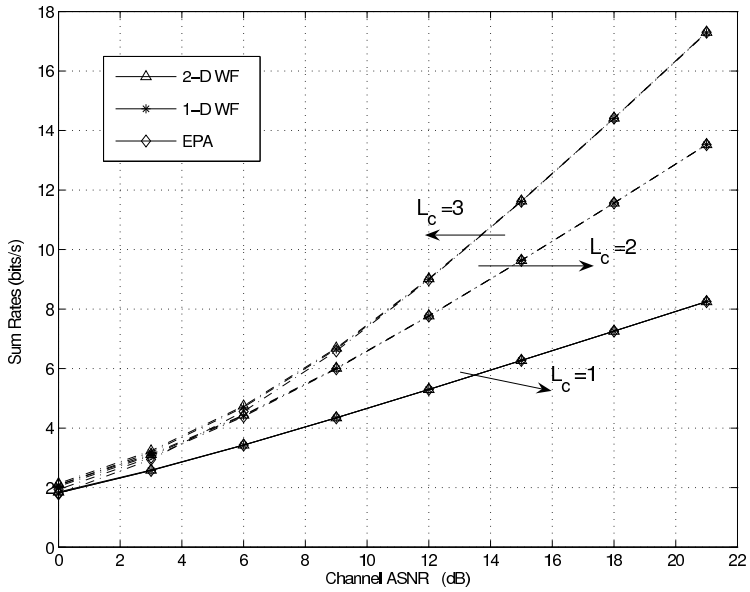

Figure 5.4 Sum rate of GSMuD (with 2-D WF, 1-D WF, and EPA) vs. ASNR with 6 users over the i.n.d. Rayleigh fading channels.

sis. Numerical results have shown that the performance advantage of 2-D WF over EPA is the largest for low SNRs and the gap increases with N_c but decreases with the SNR. The sum rates of the GSMuD 2-D and 1-D WF algorithms are monotonically non-decreasing as N_c increases, but that of the EPA may decrease due to the (equal) splitting of power into weak channels. The presented results provide a benchmark and useful tools for parallel scheduling multiuser diversity.

However, a tradeoff for providing maximal sum-rate is the fairness among users waiting for transmission. The proposed 1-D WF and 2-D WF schemes will undoubtedly favor those users with stronger channels and will assign more power to them. In the next chapter, we will explicitly address the issue of fairness among users with different fading channel models and gains under GSMuD scheme. We will propose the fairness-enhancing normalized-SNR based ranking for GSMuD and compare some of the fairness and throughput metrics with the absolute-SNR based ranking for GSMuD. We observed through numerical analysis in this chapter that the EPA is near-optimal for many cases of practical interest. Thus in the next chapter, we will adopt the EPA strategy in our analysis on the throughput performance comparison of the two

www.manaraa.com

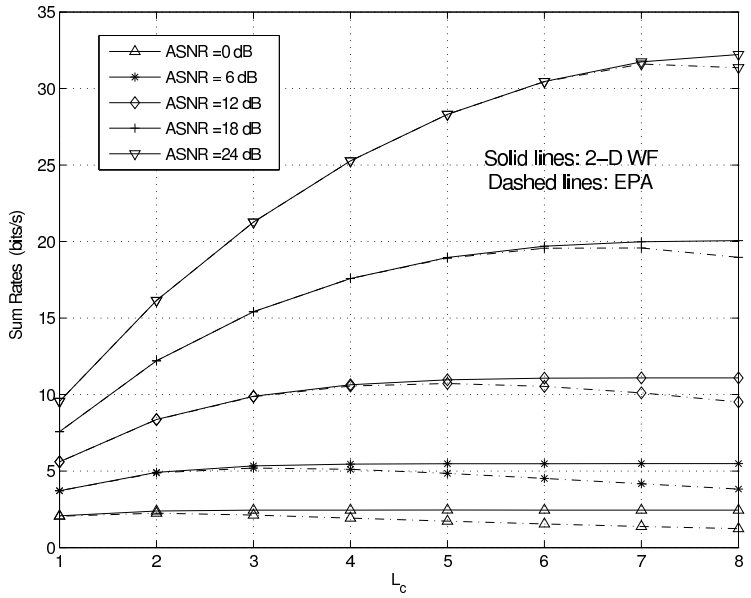

Figure 5.5 Sum rate of GSMuD (with 2-D WF and EPA) vs. N_c with different ASNRs for 8 users over the i.n.d. Rayleigh fading channels.

approaches.

5.6 Appendix 5.A Closed-form Evaluation of (5.18) for Rayleigh Fading Case

To efficiently solving for (5.18) for Rayleigh-faded users, we use (5.5) and have

$$f_{\gamma_{(N)}}(y) = \sum_{n_1,\ldots,n_N \in \mathcal{I}} \frac{\exp(-y/\bar{\gamma}_{n_N})}{\bar{\gamma}_{n_N}} \cdot \left[\prod_{l=1}^{N-1} \exp(-y)/\bar{\gamma}_{n_l}\right] \left[\prod_{l'=N+1}^{L} \left(1 - \exp(-y/\bar{\gamma}_{n_{l'}})\right)\right]. \quad (5.26)$$

Define the expansion

$$\prod_{l'=N+1}^{L} \left(1 - \exp(-y/\bar{\gamma}_{n_l'})\right) = \sum_{\tau \in J_{L-N}\left(\left\{\frac{1}{\bar{\gamma}_{n_l}}\right\}_{l=N+1}^{L}\right)} e^{-y|\tau|}\text{sign}(\tau),$$

where $J_{L-N}(\left\{\frac{1}{\bar{\gamma}_{n_l}}\right\}_{l=N+1}^{L})$ is a set of expansion elements defined for $\left\{\frac{1}{\bar{\gamma}_{n_l}}\right\}_{l=N+1}^{L}$ as:

$$J_{L-N}\left(\left\{\frac{1}{\bar{\gamma}_{n_l}}\right\}_{l=N+1}^{L}\right) = \left\{0, T_1\left(\left\{\frac{1}{\bar{\gamma}_{n_l}}\right\}_{l=N+1}^{L}\right), \ldots, T_{L-N}\left(\left\{\frac{1}{\bar{\gamma}_{n_l}}\right\}_{l=N+1}^{L}\right)\right\}. \quad (5.27)$$

www.manaraa.com

Here, $T_k\left(\left\{\frac{1}{\bar{\gamma}_{n_l}}\right\}_{l=N+1}^{L}\right) = \left\{(-1)^k \sum_{n_{l_1},n_{l_2},\ldots,n_{l_k}} \frac{1}{\bar{\gamma}_{n_{l_k}}}\right\}$, and $\sum_{n_{l_1},n_{l_2},\ldots,n_{l_k}}$ refers to all the possible $\binom{L-N}{k}$ combinations of choosing k elements out of the set $\left\{\frac{1}{\bar{\gamma}_{n_l}}\right\}_{l=N+1}^{L}$.

For example, for the first two terms, we have

$$T_1\left(\left\{\frac{1}{\bar{\gamma}_{n_l}}\right\}_{l=N+1}^{L}\right) = \left\{-\frac{1}{\bar{\gamma}_{n_{N+1}}},\ldots,-\frac{1}{\bar{\gamma}_{n_L}}\right\},$$

and

$$T_2\left(\left\{\frac{1}{\bar{\gamma}_{n_l}}\right\}_{l=N+1}^{L}\right) = \left\{\frac{1}{\bar{\gamma}_{n_{N+1}}}+\frac{1}{\bar{\gamma}_{n_{N+2}}},\frac{1}{\bar{\gamma}_{n_{N+1}}}+\frac{1}{\bar{\gamma}_{n_{N+3}}},\ldots,\frac{1}{\bar{\gamma}_{n_{L-1}}}+\frac{1}{\bar{\gamma}_{n_L}}\right\}.$$

Thus, $J_{L-N}\left(\left\{\frac{1}{\bar{\gamma}_{n_l}}\right\}_{l=N+1}^{L}\right)$ contains $\binom{L-N}{0}+\binom{L-N}{1}+\ldots+\binom{L-N}{L-N} = 2^{L-N}$ elements in total.

We have

$$f_{\gamma_{(N)}}(y) = \sum_{n_1,\ldots,n_N\in\mathcal{I}} \cdot \sum_{\tau\in J_{L-N}} \frac{\text{sign}(\tau)}{\bar{\gamma}_{n_N}} \exp(-yB),$$

where

$$B = |\tau| + \sum_{l=1}^{N} \frac{1}{\bar{\gamma}_{n_l}}, \tag{5.28}$$

and J_{L-N} is a shorthand for $J_{L-N}(\left\{\frac{1}{\bar{\gamma}_{n_l}}\right\}_{l=N+1}^{L})$. After some manipulations, a closed-form expression (5.18) is obtained as

$$\sum_{N=1}^{N_c} \int_{\lambda}^{\infty} (1/\lambda - 1/y) f_{\gamma_{(N)}}(y) dy = \sum_{N=1}^{N_c} \sum_{n_1,\ldots,n_N\in\mathcal{I}} \sum_{\tau\in J_{L-N}} \frac{\text{sign}(\tau)}{\bar{\gamma}_{n_N}} \left(\frac{\exp(-\lambda B)}{\lambda B} - E_1(\lambda B)\right) \tag{5.29}$$

where $E_1(B) = \int_1^{\infty} \frac{\exp(-yB)}{y} dy$ is the exponential-integral function [66,80], which has a closed-form expression.

www.manaraa.com

CHAPTER 6. FAIRNESS IN GSMuD

6.1 Introduction

Fairness is an important issue to multiuser systems. The SMuD and the proposed GSMuD schemes try to maximize the multiuser sum rate but may cause the channel access fairness problem because users with the stronger average channel strengths may monopolize the channel assignment resources [65, 66, 75, 79]. In [65], the authors analyzed the performance of a fair scheduling algorithm called proportional fair scheduling (PFS) where the scheduler will select the current user based on its rate in the recent history. It's proved in the paper that if all users have the same ASNRs, PFS will indeed always select the user with largest instantaneous SNR. A proportional fair scheduler is also proposed in the downlink design of IS-856 (CDMA 2000 EV-DO) by Tse [44]. Authors in [66, 79, 81] studied another kind of fair scheduling algorithm where instead of selecting the user with the largest absolute SNR for transmission at each time slot, the user with the largest normalized SNR (**n**-SNR) will be selected for transmission.

Multiuser diversity schemes that employed the **n**-SNR to rank the users to provide proportional fairness were proposed and studied in [66, 75, 79–81]. It is known that the normalized-SNR-based ranking for the SMuD provides proportional fairness for the non-identically distributed (with different channel variance) Rayleigh-faded users [66, 79–81]. In [80], the channel throughput and fairness performance metrics of the SMuD over Rayleigh fading channels were analyzed. Furthermore, the channel access statistics, including the average channel access rate (AAR), the average access time (AAT), and the average waiting time (AWT), were evaluated.

In the above-mentioned schemes and related performance analysis in terms of throughput and fairness metrics, only SMuD schemes are considered where exactly one user is allowed to communicate in any time slot. In [67], the authors considered an asymptotic analysis for a

www.manaraa.com

fair scheduler that could schedule more than one user at a time slot in CDMA fashion, where fairness accounts for providing certain channel access time fractions among the users. That is, equal expected throughput is not necessarily guaranteed, rather the access to the channel. This will mean that the scheduler is resource fair in the sense that each user will asymptotically be allocated the same amount of energy. This result is only applicable to Rayleigh fading channels.

In Chapter 4, we study the CDMA downlink channel where a total of L users are waiting for downlink access and each of them uses a single spreading code with a fixed spreading gain. We point out that in order to provide better fairness (e.g., to reduce the waiting time of every user) than SMuD a single user cannot occupy all the channels (or that multi-code assignment is excluded), and this is important especially for slow fading channels. To improve the fairness issue for the SMuD and absolute-SNR based ranking GSMuD schemes, we propose and study the normalized-SNR based ranking GSMuD scheme in this chapter. We will also solve the important question of how good the fairness metrics are for both **a**-SNRs and **n**-SNRs based ranking? We note that the GSMuD method may also be useful for OFDMA system. For example, a user can be assigned N_c best sub-channels among L channels that are available in OFDMA.

Our major fairness-related performance analysis results for both **a**-SNRs and **n**-SNRs based ranking with GSMuD may be summarized as follows: (i) We derive the PDF and MGF statistics of the ordered **n**-SNRs for all the L users; (ii) We analyze the level-crossing rate (LCR) and the average fade duration (AFD) of each user; (iii) We derive fairness metrics and channel access statistics, including the average channel access probability (AAP), the AAR, AAT and AWT of every ranked user in the system with GSMuD.

The AAP is closely related to the proportional fairness. The AAR, AAT and AWT performance of GSMuD is important to the design of system parameters, such as the transmission packet size and the buffer length. For example, a longer AAT allows a larger data frame size, while a longer AWT of a user will cause a larger access delay and also affect the buffering process. Consequently, these metrics should be taken into account in the cross-layer design.

www.manaraa.com

Similar to the analysis in Chapter 4, our results are applicable to the case that the different users' channels are i.n.d distributed where they may have non-identical statistics, or follow different families of fading distributions including Rayleigh, Rician and Nakagami-m or Weibull models.

Our analytical and simulation results show that the GSMuD, even with **a**-SNR ranking, significantly improves the channel access probability and fairness for all the users than SMuD. The GSMuD with normalized SNR ranking (**n**-SNR GSMuD) will further improve the fairness for all the users in general i.n.d. channels. Compared to the round robin scheduling without SNR ranking, the **n**-SNR GSMuD achieves a substantially higher sum rate while maintaining fairness. The presented scheme is useful for the parallel channel access multiuser scheduling design, and the analytical results provide a benchmark and mathematical tools to understand the effects of different channel and system parameters on the scheduling performance.

6.2 Signal Model

In a CDMA downlink there are a total of L users awaiting channel assignment using N_c parallel orthogonal channels ($N_c \leq L$). The spreading gain of the considered CDMA system may be larger than N_c to provide a capability to suppress external interference. As in Chapter 4, the fading channels for different users may follow different fading types, and may furthermore experience non-identical mean signal strengths and channel parameters. The channel SNR of user k is given by $\gamma_k = |h_k|^2/\mathcal{N}_k$, where h_k and $\mathcal{N}_k$ are the complex channel gain and the noise power of user k, respectively. The average channel SNR for user k is defined as by $\bar{\gamma}_k = E[\gamma_k]$.

We denote the scheme to select users for transmission introduced in Chapter 4 as the **a**-SNR-GSMuD scheme. In this scheme the scheduler ranks the instantaneous channel SNRs of all the L users in a descending order, denoted by $\gamma_{(1)}, \gamma_{(2)}, \ldots, \gamma_{(L)}$ (with $\gamma_{(1)} \geq \gamma_{(2)} \geq \cdots \geq \gamma_{(L)}$), where $\gamma_{(k)}$ is the kth largest SNR. The scheduler chooses the N_c users with the largest SNRs for simultaneous transmission in the next available time slot (e.g., a packet duration). The receiver SNR of the kth strongest user is given by $P_{(k)}\gamma_{(k)} = \gamma_{(k)}P_T/N_c$ ($k = 1, \ldots, N_c$).

In this chapter, we are more concerned with the performance metrics on fairness of the

www.manaraa.com

proposed GSMuD scheme and thus we assume that we have CSI at the receiver and that the SNR feedback process is perfect. The case for ICE can be easily obtained by putting in the ICE effective-SNR distribution into our results. We will first present the **n**-SNR-based ranking algorithm for GSMuD and then discuss the sets of fairness metrics we will investigate later in this chapter. Intuitively, **n**-SNR-based ranking algorithm provides better fairness for users at the price of a reduced sum-rate. Thus we will also investigate the sum-rate of the proposed **n**-SNR-based GSMuD and compare the result with that of the **a**-SNR-based GSMuD. For tractability of performance analysis, we consider the equal transmit power allocation of the selected users shown in Chapter 5. Equal power allocation for GSMuD has a small performance loss compared to the optimal waterfilling power allocation in many cases of practical interest. A thorough performance analysis of both **a**-SNR-based and **n**-SNR-based GSMuD is implemented in this chapter.

6.2.1 n-SNR based Ranking

In the **a**-SNR-GSMuD scheme proposed in Chapter 4, the scheduler didn't explicitly address the fairness issues in that users with stronger channel gain will likely monopolize the channel access. The total system sum-rate can be maximized by adopting the 1-D or 2-D waterfilling power allocation strategy as discussed in Section 5.3. For comparison, in the round robin scheme, at each time slot N_c users are selected for access by turns at the base station. This scheme ensures perfect fairness but does not employ multiuser diversity and consequently provides a less total sum-rate.

By combining GSMuD and **n**-SNR ranking, both multiuser diversity gain and fairness can be achieved. Let $\tilde{\gamma}_k = \gamma_k/\bar{\gamma}_k$ be the normalized SNR of the kth user. Here $\bar{\gamma}_k$ is the statistical mean SNR for the kth user, which could be different for different users even if they follow the same fading model. Ranking $\tilde{\gamma}_l$ $(l = 1, \ldots, L)$ in a descending order as $\tilde{\gamma}_{(1)}, \ldots, \tilde{\gamma}_{(L)}$, where $\tilde{\gamma}_{(1)} \geq \ldots \geq \tilde{\gamma}_{(L)}$. The users with the N_c largest **n**-SNRs are scheduled for transmission.

The purpose of **n**-SNR ranking is to ensure improved fairness for all the users. We show later in this chapter that **n**-SNR GSMuD ensures a uniform AAP for all the users for Rayleigh

www.manaraa.com

fading channels, and provides a near-uniform AAP for more general fading types (such as Nakagami-m, -q, or Rician distributions).

6.2.2 Performance Metrics to be Studied

Next we define the performance metrics to be studied for GSMuD (with both **a**-SNR and **n**-SNR ranking). They include LCR and AFD of each ranked user, AAP, degree of fairness, AAR, AAT, and AWT.

1. The level crossing rate ($\text{LCR}_\alpha(R)$) is defined as the number of times that signal envelope (the square root of SNR, $\alpha = \sqrt{\gamma}$, assuming constant noise power) α crosses level R at the positive direction in a unit time, and the average fade duration (AFD) is the average duration when α stays below R, and is given by $T_\alpha(R) = \Pr(\alpha < R)/\text{LCR}_\alpha(R)$, where $\Pr(\alpha < R)$ is the probability of $\alpha < R$. In Fig. 6.1, adapted from Fig 3.10 in [72], the LCR can be calculated by counting how many times it has crossed the level R in a unit time (in the example, 2 times) and AFD can be obtained by averaging the durations t_1 and t_2 when signal envelope level is below the level R. These two metrics measure the properties of the underlying fading channel.

2. We denote the AAP_k as the average channel access probability for the kth user. A fair scheduling requires the AAP_k to be identical for all k. It is related to the degree of fairness (DoF) for each user. The DoF for user k in the SMuD is defined as [80, 87] $\text{FA}_k = -\log(\text{AAP}_k)/\log(\frac{1}{L})$, and $\frac{1}{L}$ is the AAP for the perfect fair case where each user has equal probability of accessing the channel. We observe that when $\text{FA}_k > 1$, user k has less than average chance of accessing the channel. The sum DoF $\sum_{k=1}^{L} \text{AAP}_k\text{FA}_k$ lies between 0 and 1, with 1 denoting the perfect fairness. The DoF metric for GSMuD will be defined and studied in Section 6.3.1.

3. AAR_k is the average rate (or frequency) that user k (unranked) gains channel access. AAT_k is the average duration each time when user k has channel access. AWT_k is the average waiting time for user k to gain channel access again after releasing it [80].

www.manaraa.com

4. We will calculate sum-rate for the proposed ranking algorithms as the metric to gauge system performance from another perspective. Throughout this chapter the defined throughput and sum-rate has been normalized by the B/N_s, where B is the total bandwidth and N_s is the spreading gain.

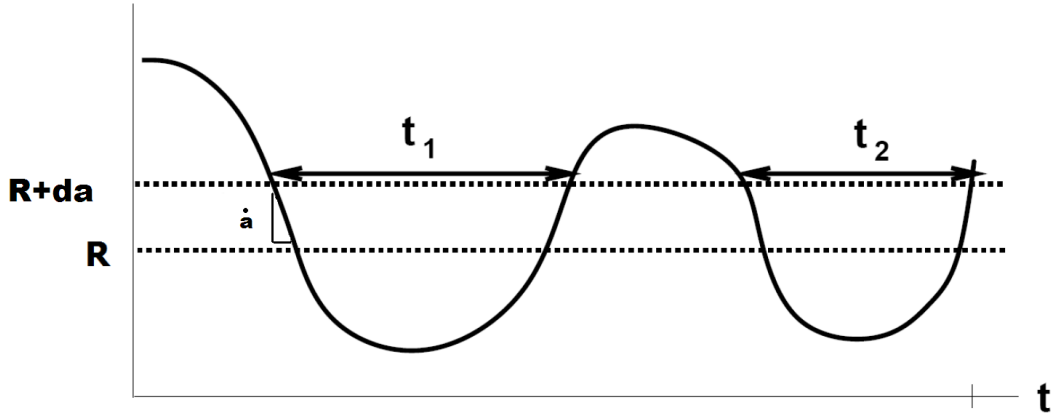

Figure 6.1 Illustration of LCR and AFD

6.3 Performance of a-SNR-based Ranking

Using the results obtained in Section 4.3, we now will formulate and derive the fairness-related performance metrics for the **a**-SNR-based GSMuD schemes.

6.3.1 Throughput and Fairness

The channel throughput of the (N)th user is given by

$$C_{(N)} = \int_0^\infty \log_2(1+P_{(N)}x) f_{\gamma_{(N)}}(x)dx$$
$$= \int_1^\infty (\log_2 y) \cdot \sum_{n_1,\ldots,n_N \in \mathcal{I}} f_{\gamma_{n_N}}\left(\frac{y-1}{P_{(N)}}\right) \left[\prod_{l=1}^{N-1}\left(1-F_{\gamma_{n_l}}\left(\frac{y-1}{P_{(N)}}\right)\right)\right] \left[\prod_{l'=N+1}^{L} F_{\gamma_{n_{l'}}}\left(\frac{y-1}{P_{(N)}}\right)\right] dy. \tag{6.1}$$

Generally speaking, (6.1) has to be evaluated using the numerical technique, such as the trapezoidal summation.

www.manaraa.com

When all the L users experience Rayleigh fading channels, using the similar results in Section 5.6, we derive a closed-form formula as

$$C_{(N),\text{Ray}} = \sum_{n_1,\ldots,n_N \in \mathcal{I}} \cdot \sum_{\tau \in J_{L-N}} \frac{\text{sign}(\tau)}{\bar{\gamma}_{n_N} A} \log_2 e \cdot \exp(A) E_1(A) \tag{6.2}$$

where $A = (\sum_{l=1}^{N} \frac{1}{\bar{\gamma}_{n_l}} + |\tau|)/P_{(N)}$, $P_{(N)} = P_T/N_c$, and J_{L-N} is a shorthand for $J_{L-N}\left(\left\{\frac{1}{\bar{\gamma}_{n_l}}\right\}_{l=N+1}^{L}\right)$ (defined in (5.27)), and $E_1(A) = \int_1^\infty \frac{\exp(-yA)}{y} dy$ is the exponential-integral function [66, 80], which has a closed-form expression.

The fairness metric is studied next. For the GSMuD (L, N_c), since the access probability averaged over all the users is N_c/L instead of $1/L$, we propose to define the DoF for user k as

$$\text{FA}_k = \log(\text{AAP}_k)/\log(N_c/L). \tag{6.3}$$

The sum DoF of all the users is given by:

$$\text{FA}_{\text{all}} = \sum_{k=1}^{L} \text{AAP}_k \text{FA}_k = \sum_{k=1}^{L} \text{AAP}_k \log(\text{AAP}_k)/\log(N_c/L).$$

The AAP for user k (for $k = 1, \ldots, L$) is given by the probability that the **a**-SNR γ_k is larger than the N_cth largest SNR among those of the remaining $L-1$ users. Thus,

$$\text{AAP}_k = \Pr\{\gamma_k > \gamma_{(N_c),\tilde{k}}\} \tag{6.4}$$

where $\Pr\{A\}$ is the probability of event A, and $\gamma_{(N_c),\tilde{k}}$ is the N_cth largest SNR among the remaining $L-1$ users (excluding user k). Some integral-form and closed-form expressions for AAP_k are given in Appendix 6.A.

We may evaluate the individual throughput of user k (unranked) as

$$C_k = \int_0^\infty \log_2(1 + P_k x) f_{\gamma_k}(x) \left[\int_0^x f_{\gamma_{(N_c),\tilde{k}}}(y) dy\right] dx \tag{6.5}$$

where $f_{\gamma_{(N_c),\tilde{k}}}(y)$ is the PDF of $\gamma_{(N_c),\tilde{k}}$ and is given in Appendix 6.A. Assuming all Rayleigh-faded users, using a procedure similar to that for deriving (6.37) appeared in Appendix 6.A, we have a closed-form capacity formula for Rayleigh channels as

$$C_{k,\text{Ray}} = \sum_{n_1,\ldots,n_{N_c} \in \mathcal{I}_{\tilde{k}}} \sum_{\tau \in J_{L-N_c-1}} \log_2 e \cdot \frac{\text{sign}(\tau)}{\bar{\gamma}_{n_{N_c}} \bar{\gamma}_k B} \left[e^{A_1} E_1(A_1)/A_1 + e^{A_2} E_1(A_2)/A_2\right] \tag{6.6}$$

www.manaraa.com

where $A_1 = 1/(P_k\bar{\gamma}_k)$, $P_k = P_T/N_c$, $A_2 = (1/P_k)(B + 1/\bar{\gamma}_k)$, and $B = \sum_{l=1}^{N_c} \frac{1}{\bar{\gamma}_{n_l}} + |\tau|$. J_{L-N_c-1} is a shorthand for $J_{L-N_c-1}\left(\left\{\frac{1}{\bar{\gamma}_{n_l}}\right\}_{l=N_c+1}^{L-1}, n_l \neq k\right)$, which follows the definition in (5.27) and contains 2^{L-N_c-1} elements.

6.3.2 LCR and AFD

The LCR and AFD are important second-order channel statistics which depict the channel fading rate and dynamic channel changes, and their performance evaluation has been an interesting topic of study [80, 93–96]. Derivation of the LCR and AFD will also help the evaluation of user channel access metrics in Section 6.3.3.

Define $\alpha_k = \sqrt{\gamma_k}$ to be the signal envelop. Let $\dot{\alpha}_k$ denote the first-order time derivative of α_k, and we denote $f_{\alpha_{(N)},\dot{\alpha}_{(N)}}(\alpha_k, \dot{\alpha}_k)$ as their joint PDF. To obtain the number of crossings in a unit time of the signal envelop over the level R, we first derive two interim values. From Fig. 6.1, we observe that the expected amount of time α_k falls in the interval $[R, R + d\alpha_k]$ with the slope $\dot{\alpha}_k$ falling in the range $[\dot{\alpha}_k, \dot{\alpha}_k + d\dot{\alpha}_k]$ over the time duration dt is $T = f_{\alpha_{(N)},\dot{\alpha}_{(N)}}(\alpha_k, \dot{\alpha}_k)d\alpha_k d\dot{\alpha}_k dt$. When the slope is $\dot{\alpha}_k$, the amount of time it takes for the signal envelop to cross from level R to $R + d\alpha_k$ is $P = d\alpha_k/\dot{\alpha}_k$. We thus have the expected number of crossings over the level R with the slope between $\dot{\alpha}_k$ and $\dot{\alpha}_k + d\dot{\alpha}_k$ in a unit time as the ratio $T/P = \dot{\alpha}_k f_{\alpha_{(N)},\dot{\alpha}_{(N)}}(\alpha_k, \dot{\alpha}_k)d\dot{\alpha}_k dt$. When averaged over time and the distribution of $\dot{\alpha}_k$, we derive the LCR of the Nth largest amplitude, $\alpha_{(N)}$, at the signal level R as:

$$\mathrm{LCR}_{\alpha_{(N)}}(R) = \int_0^\infty \dot{x} f_{\alpha_{(N)},\dot{\alpha}_{(N)}}(R, \dot{x})d\dot{x} \tag{6.7}$$

where $f_{\alpha_{(N)},\dot{\alpha}_{(N)}}(x, \dot{x})$ is the joint PDF of signal envelop $\alpha_{(N)}$ and its first-order derivative $\dot{\alpha}_{(N)}$, and is given by (6.41) (the independent case) and (6.43) (the non-independent case) in the Appendix 6.B respectively.

It is known that $\dot{\alpha}_k$ follows a zero-mean Gaussian distribution for Rayleigh, Rician and Nakagami-m channels, and its PDF is given by [80, 93–96]

$$f_{\dot{\alpha}_k}(\dot{\alpha}) = \frac{1}{\sqrt{2\pi}\dot{\sigma}_{\dot{\alpha}_k}} \exp\left(-\frac{\dot{\alpha}^2}{2\dot{\sigma}^2_{\dot{\alpha}_k}}\right) \tag{6.8}$$

www.manaraa.com

where $\dot{\sigma}^2_{\dot{\alpha}_k}$ is the variance of $\dot{\alpha}_k$. Assume the Jakes' Doppler fading spectrum. It is known that $\dot{\sigma}^2_{\dot{\alpha}_k} = \pi^2 f^2_{\text{Dop},k}\Omega_k$, where $f_{\text{Dop},k}$ is the Doppler fading bandwidth of the kth user, and Ω_k is the variance of the underlying Gaussian process. For the Rayleigh, Rician [94] and Nakagami-m [95] fading channels, we have $\Omega_k = \bar{\gamma}_k$, $\Omega_k = \bar{\gamma}_k/(1+K_k)$, and $\Omega_k = \bar{\gamma}_k/m_k$, respectively, where K_k and m_k are the Rice-K factor and m-parameter for user k. In these channels, $\dot{\alpha}_k$ and α_k are independent. For Weibull and Nakagami-q fading channels $\dot{\alpha}_k$ and α_k are not independent. For the Weibull fading channels, $\dot{\alpha}_k$ still follows a Gaussian distribution with the PDF shown in (6.8), where $\dot{\sigma}_{\dot{\alpha}_k}$ can be obtained from [96, eq. (9)]. For the Nakagami-q channels, a joint PDF expression of $\dot{\alpha}_k$ and α_k was given in [97, eq.(11)].

Below, we use $\dot{\sigma}^2_k$ as a shorthand for $\dot{\sigma}^2_{\dot{\alpha}_k}$. For i.n.d.-faded users over Rayleigh, Rician and Nakagami-m fading channels, using (6.41) we derived a closed-form expression of (6.7) as

$$\begin{aligned}\text{LCR}_{\alpha_{(N)}}(R) &= \sum_{n_1,\ldots,n_N\in\mathcal{I}} f_{\alpha_{n_N}}(R)\left[\prod_{l=1}^{N-1}(1-F_{\alpha_{n_l}}(R))\right]\left[\prod_{l'=N+1}^{L}F_{\alpha_{n_{l'}}}(R)\right]\int_0^\infty \dot{x} f_{\dot{\alpha}_{n_N}}(\dot{x})d\dot{x} \\ &= \sum_{n_1,\ldots,n_N\in\mathcal{I}} f_{\alpha_{n_N}}(R)\left[\prod_{l=1}^{N-1}(1-F_{\alpha_{n_l}}(R))\right]\left[\prod_{l'=N+1}^{L}F_{\alpha_{n_{l'}}}(R)\right]\dot{\sigma}_{n_N}/\sqrt{2\pi} \qquad (6.9)\end{aligned}$$

The second equation is using the properties of the Gaussian distribution of $\dot{\alpha}_k$. Furthermore, LCR results for GSMuD over Weibull and Nakagami-q fading channels can be similarly derived using (6.7), (6.43), and results in [96, eq. (9)] and [97, eq.(11)], respectively.

The AFD is given by $T_{\alpha_{(N)}}(R) = \Pr\{\alpha_{(N)} < R\}/\text{LCR}_{\alpha_{(N)}}$, where $\Pr\{\alpha_{(N)} < R\}$ is simply the CDF (or the outage probability) of $\alpha_{(N)}$. Using a procedure similar to that for deriving (5.5) we obtain the PDF of $\alpha_{(N)}$ as

$$f_{\alpha_{(N)}}(y) = \sum_{n_1,\ldots,n_N\in\mathcal{I}} f_{\alpha_{n_N}}(y)\left[\prod_{l=1}^{N-1}(1-F_{\alpha_{n_l}}(y))\right]\left[\prod_{l'=N+1}^{L}F_{\alpha_{n_{l'}}}(y)\right]. \qquad (6.10)$$

where $f_{\alpha_{n_N}}(y)$ and $F_{\alpha_{n_l}}(y)$ are the PDF and CDF of α_{n_N}, respectively, and are the standard Rayleigh, Rician or Nakagami-m distribution PDF and CDF respectively for the different fading models. For i.n.d. Rayleigh-faded users, we derived a closed-form expression for

www.manaraa.com

$\Pr\{\alpha_{(N)} < R\}$ as

$$\Pr\{\alpha_{(N)} < R\} = F_{\alpha_{(N)}}(R) = \int_0^R f_{\alpha_{(N)}}(y)dy$$
$$= \sum_{n_1,\ldots,n_N \in \mathcal{I}} \sum_{\tau \in J_{L-N}} \frac{1}{\bar{\gamma}_{n_N}} \left[1 - \exp\left(-R^2\left(\sum_{l=1}^{N} \frac{1}{\bar{\gamma}_{n_l}} + |\tau|\right)\right)\right] \Bigg/ \left[\sum_{l=1}^{N} \frac{1}{\bar{\gamma}_{n_l}} + |\tau|\right] \quad (6.11)$$

where J_{L-N} is a shorthand for $J_{L-N}\left(\left\{\frac{1}{\bar{\gamma}_{n_l}}\right\}_{l=N+1}^{L}\right)$. The AFD can now be evaluated.

6.3.3 Channel Access Statistics

The AAR, AAT and AWT are important performance metrics affecting the scheduling and the cross-layer design. For example, AWT is pertaining to the waiting time of users awaiting scheduling and its value will influence the buffer length design and the expected scheduling delay. AAT on the other hand will affect the choice of optimal packet size. In this section, AAR is used to obtain AAT and AWT, and can be obtained in similar fashion as LCR. It should be noted that AAR, AAT, and AWT are fairness metrics for multiuser channels and they are related but are different from the fading channel metrics LCR and AFD.

When AAP_k (derived in Section 6.3.1 and Appendix 6.A) and AAR_k are known, the AAT and AWT are, respectively, given by

$$\text{AAT}_k = \text{AAP}_k/\text{AAR}_k, \qquad \text{AWT}_k = (1 - \text{AAP}_k)/\text{AAR}_k. \quad (6.12)$$

Now, we derive AAR_k. Define $r_k = \alpha_k/\alpha_*$, where $\alpha_* = \alpha_{(N_c),\tilde{k}} = \sqrt{\gamma_{(N_c),\tilde{k}}}$, and $\gamma_{(N_c),\tilde{k}}$ is the N_cth largest SNR among the $L-1$ users (excluding user k). We use $\dot{\alpha}_*$ to denote the first-order time derivation of α_*. The AAR of the kth user, AAR_k, is the crossing rate (at the positive direction) of the kth users' signal envelop at the level $r_k = 1$. Thus,

$$\text{AAR}_k = \int_0^\infty \dot{r} f_{r_k,\dot{r}_k}(r = 1, \dot{r})d\dot{r}, \quad (6.13)$$

where $\dot{r}_k$ is the first-order time derivation of r_k, and $f_{r_k,\dot{r}_k}(r,\dot{r})$ is the joint PDF of r_k and $\dot{r}_k$. As discussed in Section 6.3.2, we assume that α_k and $\dot{\alpha}_k$ are independent, which is valid for Rayleigh, Rician and Nakagami-m fading channels. The result for Nakagami-q and Weibull channels may be obtained by using a similar procedure after a proper modification.

www.manaraa.com

Based on [80, eq. (9)], $f_{r_k,\dot{r}_k}(r,\dot{r})$ is given by

$$f_{r_k,\dot{r}_k}(r,\dot{r}) = \int_0^\infty \int_{-\infty}^\infty \alpha_*^2 f_{\alpha_k}(\alpha_* r) f_{\dot{\alpha}_k}(\dot{r}\alpha_* + \dot{\alpha}_* r) f_{\dot{\alpha}_*,\dot{\alpha}_*}(\alpha_*,\dot{\alpha}_*) d\dot{\alpha}_* d\alpha_* \tag{6.14}$$

where $f_{\alpha_*,\dot{\alpha}_*}(\alpha_*,\dot{\alpha}_*)$ is the joint PDF of α_* and $\dot{\alpha}_*$. We show that the PDF $f_{\alpha_*}(x)$ of α_* is given by

$$\begin{aligned} f_{\alpha_*}(x) &= f_{\gamma_{(N_c),\tilde{k}}}(x) \\ &= \sum_{n_1,\ldots,n_{N_c}\in\mathcal{I}_{\tilde{k}}} f_{\alpha_{n_{N_c}}}(x) \left[\prod_{l=1}^{N_c-1}(1-F_{\alpha_{n_l}}(x))\right]\left[\prod_{l'=N_c+1}^{L-1} F_{\alpha_{n_{l'}}}(x)\right], \end{aligned} \tag{6.15}$$

and by using a procedure similar to that for deriving (6.41), we have

$$f_{\alpha_*,\dot{\alpha}_*}(\alpha_*,\dot{\alpha}_*) = \sum_{n_1,\ldots,n_{N_c}\in\mathcal{I}_{\tilde{k}}} f_{\alpha_{n_{N_c}}}(\alpha_*) \times \left[\prod_{l=1}^{N_c-1}(1-F_{\alpha_{n_l}}(\alpha_*))\right]\left[\prod_{l'=N_c+1}^{L-1} F_{\alpha_{n_{l'}}}(\alpha_*)\right] f_{\dot{\alpha}_{n_{N_c}}}(\dot{\alpha}_*) \tag{6.16}$$

Equation (6.13) (with (6.14) and (6.16)) involves a three-fold integral. For the most general case of i.n.d. users with different fading parameters we can reduce (6.13) to a single integral. Furthermore, for Rayleigh-faded users closed-form AAR expression are obtained. The procedure and results are detailed in Appendix 6.C.

6.4 Performance of n-SNR-based Ranking

In this section, we propose the **n**-SNR-based GSMuD algorithms and derive the performance and fairness related metrics for comparison with **a**-SNR-based GSMuD.

6.4.1 SNR Statistics

The normalized-SNR based ranking is introduced to provide proportional fairness. To evaluate the throughput and fairness performance of **n**-SNR-GSMuD, the output absolute SNR $\hat{\gamma}_{(N)}$ has to be analyzed. Here we use the hat in $\hat{\gamma}_{(N)}$ to denote the **a**-SNR of the user with Nth largest **n**-SNR $\tilde{\gamma}_{(N)}$.

Now we derive the statistics of the **a**-SNR $\hat{\gamma}_{(N)}$. When we rank the **n**-SNR set $\{\tilde{\gamma}_{n_l}\}_{l=1}^L$, namely $\gamma_{n_1}/\bar{\gamma}_{n_1},\ldots,\gamma_{n_k}/\bar{\gamma}_{n_k},\ldots,\gamma_{n_L}/\bar{\gamma}_{n_L}$, we may use $\bar{\gamma}_{n_N}$ as an anchor element, and reformulate the **n**-SNR-ranking problem as: Compare the set $\bar{\gamma}_{n_N}\gamma_{n_1}/\bar{\gamma}_{n_1},\ldots,\gamma_{n_N},\ldots,\bar{\gamma}_{n_N}\gamma_{n_L}/\bar{\gamma}_{n_L}$,

www.manaraa.com

and choose the Nth largest element. Note that the new set may be written as $w_{n_1}\gamma_{n_1}, \ldots, \gamma_{n_N}, \ldots, w_{n_L}\gamma_{n_L}$ (where $w_{n_l} = \bar{\gamma}_{n_N}/\bar{\gamma}_{n_l}$) and it is simply a weighted version of the original SNR set $\gamma_{n_1}, \ldots, \gamma_{n_N}, \ldots, \gamma_{n_L}$. When the n_Nth user has the Nth largest **n**-SNR, the event may be written as $\{\gamma_{n_N} \leq \bar{\gamma}_{n_N}\tilde{\gamma}_{(1)}, \ldots, \gamma_{n_N} \leq \bar{\gamma}_{n_N}\tilde{\gamma}_{(N-1)}, \gamma_{n_N} \geq \bar{\gamma}_{n_N}\tilde{\gamma}_{(N+1)}, \ldots, \gamma_{n_N} \geq \bar{\gamma}_{n_N}\tilde{\gamma}_{(L)}\}$ or equivalently $\{\gamma_{n_N} \leq w_{(1)}\hat{\gamma}_{(1)}, \ldots, \gamma_{n_N} \leq w_{(N-1)}\hat{\gamma}_{(N-1)}, \gamma_{n_N} \geq w_{(N+1)}\hat{\gamma}_{(N+1)}, \ldots, \gamma_{n_N} \geq w_{(L)}\hat{\gamma}_{(L)}\}$.

Following the same procedure for deriving (4.12), we derive the MGF of $\hat{\gamma}_{(N)}$ for the general case of i.n.d. users as

$$\Phi_{\hat{\gamma}_{(N)}}(s) = \sum_{n_1,\ldots,n_N \in \mathcal{I}} \int_0^\infty e^{-sx} f_{\gamma_{n_N}}(x) \left[\prod_{l=1}^{N-1} \left(1 - F_{\gamma_{n_l}}\left(\frac{x\bar{\gamma}_{n_l}}{\bar{\gamma}_{n_N}}\right)\right)\right] \left[\prod_{l'=N+1}^{L} F_{\gamma_{n_{l'}}}\left(\frac{x\bar{\gamma}_{n_{l'}}}{\bar{\gamma}_{n_N}}\right)\right] dx \tag{6.17}$$

Here, $f_{\gamma_{n_l}}$, and $F_{\gamma_{n_l}}$ are PDF, CDF of the n_lth unranked user **a**-SNR respectively.

The PDF of $\hat{\gamma}_{(N)}$ can be derived as

$$f_{\hat{\gamma}_{(N)}}(x) = \sum_{n_1,\ldots,n_N \in \mathcal{I}} f_{\gamma_{n_N}}(x) \left[\prod_{l=1}^{N-1} \left(1 - F_{\gamma_{n_l}}\left(\frac{x\bar{\gamma}_{n_l}}{\bar{\gamma}_{n_N}}\right)\right)\right] \left[\prod_{l'=N+1}^{L} F_{\gamma_{n_{l'}}}\left(\frac{x\bar{\gamma}_{n_{l'}}}{\bar{\gamma}_{n_N}}\right)\right]. \tag{6.18}$$

For verification purpose, we show two special cases of (6.18) below.

1. For the special case of $N = 1$, (6.18) simplifies to the PDF of the **n**-SNR-ranking SMuD selected user's **a**-SNR as

$$f_{\hat{\gamma}_{(1)}}(x) = \sum_{n_1=1}^{L} f_{\gamma_{n_1}}(x) \cdot \left[\prod_{l'=2}^{L} F_{\gamma_{n_{l'}}}(x\bar{\gamma}_{n_{l'}}/\bar{\gamma}_{n_1})\right]. \tag{6.19}$$

   For i.n.d. Rayleigh-faded users, we have $F_{\gamma_{n_{l'}}}(x\bar{\gamma}_{n_{l'}}/\bar{\gamma}_{n_1}) = 1 - e^{-x/\bar{\gamma}_{n_1}}$, and $f_{\gamma_{n_1}}(x) = \frac{e^{-x/\bar{\gamma}_{n_1}}}{\bar{\gamma}_{n_1}}$. Thus, (6.19) is reduced to

$$f_{\hat{\gamma}_{(1)}}(x) = \sum_{l=1}^{L} f_{\gamma_l}(x) \cdot [F_{\tilde{\gamma}}(x/\bar{\gamma}_l)]^{L-1} = \sum_{l=1}^{L} \frac{\exp(-x/\bar{\gamma}_l)}{\bar{\gamma}_l} [1 - \exp(-x/\bar{\gamma}_l)]^{L-1}. \tag{6.20}$$

   which is the identical to that given in [81] and [80, eq. (39)], as expected.

2. When all the L users have i.i.d. channels, (6.18) reduces to

$$f_{\hat{\gamma}_{(N)}}(x) = N\binom{L}{N} f_{\gamma_{n_N}}(x) \left[1 - F_\gamma(x)\right]^{N-1} \left[F_\gamma(x)\right]^{L-N}. \tag{6.21}$$

   which is identical to the case of **a**-SNR based ranking.

www.manaraa.com

We note that i.i.d is a prerequisite that (6.18) can be reduced to (6.21). When all the users follow different fading channel parameters (such as Nakagami-m, -q parameters and Rice-K factors), even when their average SNRs are identical, i.e., $\bar{\gamma}_1 = \ldots = \bar{\gamma}_L$, (6.18) cannot be reduced to (6.21), which means that the users' statistics are not exchangeable. We will show in Section 6.4.2 and Section 6.5 that if this is the case, fair AAP for all users are not possible even under **n**-SNR-ranking.

6.4.2 Throughput and Fairness

The channel throughput of the user with the Nth largest **n**-SNR is given by

$$C_{(N)} = \int_0^\infty \log_2(1 + xP_T/N_c) f_{\hat{\gamma}_{(N)}}(x) dx \tag{6.22}$$

where $f_{\hat{\gamma}_{(N)}}(x)$ is given by (6.18). When all the L users experience Rayleigh fading channels, we derive a closed-form throughput formula as

$$\begin{aligned} C_{(N),\text{Ray}} &= \int_0^\infty \log_2(1 + xP_T/N_c) \sum_{n_1,\ldots,n_N \in \mathcal{I}} \frac{\exp(-x/\bar{\gamma}_{n_N})}{\bar{\gamma}_{n_N}} \cdot \exp(-(N-1)x) \cdot \left(1 - e^{-x}\right)^{L-N} dx \\ &= \sum_{n_1,\ldots,n_N \in \mathcal{I}} \frac{1}{\bar{\gamma}_{n_N}} \sum_{k=0}^{L-N} \binom{L-N}{k} (-1)^k e^B E_1(B)/B \log_2 e \end{aligned} \tag{6.23}$$

where $B = (\frac{1}{\bar{\gamma}_{n_N}} + N + k - 1)N_c/P_T$. For general fading cases a numerical integration is required to evaluate $C_{(N)}$.

Using the **n**-SNR based ranking, the AAP for user with original index k is given by $\text{AAP}_k = \Pr\{\tilde{\gamma}_k > \tilde{\gamma}_{(N_c),\tilde{k}}\}$, where $\tilde{\gamma}_k = \gamma_k/\bar{\gamma}_k$, and $\tilde{\gamma}_{(N_c),\tilde{k}}$ is the N_cth largest **n**-SNR among the remaining $L-1$ users (excluding user k). Using similar approach in Appendix 6.A, we have

$$\text{AAP}_k = \int_0^\infty f_{\tilde{\gamma}_k}(x) \left[\int_0^x f_{\gamma_{(N_c),\tilde{k}}}(y) dy \right] dx \tag{6.24}$$

where

$$f_{\tilde{\gamma}_{(N_c),\tilde{k}}}(x) = \sum_{n_1,\ldots,n_{N_c} \in \mathcal{I}_{\tilde{k}}} f_{\tilde{\gamma}_{n_{N_c}}}(x) \times \left[\prod_{l=1}^{N_c-1} (1 - F_{\tilde{\gamma}_{n_l}}(x)) \right] \left[\prod_{l'=N_c+1}^{L-1} F_{\tilde{\gamma}_{n_{l'}}}(x) \right] \tag{6.25}$$

Here, $f_{\tilde{\gamma}_{n_l}}(x)$ and $F_{\tilde{\gamma}_{n_l}}(x)$ are PDF and CDF of the **n**-SNR $\tilde{\gamma}_{n_l}$ of the n_lth unranked user and can be obtained by a change of variable operation on their corresponding **a**-SNR PDF and CDF.

www.manaraa.com

When all the users experience the identical Rice K factors, or m, q parameters over Rician or Nakagami fading channels (though with different mean SNRs $\bar{\gamma}_{n_l}$), the CDF $F_{\tilde{\gamma}_l}(x)$ is independent of user index l, and we have $f_{\tilde{\gamma}_{(N_c),\tilde{k}}}(x) = N_c\binom{L-1}{N_c} f_{\tilde{\gamma}}(x)(1-F_{\tilde{\gamma}(x)})^{N_c-1}\left[F_{\tilde{\gamma}}(x)\right]^{L-N_c-1}$.

Using (6.24), the throughput of user k with **n**-SNR-GSMuD (L, N_c) is given by

$$C_k = \int_0^\infty \log_2(1+\bar{\gamma}_k P_T/N_c x) f_{\tilde{\gamma}_k}(x) \left[\int_0^x f_{\gamma_{(N_c),\tilde{k}}}(y)dy\right] dx \tag{6.26}$$

For the i.n.d. Rayleigh-faded users, we derive a closed-form expression for AAP_k as

$$\begin{aligned}\mathrm{AAP}_k &= \int_0^\infty e^{-x}\int_0^x N_c\binom{L-1}{N_c} e^{-y}(e^{-y(N_c-1)})\left[1-e^{-y}\right]^{L-N_c-1} dydx \\ &= N_c\binom{L-1}{N_c}\sum_{k=0}^{L-N_c-1}\binom{L-N_c-1}{k}\frac{(-1)^k}{N_c+k+1} = N_c/L \end{aligned} \tag{6.27}$$

This result shows that for i.n.d Rayleigh fading channels with **n**-SNR ranking all the users have the same channel access probabilities, which increases with N_c. We note that when $N_c = 1$, (6.27) reduces to $\mathrm{AAP}_k = 1/L$, which is identical to that given by [80, eq. (37)] for the SMuD case.

6.4.3 LCR and AFD

Let we define $\tilde{\alpha}_k = \sqrt{\tilde{\gamma}_k}$, where $\tilde{\gamma}_k$ is the **n**-SNR of the kth unranked users. Define $\dot{\tilde{\alpha}}_k$ as the first-order time derivation of $\tilde{\alpha}_k$. By the change of variables using (6.8), we show that $\dot{\tilde{\alpha}}_k$ for Rayleigh, Rician and Nakagami-m fading channels also follows a zero-mean Gaussian distribution and its PDF is given by

$$f_{\dot{\tilde{\alpha}}_k}(\dot{\tilde{\alpha}}) = \frac{1}{\sqrt{2\pi}\dot{\sigma}_{\dot{\tilde{\alpha}}_k}} \exp\left(-\frac{\dot{\tilde{\alpha}}^2}{2\dot{\sigma}^2_{\dot{\tilde{\alpha}}_k}}\right), \tag{6.28}$$

where $\dot{\sigma}^2_{\dot{\tilde{\alpha}}_k}$ is the variance of $\dot{\tilde{\alpha}}_k$ given by $\dot{\sigma}^2_{\dot{\tilde{\alpha}}_k} = \pi^2 f^2_{\mathrm{Dop},k}$, $\dot{\sigma}^2_{\dot{\tilde{\alpha}}_k} = \pi^2 f^2_{\mathrm{Dop},k}/(1+K_k)$, and $\dot{\sigma}^2_{\dot{\tilde{\alpha}}_k} = \pi^2 f^2_{\mathrm{Dop},k}/m_k$ for the Rayleigh, Rician and Nakagami-m fading channels, respectively, and $f_{\mathrm{Dop},k}$ is the Doppler fading bandwidth of the kth user. Below, we use $\dot{\tilde{\sigma}}^2_k$ as a shorthand for $\dot{\sigma}^2_{\dot{\tilde{\alpha}}_k}$.

Now we derive the LCR and AFD of the Nth largest normalized amplitude, $\tilde{\alpha}_{(N)} = \sqrt{\tilde{\gamma}_{(N)}}$. The LCR of $\tilde{\alpha}_{(N)}$ at the signal level R is given by

$$\mathrm{LCR}_{\tilde{\alpha}_{(N)}}(R) = \int_0^\infty \dot{x} f_{\tilde{\alpha}_{(N)},\dot{\tilde{\alpha}}_{(N)}}(R,\dot{x})d\dot{x} \tag{6.29}$$

www.manaraa.com

where $f_{\tilde{\alpha}_{(N)},\dot{\tilde{\alpha}}_{(N)}}(x,\dot{x})$ is the joint PDF of $\tilde{\alpha}_{(N)}$ and $\dot{\tilde{\alpha}}_{(N)}$.

Using a similar procedure in Section 6.3.2, we derived a closed-form expression of (6.29) for i.n.d. faded users as

$$\begin{aligned}\mathrm{LCR}_{\tilde{\alpha}_{(N)}}(R) &= \sum_{n_1,\ldots,n_N\in\mathcal{I}} f_{\tilde{\alpha}_{n_N}}(R)\left[\prod_{l=1}^{N-1}(1-F_{\tilde{\alpha}_{n_l}}(R))\right]\left[\prod_{l'=N+1}^{L}F_{\tilde{\alpha}_{n_{l'}}}(R)\right]\int_0^\infty \dot{x} f_{\dot{\tilde{\alpha}}_{n_N}}(\dot{x})d\dot{x} \\ &= \sum_{n_1,\ldots,n_N\in\mathcal{I}} f_{\tilde{\alpha}_{n_N}}(R)\left[\prod_{l=1}^{N-1}(1-F_{\tilde{\alpha}_{n_l}}(R))\right]\left[\prod_{l'=N+1}^{L}F_{\tilde{\alpha}_{n_{l'}}}(R)\right]\dot{\tilde{\sigma}}_{n_N}/\sqrt{2\pi}, \qquad (6.30)\end{aligned}$$

where $\dot{\tilde{\sigma}}_{n_N}=\dot{\sigma}_{n_N}/\sqrt{\tilde{\gamma}_{n_N}}$.

The AFD is given by $T_{\tilde{\alpha}_{(N)}}(R)=\Pr\{\tilde{\alpha}_{(N)}<R\}/\mathrm{LCR}_{\tilde{\alpha}_{(N)}}$. For i.n.d. Rayleigh faded users, we derived a closed-form expression for $\Pr\{\tilde{\alpha}_{(N)}<R\}$ as

$$\Pr\{\tilde{\alpha}_{(N)}<R\} = N\binom{L}{N}\sum_{k=0}^{L-N}(-1)^k\binom{L-N}{k}[1-\exp(-R^2(N+k))]/(N+k)$$

6.4.4 Channel Access Statistics

The AAR, AAT and AWT of GSMuD (L,N_c) with **n**-SNR ranking are derived here. Let we define $\tilde{\alpha}_*=\tilde{\alpha}_{(N_c),\tilde{k}}=\sqrt{\tilde{\gamma}_{(N_c),\tilde{k}}}$, where $\tilde{\gamma}_{(N_c),\tilde{k}}$ is the N_cth largest **n**-SNR among $L-1$ users (excluding user k). Define $\dot{\tilde{\alpha}}_*$ as the first-order time derivation of $\tilde{\alpha}_*$.

Define $\tilde{r}_k=\tilde{\alpha}_k/\tilde{\alpha}_{(N_c),\tilde{k}}=\tilde{\alpha}_k/\tilde{\alpha}_*$. The AAR of the kth user , AAR_k, is equivalent to the LCR at the positive direction of the kth users' signal envelop at the level that $\tilde{r}_k=1$. $\mathrm{AAR}_k=\Pr\{\tilde{r}=1,\dot{\tilde{r}}_k>0)$ Following a procedure given in [80], the AAR of user k is given by

$$\mathrm{AAR}_k=\int_0^\infty \dot{\tilde{r}} f_{\tilde{r}_k,\dot{\tilde{r}}_k}(\tilde{r}=1,\dot{\tilde{r}})d\dot{\tilde{r}}, \qquad (6.31)$$

where $\dot{\tilde{r}}_k$ is the first-order time derivation of $\tilde{r}_k$, and $f_{\tilde{r}_k,\dot{\tilde{r}}_k}(\tilde{r},\dot{\tilde{r}})$ is the joint PDF of $\tilde{r}_k$ and $\dot{\tilde{r}}_k$.

Using the procedure similar to that for deriving the case of **a**-SNR ranking in Section 6.3.3 and Appendix 6.C, we obtain a single integral expression of AAR_k with **n**-SNR ranking as

$$\begin{aligned}\mathrm{AAR}_k &= \int_0^\infty f_{\tilde{\alpha}_k}(\tilde{\alpha}_*)\sum_{n_1,\ldots,n_{N_c}\in\mathcal{I}_{\tilde{k}}} f_{\tilde{\alpha}_{n_{N_c}}}(\tilde{\alpha}_*)\left[\prod_{l=1}^{N_c-1}(1-F_{\tilde{\alpha}_{n_l}}(\tilde{\alpha}_*))\right] \\ &\quad\times\left[\prod_{l'=N_c+1}^{L-1}F_{\tilde{\alpha}_{n_{l'}}}(\tilde{\alpha}_*)\right]\sqrt{\frac{(\dot{\tilde{\sigma}}_k^2+\dot{\tilde{\sigma}}_{n_{N_c}}^2)}{2\pi}}d\tilde{\alpha}_* \qquad (6.32)\end{aligned}$$

www.manaraa.com

For Rayleigh fading channels, $f_{\tilde{\alpha}_k}(x) = 2x\exp(-x^2)$ and $F_{\tilde{\alpha}_k}(x) = 1-\exp(-x^2)$. Assume the general case that all the users may have different Doppler shifts. From (6.32) we obtain a closed-form AAR expression as

$$\mathrm{AAR}_k = \sum_{n_1,\ldots,n_{N_c}\in\mathcal{I}_{\tilde{k}}} \sum_{l=0}^{L-1-N_c} (-1)^l \binom{L-1-N_c}{l} (N_c+1+l)^{-3/2}\pi\sqrt{(f_{\mathrm{Dop},k}^2 + f_{\mathrm{Dop},n_{N_c}}^2)/2} \quad (6.33)$$

Furthermore, if $f_{\mathrm{Dop},1} = \cdots = f_{\mathrm{Dop},L} = f_{\mathrm{Dop}}$, we have

$$\mathrm{AAR}_k = \pi f_{\mathrm{Dop}} N_c \binom{L-1}{N_c} \sum_{l=0}^{L-1-N_c} (-1)^l \binom{L-1-N_c}{l} (N_c+1+l)^{-3/2} \quad (6.34)$$

Finally, we have $\mathrm{AAT}_k = \mathrm{AAP}_k/\mathrm{AAR}_k$, and $\mathrm{AWT}_k = (1-\mathrm{AAP}_k)/\mathrm{AAR}_k$.

6.5 Numerical Results

We provide some numerical examples and simulation results to illustrate the performance of our proposed GSMuD scheme with both **a**-SNR- and **n**-SNR-based rankings for i.i.d. and i.n.d. users over Rayleigh and Nakagami-m fading channels. For i.i.d. channels we assume all the users's signals have the same average SNRs, and $m = 2.1$ in the Nakagami-m fading channel. For all the i.n.d. channels considered in this section, we assume the average SNRs differ successively by 1.5 dB from the strongest user to the weakest one, i.e., $\bar{\gamma}_{k+1} = \bar{\gamma}_k 10^{-1.5/10}$, for $k = 1,\ldots,L-1$. Furthermore, following the same branch order $m = [3, 2.6, 2.2, 1.8, 1.4, 1]$ in the i.n.d. Nakagami channels.

Next we present the numerical and simulation results for the throughput and fairness metrics of the propose **n**-SNR-ranking GSMuD and the **a**-SNR-ranking GSMuD proposed in Chapter 4. We used the Nakagami-m fading channel simulator proposed in Chapter 7.2 to generate the desired channel coefficients in our simulation.

6.5.1 Throughput

We assume $P_T = 1$ for different N_c and L in Fig. 6.2 and Fig. 6.3. Thus, $P_N = 1/N_c$. All throughput results have been normalized by B/N_s. In Fig. 6.2 we present the individual throughput of GSMuD (with the **a**-SNR-based and the **n**-SNR-based rankings) vs. the user-average channel SNR $\bar{\gamma}$ ($\bar{\gamma} = \frac{1}{L}\sum_{k=1}^{L}\bar{\gamma}_k$) over i.n.d. Rayleigh fading channels, with $L = 6$,

www.manaraa.com

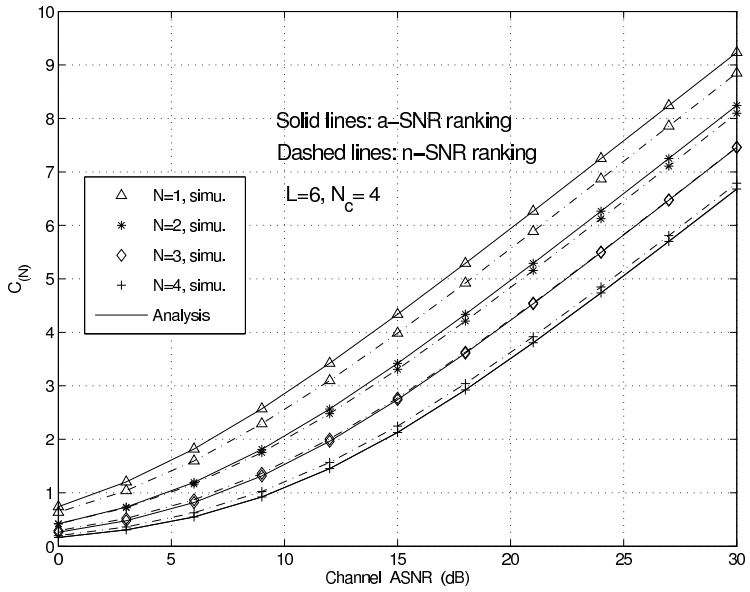

Figure 6.2 Analytical and simulated individual throughput of ranked users with GSMuD (with **a**-SNR- and **n**-SNR-based rankings) vs. the user-average channel SNR over i.n.d. Rayleigh fading channels. The channel average SNRs for the $L = 6$ users differ by 1.5 dB from the strongest user to the weakest one.

$N_c = 4$ and $N = \{1, 2, 3, 4\}$ (the first 4 strongest users). With the **n**-SNR ranking the throughput gap between the strongest user ($N = 1$) and the 4th strongest user ($N = 4$) is reduced compared to that with the **a**-SNR ranking, which implies an improved fairness. On the other hand, the throughput of the **n**-SNR ranking for $N = 1$ is smaller than that with the **a**-SNR ranking.

In Fig. 6.3 we show the sum-throughput of GSMuD vs. the channel average SNR over i.n.d. Nakagami-m fading channels with $L = 6$. The results show that the sum-throughput for each N_c with the **n**-SNR ranking is slightly lower than that of the **a**-SNR ranking. As N_c increases the sum throughput increases. For $N_c = L$, the rates of the **a**-SNR-GSMuD and the **n**-SNR-GSMuD become identical, as expected. In both Fig. 6.2 and Fig. 6.3, the analytical curves for both the **a**-SNR- and the **n**-SNR-ranking excellently match the simulation results (in markers), which verified the validity and accuracy of our analysis.

In Fig. 6.4, the sum rates of the **n**-SNR GSMuD and the round robin schemes are given

www.manaraa.com

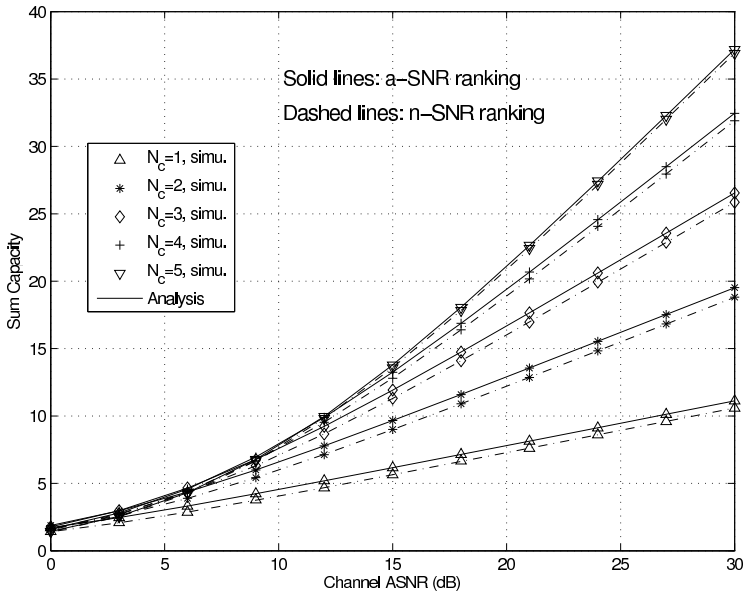

Figure 6.3 Analytical and simulated sum throughput of GSMuD vs. the channel average SNR over i.n.d. Nakagami-m fading channels (with $L = 6$), with both **a**-SNR-based (in solid lines) and **n**-SNR-based (in dashed lines) rankings. For the i.n.d. channels, the average SNRs differ by 1.5 dB from the strongest user to the weakest one, and $m = [3, 2.6, 2.2, 1.8, 1.4, 1]$.

assuming $L = 6$ i.i.d. Rayleigh faded users and $N_c = [1, 2, 3]$. The **n**-SNR GSMuD, while maintaining fairness, has a larger throughput than the RR scheme due to the SNR ranking. In Fig. 6.5, individual user throughput of GSMuD with **a**-SNR and **n**-SNR-based rankings vs. original user index k over i.n.d. Rayleigh fading channels is shown. As N_c increases, every user has a larger rate. The **n**-SNR ranking brings more uniform throughput rates for different users and thus better fairness than **a**-SNR ranking.

6.5.2 Fairness Metrics

We study the fairness metrics (including the AAP and DoF). For all the examples studied below, we assume $P_N = 1$ for all the N_c selected users, so that $P_T = N_c$. We show the AAP of every unordered user k ($k = 1, \ldots, L$) with the **n**-SNR-GSMuD and the **a**-SNR-GSMuD schemes in the i.n.d. Rayleigh and i.n.d. Nakagami-m fading channels in Fig. 6.6 and Fig. 6.7, respectively. In both figures the user index k is shown in a descending order of their

www.manaraa.com

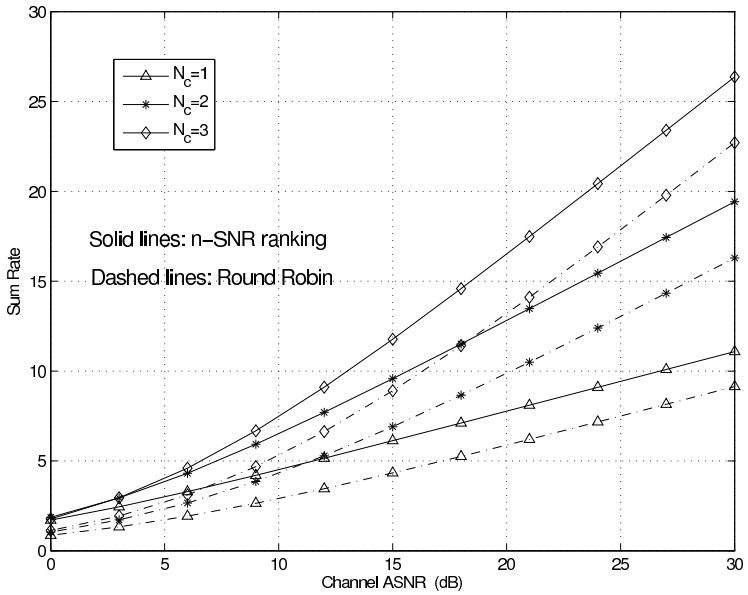

Figure 6.4 Sum throughput vs. the channel average SNR for both **n**-SNR-GSMuD and round robin schemes over i.i.d. Rayleigh fading channels with $L = 6$.

average SNRs. For both Fig. 6.6 and Fig. 6.7, the analytical curves again excellently agree with the simulation results (in markers).

The result in Fig. 6.6 shows that as N_c increases the AAP increases for every user k. The **n**-SNR ranking ensures an uniform AAP ($\text{AAP}_k = N_c/L$) for every k and N_c and thus provides perfect proportional fairness.

Fig. 6.7 shows that for the i.n.d. Nakagami fading channels **n**-SNR-ranking significantly improves the fairness, though it does not provide perfectly uniform AAPs. Though the disparateness of the average SNRs has been compensated by the **n**-SNR ranking, the differences of Nakagami-m parameters among the users cause the slightly non-uniform AAPs. This is due to the difference of other types of channels (such as the Nakagami and Rician distributions) than the Rayleigh channels. The non-uniform fading parameters (such as Nakagami-m, q and Rice-K parameters) among the users may not be perfectly compensated by the SNR normalization alone but the **n**-SNR ranking can improve it. We also observe in Fig. 6.7 that for $N_c = 1$ the user $k = 6$ (with $m = 1$) has the largest AAP among the six users. This is because

www.manaraa.com

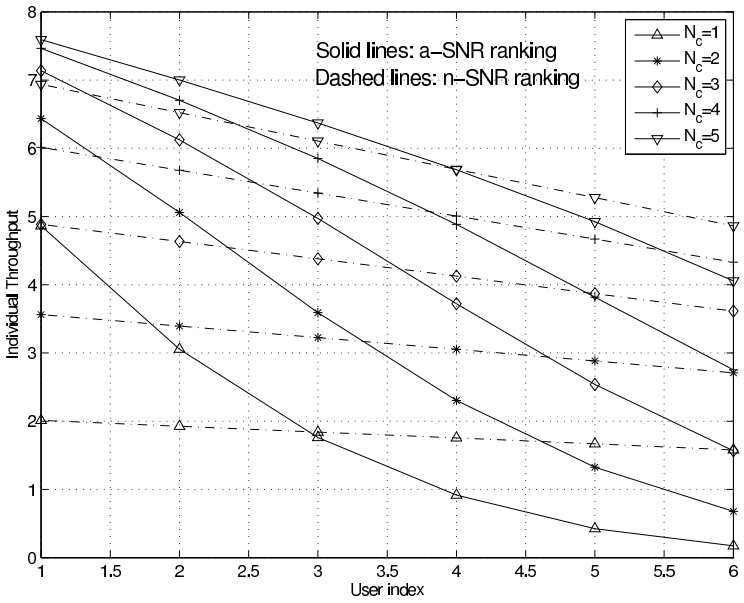

Figure 6.5 Individual user throughput of GSMuD with **a**-SNR and **n**-SNR-based rankings vs. original user index k over i.n.d. Rayleigh fading channels with $L = 6$.

that in the $N_c = 1$ case, the PDF of the Nakagami channel envelop with a smaller m-parameter has a larger tail towards infinity than the PDF with a larger m-parameter (given the same average SNR, see Fig. 7.2), and so the former (user 6) has an advantage of competing for the best-ranked user. When N_c increases, a small m-parameter is not advantageous to compete for the second and third largest SNRs, since it also has a bulky tail toward the low SNR region as compared to the case with a larger m-parameter. Thus, we observe that as N_c increases, users with larger m parameters have larger AAPs.

Fig. 6.8 shows the sum DoF vs. N_c for i.n.d. Rayleigh and Nakagami channels. The result shows that the sum DoF of **a**-SNR ranking over i.n.d. Nakagami channel is highly unfair for $N_c = 1$, but improves as N_c increases. On the other hand, the **n**-SNR ranking brings near-perfect fairness for all cases.

www.manaraa.com

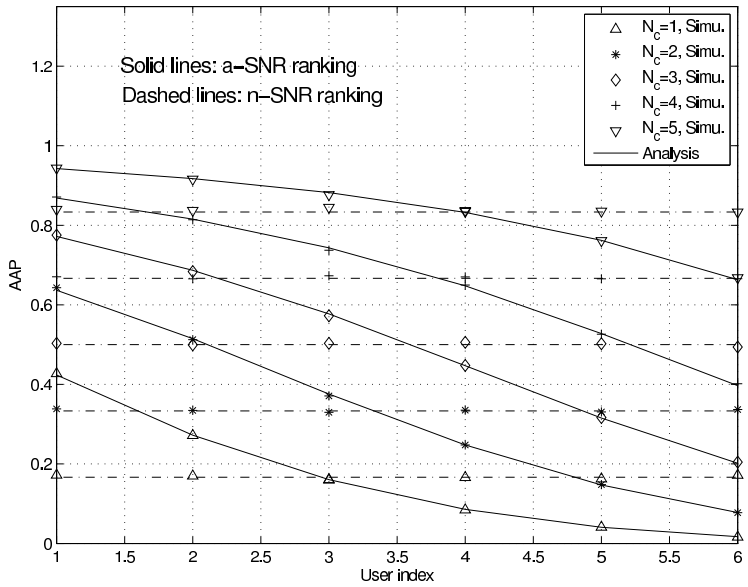

Figure 6.6 Analytical and simulated AAPs of GSMuD with **a**-SNR and **n**-SNR-based rankings vs. original user index k over i.n.d. Rayleigh fading channels with $L = 6$. The user index is ranged in the decreasing order of the channel average SNRs.

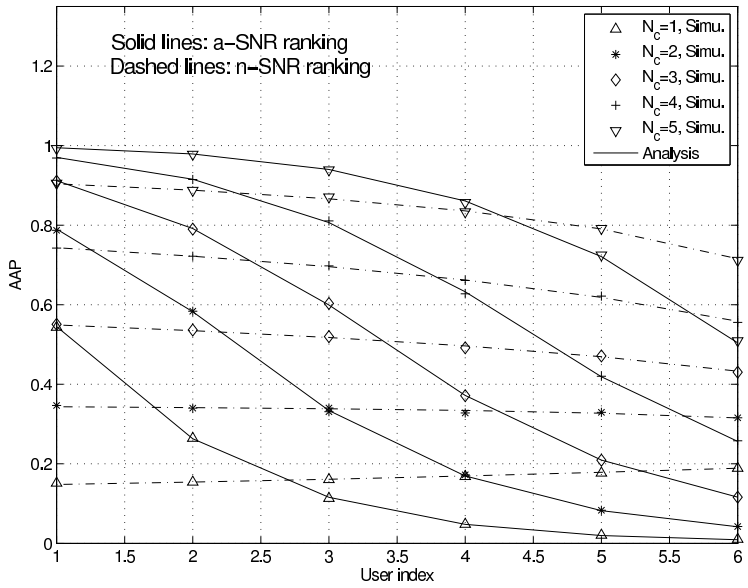

Figure 6.7 Analytical and simulated AAPs of GSMuD with **a**-SNR and **n**-SNR-based rankings vs. user index k over i.n.d. Nakagami fading channels with $L = 6$, and $m = [3, 2.6, 2.2, 1.8, 1.4, 1]$.

www.manaraa.com

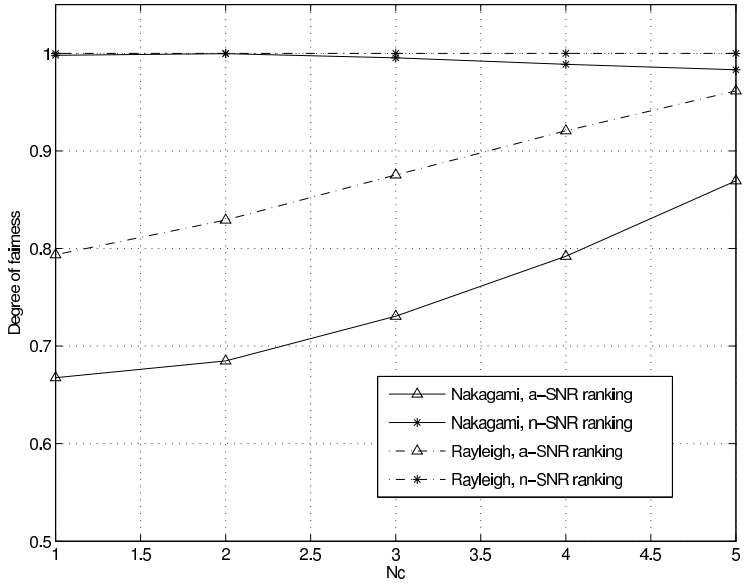

Figure 6.8 Sum DoF of GSMuD vs. N_c over i.n.d. Rayleigh and Nakagami-m fading channels, with $L = 6$ and $N_c = [1 - 5]$.

6.5.3 LCR, AFD, and Channel Access Statistics

Below, we assume all the users have the same Doppler bandwidth, i.e., $f_{\text{Dop},1} = \ldots = f_{\text{Dop},L} = f_{\text{Dop}}$. As a result, the normalized LCR and normalized AFD are independent of f_{Dop}. The normalized LCR $\text{LCR}_{\alpha_{(N)}}(R)/f_{\text{Dop}}$ and the normalized AFD $T_{\alpha_{(N)}}(R) \cdot f_{\text{Dop}}$ (with $N = [1, 3, 5]$ and $N_c = L = 6$) of **a**-SNR-GSMuD vs. threshold R over the i.n.d. Nakagami-m fading channels are presented in Fig. 6.9 and Fig. 6.10, respectively. Fig. 6.9 shows that as N increases (towards lower-ranked users), the LCR happens more frequently at the lower values of R. Fig. 6.10 illustrates that at a lower threshold level R a weaker user (e.g., $N = 3$) has a larger AFD than a stronger user (e.g., $N = 1$) does.

The AAR, AAT and AWT of GSMuD are important performance metrics to the scheduling and cross-layer design. The normalized AAR ($\text{AAR}_k/f_{\text{Dop}}$) vs. user index k over the i.n.d. Nakagami channels is shown in Fig. 6.11, with $L = 6$ and $N_c = 3$. With **a**-SNR ranking the strongest user ($k = 1$) and the weakest user ($k = 6$) have lower AARs than the users with medium average SNRs ($k = 3, 4$). For **n**-SNR ranking, however, user 1 is the most active and user 6 is the least active in acquiring and releasing the channel access.

www.manaraa.com

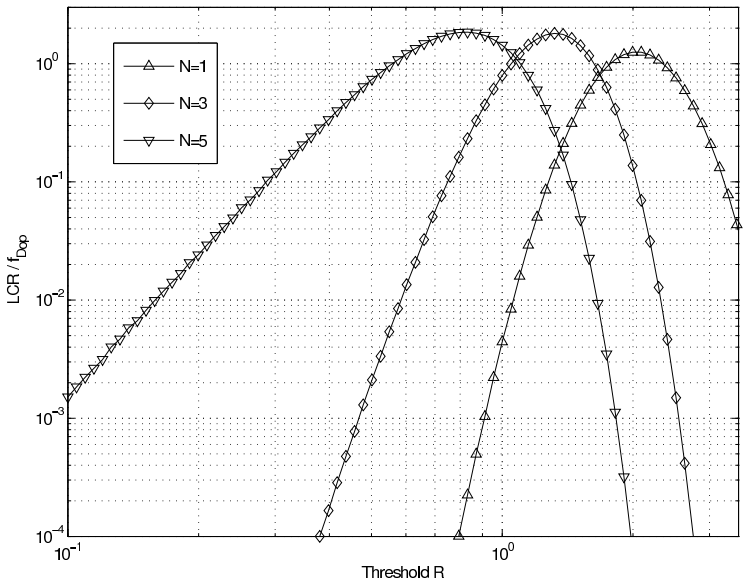

Figure 6.9 Normalized LCR ($\mathrm{LCR}_{\alpha_{(N)}}(R)/f_{\mathrm{Dop}}$) of GSMuD vs. threshold R over i.n.d. Nakagami-m fading channels, with $L = 6$, $N = [1, 3, 5]$, and $m = [3, 2.6, 2.2, 1.8, 1.4, 1]$. $f_{\mathrm{Dop},1} = \ldots = f_{\mathrm{Dop},L} = f_{\mathrm{Dop}}$.

The normalized AAT ($\mathrm{AAT}_k \cdot f_{\mathrm{Dop}}$) vs. user index k over the i.n.d. Rayleigh channel is shown in Fig. 6.12, with $L = 6$ and $N_c = [1 - 5]$. In Fig. 6.12 the simulation results are shown which verify our analytical results on the AAT (and also the AAR and the AWT, since the AAP has already been verified). The result in Fig. 6.12 shows that the users with larger average SNRs generally have larger AATs than users with weaker average SNRs for **a**-SNR ranking. With the **n**-SNR ranking, the AATs of weaker users are significantly improved than with the **a**-SNR ranking.

The normalized AWT ($\mathrm{AWT}_k \cdot f_{\mathrm{Dop}}$) for each user over the i.n.d. Nakagami channels is presented in Fig. 6.13, which shows that the AWTs for all the users decrease as N_c increases, which is an advantage of GSMuD over the SMuD. With the **n**-SNR ranking the AWTs among the users become nearly uniform.

www.manaraa.com

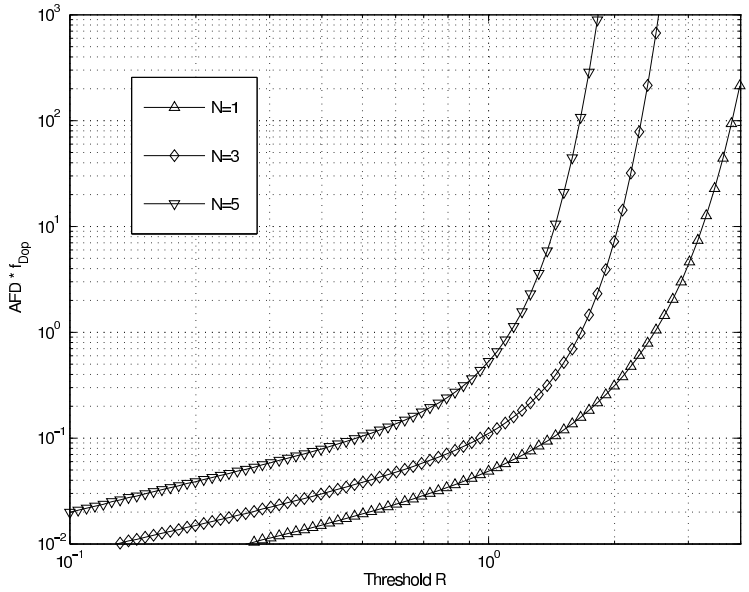

Figure 6.10 Normalized AFD ($T_{\alpha_{(N)}}(R) \cdot f_{\text{Dop}}$) of GSMuD vs. threshold R over i.n.d. Nakagami-m fading channels with $L = 6$, $N = [1, 3, 5]$, and $m = [3, 2.6, 2.2, 1.8, 1.4, 1]$. $f_{\text{Dop},1} = \ldots = f_{\text{Dop},L} = f_{\text{Dop}}$.

6.6 Summary

To address the fairness issues in GSMuD, we have proposed the normalized-SNR-ranking based approach, which ranks a total of L users awaiting for transmission by their SNRs and selects N_c number of users with the largest absolute or normalized SNRs for channel access. We also analyzed the fairness metrics and throughput performance of the absolute- or normalized-SNR-ranking based GSMuD schemes assuming the equal transmit power allocation among the selected users. The individual- and sum-rates, second-order statistics (LCR and AFD), fairness (DoF and AAP), and channel access statistics (including AAR, AAT and AWT) have been evaluated. The results are valid for generalized fading channels, and have been verified by simulations. Numerical results show that **a**-SNR-based GSMuD significantly improves the proportional fairness of all the users than the SMuD and the **n**-SNR-based GSMuD further extends this benefit. Specifically, as N_c increases, the GSMuD improves the AAT and reduces the AWT for every user than the SMuD. With the **n**-SNR ranking, the users with weaker aver-

www.manaraa.com

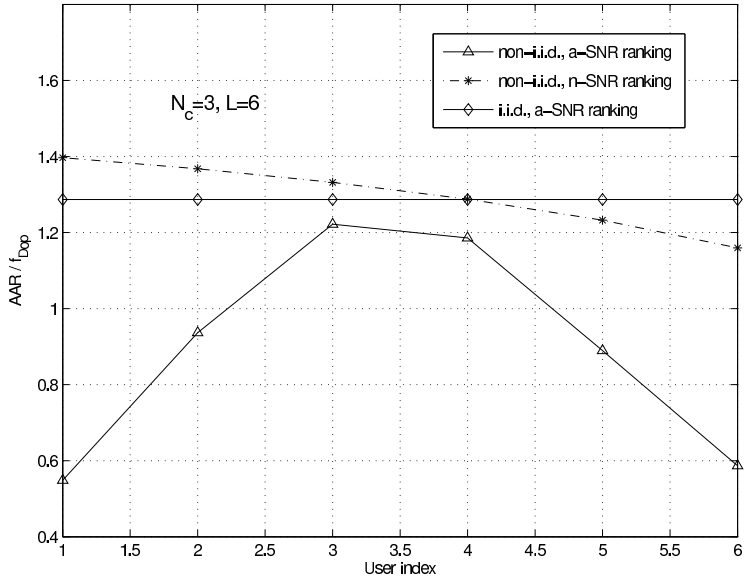

Figure 6.11 Normalized AAR ($\mathrm{AAR}_k/f_{\mathrm{Dop}}$) of GSMuD with **a**-SNR- and **n**-SNR-based rankings vs. user index k over i.i.d. and i.n.d. Nakagami-m fading channels, with $L = 6$ and $N_c = 3$. For the i.n.d. channels, $m = [3, 2.6, 2.2, 1.8, 1.4, 1]$ and the user index is ranged in the decreasing order of the channel average SNRs. For the i.i.d. channels, $m = 2.1$ and the channel average SNRs are identical for all the users.

age SNRs gain more resources in terms of the AAP and the AAT, and thus better proportional fairness. These results will be useful for the cross-layer design of multiuser parallel scheduling systems. We further show that **a**-SNR-based GSMuD can provide a larger sum-rate than **n**-SNR-based GSMuD for all cases, and thus these two schemes provide a tradeoff between fairness and performance.

This concludes our discussion on GSMuD-related algorithms and analysis. In the next chapter, we address another important problem for researchers and engineers alike: the Nakagami-m fading channel simulator. As a matter of fact, many of the simulation results from previous chapters actively applied the approaches we present next to generating the Nakagami-m fading channels.

www.manaraa.com

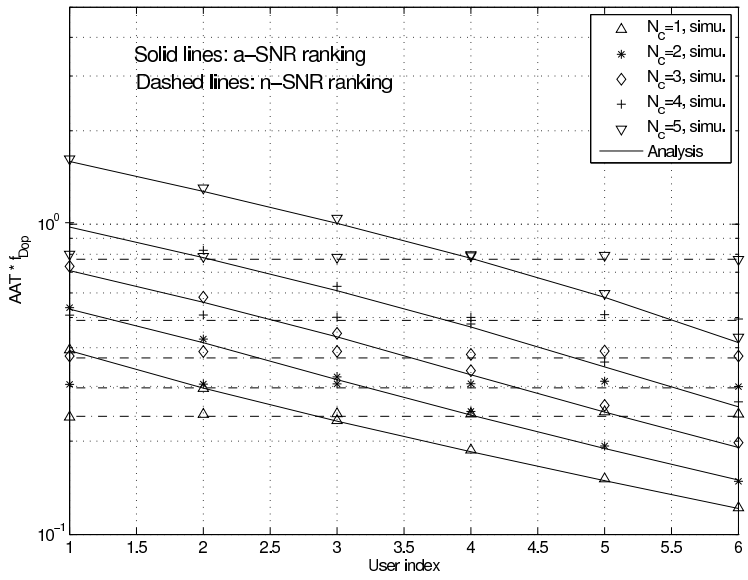

Figure 6.12 Analytical and simulated normalized AAT ($\mathrm{AAT}_k \cdot f_{\mathrm{Dop}}$) of GSMuD with **a**-SNR- and **n**-SNR-based rankings vs. user index k over i.n.d. Rayleigh fading channels. $L = 6$ and $N_c = [1 - 5]$.

6.7 Appendix 6.A AAP Expressions for a-SNR GSMuD

Define $f_{\gamma_{(N_c),\tilde{k}}}(x)$ as the PDF of $\gamma_{(N_c),\tilde{k}}$. Using a similar procedure similar to that for deriving $f_{\gamma_{(N)}}(x)$, we may obtain

$$f_{\gamma_{(N_c),\tilde{k}}}(x) = \sum_{n_1,\ldots,n_{N_c} \in \mathcal{I}_{\tilde{k}}} f_{\gamma_{n_{N_c}}}(x) \times \left[\prod_{l=1}^{N_c-1} (1 - F_{\gamma_{n_l}}(x))\right] \left[\prod_{l'=N_c+1}^{L-1} F_{\gamma_{n_{l'}}}(x)\right], \tag{6.35}$$

where in $\sum_{n_1,\ldots,n_{N_c} \in \mathcal{I}_{\tilde{k}}}$, $\mathcal{I}_{\tilde{k}}$ is the set for all combinations of $\{n_1, \ldots, n_{L-1}\}$ (excluding the case of $n_l = k$), in which the subset $\{n_1, \ldots, n_{N_c}\}$ are the indices of N_c users with largest SNRs among $L - 1$ users. We have

$$\mathrm{AAP}_k = \int_0^\infty f_{\gamma_k}(x) \left[\int_0^x f_{\gamma_{(N_c),\tilde{k}}}(y) dy\right] dx \tag{6.36}$$

www.manaraa.com

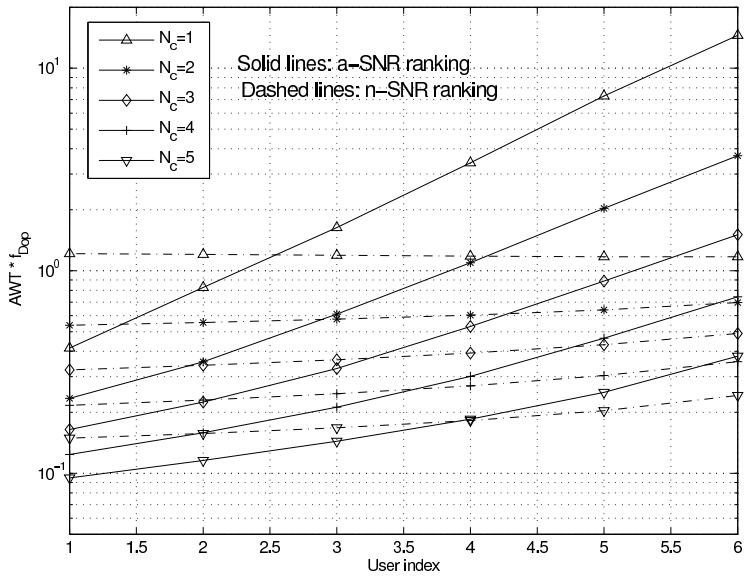

Figure 6.13 Normalized AWT ($\mathrm{AWT}_k \cdot f_{\mathrm{Dop}}$) of GSMuD with **a**-SNR- and **n**-SNR-based rankings vs. user index k over i.n.d. Nakagami-m fading channels. $L = 6$ and $N_c = [1 - 5]$.

For the Rayleigh-faded users, we derive a closed-form expression for AAP_k as

$$\begin{aligned}
\mathrm{AAP}_k &= \int_0^\infty \frac{e^{-x/\bar{\gamma}_k}}{\bar{\gamma}_k} \int_0^x \sum_{n_1,\ldots,n_{N_c} \in \mathcal{I}_{\tilde{k}}} \frac{\exp(-y/\bar{\gamma}_{n_{N_c}})}{\bar{\gamma}_{n_{N_c}}} \left[\prod_{l=1}^{N_c-1} e^{-y/\bar{\gamma}_{n_l}}\right] \prod_{l'=N_c+1}^{L-1} \left[1 - e^{-y/\bar{\gamma}_{n_{l'}}}\right] dydx \\
&= \int_0^\infty \exp(-x/\bar{\gamma}_k)/\bar{\gamma}_k \sum_{n_1,\ldots,n_{N_c} \in \mathcal{I}_{\tilde{k}}} \sum_{\tau \in J_{L-N_c-1}} \mathrm{sign}(\tau) \frac{(1 - e^{-Bx})}{\bar{\gamma}_{n_{N_c}} B} dx \\
&= \sum_{n_1,\ldots,n_{N_c} \in \mathcal{I}_{\tilde{k}}} \sum_{\tau \in J_{L-N_c-1}} \mathrm{sign}(\tau) \cdot \frac{1}{\bar{\gamma}_{n_{N_c}}} \left[\bar{\gamma}_k/(B\bar{\gamma}_k + 1)\right] \qquad (6.37)
\end{aligned}$$

where $B = \sum_{l=1}^{N_c} \frac{1}{\bar{\gamma}_{n_l}} + |\tau|$, and J_{L-N_c-1} is a shorthand for $J_{L-N_c-1}\left(\left\{\frac{1}{\bar{\gamma}_{n_l}}\right\}_{l=N_c+1}^{L-1}, n_l \neq k\right)$, which follows the definition in (5.27) and contains 2^{L-N_c-1} elements.

6.8 Appendix 6.B Joint PDF of α and $\dot{\alpha}$ for GSMuD

We derive the joint PDF of $\alpha_{(N)}$ and $\dot{\alpha}_{(N)}$ here. The joint CDF of $\alpha_{(N)}$ and $\dot{\alpha}_{(N)}$ is given by

$$F_{\alpha_{(N)},\dot{\alpha}_{(N)}}(x, \dot{x}) = \sum_{n_1,\ldots,n_N \in \mathcal{I}} \Pr\{\alpha_{n_N} < x, \dot{\alpha}_{n_N} < \dot{x} | \alpha_{n_N} = \alpha_{(N)}\} \cdot \Pr\{\alpha_{n_N} = \alpha_{(N)}\} \qquad (6.38)$$

www.manaraa.com

where $\{\alpha_{n_N} = \alpha_{(N)}\}$ is the event that the user n_N ($n_N = 1, \ldots, L$) has the Nth largest SNR. The summation set $\mathcal{I}$ is the set for all combinations of $\{n_1, \ldots, n_L\}$ in which the subset $\{n_1, \ldots, n_N\}$ are the indices of N users with largest SNRs. We first consider the case that α_{n_N} and $\dot{\alpha}_{n_N}$ are independent, and then study the case that they are correlated.

When α_{n_N} and $\dot{\alpha}_{n_N}$ are independent, we have

$$F_{\alpha_{(N)},\dot{\alpha}_{(N)}}(x,\dot{x}) = \sum_{n_1,\ldots,n_N \in \mathcal{I}} \Pr\{\alpha_{n_N} < x | \alpha_{n_N} = \alpha_{(N)}\} \cdot \Pr\{\dot{\alpha}_{n_N} < \dot{x}\} \tag{6.39}$$

where $\Pr\{\alpha_{n_N} < x | \alpha_{n_N} = \alpha_{(N)}\} = \int_0^x f_{\alpha_{n_N}}(y|\alpha_{n_N} = \alpha_{(N)})dy$, and $\Pr\{\dot{\alpha}_{n_N} < \dot{x}\} = \int_0^{\dot{x}} f_{\dot{\alpha}_{n_N}}(y)dy$. Using a procedure similar to that for deriving (5.5) we obtain

$$f_{\alpha_{n_N}}(y|\alpha_{n_N} = \alpha_{(N)}) = f_{\alpha_{n_N}}(y)\left[\prod_{l=1}^{N-1}(1 - F_{\alpha_{n_l}}(y))\right]\left[\prod_{l'=N+1}^{L} F_{\alpha_{n_{l'}}}(y)\right]. \tag{6.40}$$

Taking double derivative of (6.39) w.r.t to x and $\dot{x}$ leads to

$$f_{\alpha_{(N)},\dot{\alpha}_{(N)}}(x,\dot{x}) = \sum_{n_1,\ldots,n_N \in \mathcal{I}} f_{\alpha_{n_N}}(x)\left[\prod_{l=1}^{N-1}(1 - F_{\alpha_{n_l}}(x))\right]\left[\prod_{l'=N+1}^{L} F_{\alpha_{n_{l'}}}(x)\right] f_{\dot{\alpha}_{n_N}}(\dot{x}) \tag{6.41}$$

Next, when α_{n_N} and $\dot{\alpha}_{n_N}$ are not independent, we have

$$F_{\alpha_{(N)},\dot{\alpha}_{(N)}}(x,\dot{x}) = \sum_{n_1,\ldots,n_N \in \mathcal{I}} \Pr\{\alpha_{n_N} < x, \dot{\alpha}_{n_N} < \dot{x} | \alpha_{n_N} = \alpha_{(N)}\} \tag{6.42}$$

Taking double derivative of (6.42) w.r.t to x and $\dot{x}$ leads to

$$f_{\alpha_{(N)},\dot{\alpha}_{(N)}}(x,\dot{x}) = \sum_{n_1,\ldots,n_N \in \mathcal{I}} f_{\alpha_{n_N},\dot{\alpha}_{n_N}}(x,\dot{x})\left[\prod_{l=1}^{N-1}(1 - F_{\alpha_{n_l}}(x))\right]\left[\prod_{l'=N+1}^{L} F_{\alpha_{n_{l'}}}(x)\right] \tag{6.43}$$

6.9 Appendix 6.C AAR for a-SNR GSMuD

We first evaluate the integral with respect to (w.r.t.) $\dot{\alpha}_*$ and obtain (setting $r = 1$)

$$\begin{aligned}\int_{-\infty}^{\infty} f_{\dot{\alpha}_k}(\dot{r}\alpha_* + \dot{\alpha}_*) f_{\dot{\alpha}_{n_{N_c}}}(\dot{\alpha}_*)d\dot{\alpha}_* &= \frac{1}{2\pi\dot{\sigma}_k\dot{\sigma}_{n_{N_c}}}\int_{-\infty}^{\infty}\exp\left(-\frac{(\dot{r}\alpha_* + \dot{\alpha}_*)^2}{2\dot{\sigma}_k^2} - \frac{\dot{\alpha}_*^2}{2\dot{\sigma}_{n_{N_c}}^2}\right)d\dot{\alpha}_* \\ &= \frac{1}{\sqrt{2\pi(\dot{\sigma}_k^2 + \dot{\sigma}_{n_{N_c}}^2)}}\exp\left(-\frac{\dot{r}^2\alpha_*^2}{2\dot{\sigma}_k^2 + 2\dot{\sigma}_{n_{N_c}}^2}\right)\end{aligned} \tag{6.44}$$

Next, we interchange the integral order of α_* and $\dot{r}$. The integral w.r.t. $\dot{r}$ gives

$$\frac{1}{\sqrt{2\pi(\dot{\sigma}_k^2 + \dot{\sigma}_{n_{N_c}}^2)}}\int_0^{\infty}\dot{r}\exp\left(-\frac{\dot{r}^2\alpha_*^2}{2\dot{\sigma}_k^2 + 2\dot{\sigma}_{n_{N_c}}^2}\right)d\dot{r} = \frac{1}{\alpha_*^2}\sqrt{(\dot{\sigma}_k^2 + \dot{\sigma}_{n_{N_c}}^2)/(2\pi)} \tag{6.45}$$

www.manaraa.com

Substituting (6.45) into (6.13) we obtain a single integral expression of AAR_k valid for i.n.d.-faded users over Rayleigh, Rician and Nakagami-m channels as

$$\mathrm{AAR}_k = \int_0^\infty f_{\alpha_k}(\alpha_*) \sum_{n_1,\ldots,n_{N_c}\in\mathcal{I}_{\tilde{k}}} f_{\alpha_{n_{N_c}}}(\alpha_*) \left[\prod_{l=1}^{N_c-1}\left(1-F_{\alpha_{n_l}}(\alpha_*)\right)\right] \times \left[\prod_{l'=N_c+1}^{L-1} F_{\alpha_{n_{l'}}}(\alpha_*)\right] \sqrt{\frac{(\dot{\sigma}_k^2+\dot{\sigma}_{n_{N_c}}^2)}{2\pi}}\, d\alpha_* \quad (6.46)$$

Furthermore, for i.n.d. Rayleigh-faded users, (6.46) can be reduced to a closed form. For Rayleigh fading channels $f_{\alpha_k}(x) = \frac{2x}{\bar{\gamma}_k}\exp(-x^2/\bar{\gamma}_k)$ and $F_{\alpha_k}(x) = 1-\exp(-x^2/\bar{\gamma}_k)$. The product $\prod_{l'=N_c+1}^{L-1} F_{\alpha_{n_{l'}}}(\alpha_*)$ in (6.46) may be decomposed to

$$\prod_{l'=N_c+1}^{L-1} F_{\alpha_{n_{l'}}}(\alpha_*) = \sum_{\tau\in J_{L-N_c-1}} \mathrm{sign}(\tau)\exp(-\alpha_*^2|\tau|)$$

where J_{L-N_c-1} is a shorthand for $J_{L-N_c-1}(\{\frac{1}{\bar{\gamma}_{n_l}}\}_{l=N_c+1}^{L-1}, n_l\neq k)$. Using the integral equality that $\int_0^\infty x^2\exp(-x^2C)dx = \sqrt{\pi}C^{-3/2}/4$, we have

$$\mathrm{AAR}_k = \sum_{n_1,\ldots,n_{N_c}\in\mathcal{I}_{\tilde{k}}} \sum_{\tau\in J_{L-N_c-1}} \mathrm{sign}(\tau)\frac{\sqrt{(\dot{\sigma}_k^2+\dot{\sigma}_{n_{N_c}}^2)/2}}{\bar{\gamma}_k\bar{\gamma}_{n_{N_c}}}\left(\frac{1}{\bar{\gamma}_k}+\sum_{l=1}^{N_c}\frac{1}{\bar{\gamma}_{n_l}}+|\tau|\right)^{-3/2} \quad (6.47)$$

As the verification, for $N_c = 1$, the result in (6.47) reduces to

$$\mathrm{AAR}_k = \sum_{\substack{n_1=1\\ n_1\neq k}}^{L} \sum_{\tau\in J_{L-2}} \mathrm{sign}(\tau)\frac{\sqrt{(\dot{\sigma}_k^2+\dot{\sigma}_{n_1}^2)/2}}{\bar{\gamma}_k\bar{\gamma}_{n_1}}\left(\frac{1}{\bar{\gamma}_k}+\frac{1}{\bar{\gamma}_{n_1}}+|\tau|\right)^{-3/2} \quad (6.48)$$

where J_{L-2} is a shorthand for $J_{L-2}(\{\frac{1}{\bar{\gamma}_{n_l}}\}_{l=2}^{L}, n_l\neq k)$. We can readily show that (6.48) is equivalent to the case of SMuD given by [80, eq.(11)].

www.manaraa.com

CHAPTER 7. ACCURATE COMPLEX NAKAGAMI-m FADING CHANNEL SIMULATOR

7.1 Introduction

The Nakagami-m [123] channel model has been widely used to model the fading distribution in various wireless channels [98–102, 104, 105]. Its popularity stems from the fact that Nakagami-m fading model can better fit the experimental results [106] than Rayleigh, Rice or log-normal fading models for certain types of fading environment. Simulation of Nakagami channel sequences which accurately captures the pre-specified temporal auto-correlation property is important for fading channel transceiver design and performance evaluation for wireless communication, including, for example, simulation of pilot-symbol-based channel estimators. and cross-layer design in packet transmissions [76] for Nakagami channels.

For Nakagami-m fading channel simulation, in [95] a method for generating Nakagami-m distributed samples valid for integer and half-integer valued m-parameters was proposed. This method relies on the fact that the square-root of a sum of the square of n zero-mean independent and i.i.d. real Gaussian variables has a Nakagami-m distribution with $m = n/2$. This technique can generate samples which follow the pre-specified multi-branch spatial correlation matrix, but it is not clear how to use this method to fulfill pre-specified temporal correlation function. In [110], a method was proposed to generate Nakagami-m fading channels based on the product of a square-root beta process and a complex Gaussian process. This result can account for temporally-correlated channels but is only valid for the case $0.5 \leq m \leq 1$. The recently proposed Nakagami-m fading channel simulator [111] discussed in Section 1.5 takes into account arbitrary temporal correlation. In this approach [111], a Rayleigh fading channel realization with a pre-specified temporal correlation (such as the Clarke's model) is

www.manaraa.com

first generated. The Rayleigh fading amplitude is then mapped to the Nakagami-m fading amplitude via the relationship between CDFs of Rayleigh and Nakagami distributions. Furthermore, the authors heuristically designed a process so that the phase components of the generated Nakagami-m fading channels were taken directly from those of the Rayleigh channel samples. As pointed out in Section 1.6, this technique provides a low-complexity solution to generate Nakagami samples, but with two technical problems left open: (1) It is not known what the generated Nakagami temporal autocorrelation function is. An even more significant question is, in order to fulfill a specified Nakagami temporal autocorrelation function, what should the original Rayleigh temporal autocorrelation function be? (2) The phase property of the generated Nakagami sequences have not been adequately addressed.

In this chapter, we design simulation techniques to solve these two open problems and also provide an in-depth analysis. We propose a novel approach to generate the Nakagami-m fading channel sequences which satisfies (1) arbitrary pre-specified temporal autocorrelation function, (2) proper non-uniform phase distribution following that given in [112], (3) arbitrary pre-specified m parameter and signal power, (4) independent real and imaginary parts (for $m \geq 1$). Our new method has a low complexity, versatile for different channel parameters, and theoretically more strict than available approaches.

7.2 Nakagami-m Fading Channel Model

The PDF of a Nakagami-m distributed fading channel amplitude α is given by

$$p(\alpha) = \frac{2m^m \alpha^{2m-1}}{\Omega^m \Gamma(m)} \exp(-\frac{m\alpha^2}{\Omega}) \tag{7.1}$$

We noticed this PDF expression is a central chi-square distribution in essence. Here $\Omega = E[\alpha^2]$ is the average power of α and called the shaping factor, and

$$m = \frac{\Omega^2}{E[\alpha^2 - \Omega]} \geq \frac{1}{2} \tag{7.2}$$

is the m-parameter which determines the severity of fading. The amount of fading (AF) [103] for the Nakagami-m distributed RV is:

$$AF = \frac{1}{m} \tag{7.3}$$

www.manaraa.com

where AF for any RV α is defined as:

$$AF = \frac{var(\alpha^2)}{\Omega^2} \tag{7.4}$$

AF quantifies the fading severity, with a larger value meaning more severe fading. We can see that Nakagami-m distribution has the widest range of AF from 0 to 2 among all the commonly used multipath distributions such as Rayleigh, Rice,Nakagami-q, etc. The one sided Gaussian ($m = \frac{1}{2}$) and Rayleigh ($m = 1$) are special cases of Nakagami-m distribution. The m factor also determines the severity of fading evident from the AF. When $m < 1$, $AF > 1$ is the situation where fading is more sever than Rayleigh fading and the smaller the m parameter, the larger the AF thus the more severity the fading. On the other hand, when $m > 1$, $AF < 1$ is the situation where fading is less sever than Rayleigh fading and the larger the m parameter the less severity the fading is. In the extreme case where $m \to +\infty$, the Nakagami-m fading channel converges to a nonfading AWGN channel.

The relationship is also evident in the shape of the Nakagami-m PDF with the value of the m parameter. In Fig.7.1, RVs with smaller m value tends to have longer tails and concentrate more in low SNR region while larger m tends to drag the PDF toward higher SNR region with smaller tails. When m is really large (in this case, $m = 100$), the most majority of mass of PDF centers around 1 in α-axis with the extreme of becoming an impulse function at $\alpha = 1$. In this extreme case, the Nakagami-m fading channel is no longer a fading channel because the $AF = 0$ and it becomes the AWGN channel.

Although several experimental and theoretical works have shown that the Nakagami-m distribution is the best-fit distribution for the amplitude by data obtained from many urban multipath wireless channels [123], [113], [114], there's no empirical data available discussing the distribution for the phase of the channel. Actually this ambiguity on the phase distribution is the base of some criticism on the Nakagami-m fading model [115]. Some previous works on Nakagami-m fading channel simulation either ignore the phase problem [117], or try to assign a uniform distribution on the phase [110] [111]. Using the fact that Nakagami-m distribution is Rayleigh distribution when $m = 1$ and approximates that of Hoyt [119] ($m < 1$) and Rice ($m > 1$), a reasonable assumption is that the phase distribution would also closely approximate

www.manaraa.com

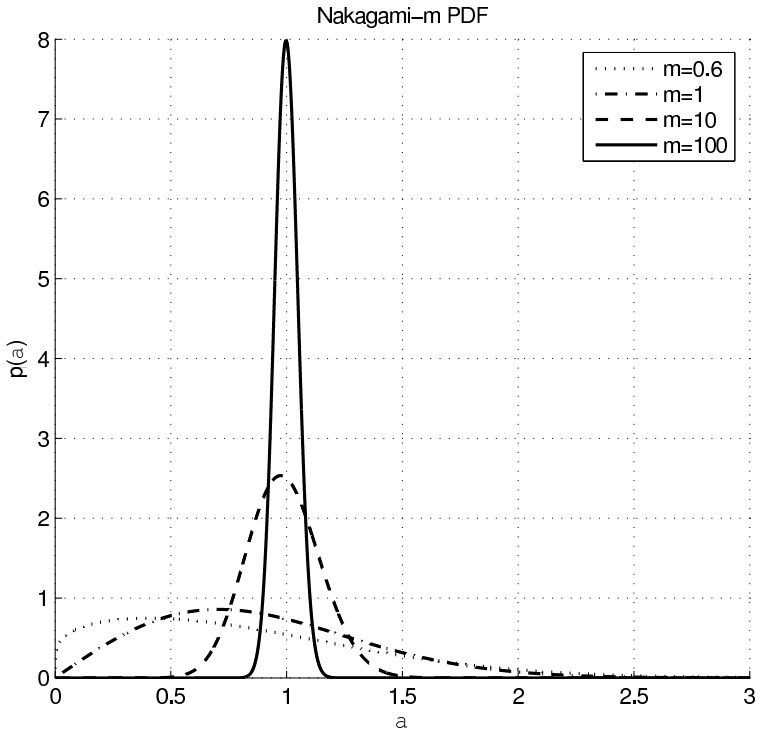

Figure 7.1 Nakagami-m PDF with different m parameter

that of the corresponding distributions. A phase-amplitude joint distribution is obtained in [112] by using the fact that the Nakagami-m distribution reduces to a Rayleigh distribution and its uniform phase distribution. The obtained marginal phase distribution, given in (7.5), closely matches that of the Rayleigh ($m = 1$), Hoyt ($m < 1$) and Rice ($m > 1$) case. We observed that this model is more reasonable than assuming a uniform phase distribution for any m parameters and simulation results in Section 7.5 obtained by the proposed simulator will confirm this claim.

Another characteristic of fading channels is that the channel coefficients are temporally correlated [118]. One question is what would be the fading spectrum model that fits the physical channel best. However, in spite of its importance in practice (i.e. the performance of PSAM would be different under different models) there's been no empirical data nor explicit theoretical analysis on this matter presented in the literature. The authors in [111] argued for the legitimacy of accepting the auto-correlation property of the output sequence of their proposed amplitude mapper but no justification was given in the paper as whether the auto-

www.manaraa.com

correlation property of the output indeed approximate that of the physical phenomenon. The simulator proposed there has no component taking care of the auto-correlation property of the output sequence but rather blindly accept any sequence with any auto-correlation property that might come out from the proposed amplitude mapper. We observe that indeed before any specific physical models or empirical data are available in the literature, it's difficult to argue which auto-correlation property of the output sequence from the Nakagami-m simulator is best fit for the real physical phenomenon. We thus take a more adaptive approach on the auto-correlation property in that we design a part in our proposed simulator that make sure the output sequence follow any arbitrary auto-correlation model of choice. The inclusion of this part in the proposed simulator would greatly improve the adaptability in that: (1) it can be quickly adapted to any auto-correlation model if such model is found using new empirical data and (2) in most analytical analysis in the published work, a certain auto-correlation model is assumed (usually Jakes' fading channel power spectrum density model), our proposed simulator will provide the output based on the model used in analytical analysis to test the accuracy of the analysis itself, which is not possible using the simulator proposed in [111].

In Rayleigh fading model, the complex channel coefficients are considered circular symmetric, i.e. independent real and imaginary quadrature parts. This assumption of independent quadrature parts in Nakagami-m fading model is also valid and indeed adopted as a basic assumption in most analytical analysis of different system in Nakagami-m fading channels [98–100, 102, 104, 105].

7.3 Simulator Design

The main design objective for the simulator is to generate complex Nakagami sequences with pre-specified temporal auto-correlation property and also correct phase property as shown by [112]

$$p_{\Theta}(\theta) = \frac{\Gamma(m)|\sin(2\theta)|^{m-1}}{2^m\Gamma^2(m/2)} \tag{7.5}$$

This requires the real and imaginary parts of the channel to be independent but not circularly symmetric. To our knowledge, a simulation technique to fulfill such a requirement is not known

www.manaraa.com

in the literature.

To solve this problem, we proposed a new simulator structure that guarantees the independence of the quadrature components of the generated channel samples as well as pre-specified temporal autocorrelation characteristic. We design a technique which maps the real and imaginary parts of Gaussian sequence separately to Nakagami-m sequences with parameters $m/2$, and then sum them up to get a complex Nakagami channel which has independent real and imaginary parts.

We need to generate a temporally correlated complex Nakagami sequence $y(t)$ with zero-mean, variance σ_y^2, and a pre-specified auto-correlation function $R_y(\tau) = R_{\text{tar}}(\tau)$, where $R_{\text{tar}}(\tau)$ is the target temporal correlation function. Two mapping methods are designed next.

7.3.1 First Approach

The schematic plot of the proposed first mapping algorithm is shown in Fig. 7.2. The scheme is described below (**Algorithm I**).

1. Generate two independent real Gaussian sequences $x_R(t)$ and $x_I(t)$, both have the identical temporal auto-correlation function $R_x(\tau) = E[x_R(t)x_R^*(t-\tau)] = E[x_I(t)x_I^*(t-\tau)]$. Furthermore, $x_R(t) \sim N(0,1)$ and $x_I(t) \sim N(0,1)$. We can readily show that $x(t) = x_R(t) + jx_I(t) \sim \text{CN}(0,2)$ is a circularly symmetric complex Gaussian sequence.

2. Map $x_R(t)$ and $x_I(t)$ independently to Nakagami channel samples. The procedure is outlined below. We note that $|x_R(t)|$ and $|x_I(t)|$ are both Chi- (χ) random variables with one degree of freedom (d.o.f.). Denote their CDF as $u = F_\chi(x) = \int_0^x f_\chi(z)dz$.

   Map $|x_R(t)|$ to a variable u_R which has uniform distribution in $[0,1)$, and then map u_R to $|y_R(t)|$ by the inverse CDF of the Nakagami-m amplitude variable (with parameters $\sigma_y^2/m, m/2$).

   Since the PDF $f_{\text{Naka}}(z)$ for Nakagami-m amplitude is known, we can evaluate the CDF by $u_R = F_{\text{Naka}}(|y_R|) = \int_0^{|y_R|} f_{\text{Naka}}(z)dz$. The inverse CDF calculation $|y_R| = F_{\text{Naka}}^{-1}(u_R)$ can be implemented using a numerical search, or by using the inverse CDF approximation proposed in [111] based on the Hasting's approach.

www.manaraa.com

3. The generated real part of the Nakagami channel component is given by

$$\begin{aligned} y_R &= |y_R|\text{sign}(x_R) = F^{-1}_{\text{Naka}}(F_{\chi(x_R)})\text{sign}(x_R) \\ &= g(x_R) \end{aligned} \tag{7.6}$$

4. Similarly, the same mapping is implemented for $x_I(t)$, generating $y_I(t) = g(x_I(t))$. In short, the real and imaginary components of the Nakagami-m channel samples are generated independently by the proposed procedure. The complex Nakagami-m sequence is given by $y(t) = y_R(t) + jy_I(t)$, cf. Fig. 7.2. It is obvious that $y(t)$ is a complex Nakagami sequence with the pre-specified m-parameter. ■

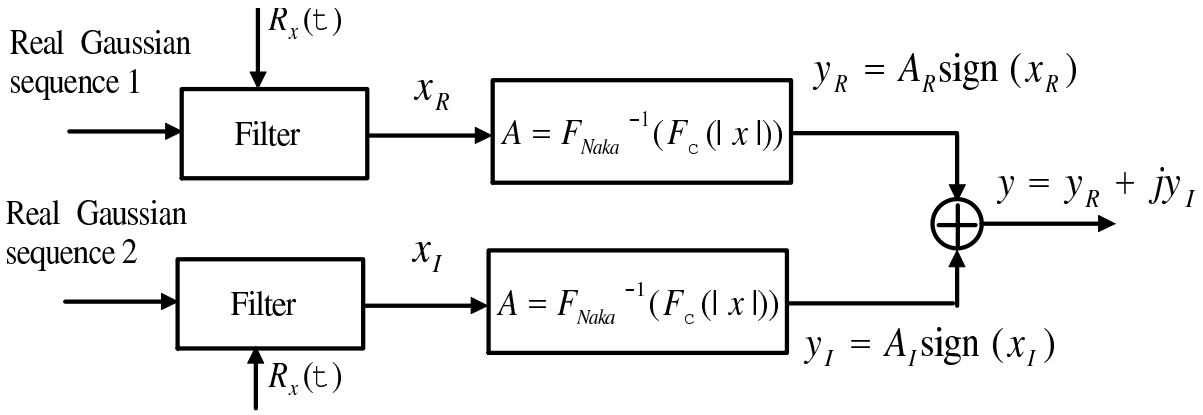

Figure 7.2 Diagram of the proposed complex Nakagami channel simulator (method 1). $F_\chi(r)$ and $F_{\text{Naka}}(r)$ refer to the CDFs of the Chi-(χ) and Nakagami-distributed variables, respectively.

7.3.2 Second Approach

In the first method, $|x_R|$ is a χ-variable with 1 d.o.f., and its CDF evaluation may not be numerically stable for $|x_R|$ being close to zero. We design a numerically more stable and also computationally more efficient approach below. The diagram of the second simulator is shown in Fig. 7.3.

We note that $x_R^2(t)$ and $x_I^2(t)$ are both χ^2 variables with 1 d.o.f., or the Gamma variables with $m = 1$. Consequently, their CDF evaluation is much more stable and accurate than that

www.manaraa.com

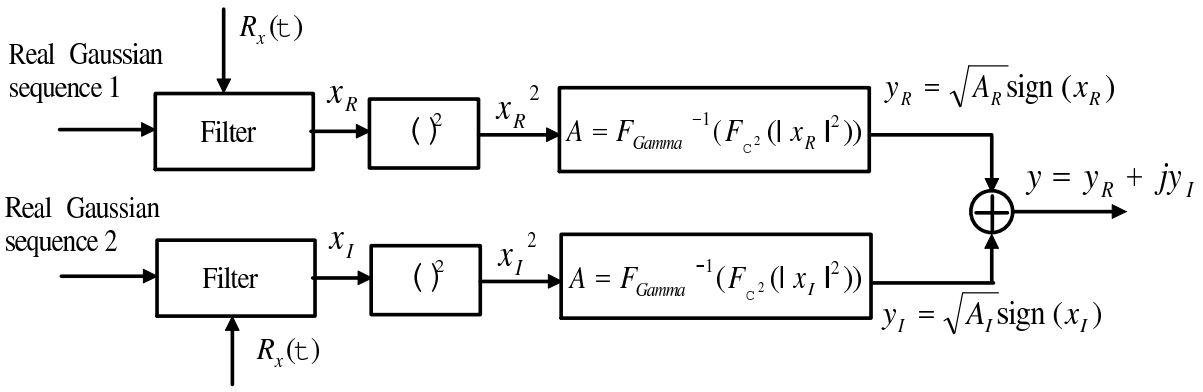

Figure 7.3 Diagram of the proposed complex Nakagami channel simulator (method 2). $F_{\chi^2}(r)$ and $F_{\text{Gamma}}(r)$ refer to the CDFs of the Chi-square (χ^2) and Gamma variables, respectively.

of $x_R(t)$. Furthermore, inverse-mapping the CDF of Gamma variables (to that of uniform distribution) is also much easier than inverse-mapping Nakagami amplitudes, and has been included in many available programming tools. For example, in *Matlab* the CDF of χ^2 variables and inverse CDF of Gamma variables can be evaluated using *chi2CDF* (or *gamcdf*) and *gaminv* commands, respectively.

The second approach (**Algorithm II**) is outlined below (index t of $x_R(t)$, $x_I(t)$, $y_R(t)$, $y_I(t)$ is suppressed when no confusion arises).

1. After the sequence x_R is generated, we evaluate the CDF of x_R^2, denoted by $u_R = F_{\chi^2}(x_R^2) \in [0, 1)$, and

$$\begin{aligned} u_R &= \int_0^{x_R^2} f_{\chi^2}(z)dz \\ &= \int_0^{x_R^2} \frac{z^{-1/2}\exp(-z/2)}{\sqrt{2\pi}}dz \end{aligned}$$

where $f_{\chi^2}(z)$ and u_R are the PDF and the CDF of x_R^2, respectively.

Next, map u_R to real Gamma variable A_R (which is the square of Nakagami amplitude y_R) with m-parameter $m/2$. This is achieved by exploiting the inverse Gamma CDF, $A_R = F_{\text{Gamma}}^{-1}(u_R)$, where $F_{\text{Gamma}}^{-1}(u_R)$ denotes the inverse function of Gamma CDF $u_R = F_{\text{Gamma}}(A_R)$. For example, $F_{\text{Gamma}}^{-1}(u_R) = A_R$ leads to $u_R = F_{\text{Gamma}}(A_R)$. The Gamma

www.manaraa.com

CDF $F_{\text{Gamma}}(A)$ is given by

$$u = F_{\text{Gamma}}(A) = \frac{1}{b^2\Gamma(a)} \int_0^A z^{a-1} \exp(-\frac{z}{b}) dz$$

where $a = m/2$ and $b = \sigma_y^2/(2a) = \sigma_y^2/m$ holds.

2. The real part of generated Nakagami-m sequence is given by

$$y_R = \sqrt{A_R}\text{sign}(x_R) = g(x_R) \tag{7.7}$$

where $g(x)$ is the mapping function from x_R to y_R, and is given by

$$g(x) = \sqrt{F^{-1}_{\text{Gamma}}(F_{\chi^2}(x))}\text{sign}(x) \tag{7.8}$$

We can show that $y_R = \begin{cases} \sqrt{A_R}, & \text{if} x_R \geq 0, \\ -\sqrt{A_R}, & \text{if} x_R < 0. \end{cases}$.

3. The same procedure is used to generate sequence y_I from input Gaussian sequence x_I. The generated complex Nakagami-m sequence is given by $y(t) = y_R(t) + jy_I(t)$, cf. Fig. 7.3. ■

With the sign function used in (7.6) and (7.8) for the CDF mapping process, the phase of the generated sequences are symmetric within the ranges $(0, \pi/2), (\pi/2, \pi), (\pi, 3\pi/2)$, and $(3\pi/2, 2\pi)$, and fits the result predicted in (7.5).

We note that in [111] the amplitude $|x(t)| = \sqrt{x_R^2(t) + x_I^2(t)}$ is mapped to the Rayleigh CDF $u_{\text{Ray}}(t)$, which is then mapped to Nakagami amplitude modulus $|y_{\text{Naka}}(t)|$. The phase of the resulting sequence is directly taken from the phase of $x(t)$, and $\angle x(t)$ follows a uniform distribution. The output sequence is given by $y(t) = |y_{\text{Naka}}(t)| \exp(j\angle x(t))$, where $j = \sqrt{-1}$.

We point out that there are two approximations in the approach designed in [111]:

1. The real and imaginary parts of generated Nakagami sequences are not strictly independent.

2. The phase of $y_{\text{Naka}}(t)$ also follows a uniform distribution as that of $x(t)$. However, as pointed out in [112] when $m \neq 1$, the phase of $y_{\text{Naka}}(t)$ is no longer uniformly distributed, i.e., $y_{\text{Naka}}(t)$ is not a circularly symmetric process.

www.manaraa.com

The sequence generation approach we proposed above has solved these problems. Our CDF mapping method is different from that in [111]. In [111], the CDF method uses the $(0, \infty)$ to $(0, \infty)$ mapping for channel absolute amplitudes. In our method, the mapping function $g(x)$ includes the phases of real and imaginary parts of $x(t)$, and it uses $(-\infty, \infty)$ to $(-\infty, \infty)$ mapping, and guarantees that the y_R and y_I are independent. Furthermore, in our method, the one-to-one mapping between Gaussian processes (x_R and x_I) and Nakagami-process (y_R and y_I) is used, and thus the phase of resulting complex Nakagami sequence is uniquely determined by both the phases and amplitudes of the original Gaussian sequence. Since the sequence also has the correct m-parameter, we show later by simulations that the sequence-phase distribution follows (7.5), as analytically predicted in [112].

7.4 Mapping of Temporal Correlation Functions

To implement our algorithm, there is still a significant problem to be solved, which is, given the desired output auto-correlation function $R_{\text{tar}}(\tau)$ (i.e., $R_y(\tau) = R_{\text{tar}}(\tau)$ must hold), what should the Rayleigh channel auto-correlation function $R_x(\tau)$ be? To our knowledge, this is a critical open problem which has not been addressed in the literature. In [95] and [111], the generated Rayleigh channels follows the Jakes' model, and then the sequences are mapped to Nakagami channels using different techniques. These results have not answered these questions: 1) Given that the Rayleigh channels follow the Jakes' model, what would be temporal auto-correlation function of the generated Nakagami-channels? 2) More significantly, given the specified Nakagami-channel autocorrelation function $R_y(\tau) = R_{\text{tar}}(\tau)$, how to determine $R_x(\tau)$ so that the resulting Nakagami channel $y(t)$ after CDF mapping follows the specified autocorrelation function $R_y(\tau) = R_{\text{tar}}(\tau)$?

We provide a new technique to solve this open problem using a two-step procedure: (1) For the channel mapping function $y_R = g(x_R)$ (and $y_I = g(x_I)$), find the auto-correlation function mapping function $g_R(\cdot)$ so that $R_y(\tau) = g_R(R_x(\tau))$. This answers the first question given in the above. (2) Based on $g_R(\cdot)$, find the inverse function $g_R^{-1}(\cdot)$, such that $R_x(\tau) = g_R^{-1}(R_y(\tau)) = g_R^{-1}(R_{\text{tar}}(\tau))$. In short, given a required $R_y(\tau) = R_{\text{tar}}(\tau)$, the solution of original

www.manaraa.com

Gaussian correlation function is given by $R_x(\tau) = g_R^{-1}(R_{\text{tar}}(\tau))$.

The first step is presented below. The output correlation $R_{y_R}(\tau)$ is calculated by (using real parts)

$$\begin{aligned} R_{y_R}(\tau) &= E[y_R(t+\tau)y_R(t)] \\ &= E[g(x_R(t+\tau))g(x_R(t))] \end{aligned} \tag{7.9}$$

Below, we use $x_1 = x_R(t+\tau)$ and $x_2 = x_R(t)$ as a shorthand. Assume that the sequences are stationary and ergodic. We may replace the time average in (7.9) with the ensemble average over $x_R(t)$, and obtain

$$R_y(\tau) = \int_{-\infty}^{\infty}\int_{\infty}^{\infty} g(x_1)g(x_2)f(x_1,x_2)dx_1dx_2 \tag{7.10}$$

where $f(x_1, x_2)$ is the joint PDF of Gaussian variables x_1 and x_2, and is given by

$$f(x_1,x_2) = \frac{1}{2\pi(1-\tilde{R}_x^2(\tau))^{1/2}} \exp\left(-\frac{x_1^2+x_2^2-2\tilde{R}_x(\tau)x_1x_2}{2(1-\tilde{R}_x^2(\tau))}\right) \tag{7.11}$$

where $\tilde{R}_x(\tau) = R_x(\tau)/R_x(0)$ is the normalized autocorrelation function of $x(t)$. Based on the assumption that $x_1 \sim N(0,1)$ and $x_2 \sim N(0,1)$, we have $R_x(0) = 1$ and $\tilde{R}_x(\tau) = R_x(\tau)$. For example, assuming the Jakes' spectrum for input sequence $x(t)$, we have $\tilde{R}_x(\tau) = J_0(2\pi B_f\tau)$, where B_f is the maximum Doppler shift, and $J_0(x)$ is the zeroth order Bessel function of the first kind. Below, we use $\tilde{R}_x(\tau)$ and $R_x(\tau)$ interchangeably.

Equation (7.10) can be evaluated efficiently by using a transform technique given in [110]. Define $x_1 = \sqrt{2s}\cos(\theta)$, and $x_2 = \tilde{R}_x(\tau)\sqrt{2s}\cos(\theta) + \sqrt{1-\tilde{R}_x^2(\tau)}\sqrt{2s}\sin(\theta)$. We have

$$R_y(\tau) = \int_0^{2\pi}\int_0^{\infty} g\left(\sqrt{2s}\cos(\theta)\right) g(\tilde{R}_x(\tau)\sqrt{2s}\cos(\theta) + \sqrt{1-\tilde{R}_x^2(\tau)}\sqrt{2s}\sin(\theta))\exp(-s)dsd\theta \tag{7.12}$$

which can be evaluated efficiently using Gaussian quadrature and by the change of integrand (s into $\tan(\alpha)$, thus change integration range from infinite into finite). For convenience, we may re-write (7.12) as $R_y(\tau) = M_R(R_x(\tau))$.

www.manaraa.com

In the second step, we need to find the solution of $R_x(\tau)$ given a specified $R_y(\tau) = R_{\text{tar}}(\tau)$. Following (7.9), we may write

$$\begin{aligned} R_x(\tau) &= E_x[x_R(t+\tau)x_R(t)] \\ &= E_y[g^{-1}(y_R(t+\tau))g^{-1}(y_R(t))] \end{aligned} \tag{7.13}$$

where $g^{-1}(y)$ is the inverse function of $g(x)$ and can be easily evaluated. However, the expectation in (7.13) is with respect to the joint PDF of real Nakagami variable $y_R(t+\tau)$ and $y_R(t)$ with correlation coefficient $R_{\text{tar}}(\tau)$, and such a PDF is known only for special cases and also very involved to manipulate [123].

To bypass this technical difficulty, we design an iterative search technique to solve (7.13). Define $R_y(\tau) = M_R(R_x(\tau))$. We may remodel the solution of (7.13) as

$$\min_{R_x(\tau)} |R_y(\tau) - R_{\text{tar}}(\tau)|^2, \tag{7.14}$$

for all τ. We may rewrite the optimization problem in (7.14) as

$$R_x(\tau) = \min_{\tilde{R}_x(\tau)} |M_R(\tilde{R}_x(\tau)) - R_{\text{tar}}(\tau)|^2 \tag{7.15}$$

Since (7.15) is a quadratic form, the solution to (7.15) exists and is unique. We design a numerical algorithm to solve (7.13) using the gradient search, as described below.

Define an error cost function $\mathcal{L}(R_x(\tau)) = |M_R(R_x(\tau)) - R_{\text{tar}}(\tau)|^2$. The partial derivative of $\mathcal{L}(R_x(\tau))$ with respect to (w.r.t.) $R_x(\tau)$ is given by

$$\frac{\partial \mathcal{L}(R_x(\tau))}{\partial R_x(\tau)} = 2(M_R(R_x(\tau)) - R_{\text{tar}}(\tau))M_R'(R_x(\tau))$$

where $M_R'(R_x(\tau)) = \frac{\partial M_R(R_x(\tau))}{\partial R_x(\tau)}$ is the partial derivative of $M_R(R_x(\tau))$ w.r.t. $R_x(\tau)$ and may be evaluated numerically by

$$M_R'(R_x(\tau)) = \frac{\partial M_R(R_x(\tau))}{\partial R_x(\tau)} \tag{7.16}$$

$$= \lim_{\Delta R_x(\tau) \to 0} \frac{M_R(R_x(\tau)) - M_R(R_x(\tau) - \Delta R_x(\tau))}{\Delta R_x(\tau)} \tag{7.17}$$

The procedure is listed as (**Algorithm III**)

www.manaraa.com

1. Set $n = 0$. Let the initial value of $R_x^{(n)}(\tau)$, denoted by $R_x^{(0)}(\tau)$, be given by $R_x^{(0)}(\tau) = R_{\text{tar}}(\tau)$.

2. Increase n by 1. Update $R_x^{(n)}(\tau)$ by

$$R_x^{(n)}(\tau) = R_x^{(n-1)}(\tau) - a \cdot [M_R(R_x^{(n-1)}(\tau)) - R_{\text{tar}}(\tau)] M_R'(R_x^{(n-1)}(\tau)) \tag{7.18}$$

   where a $(0 < a \leq 1)$ is a scalar used to control the convergence speed. For numerical stability, we suggest setting $\Delta R_x(\tau) = 0.01 R_x(\tau)$.

3. Calculate the residual error cost function $\mathcal{L}(\tilde{R}_x^{(n)}(\tau)) = |M_R(\tilde{R}_x^{(n)}(\tau)) - R_{\text{tar}}(\tau)|^2$, and compare it with a predefined threshold ϵ ($\epsilon \ll 1$). If $\mathcal{L}(\tilde{R}_x^{(n)}(\tau)) > \epsilon$, go to step 2; otherwise, stop.

   Alternatively, we may define another error cost function $\hat{\mathcal{L}}(\tilde{R}_x^{(n)}(\tau)) = |\tilde{R}_x^{(n)}(\tau) - R_x^{(n-1)}(\tau)| / |R_x^{(n-1)}(\tau)|$, when $\hat{\mathcal{L}}(\tilde{R}_x^{(n)}(\tau)) > \epsilon$ holds, go to step 2; otherwise, stop.

The output $R_x^{(n)}(\tau)$ now gives the required temporal auto-correlation function of $x_R(t)$ (and $x_I(t)$) which leads to the pre-specified $R_y(\tau) = R_{\text{tar}}(\tau)$.

Exploiting the above procedures, the $R_x(\tau)$ function which generates desired $R_y(\tau)$ is obtained. The further procedure to generate sequence $y_{\text{Naka}}[n] = y_{\text{Naka}}(nT_s)$ is described below, where T_s is a symbol duration. Assume we need to generate a stationary Nakagami-m sequence with power σ_y^2, length N, parameter m, and auto-correlation function $R_y[n] = R_{\text{tar}}[n]$, for $n = 1, \ldots, N$.

1. Using $R_{\text{tar}}(\tau)$ and $\tau = nT_s$, form sequence $R_{\text{tar}}[n]$. Using Algorithm III, find $R_x(\tau)$, for $\tau = nT_s$, $n = 1, \ldots, N$.

2. Using N-point DFT of $R_x[n]$, transform the auto-correlation function to frequency domain resulting in the power spectrum shaping function $F_x[n]$. A technique proposed in [108, 126] can be used for this step.

3. Using the N-point inverse DFT of the product of $F_x[n]$ and a zero-mean white Gaussian sequence, generate a time-domain Gaussian channel sequence $x[n] = x(nT_s)$.

4. Using Algorithm I or II and sequence $x[n]$, find $y_{Naka}[n] = y_{Naka}(nT_s)$.

www.manaraa.com

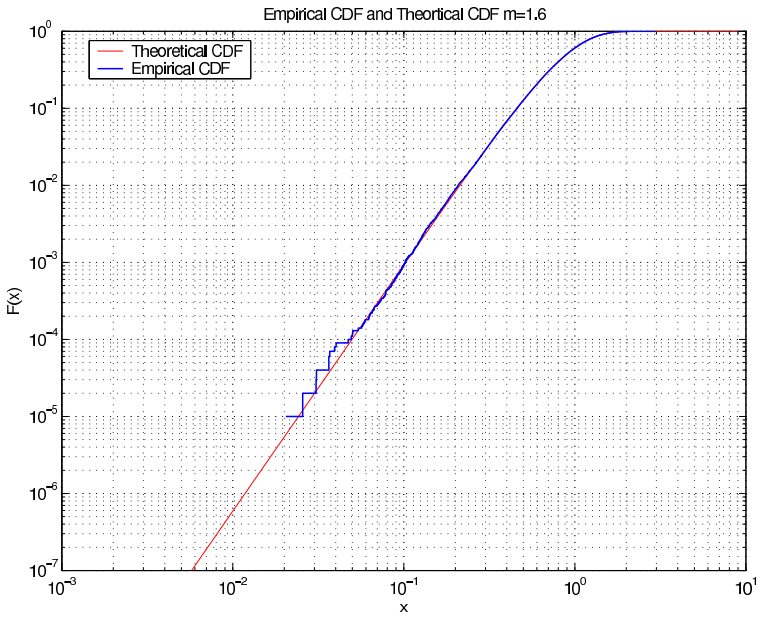

Figure 7.4 Theoretical and simulated CDFs (lower tail) of generated Nakagami channels, $m = 1.6$.

7.5 Simulation Results

In this section, we provide simulation results to compare the techniques we proposed and those available in the literature. For each simulation test, we set the Nakagami sequence length to be $N = 2^{14}$, and generated 50 independent Nakagami sequences to obtain the simulator output statistics.

Test 1: Accuracy of CDF of generated Nakagami-m sequences. Fig 7.4 is the comparison of the empirical CDF of the amplitude of the channel samples with the analytical Nakagami-m CDF with $m = 1.6$. The x-axis is in log-scale so that the lower tail of the CDF is magnified. In Fig. 7.5, the analytical and complementary CDFs (upper tail) of the channel samples are presented. Both analytical curves are obtained using (7.1), and for simulations the channel samples are generated using Algorithms II and III. The result shows that both the lower and upper CDF tail of the Nakagami amplitudes generated using the proposed simulation schemes fit the analytical ones very well. The noticalbe zigzag shown on the empirical CDF is an expected artifacts which could be fixed by increasing the simulator sequence's length.

Test 2: Phase property of generated Nakagami-m sequences.

www.manaraa.com

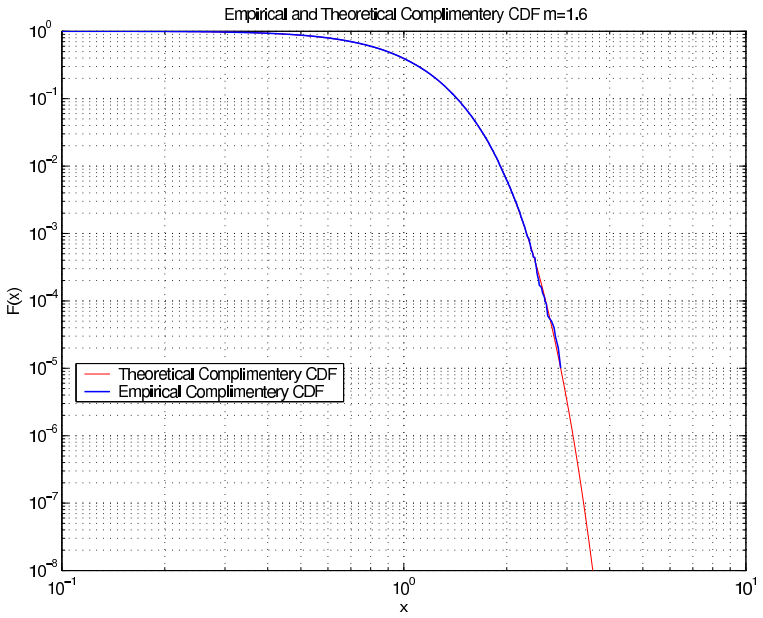

Figure 7.5 Theoretical and simulated complementary CDFs (upper tail) of generated Nakagami channels, $m = 1.6$.

In Fig. 7.6, the phase distribution is obtained by simulation of the generated Nakagami channels using the proposed method (with $m = 2.5$), and the analytical curves is generated using (7.5). The result shows that the phase property of generated sequence fit the analysis very well. This observation demonstrates that our proposed technique (at least partially) has solved the Nakagami channel simulator phase-ambiguity problem. We also verified the validity of (7.5), the analytical results on phase distribution of Nakagami-m fading channels in [112].

Test 3: Analytical relation between $R_x(\tau)$ and $R_{\text{tar}}(\tau)$.

Given the target Nakagami normalized correlation function $\tilde{R}_y(\tau) = R_{\text{tar}}(\tau) = J_0(2\pi B_f \tau)$, what should the temporal auto-correlation function $R_x(\tau)$ of original Gaussian sequences should be? This question is answered in Fig. 7.7, where (Rayleigh channels) we show the $R_x(\tau)$, calculated by the proposed auto-correlation function mapping method (Algorithm III), with $m = 2.5$ and $B_f T = 0.03$. Fig. 7.7 shows that generally $R_x(\tau) \neq R_y(\tau)$ for $\tau > 0$. When $R_y(\tau)$ is defined to follow the Jakes' model, it turns out that $R_x(\tau)$ does not follow Jakes' model. The divergence between $R_x(\tau)$ and $R_y(\tau)$ is most significant for negative and minimum values of correlation, e.g., for $R_y(\tau) \in (-0.2, -0.4)$. Therefore, it is interesting to know if

www.manaraa.com

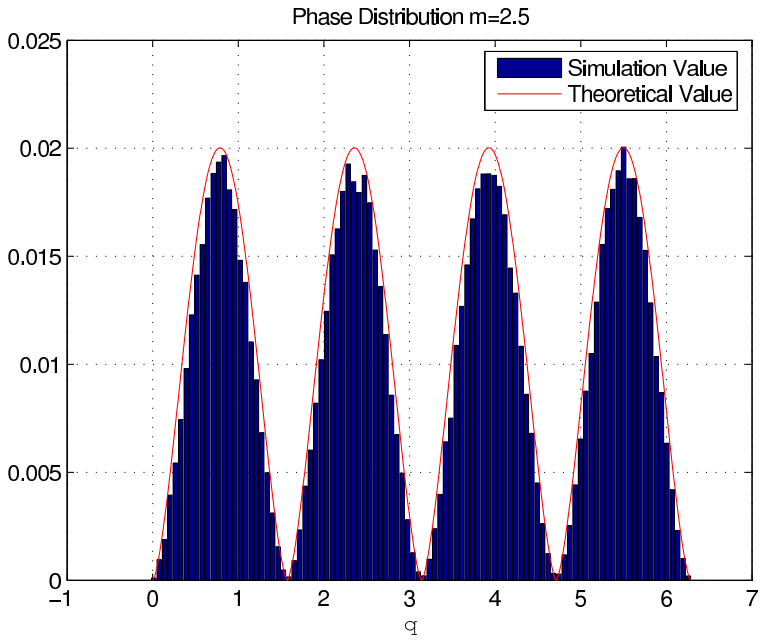

Figure 7.6 Analytical and simulated phase distribution of the generated Nakagami-m sequence for $m = 2.5$

one uses $R_x(\tau) = J_0(2\pi B_f \tau)$, and the $R_x(\tau)$ generated using Algorithm III, respectively, what will the $R_y(\tau)$ be, respectively.

Assume that we need a Nakagami sequence with $\tilde{R}_y(\tau) = R_{\text{tar}}(\tau) = J_0(2\pi B_f \tau)$. This may be obtained using CDF method and Rayleigh Gaussian sequences $x(t)$ with the following auto-correlation functions (1) $R_x(\tau) = R_{\text{tar}}(\tau) = J_0(2\pi B_f \tau)$, which we call traditional direct mapping method, and it involves approximations; (2) $R_x(\tau)$ is generated using the proposed mapping technique (Algorithm III). This is a strict approach but requires a larger complexity than the direct mapping method. With the help of (7.12), the resulting analytical auto-correlation function $R_y(\tau)$ of generated Nakagami channels are given in Fig. 7.8, respectively, based on direct mapping of $R_{\text{Ray}}(\tau)$ to $R_{\text{Naka}}(\tau)$. for $m = 2.5$ and $B_f T = 0.03$. The result shows that (1) the proposed technique can achieve the near-perfect target temporal correlation; (2) If we use $R_x(\tau) = R_{\text{tar}}(\tau)$, thus the traditional direct mapping, the resulting Nakagami temporal correlation will be different from the target correlation, but the mismatch is still a tight approximation. Therefore, as a low complexity approximation, Algorithm I (or II) and direct mapping of $R_x(\tau)$ can be combined to achieve a correct non-uniform phase distribution

www.manaraa.com

and tight approximation of $\tilde{R}_y(\tau) = R_{\text{tar}}(\tau)$.

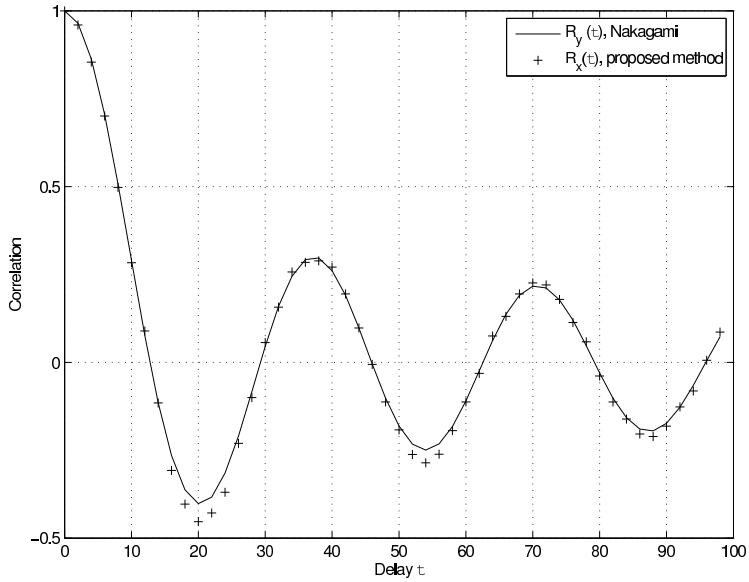

Figure 7.7 Auto-correlation function $R_x(\tau)$ of original Gaussian sequence calculated by the proposed mapping method vs. τ, given that $R_y(\tau) = R_{\text{tar}}(\tau) = J_0(2\pi B_f \tau)$, $m = 2.5$, and $B_f T = 0.03$.

Test 4: Relation between $R_x(\tau)$ and $R_y(\tau)$ by simulation.

We assume that the target normalized auto-correlation function for Nakagami sequence is $R_y(\tau) = J_0(2\pi B_f \tau)$. In Fig. 7.9, simulated auto-correlation sequences $R_y(\tau)$ of generated Nakagami channels vs. τ using the traditional direct mapping ($R_x(\tau) = R_{\text{tar}}(\tau)$) and the proposed mapping methods (Algorithm III) are presented, assuming $m = 4.5$ and $B_f T = 0.04$. Since the complexity involved in Algorithm III may be large for a large sequence length N, in the simulation we generated $R_x[n] = R_x(nT_s)$ only for the first 1024 values of n, $(n = 0, 1, \ldots, 1023)$, and then use direct mapping for the remaining values of $R_x[n]$. This approximation involves actually negligible effect on the accuracy of simulation statistics. The results in Fig. 7.9 show that Algorithms III attains a near-perfect matching between the resulting auto-correlation function $R_y(\tau)$ and the target Jakes' model, while the conventional direct mapping method causes some mismatches, especially for peak negative values of correlation. However, this may still be acceptable as a tight approximation.

www.manaraa.com

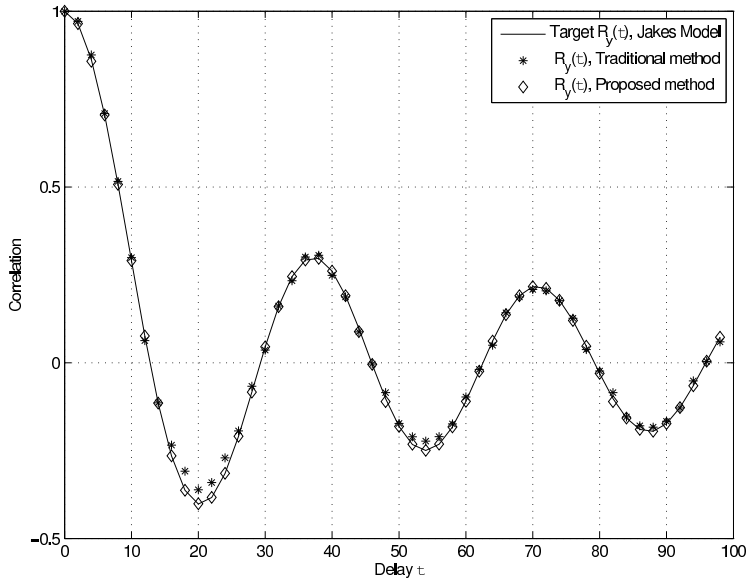

Figure 7.8 Analytical auto-correlation function $R_y(\tau)$ of generated Nakagami channels using the direct mapping method ($R_x(\tau) = R_{\text{tar}}(\tau) = J_0(2\pi B_f \tau)$) and the proposed inverse mapping vs. τ. $m = 2.5$, and $B_f T = 0.03$.

7.6 Conclusions

In this chapter, we have provided a systematic procedure on the reconstruction of complex Nakagami-m fading channels with correct non-uniform phase distribution, independent real and imaginary parts of the channel, and fitting any pre-specified Nakagami-m temporal auto-correlation function. We have shown the previously unknown fact that the Rayleigh auto-correlation function is different from that for Nakagami channels, and also provided a numerical search technique to calculate what the corresponding Rayleigh auto-correlation function should be in order to generate the Nakagami-m sequences with pre-specified temporal correlation function. Simulation results have verified the accuracy and validity of our analysis, and shown that our approach can accurately reconstruct arbitrary pre-specified auto-correlation function for the Nakagami channel simulation.

www.manaraa.com

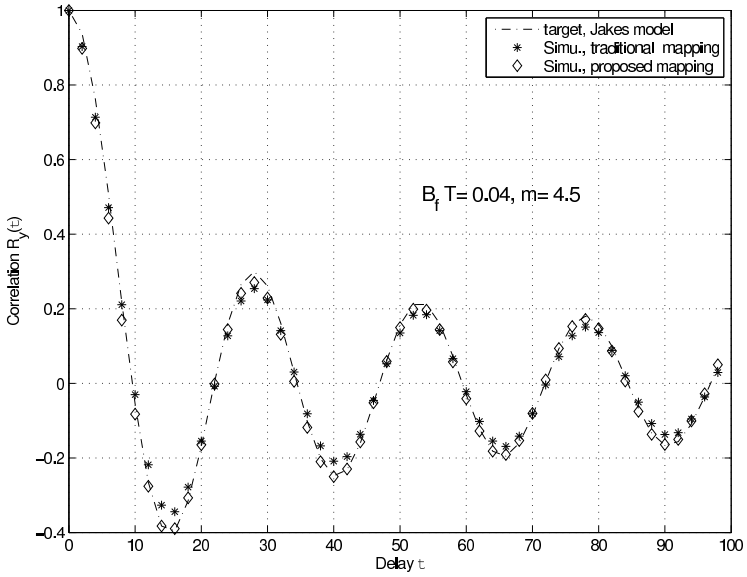

Figure 7.9 Simulated auto-correlation sequences $R_y(\tau)$ of generated Nakagami channel vs. τ using the direct correlation-function mapping ($R_x(\tau) = R_{\text{tar}}(\tau)$) and the proposed mapping (Algorithm III) methods, respectively. $m = 4.5$, and $B_f T = 0.04$.

www.manaraa.com

CHAPTER 8. CONCLUSIONS AND FUTURE WORK

In this thesis, we studied three important issues in multiuser wireless communication systems to provide insights of how to provide higher throughput, lower communication error, and better support for simultaneous communication of multiple users under fading channels. First we investigated the performance of MRC and GSC diversity receivers for M-QAM modulations under different fading channel models with imperfect channel estimation. We presented the exact BER performance results that take into account of fading channel conditions the system experienced, the modulation scheme used and the type of channel estimators employed. By applying these results on practical systems, we predicted with high accuracy how the system would perform under practical choice of channel estimation parameters. We then focused on a different class of problems, namely multiuser diversity-based scheduling and power allocation algorithms. Motivated by the fact that conventional CDMA systems ignore the multiuser diversity and the existing selection multiuser diversity systems are not designed explicitly for CDMA multiuser systems, we propose a novel GSMuD scheduling algorithm that schedules multiple users for simultaneous communication in a CDMA fashion. The proposed algorithms take into account whether perfect or imperfect channel state information is available at the scheduler and act accordingly. Several schemes to allocate the total system power to selected users are proposed, namely simple-to-implement equal power allocation, and the optimal 1-D and 2-D power allocation. We analyzed the various fairness metrics of the proposed **a**-SNR-based GSMuD as well as the **n**-SNR-based GSMuD, and the latter balances the need to provide better performance and fairness in the user selection process. We presented our contribution on the design and analysis of diversity receiver and multiuser diversity systems in this thesis in the context of wireless multipath fading channels. However, during the course of generating the

www.manaraa.com

simulation results for Chapter 3 through Chapter 6, we discovered that the existing methods in the literature to simulate the Nakagami-m fading channel coefficients are limited both in scope and accuracies, despite the fading channel model's widespread adoption. We designed a novel fading channel simulator for the Nakagami-m model with the correct phase distribution, accurate auto-correlation properties and low complexity. We presented the results in Chapter 7. As a matter of fact, we used this proposed approach to generate the fading channels in all the simulations that require the Nakagami-m fading channel models throughout this thesis. Their accuracy in matching the respective analytical results verifies both the validity of the presented analysis and the accuracy of the proposed fading channel simulator.

We have the following three topics for possible future research and extension that are closely related to the works and approaches discussed in this thesis.

- *BER performance of M-QAM for GSC in arbitrarily correlated generalized fading channels* We derived the signal constellation dependent combiner output SNR in our approach to evaluate the performance of M-QAM with GSC in generalized fading channels. In this framework, the i.i.d fading channels among all the diversity branches are assumed. We noticed that this framework can be readily extended to the i.n.d fading case by deriving the MGF of the SNR for i.n.d channels. Another topic of interest is to study the effect of correlated diversity branches on the BER performance of GSC combiners. This is an important extension because in practice the available diversity branches are often correlated and thus how to design and evaluate the performance of GSC with correlated branches is more relevant. Authors in [128] proposed a way to obtain distribution of output SNR of the correlated branches in Nakagami-m fading channel. But the approach and result therein are not directly applicable to GSC case. Further study on this topic would be required.

- *GSMuD in practical CDMA/OFDMA/SDMA systems* In the design and analysis of GSMuD related algorithms, we assume that each user experience an independent fading. There are some practical cases where this assumption does not hold, i.e. when users are physically close to each other. We plan to extend our analysis to the situation where the

www.manaraa.com

channels between users may have arbitrary correlation. We also plan to extend our results to the Weibull and Nakagami-q fading case due to the reasons cited above. In the thesis, we assume the orthogonal spreading code for CDMA or separate carriers for OFDM case. We note that the in practice, non-orthogonal spreading code might be used. We plan to include the effect of channel non-orthogonality and interferences in the design of GSMuD algorithm, by implementing the user ranking based on the signal-to-interference-plus-noise ratio (SINR) instead of the SNR [67, 68, 79]. The power allocation algorithms and the related performance and fairness metric need to be re-designed. We assumed the base station has the accurate and up-to-date user channel condition feedback (in terms of SNR) from the user. However, this assumption is not always valid. In practice, this SNR feedback may not track the current channel status if the channel experience fast fading, or inaccurate if there are communication errors during the feedback. We proved in [82] that under delayed feedback assumptions, the delayed channel SNR and SNR feedback error are independent and thus the ICE model (4.2) can also be used for the delayed SNR feedback case. This would facilitate the effort to readily incorporate this problem of out-dated SNR information into GSMuD error analysis and scheduler design.

A more general extension of GSMuD is to adapt the proposed algorithms to OFDMA and spacial division multiple access (SDMA), hybrid OFDMA/SDMA, CDMA/SDMA, and CDMA/OFDAM/SDMA systems. For example, hybrid OFDMA/SDMA scheme has been selected as a promising standard in next generation WiMax systems (IEEE 802.16e). In such systems, multiple users can be selected to occupy the same subcarrier of OFDM, thus increasing system capacity. This is made possible by using of advanced antenna systems (AAS) to separate user traffic by beamforming and interference cancelation. Apparently, SDMA channelization is not orthogonal and SINR must be used as the ranking criteria instead of SNR. We need to develop a "two-dimensional" GSMuD scheme where users are selected based on their SINR and spacial location properties and are assigned subcarriers to share with some other users. GSMuD scheme needs to consider the optimal ways of selecting and arranging users based on their spacial relationships for

www.manaraa.com

transmitting on the same subcarriers, in addition to SINR rankings.

- *MIMO fading channel simulator* We plan to extend our framework to include the MIMO channel case. Co-channel cross-correlation is inherent in practical wireless MIMO channels [118]. We plan to extend our simulator's capability to generate MIMO channel realizations that has co-channel correlation, while each channel could have its own temporal autocorrelation identical or not. Using the channel coefficients mapping and auto-correlation mapping method, we could extend our simulator to other non-Gaussian RV based fading models such as Weibull fading. We noticed that under certain conditions, Weibull model is a better fit for describing multipath fading channels in both indoor [42] and outdoor radio propagation environments [43]. However, a technical difficulty in generating Weibull fading channel coefficients with the independent quadrature parts using the proposed approach lies in the fact that unlike Nakagami-m case, the quadratures of Weibull fading channel coefficients no longer follow the Weibull fading. Thus if unmodified, our approach could only generate Weibull fading coefficients that has correlated quadrature parts, as in [111] for the case of Nakagami-m fading. One possible extension is to look into ways to generate independent quadrature parts for Weibull fading. Fortunately, the other parts of our proposed approach can still be applied.

www.manaraa.com

BIBLIOGRAPHY

[1] A. Annamalai, C. Tellambura and V. K. Bhargava, "Equal-gain diversity receiver performance in wireless channels," *IEEE Trans. Commun.*, vol. 48, pp. 1732–1745, Oct. 2000.

[2] L. Najafizadeh and C. Tellambura, "Exact BER analysis of an arbitrary square/rectangular QAM for MRC diversity with ICE in nonidentical Rayleigh fading channels", *IEEE International Conference on Communications, 2005. ICC 2005.* vol 4, pp 2190 - 2194, May 2005

[3] Chang-Joo Kim, Young-Su Kim and Coo-Young Jung, "BER analysis of QAM with MRC space diversity in Rayleigh fading channel", *Personal, Indoor and Mobile Radio Communications, 1995. PIMRC'95.* vol 2, pp 482 - 485, Sept. 1995

[4] M. P. Fitz and J. P. Seymour, "On the Bit Error Probability of QAM Modulation," *International Journal of Wireless Information Networks*, vol. 1, no. 2, pp. 131-139, 1994.

[5] Y. Ma, R. Schober, and S. Pasupathy, "Effect of Channel Estimation Errors on MRC Diversity in Rician Fading Channels," *IEEE Trans. Vehicular Technology,*. pp. 2137-2142, Nov, 2005.

[6] L. Hanzo, W. Webb, and T. Keller, *Single- and Multi-Carrier Quadrature Amplitude Modulation.* New York:Wiley, 2000.

[7] P. Gupta, N. Bansal, and R.K. Mallik, "Analysis of minimum selection GSC in Rayleigh fading", *2004 IEEE International Conference on Communications*, Volume 6, pp. 3364-3368, Jun. 2004

www.manaraa.com

[8] Y. Ma, D. Zhang, and R. Schober, "Effect of channel estimation errors on M-QAM with GSC diversity in fading channels," in *Proc. IEEE Int. Conf. Commun. (ICC)*, pp. 2190–2194, May 2005.

[9] G. L. Stuber, *Principles of Mobile Communications*. Norwell, MA: Kluwer Academic Publishers, second ed., 2003. Third Printing.

[10] J. K. Cavers, "An analysis of pilot symbol assisted modulation for Rayleigh fading channels," *IEEE Trans. Veh. Technol.*, vol. 40, pp. 686–693, Nov. 1991.

[11] M. G. Shayesteh and A. Aghamohammadi, "On the error probability of linearly modulated signals on frequency-flat Ricean, Rayleigh and AWGN channels," *IEEE Trans. Commun.*, vol. 43, pp. 1454–1466, Feb./Mar./Apr. 1995.

[12] S. K. Wilson and J. M. Cioffi, "Probability density functions for analyzing multi-amplitude constellations in Rayleigh and Ricean channels," *IEEE Trans. Commun.*, vol. 47, pp. 380–386, March 1999.

[13] X. Tang, M. S. Alouini, and A. J. Goldsmith, "Effect of channel estimation error on M-QAM BER performance in Rayleigh fading," *IEEE Trans. Commun.*, vol. 47, pp. 1856–1864, Dec. 1999.

[14] K. Cho and D. Yoon, "On the general BER expression of one- and two-dimensional amplitude modulations," *IEEE Trans. Commun.*, vol. 50, pp. 1074–1080, July 2002.

[15] X. Dong and L. Xiao, "Two-dimensional signaling in Ricean fading with imperfect channel estimation," in *Proc. IEEE Wireless Communications and Networking Conference (WCNC)*, pp. 1159–1164, 21-25 March 2004.

[16] X. Dong and L. Xiao, "Symbol error probability of two-dimensional signaling in Ricean fading with imperfect channel estimation," *IEEE Trans. Veh. Technol.*, vol. 54, pp. 538–549, March 2005.

www.manaraa.com

[17] L. Cao and N. C. Beaulieu, "Exact error-rate analysis of diversity 16-QAM with channel estimation error," *IEEE Trans. Commun.*, vol. 52, pp. 1019–1029, June 2004.

[18] B. Xia and J. Wang, "Effect of channel-estimation error on QAM systems with antenna diversity," *IEEE Trans. Commun.*, vol. 53, pp. 481–488, March 2005.

[19] L. Cao and N. C. Beaulieu, "Closed-form ber results for MRC diversity with channel estimation errors in Ricean fading channels," *IEEE Trans. Wireless Commun.*, vol. 4, pp. 1440–1447, July 2005.

[20] Y. Ma, R. Schober, and D. Zhang, "Exact BERs for M-QAM with MRC and channel estimation errors in Rician channels," in *Proc. IEEE Wireless Commun. and Networking Conference (WCNC)*, vol. 2, pp. 967–972, March 2005.

[21] Y. Ma, R. Schober and D. Zhang, "Exact BER of M-QAM with MRC and Imperfect Channel Estimation in Rician Fading Channels", *IEEE Transactions on Wireless Communications,* pp. 926-936, March 2007.

[22] R. A. Horn and C. R. Johnson, *Topics in Matrix Analysis.* Cambridge University Press, 1991.

[23] S. Haykin, *Adaptive filter theory.* Englewood Cliffs, NJ: Prentice Hall, 3rd ed., 1996.

[24] F. D. Neeser and J. L. Massey, "Proper complex random processes with applications to information theory," *IEEE Trans. Inform. Theory*, vol. 39, pp. 1293–1302, July 1993.

[25] G. L. Turin, "The characteristic function of hermitian quadratic forms in complex normal variables," *Biometrika*, vol. 47, pp. 199–201, 1960.

[26] M. Schwartz, W. Bennett, and S. Stein, *Communication Systems and Techniques.* McGraw Hill, 1966.

[27] C. W. Helstrom, "Calculating error probabilities for intersymbol and cochannel interference," *IEEE Trans. Commun.*, vol. 34, pp. 430–435, May 1986.

www.manaraa.com

[28] M. Abramowitz and I. A. Stegun, *Handbook of Mathematical Functions with Formulas, Graphs, and Mathematical Tables*. New York: Dover, 9th ed., 1970.

[29] Y. Ma and T. J. Lim, "Bit error probability for MDPSK and NCFSK over arbitrary Rician fading channels," *IEEE J. Sel. Areas Commun.*, vol. 18, pp. 2179–2189, Nov. 2000.

[30] J. G. Proakis, *Digital Communications*. McGraw-Hill, 3rd ed., 1995.

[31] X. Cai and G. B. Giannakis, "Adaptive PSAM accounting for channel estimation and prediction errors," *IEEE Trans. Wireless Commun.*, vol. 4, pp. 246–256, Jan. 2005.

[32] Y. Ma, "Impact of correlated diversity branches in Rician fading channels," in *Proc. IEEE Int. Conf. Commun. (ICC)*, vol. 1, (Seoul, Korea), pp. 473–477, May 16-20 2005.

[33] E. W. Weisstein, "Eigenvalue.," *MathWorld: A Wolfram Web Resource*. URL: mathworld.wolfram.com/Eigenvalue.html.

[34] Y. Ma and C. C. Chai, "Unified error probability analysis for generalized selection combining in Nakagami fading channels," *IEEE J. Sel. Areas Commun.*, vol. 18, pp. 2198–2210, Nov. 2000.

[35] A. Annamalai and C. Tellambura, "A new approach to performance evaluation of generalized selection diversity receivers in wireless channels," in *Proc. IEEE Vehicular Technology Conference (VTC)*, pp. 2309–2313, Fall 2001.

[36] Y. Ma and S. Pasupathy, "Efficient performance evaluation for generalized selection combining on generalized fading channels," *IEEE Trans. Wireless. Commun.*, vol. 3, pp. 29–34, Jan. 2004.

[37] M. J. Gans, "The effect of Gaussian error in maximal ratio combiners," *IEEE Trans. Commun. Technol.*, vol. 19, pp. 492–500, Aug. 1971.

[38] A. Annamalai and C. Tellambura, "Analysis of hybrid selection/maximal-ratio diversity combiners with Gaussian errors," *IEEE Trans. Wireless Commun.*, vol. 1, pp. 498–511, July 2002.

www.manaraa.com

[39] Y. Ma, R. Schober, and S. Pasupathy, "Effect of imperfect channel estimation on MRC diversity in fading channels," in *Proc. IEEE Int. Conf. Commun. (ICC)*, pp. 3163–3167, June. 2004.

[40] Y. Ma, R. Schober, and S. Pasupathy, "Performance of M-PSK with GSC and EGC with Gaussian weighting errors," *IEEE Trans. Veh. Technol.*, vol. 54, pp. 149–162, Jan. 2005.

[41] M. S. Alouini and M. K. Simon, "An MGF-based performance analysis of generalized selection combining over Rayleigh fading channels," *IEEE Trans. Commun.*, vol. 48, pp. 401-415, March 2000.

[42] F. Babich and G. Lombardi, "Statistical analysis and characterization of the indoor propagation channel," *IEEE Trans. Commun.*, vol. 48, pp. 455-64, Mar. 2000.

[43] N. H. Shepherd, "Radio wave loss deviation and shadow loss at 900 MHz," *IEEE Trans. Veh. Technol.*, vol. VT-26, pp. 309-13, June 1977.

[44] E.F. Chaponniere, P. Black, J. M. Holtzman and D. Tse, "Transmitter directed, multiple receiver system using path diversity to equiably maximize throughput", U.S. Patent No. 6449490, September 10, 2002

[45] Q. Liu, S. Zhou, and G. B. Giannakis, "Cross-layer combining of adaptive modulation and coding with truncated ARQ over wireless links," *IEEE Trans. Wireless Commun.*, pp. 1746-1755, Sep. 2004.

[46] N. Kong and L. B. Milstein, "Average SNR of a generalized diversity selection combining scheme," *IEEE Commun. Lett.*, vol. 3, pp. 57-59, Mar. 1999

[47] G. J. Pottie, "System design choices in personal communications," *IEEE Personal Commun.*, vol. 2, pp. 50-67, Oct. 1995.

[48] A. J. Goldsmith and S. G. Chua, "Variable-rate variable-power MQAM for fading channels," *IEEE Trans. Commun.*, vol. 45, pp. 1218-1230, Oct. 1997.

www.manaraa.com

[49] W. T. Webb and R. Steele, "Variable rate QAM for mobile radio," *IEEE Trans. Commun.*, vol. 43, pp. 2223-2230, July 1995.

[50] H. Matsuoka, S. Sampei, N. Morinaga, and Y. Kamio, "Adaptive modulation system with variable coding rate concatenated code for highquality multi-media communication systems," *Proc. IEEE VTC'96*, pp. 487-491.

[51] "IMT-2000: Standards efforts of the ITU," *IEEE Personal Commun.*, vol. 4, Aug. 1997.

[52] X. Qiu and K. Chawla, "On the Performance of Adaptive Modulation in Cellular Systems", *IEEE Transactions On Communications*, vol. 47, pp. 884-895, June 1999.

[53] F. Berggren, and R. Jantti "Asymptotically fair scheduling on fading channels" in *Proc. IEEE VTC Fall*, vol. 4, pp. 1934-1938, 2002. Also to appear in *IEEE Trans. Wireless Commun.*.

[54] N. Joshi, S. R. Kadaba, S. Patel, and G. S. Sundaram, "Downlink scheduling in CDMA data networks," in *Proc. ACM MobiCom*, pp. 179-190, 2000.

[55] M. Andrews, K. Kumaran, K. Ramanan, A. Stoylar, and P. Whiting, "Providing quality of service over a wireless link", *IEEE Commun. Mag.*, vol. 39, no. 2, pp. 150-154, 2001.

[56] X. Liu, E. K. P. Chong, and N. B. Shroff, "Opportunistic transmission scheduling with resource-sharing constraints in wireless networks," *IEEE J. Sel. Areas Commun.*, vol. 19, no. 10, pp. 2053-2064, 2001.

[57] S. Borst, and P. Whiting, "Dynamic rate control algorithms for HDR throughput optimization," in *Proc. IEEE INFOCOM*, vol. 2, pp. 976-985, 2001.

[58] J. M. Holtzman, "CDMA forward link waterfilling power control," in *Proc. IEEE VTC Spring*, vol. 3, pp. 1663-1667, 2000.

[59] J. M. Holtzman, "Asymptotic analysis of proportional fair algorithm," in *Proc. IEEE PIMRC*, vol. 2, pp. 33-37, 2001.

www.manaraa.com

[60] Y. Ma and D. Zhang, "Performance of Generalized Selection Multiuser Scheduling Over Generalized Fading Channels", *Int. Conf. on Wireless Commun. Mobile Comput. (iWCMC),* VanCouver, Canada, July, 2006.

[61] Y. Ma and D. Zhang, "Performance of Generalized Selection Multiuser Scheduling with Channel Estimation Errors", in *Proc. IEEE Conf. on Global Communications (GlobeCom),* Nov., 2006.

[62] W. P. Siriwongpairat, H. Zhu, and K. J. R. Liu, "Energy-efficient resource allocation for multiband UWB communication systems," *Proc. IEEE Wireless Commun. and Networking Conf. (WCNC)*, vol. 2, pp. 813–818, Mar. 2005.

[63] R. Negi and A. Rajeswaran, "Scheduling and power adaptation for networks in the ultra wide band regime," *IEEE Global Telecommun. Conf.*, vol. 1, pp. 139–145, Dec. 2004.

[64] R. Knopp and P. A. Humblet, "Information capacity and power control in single-cell multiuser communications," in *Proc. IEEE International Conference on Commun. (ICC)*, vol. 1, pp. 331–335, June 1995.

[65] D. Gesbert and M.-S. Alouini, "How much feedback is multi-user diversity really worth?," in *IEEE International Conference on Commun. (ICC)*, vol. 1, pp. 234–238, June 2004.

[66] L. Yang, M.-S. Alouini, and D. Gesbert, "Further results on selective multiuser diversity," in *MSWiM'04*, pp. 25–30, Oct. 2004.

[67] F. Berggren and R. Jantti, "Multiuser scheduling over Rayleigh fading channels," in *IEEE Global Telecommunications Conference (GLOBECOM'03)*, pp. 158–162, Dec. 2003.

[68] R. Kwan and C. Leung, "Downlink scheduling optimization in CDMA networks," *IEEE Commun. Letters*, vol. 8, pp. 611–613, Oct. 2004.

[69] Y. Ma and D. Zhang, "Channel Access Statistics of Parallel Multiuser Scheduling", *Proc IEEE ICC*, June 2007.

www.manaraa.com

[70] Y. Ma, J. Jin, and D. Zhang, "Throughput and Fairness of Generalized Selection Parallel Multiuser Scheduling," Submitted to *IEEE Trans. on Wireless Comm.*

[71] D. Tse and P. Viswanath, *Fundamentals of Wireless Communication.* Cambridge University Press, 2005.

[72] A. Goldsmith, *Wireless Communications.* Cambridge University Press, 2005.

[73] H. Fattah and C. Leung, "An overview of scheduling algorithms in wireless multimedia networks," *IEEE Wireless Commun.*, vol. 9, pp. 76–83, Oct. 2002.

[74] S. Shakkottai, T. Rappaport, and P. C. Karlsson, "Cross-layer design for wireless networks," *IEEE Commun. Magazine*, vol. 41, pp. 74–80, Oct. 2003.

[75] P. Viswanath, D. N. C. Tse, and R. Laroia, "Opportunistic beamforming using dumb antennas," *IEEE Trans. Inf. Theory*, vol. 48, pp. 1277–1294, June 2002.

[76] Q. Liu, S. Zhou, and G. B. Giannakis, "Queuing with adaptive modulation and coding over wireless links: cross-layer analysis and design," *IEEE Trans. Wireless Commun.*, vol. 4, pp. 1142–1153, May 2005.

[77] Q. Liu, S. Zhou, and G. B. Giannakis, "Cross-layer scheduling with prescribed QoS guarantees in adaptive wireless networks," *IEEE J. Sel. Areas in Commun.*, vol. 23, pp. 1056–1066, May 2005.

[78] D. N. Tse, "Optimal power allocation over parallel Gaussian broadcast channels," in *Proc. IEEE International Symposium on Information Theory (ISIT)*, p. 27, Jun. 29 - Jul. 4 1997.

[79] F. Berggren and R. Jantti, "Asymptotically fair transmission scheduling over fading channels," *IEEE Trans. Wireless Commun.*, vol. 3, pp. 326–336, Jan. 2004.

[80] L. Yang and M.-S. Alouini, "Performance analysis of multiuser selection diversity," *IEEE Trans. Veh. Technol.*, vol. 55, pp. 1003–1018, May 2006.

[81] Q. Ma and C. Tepedelenlioglu, "Practical multiuser diversity with outdated channel feedback," *IEEE Trans. Veh. Technol.*, vol. 54, pp. 1334–1345, July 2005.

www.manaraa.com

[82] Y. Ma and D. Zhang, "Error Rate of Transmit Beamforming with Delayed and Limited Feedback", *Proc. IEEE Conf. on Global Communications (GlobeCom),* Nov., 2007.

[83] B. S. Krongold, K. Ramchandran, and D. L. Jones, "Computationally efficient optimal power allocation algorithms for multicarrier communication systems," *IEEE Trans. Commun.*, vol. 48, pp. 23–27, Jan. 2000.

[84] T. S. Rappaport, A. Annamalai, R. M. Buehrer, and W. H. Tranter, "Wireless communications: Past events and a future perspective," *IEEE Commun. Mag.*, vol. 40, pp. 148–161, May 2002.

[85] C. Y. Wong, R. S. Ceng, K. B. Lataief, and R. D. Murch, "Multiuser OFDM with adaptive subcarrier, bit, and power allocation," *IEEE J. Selected Areas Commun.*, vol. 17, pp. 1747–1758, Oct. 1999.

[86] J. Jang and K. B. Lee, "Transmit power adaptation for multiuser OFDM systems," *IEEE Journal on Selected Areas in Commun.*, vol. 21, pp. 171–178, Feb 2003.

[87] R. Elliott, "A measure of fairness of service for scheduling algorithms in multiuser systems," in *Proc. IEEE Canadian Conf. Elect. Comp. Eng. (CCECE02)*, pp. 1583–1588, May 2002.

[88] T. Eng, N. Kong, and L. B. Milstein, "Comparison of diversity combining techniques for Rayleigh-fading channels," *IEEE Trans. Commun.*, vol. 44, pp. 1117–1129, Sep. 1996.

[89] Y. Ma, D. Zhang and R. Schober, "Optimal Power Allocation for Parallel Access Multiuser Scheduling", *Proc. IEEE Conf. on Global Communications (GlobeCom),* Nov., 2007.

[90] L. Xiao and X. Dong, "A novel normalized threshold generalized selection scheme and its performance evaluation," in *Proc. International Conf. Commun. (ICC)*, vol. 4, pp. 2377–2381, May 16-20, 2005.

www.manaraa.com

[91] A. Annamalai, G. Deora, and C. Tellambura, "Unified error probability analysis for generalized selection diversity in Rician fading channels," in *Proc. IEEE Vehicular Technology Conference (VTC)*, pp. 2042–2046, May 2002.

[92] Y. Ma, D. Zhang, and R. Schober, "Rate-maximizing multiuser scheduling for parallel channel access," *IEEE Signal Processing Letters*, vol. 14, pp. 441–444, July 2007.

[93] X. Dong and N. C. Beaulieu, "Average level crossing rate and average fade duration of selection diversity," *IEEE Commun. Letters*, vol. 5, pp. 396–398, Oct. 2001.

[94] S. O. Rice, "Statistical properties of a sine wave plus noise," *Bell Syst. Tech. J.*, vol. 27, pp. 109–157, Jan. 1948.

[95] M. Yacoub, J. Bautista, and L. Guedes, "On higher order statistics of the Nakagami distribution," *IEEE Trans. Veh. Technol.*, pp. 790–794, May 1999.

[96] N. C. Sagias, D. A. Zogas, G. K. Karagiannidis, and G. S. Tombras, "Channel capacity and second-order statistics in Weibull fading," *IEEE Commun. Letters*, vol. 8, pp. 377–379, June 2004.

[97] N. Youssef, C. X. Wang, and M. Patzold, "A study on the second order statistics of Nakagami-Hoyt mobile fading channels," *IEEE Trans. Veh. Technol.*, vol. 54, pp. 1259–1265, July 2005.

[98] X. Dong, N. C. Beaulieu and P. H. Wittke, "Signalling constellations for fading channels," *IEEE IEEE Trans. Commun.*, vol. 47, pp. 703–714, May 1999.

[99] A. Annamalai, C. Tellambura and V. K. Bhargava, "Exact evaluation of maximal-ratio and equal-gain diversity receivers for M-ary QAM on Nakagami fading channels," *IEEE Trans. Commun.*, vol. 47, pp. 1335–1344, Sept.1999.

[100] Q. T. Zhang, "Maximal-ratio combining over Nakagami fading channels with an arbitrary branch covariance matrix", *IEEE Trans. Veh. Technol.*, vol. 48, no. 4, pp. 1141-1150, Jul. 1999.

www.manaraa.com

[101] M. S. Alouini and A. J. Goldsmith, "Area spectral efficiency of cellular mobile radio system," *IEEE Trans. Veh. Technol.*, vol. 48, no. 4, pp. 1047-1066, Jul. 1999.

[102] M. S. Alouini, "A unified approach for calculating error rates of linearly modulated signals over generalized fading channels," *IEEE Trans. Commun.*, vol. 47, no. 9, pp. 1324-1334, Sep. 1999.

[103] U. Charash, "Reception through Nakagami fading multipath channels with random delays," *IEEE Trans. Commun.*, vol. 27, no. 4, pp. 657-670, Apr. 1979.

[104] X. Dong, N. C. Beaulieu, and P. H.Wittke, "Error probabilities of two-dimensional M-ary signaling in fading," *IEEE Trans. Commun.*, vol. 47, no. 3, pp. 352-355, Mar. 1999.

[105] M. K. Simon and M. S. Alouini, "A unified performance analysis of digital communication with dual selective combining diversity over correlated Rayleigh and Nakagami-m fading channels," *IEEE Trans. Commun.*, vol. 47, no. 1, pp. 33-43, Jan. 1999.

[106] T. Aulin, "Characteristics of a Digital Mobile Channel Type", *IEEE Trans. Veh. Tech.*, vol. 30, pp.89-104, Feb., 1981

[107] M. C. Jeruchim, P. Balaban, K. S. Shanmugan, "Simulation of Communication Systems," New York: Plenum Press, 1992

[108] D. J. Young and N. C. Beaulieu, "The generation of correlated Rayleigh random variates by inverse discrete Fourier transform," *IEEE Trans. Commun.*, vol. 48, no. 7, pp. 1114-1227, Jul. 2000.

[109] K. E. Baddour and N. C. Beaulieu, "Accurate Simulation of multiple cross-correlated Rician fading channels", *IEEE Trans. on Communications*, vol 52, pp.1980-1987 Nov. 2004

[110] K. W. Yip and T. S. Ng, "A simulation model for Nakagami-m fading channels, m ¡ 1," *IEEE Trans. Commun.*, vol. 48, no. 2, pp. 214-221, Feb. 2000.

www.manaraa.com

[111] N. C. Beaulieu and C. Cheng, "Efficient Nakagami-m Fading Channel Simulation," *IEEE Trans. On. Vehicular Tech.*, vol. 54, no. 2, pp. 413-424, Mar. 2005

[112] M. D. Yacoub, G. Fraidenraich and J.C.S. Santos Filho, "Nakagami-m phase-envelope joint distribution," *Electronics Letters,* Vol. 41, Issue 5, pp. 259-261, Mar 2005

[113] H. Suzuki, "A statistical model for urban radio propagation," *IEEE Trans. Commun,* vol. 25, p. 673, 1997

[114] W. Braun and U. Derscu, "A physical mobile radio channel model," *IEEE Trans. on Vehicular Tech.*, p. 472, May 1991.

[115] S. Stein, "Fading channel issues in system engineering," *IEEE Journal on Selected Areas in Communications*, vol. 5, pp. 68-69, Feb 1987.

[116] W. Zhou, D. Zhang, and D. Qiao, "Comparative Study of Routing Metrics for Multi-Radio Multi-Channel Wireless Networks," In *Proc. IEEE WCNC'2006*, Las Vegas, NV, April 03 06, 2006

[117] K. Zhang, Z. Song, and Y. L. Guan, "Simulation of nakagami fading channels with arbitrary cross-correlation and fading parameters," *IEEE Trans. Wireless Commun.*, vol. 3, no. 5, pp. 1463-1468, Sep. 2004.

[118] M. Patzold, U. Killat, F. Laue, and Y. Li, "On the statistical properties of deterministic simulation models for mobile fading channels," *IEEE Trans. on Vehicular Tech.*, vol. 47, pp. 254-269, Feb. 1998.

[119] R. S. Hoyt, "Probability functions for the modulus and angle of the normal complex variate", *Bell Syst. Techn. J.*, Vol. 26, pp. 318-359, 1947

[120] D. A. Harvile, "Matrix Algebra From a Statistician's Perspective," New York: Springer-Verlag, 1997.

[121] R.H. Clarke, "A statistical theory of mobile radio reception," *Bell Syst. Tech. J.*, pp. 957-1000, July-Aug. 1968.

www.manaraa.com

[122] W.C. Jakes, Jr., "Microwave Mobile Communications." New York: Wiley, 1974.

[123] M. Nakagami, "The m-distribution, a general formula of intensity distribution of rapid fading", *Statistical Methods in Radio Wave Propagation*, W. G. Hoffman, Ed, Oxford, U.K.: Pergamon, 1960.

[124] L. Najafizadeh, and C. Tellambura, C. "BER analysis of arbitrary QAM for MRC diversity with imperfect channel estimation in generalized ricean fading channels," in *IEEE Transactions on Vehicular Technology,* Vol. 55, Issue 4, pp.1239-1248, July 2006

[125] M. K. Simon and M.-S. Alouini, *Digital Communications over Fading Channels: A Unified Approach to Performance Analysis.* John Wiley & Sons, 2nd edition ed., 2005.

[126] J. I. Smith, "A computer generated multipath fading simulation for mobile radio," *IEEE Trans. Veh. Technol.*, vol. 24, pp. 39-40, Aug. 1975.

[127] Y. Ma and D. Zhang, "Complex Nakagami Channel Simulator with Accurate Phase and Auto-Correlation Properties", *Proc. IEEE Conf. on Global Communications (GlobeCom),* Nov., 2007.

[128] T. A. Tran, and A. B. Sesay, "Performance of MRC over Nakagami-m fading channels with arbitrary branch correlation, non-identical and non-integral fading orders," em 2004. Canadian Conference on Electrical and Computer Engineering, Vol. 3, pp. 1581-1584, May 2004

[129] Wei Li, Hao Zhang and T. A. Gulliver, "Error probability for maximal ratio combining on correlated Nakagami fading channels," *VTC2004-Fall,* Vol. 3, pp. 1786-1790, Sept. 2004

[130] Y. S. Kim, C.-J. Kim, G.-Y. Jeong, Y.-J. Bang, H.-K. Park, and S. S. Choi, "New Rayleigh fading channel estimator based on PSAM channel sounding technique," in *Proc. IEEE ICC,* June. 1997, pp. 1518-1520.

www.manaraa.com

[131] Q. T. Zhang, "A decomposition technique for efficient generation of correlated Nakagami fading channels," *IEEE J. Select. Areas Commun.*, vol. 18, pp. 2385-2392, Nov. 2000.

www.manaraa.com